JUSTUS-LIEBIG-
UNIVERSITÄT
GIESSEN

The role of small open reading frames in *Shewanella oneidensis* phage λSo in host takeover and phage proliferation

---

Dissertation

Zur Erlangung des Doktorgrades der Naturwissenschaften
(Dr. rer. Nat.)

Dem Fachbereich 08
- Biologie und Chemie -
der Justus-Liebig-Universität Gießen
vorgelegt von

Svenja Wiebke Thöneböhn

Angefertigt im Institut für Mikro- und Molekularbiologie
Gießen, August 2025

Erstgutachter:	Prof. Dr. Kai Thormann Institut für Mikrobiologie und Molekularbiologie Justus-Liebig-Universität Gießen
Zweitgutachter:	Prof. Dr. Julia Frunzke Institute of Bio- and Geoscience Forschungszentrum Jülich

Die während der Promotion erzielten Ergebnisse sind zum Teil in folgender Publikation veröffentlicht:

Svenja Thöneböhn, Dorian Fischer, Vanessa Kreiling, Alina Kemmler, Isabella Oberheim, Fabian Hager, Nicole E Schmid, Kai M Thormann:

Identifying components of the *Shewanella* phage LambdaSo lysis system.
Journal of Bacteriology, 21.04.2024

DOI: 10.1128/jb.00022-24

Eidesstattliche Erklärung

Hiermit versichere ich, die vorgelegte Dissertation selbständig und ohne unerlaubte fremde Hilfe und nur mit den Hilfen angefertigt, die ich in der Dissertation angegeben habe. Alle Textstellen, die wörtlich oder sinngemäß aus veröffentlichten Schriften entnommen sind, und alle Angaben, die auf mündlichen Auskünften beruhen, sind als solche kenntlich gemacht. Bei den von mir durchgeführten und in der Dissertation erwähnten Untersuchungen habe ich die Grundsätze guter wissenschaftlicher Praxis, wie sie in der „Satzung der Justus-Liebig-Universität Gießen zur Sicherung guter wissenschaftlicher Praxis“ niedergelegt sind, eingehalten. Gemäß § 25 Abs. 6 der Allgemeinen Bestimmung für modularisierte Studiengänge dulde ich eine Überprüfung der Thesis mittels Anti-Plagiatssoftware.

Datum: Unterschrift:

Erklärung zur Verwendung von künstlicher Intelligenz bei der Erstellung von Aufsätzen und Abschlussarbeiten

Name des Studierenden

Familienname:	Thöneböhn
Vorname:	Svenja Wiebke

Titel der Dissertation

The role of small open reading frames in *Shewanella oneidensis* phage λSo in host takeover and phage proliferation

Bitte markieren:

☐ Ich habe bei der Erstellung dieses Textes kein KI-Tool verwendet.

☐ Ich habe ein KI-Tool in den folgenden Bereichen eingesetzt (Mehrfachnennungen möglich):

- ☐ Ideen finden, meine Kreativität anregen
- ☐ Verstehen von Konzepten, Recherche von Fakten und Definitionen
- ☐ Optimierung eines von mir verfassten Textes
- ☐ Erstellen ganzer Textpassagen nach meinen Vorgaben

Wenn Sie ein KI-Tool verwendet haben, erklären Sie bitte, welche Teile Ihres Textes von dem Tool profitiert haben und wie. Fügen Sie bei Bedarf eine zusätzliche Seitehinzu oder geben Sie Hyperlinks zu den von Ihnen verwendeten Chat-Verläufen an.

Verwendet wurden DeepL, DeepL-Write sowie ChatGPT zur Übersetzung, Suche von Synonymen für gewisse Worte sowie zur Verbesserung des Vokabulars und des Wortlautes des in Englisch verfassten Textes.

Datum: Unterschrift:

Abstract

Bacteriophages are the most abundant biological entities on Earth. They wield an immense influence on microbial ecosystems in almost all habitats by regulating bacterial population dynamics. Most phages follow one of two well-characterised strategies for host exploitation: the lytic or the lysogenic cycle. In both pathways, host cell lysis represents the terminal event and is therefore central to phage fitness.

The temperate phage λSo is one of four known prophages in the genome of *Shewanella oneidensis* MR-1 and has a genome size of about 51 kbp. During lysogeny, λSo remains integrated into the host chromosome, replicating in concert with the host cell. In this study, the lysis system of λSo was characterised as a pinholin-SAR endolysin-two-component spanin pathway. The λSo holin protein, S^{So}, contains two transmembrane domains and also produces an antagonistic isoform through an alternative translation start, named antiholin. This regulatory mechanism enables precise temporal control over the initiation of host lysis. In addition to the pinholin and the SAR endolysin, the lysis system requires a two-component spanin complex, made up of an inner membrane protein (i-Spanin, Rz^{So}) and an outer membrane protein (o-Spanin, $Rz1^{So}$). The corresponding genes are present in an overlapping reading frame structure, and the encoded proteins likely form a functional dimer of two dimers. This putative dimer enables the fusion of the inner and outer membrane. In addition, this work has shown that further, previously uncharacterised gene products are involved in cell lysis.

Like many phages, λSo harbours genes encoding small proteins of unknown function. A gene cluster, so called cluster C, was identified, whose deletion significantly reduced the number of plaque-forming units. Cluster C consists of six genes (*lcc1* - *lcc6*) encoding proteins between 41 and 137 amino acids in length that have no obvious homologies to known protein domains. Bioinformatic analysis suggests that Lcc4 and Lcc6 contain putative transmembrane domains. Functional characterisation revealed that Lcc6 plays a critical role in phage-induced host cell lysis. In *lcc6* deletion strains, induction of the lytic cycle of λSo using mitomycin C resulted in the formation of phage particles, which, however, failed to lyse the host cells and are therefore not released. These findings

suggest that Lcc6 participates in an early phase of the lysis cascade, likely acting in concert with pinholin-mediated membrane disruption.

The ectopic expression of the Lcc4 protein on the other hand resulted in a pronounced elongation of the host cells and delocalisation of the FtsZ rings - a phenotype that is compatible with a disruption of cell division. The modelling of plausible protein interactions confirmed that this phenotype results from a direct interaction of Lcc4 with key components of the bacterial divisome, particularly FtsZ and ZipA. Site-directed mutagenesis identified isoleucine residues at positions 16 and 19 as essential for the interaction with FtsZ, and tryptophan 80 and arginine 84 as critical for binding to ZipA. Taken together, these results suggest that Lcc4 specifically inhibits bacterial cytokinesis following prophage induction in order to maximise the availability of the metabolic resources of the host cell during phage replication.

The Lcc proteins, encoded by genes of the cluster C, thus represents a previously undescribed phage-host effector system with profound influence on cellular organisation and the course of lysis.

Zusammenfassung

Bakteriophagen stellen die am weitesten verbreiteten biologischen Entitäten auf der Erde dar. Sie üben einen immensen Einfluss auf die mikrobiellen Ökosysteme nahezu aller Lebensräume aus, insbesondere durch die Regulation bakterieller Populationen. Die meisten Phagen verfolgen dabei eine von zwei gut charakterisierten Strategien zur Wirtsausbeutung: den lytischen oder den lysogenen Zyklus. Die Lyse der Wirtszelle bildet dabei das finale und für die Phagenfitness zentrale Ereignis beider Strategien.

Der temperente Phage λSo ist einer von vier bekannten Prophagen im Genom von *Shewanella oneidensis* MR-1 und weist eine Genomgröße von etwa 51 kbp auf. Im lysogenen Lebenszyklus ist λSo in das Wirtsgenom integriert und repliziert synchron mit der Wirtszelle. Im Rahmen dieser Arbeit konnte das Lysesystem von λSo als ein Pinholin-SAR-Endolysin-Zwei-Komponenten-Spanin-System charakterisiert werden. Das Holin-Protein S^{So} besitzt zwei Transmembrandomänen und generiert durch einen alternativen Translationsstart einen antagonistischen Isoform, welche als Antiholin fungiert und eine präzise zeitliche Regulation der Zelllyse ermöglicht. Ergänzend zum Pinholin und dem SAR-Endolysin ist ein Zwei-Komponenten-Spanin-System erforderlich, bestehend aus einem inneren Membranprotein (i-Spanin, Rz^{So}) und einem äußeren Membranprotein (o-Spanin, $Rz1^{So}$). Die entsprechenden Gene liegen in einer überlappenden Leserasterstruktur vor und bilden vermutlich funktional einen Dimer aus zwei Dimeren, der die Fusion der inneren und äußeren Membran ermöglicht. Darüber hinaus konnte durch diese Arbeit gezeigt werden, dass weitere, bislang uncharakterisierte Genprodukte an der Zelllyse beteiligt sind.

Viele Phagen enthalten zahlreiche Gene, die die für Proteine unterschiedlicher Größe kodieren, deren Funktion derzeit nicht klar ist. Das Genom von λSo enthält unter anderem ein Gencluster, Cluster C, dessen Deletion zu einer drastischen Abnahme der Produktion von Plaque-bildenden Einheiten führt. Das Cluster besteht aus sechs Genen (*lcc1* - *lcc6*), die für eher kleine Proteine im Bereich von 41 bis 137 Aminosäuren kodieren und keine offensichtliche Homologien zu bekannten Proteindomänen aufweisen. Zwei der Proteine, Lcc4 und Lcc6, besitzen vermutlich eine Transmembrandomäne. Das Protein Lcc6 konnte als zentraler Faktor in der Phagen-induzierten Zelllyse identifiziert werden. In *lcc6*-Deletionstämmen führte die Induktion des

lytischen Zyklus mittels Mitomycin C zwar zur Bildung reifer Phagenpartikel, diese konnten jedoch die Wirtszellen nicht lysieren und die Zelle final verlassen. Dies legt nahe, dass Lcc6 in einen frühen, wahrscheinlich Pinholin-vermittelten Schritt der Zelllyse eingreift.

Die ektopische Expression des Proteins Lcc4 hatte hingegen eine ausgeprägte Verlängerung der Wirtszellen sowie eine Delokalisierung der FtsZ-Ringe zur Folge: ein Phänotyp, der mit einer Störung der Zellteilung vereinbar ist. Durch Struktursimulationen konnte gezeigt werden, dass dieser Phänotyp auf eine Interaktion von Lcc4 mit Proteinen der Zellteilungsmaschinerie wie FtsZ und ZipA zurück zu führen ist. Funktionelle Mutagenese-Experimente identifizierten Isoleucin an Position 16 und 19 als essenziell für die Interaktion mit FtsZ sowie Tryptophan 80 und Arginin 84 für die Bindung an ZipA. Diese Ergebnisse deuten darauf hin, dass Lcc4 die Zellteilung gezielt hemmt, um die metabolischen Ressourcen der Wirtszelle während der Phagenreplikation vollständig verfügbar zu machen.

Das hier identifizierte Lcc-System stellt damit ein neuartiges Phagen-Wirt-Effektorsystem dar, das tiefgreifenden Einfluss auf die zelluläre Organisation und den Verlauf der phagen-vermittelten Zelllyse besitzt.

Table of contents

1 Introduction

1.1 General characteristics of bacteriophages

Bacteriophages, often called phages, are thought to be the most abundant biological entities on earth and are found in every explored biome [1–3]. They outnumber bacteria by up to tenfold, as viral concentrations can reach up to 2.5×10^8 viruses per millilitre in natural aquatic environments [4].

Phages are obligate intracellular parasites of bacteria with diverse life cycles that play a crucial role in shaping bacterial evolution and community structure and thereby influencing ecosystem dynamics. Their evolutionary significance is emphasised by the enormous extent of phage-mediated horizontal gene transfer, which is estimated to be about 2×10^{16} events every second worldwide [5,6].

As antibiotic-resistant bacteria continue to present a serious threat to global health, interest in bacteriophage-based strategies has grown significantly in recent years. Phages are estimated to account for up to 40% of bacterial mortality each day, underscoring their ecological importance and therapeutic potential. Over the past two decades, this has spurred a resurgence in research aimed at harnessing phages for use in medicine, agriculture, and food safety [7,8]. Phage therapy, employing either naturally occurring or genetically engineered lytic phages, has yielded encouraging results in clinical contexts [7]. In contrast to the slower regulatory uptake in healthcare, the food and agricultural sectors have adopted phage-based technologies more swiftly, with several products already available on the market [8]. Moreover, due to their high host specificity, phages are increasingly being investigated as tools for the sensitive and accurate detection of bacterial pathogens.

Bacteriophages display extraordinary diversity and are currently classified based on a combination of genomic features and morphological characteristics [9–11]. With the rapid increase in publicly available viral genome sequences, genome-based taxonomic approaches have become widespread and are now a central method in phage classification [10]. The genetic material of phages can consist of either double-stranded (ds) or single-stranded (ss) DNA or RNA and can include modified nucleotides as protection against restriction enzymes (**Fig. 1**) [12–14]. Genome sizes are highly variable, ranging from

approximately 3.5 kilobases in the ssRNA phage MS2 to around 500 kilobases in the dsDNA phage G [15]. The genetic material is enclosed within a capsid, which can take various forms: polyhedral (*Microviridae*, *Corticoviridae*, *Tectiviridae*, *Leviviridae*, and *Cystoviridae*), filamentous (*Inoviridae*), pleomorphic (*Plasmaviridae*), attached to a tail (*Caudoviricetes*) or possessing lipid or lipoprotein envelopes [1,16,17].

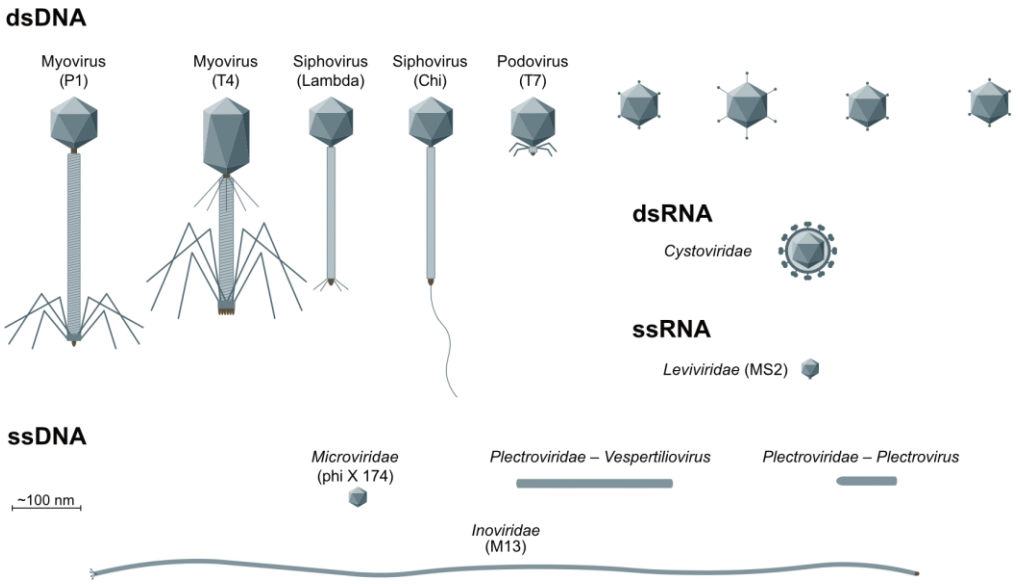

Figure 1: Viruses of bacteria. Bacterial virus sub-families are represented and grouped based on their Baltimore classification. Relative sizes and symmetries are approximate. Modified after: Hay & Lithgow [17]

1.1.2 *Caudoviricetes*

As a model belonging to the *Caudoviricetes* class was utilised in this study, the following section will provide a more detailed description of the characteristics of this class.

The class of the *Caudoviricetes* encompasses tailed bacteriophages with double-stranded DNA (dsDNA) genomes and represents the majority of phages characterised to date. This class can be divided into three morphological groups: myoviruses (phage T4), siphoviruses (phage λ) and podoviruses (phage T7) [1,9,15]. These groups differ notably in their tail morphology: myoviruses possess long, rigid, contractile tails; siphoviruses are characterised by long, flexible, non-contractile tails; and podoviruses feature short, non-contractile tails (**Fig. 1**) [18,19]. Tail structures play a crucial role in recognizing specific receptors, penetrating cell membranes, and delivering the viral genome into the bacterial cytoplasm [16]. The tails of siphoviruses and myoviruses are composed of three key elements:

the tail tip complex, which mediates host recognition and initiates the infection process; the tail tube, which serves as a conduit for the transfer of genomic DNA into the host cell; and the terminator proteins, which complete the tail assembly and form the interface for attachment to the phage head [20,21]. Capsid size varies significantly among members of the *Caudoviricetes* with diameters ranging from 45 to 185 nm, typically correlating with genome size [22]. The majority of phages in this family, around 75 %, possess icosahedral (isometric) capsids, while approximately 15% (e.g., T4) feature prolate heads. Prolate heads are icosahedral structures elongated along the five-fold axis, which aligns with the phage tail [23]. The tail is connected to the head via a so-called connector protein, which is described as a dodecameric portal protein that binds to a special pentameric vertex of the phage capsid (**Fig. 2**). This protein forms a channel essential for genome packaging during virion assembly and for genome release during infection. Phage head assembly typically begins at this vertex, where the portal protein facilitates the organization of scaffolding and major capsid proteins [16,24].

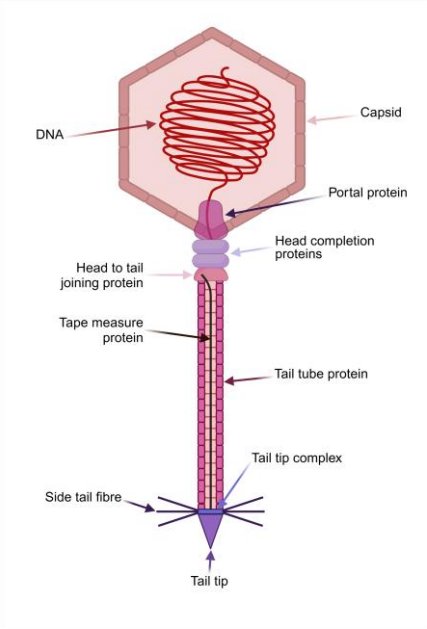

Figure 2: Phage structure. Schematic representation of a siphovirus phage tail, neck and head [24].

Capsid assembly is facilitated by internal scaffolding proteins and completed through the closure of the portal gate by head completion proteins (**Fig. 2**) [25]. These proteins typically exist as monomers in solution and do not appear to interact with other phage

proteins. However, they serve as a hub for tail assembly in podoviruses and as a platform for the attachment of the preassembled tail in siphoviruses and myoviruses [24]. Phages belonging to those families generally possess two head completion proteins, each forming a ring beneath the portal. In the mature virion, these two rings are located between the portal protein and the tail. The protein shells of the mature capsids are remarkably stable and can withstand the high internal pressure exerted by the tightly packed, encapsulated DNA [26].

1.2 Life cycles

Before the required proteins can be expressed and virions formed, the phage must first infect a host cell. This process begins with the phage identifying and attaching to specific receptors on the surface of the host cell, such as surface proteins, lipopolysaccharides, or other molecules on the bacterial cell envelope like teichoic acids, fimbriae, and flagella [21,27,28]. As soon as the phage successfully recognizes its target receptor, it permanently adsorbs to the host cell and injects its genetic material [16]. The subsequent replication strategy, including the formation, release and transmission of virions, depends on whether the phage is virulent or temperate [29].

There are four common phage life cycles: lytic, lysogenic, pseudolysogenic and chronic infection life cycle [30,31]. In the lytic life cycle, which is utilised by virulent phages such as T4, the phage employs various strategies to hijack the host's metabolism and initiate the production of viral progeny [32,33]. During this process, virion particles are assembled, packed with the respective viral nucleic acid, and ultimately released into the extracellular environment following the lysis of the infected host cell (**Fig. 3**) [16,34]. This process requires the disruption of the bacterial membrane and cell wall, which relies on specific lysis proteins, including endolysins, holins, and spanins [35,36].

In contrast, the lysogenic life cycle allows the phage not only to either lyse its host but also to establish a stable association, known as lysogeny (**Fig. 3**) [31]. During lysogeny, the viral genome, known as a prophage, replicates in synchrony with the host DNA, either as a free, plasmid-like entity (e.g., phage P1) or integrated into the bacterial chromosome (e.g. phage λ) [34]. A temperate phage has the capacity to remain dormant as a prophage, replicating alongside the host genome. In response to specific environmental cues, which often involve host cell stress, prophages have been shown to be triggered to exit lysogeny and transition

to the lytic cycle. This results in the production of new virions that are subsequently released from the bacterium [37]. The decision between lysogenic and lytic cycles in temperate phages is influenced by various factors, including carbon and nitrogen availabilty, salinity, UV radiation, temperature or pollutants [38–40]. Several studies suggest that host density-dependent quorum sensing (QS) plays a crucial role in molecular communication, both between phages and among phages and hosts, potentially guiding the lysis-lysogeny decision [41,42]. A long-term association between host and phage can be maintained over thousands of generations, potentially altering the phenotype of the host bacterium through the expression of genes that are not normally activated during infection: a phenomenon known as lysogenic conversion. A well-known example is the prophage CTXφ, which infects certain strains of *Vibrio cholerae* and encodes toxins responsible for cholera symptoms [43]. Bacteria harbouring prophages may also develop immunity to subsequent infections by homologous phages and potentially exhibit enhanced fitness [44].

Prophages that remain in the host genome but can no longer be induced are referred to as cryptic prophages [45–47]. These can be divided into four different types based on the extent of genomic degradation resulting from the integration of viral and bacterial genetic material: defective prophages, satellite phages, bacteriocins, and other prophage-related entities, such as gene transfer agents. A prophage incapable of undergoing the lytic cycle due to loss of function through mutations or the deletion of genes essential for DNA packaging into the phage capsid is called a defective prophage [48]. A satellite phage depends on a specific helper phage for its replication due to the absence of genes encoding structural proteins [49]. As the phage genome is progressively reduced, leaving only a few genes encoding for specific proteins, it can give rise to bacteriocins and eventually gene transfer agents. These phage-like particles enable the transfer of random bacterial genomic fragments to other bacteria through a process resembling generalized transduction. However, unlike true phages, gene transfer agents lack the genetic elements required for encoding phage structural components [50].

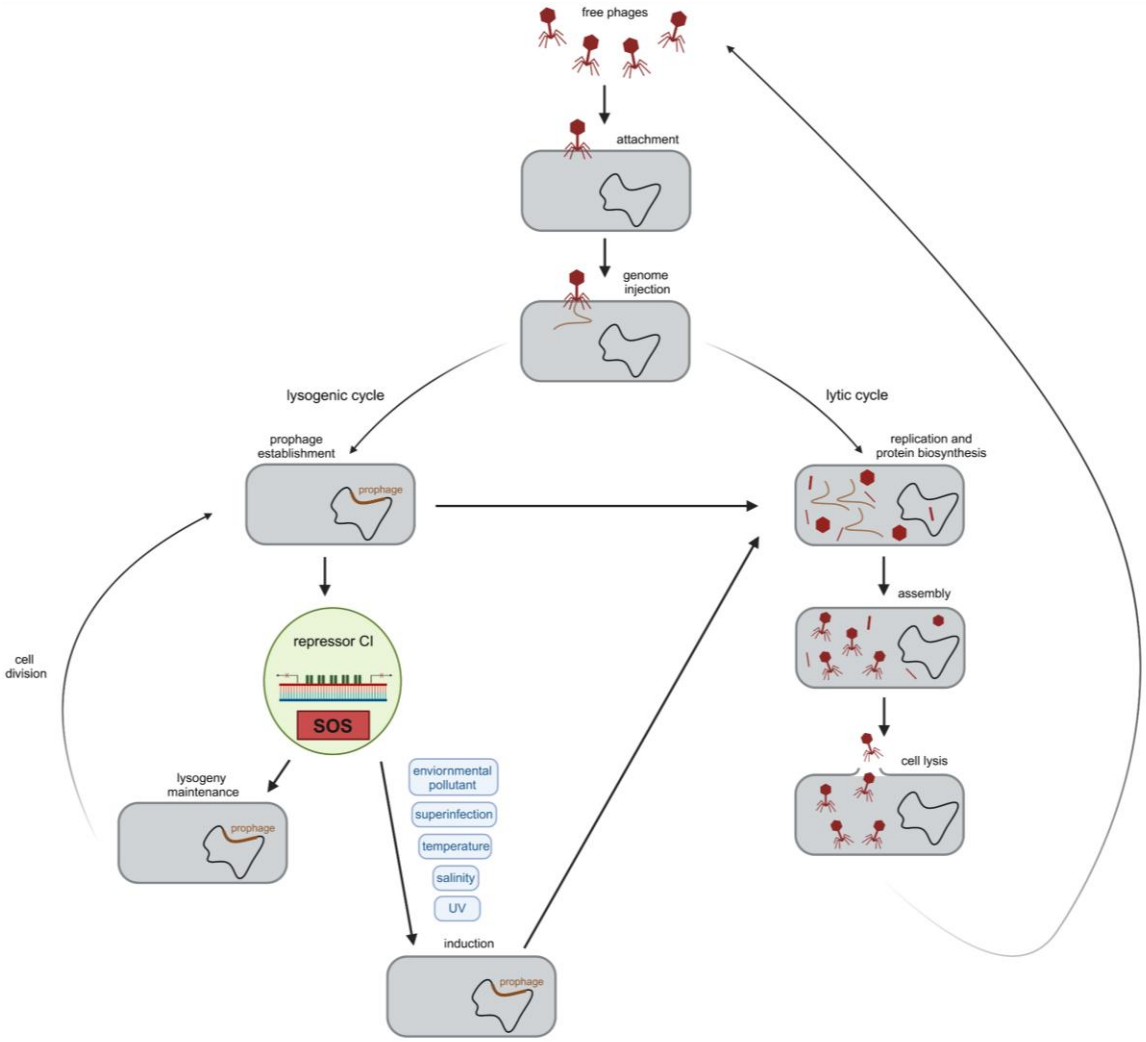

Figure 3: Possible phage life cycles. To infect a bacterial host, a phage must first recognize and bind specific surface receptors, then inject its genome into the cell. Virulent phages follow the lytic cycle: producing new virions and ultimately lysing the host. Temperate phages can either enter the lytic cycle or establish lysogeny, a dormant state maintained by a repressor protein that ensures replication of the prophage with the host genome. Stress conditions, such as those triggering the host SOS response (blue boxes), can induce the prophage to switch to the lytic cycle. In phage λ, the CI repressor maintains lysogeny by repressing early promoters (*pL*, *pR*) through octamer formation and DNA looping. Upon SOS induction, host RecA cleaves CI, reducing its levels and halting its synthesis, thereby initiating the irreversible transition to the lytic cycle [51].

In addition to the well-characterised lytic and lysogenic life cycles, phages may also adopt alternative infection strategies. One such example is pseudolysogeny, a non-canonical state in which the phage neither integrates into the host genome nor initiates lysis, thereby failing to establish a stable, long-term relationship with the host [52,53]. This condition typically arises under stressful environmental circumstances, such as nutrient starvation, and may revert to either the lysogenic or lytic cycle once favourable conditions are

restored [54]. A further alternative is the chronic infection cycle, observed in certain archaeal viruses, filamentous phages (e.g., rod-shaped single-stranded DNA phages), and plasmaviruses infecting *Mycoplasma* species. In this mode of infection, phage particles are continuously or intermittently released from the host cell without inducing immediate cell lysis, allowing prolonged coexistence between virus and host [23,29,34].

1.3 Phage mediated lysis

Phage-mediated cell lysis is an autonomous, meticulously regulated, and temporally scheduled pathway that involves multiple proteins and manifests as a sudden, explosive burst with minimal time during which the host morphology is altered. The capacity to time this process with precision is a crucial fitness factor for the phage [55,56]. The pathway is comprised of three distinct steps, each with two fundamentally different mechanisms: initiation through strictly coordinated triggering by holin or pinholin, cell wall degradation by endolysin or SAR endolysin, and outer membrane disruption by the i-spanin/o-spanin complex or the u-spanin [54].

The holin function not only triggers the lysis pathway but also plays a crucial role in regulating its duration [57]. Holin proteins always have a small cytoplasmic domain, a characteristic that is manifest at the C-terminus, in conjunction with a minimum of one transmembrane α-helical segment [58–60]. It has been demonstrated that these proteins possess the capacity to be triggered, resulting in the formation of pores within the membrane. This, in turn, leads to a collapse of the membrane potential, disruption of active transport and an increase in permeability of the inner membrane [61,62]. The classification of bacteriophage holins is determined by the topology of their transmembrane α-helical segments: Class I holins possess three transmembrane α-helical segments arranged in an N-out and C-in configuration (e.g. λ), Class II holins consist of two transmembrane α-helical segments arranged in an N-in and C-in configuration (e.g. ϕ21), and Class III holins have one transmembrane α-helical segment and a large periplasmic domain arranged in an N-in and C-out configuration (e.g. T4) [58,63,64].

1.3.1 Canonical holin lysis pathway

As the expression of late phage genes begins, holin proteins start to accumulate as freely mobile entities within the cytoplasmic membrane, while phage particle assembly continues (**Fig. 4A**). Holin proteins initially accumulate harmlessly as homodimers, with their hydrophilic faces sequestered against each other in the membrane [65–67]. Simultaneously, the endolysin proteins, which possess transglycosylase activity, also accumulate in the cytoplasm as a monomeric, properly folded and fully active enzyme [68–70]. Once the holin concentration reaches a critical, allele-specific threshold, those proteins suddenly cluster into large, two-dimensional aggregates known as death rafts (**Fig. 4B, 5B**) [71]. These large, sparse structures are lipid-depleted due to the intimate helical packing of the holins, and are thus poor insulators. This leads to local reduction or collapse of the proton motive force (PMF), and consequently to a sudden halt in culture growth and respiration of the infected bacterial cell [72]. The disturbance of the PMF gives rise to alterations in the orientation of certain TMDs of the holins, which in turn results in further leakage of protons [62,73]. As the PMF continues to decline, the death rafts undergo a massive reorganization, terminating in the sudden formation of a small number of micron-scale holes lined by a single layer of holin molecules, averaging >340 nm in diameter [74]. These large holes permit the endolysin to escape into the periplasmic space, thus facilitating the degradation of the peptidoglycan (**Fig. 4B**). The infected cells elongate until the actual lysis occurs, a process referred to as a 'blow out'. This is characterised by the sudden expulsion of cytoplasmic content including the progeny virions (**Fig. 4C**). This phenomenon is hypothesized to be caused by the degradation of the peptidoglycan in relation to the large lesions in the cytoplasmic membrane by escaped endolysins [75].

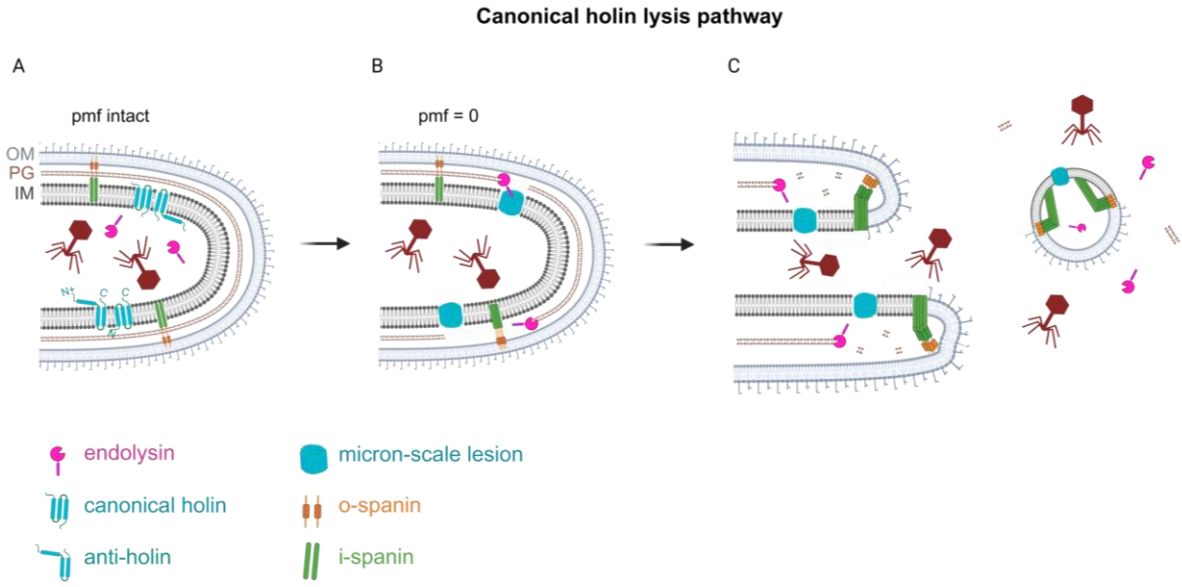

Figure 4: Phage lysis, the canonical holin-endolysin lysis pathway. Cartoon model of one of the two pathways of phage lysis of Gram-negative hosts exemplified by phage λ for the canonical holin-endolysin lysis pathway. During the expression of the late phage genes, the respective holins accumulate together with their antiholins in the inner membrane (**A**). In a similar manner, the endolysins have been observed to accumulate in the cytoplasm (**A**). Once a critical holin concentration is attained, holin triggering results in micron-scale holes (**B**), which release the endolysin into the periplasm (**B**). The subsequent peptidoglycan degradation results in the activation of the spanins, which overcome the barrier of the outer membrane by fusing the inner and outer membrane (see Chapter 2.1.1.2 and 3.1.2) and thus releasing the phage progeny (**C**) [54].

In order to ensure that this process occurs in the correct sequence and at the appropriate time, the holin is controlled by the so-called antiholin prior to the triggering event [76]. In phage λ, both protein products are generated from the same locus, which contains two Shine-Dalgarno (SD) sequences and two start codons [63,77]. These elements are involved in ensuring an adequate translation, as well as a specific ratio of holin to antholin molecules. The holin-antiholin ratio for the bacteriophage λ is 2.5:1 under normal conditions, as a stem-loop structure in the mRNA determines the relative initiation frequency [78]. The λ antiholin carries an additional positively charged residue at its N-terminus, thereby hindering the integration of this TMD1 into the membrane (**Fig. 5A**) [63]. The antiholin then heterodimerizes preferentially with the holin, forming inactive holin-antiholin heterodimers that control the timing of lysis [79]. However, depolarization induced after the triggering event ensures that the TMD1 of the antiholin can enter the membrane and convert the inactive antiholin to an active holin. As a result, given that only about one-third of the total holin gene products accumulate as homodimeric holins, while approximately two-thirds exist as holin-antiholin

heterodimers, the instantaneous triggering event leads to a threefold increase in the number of active holin dimers [80].

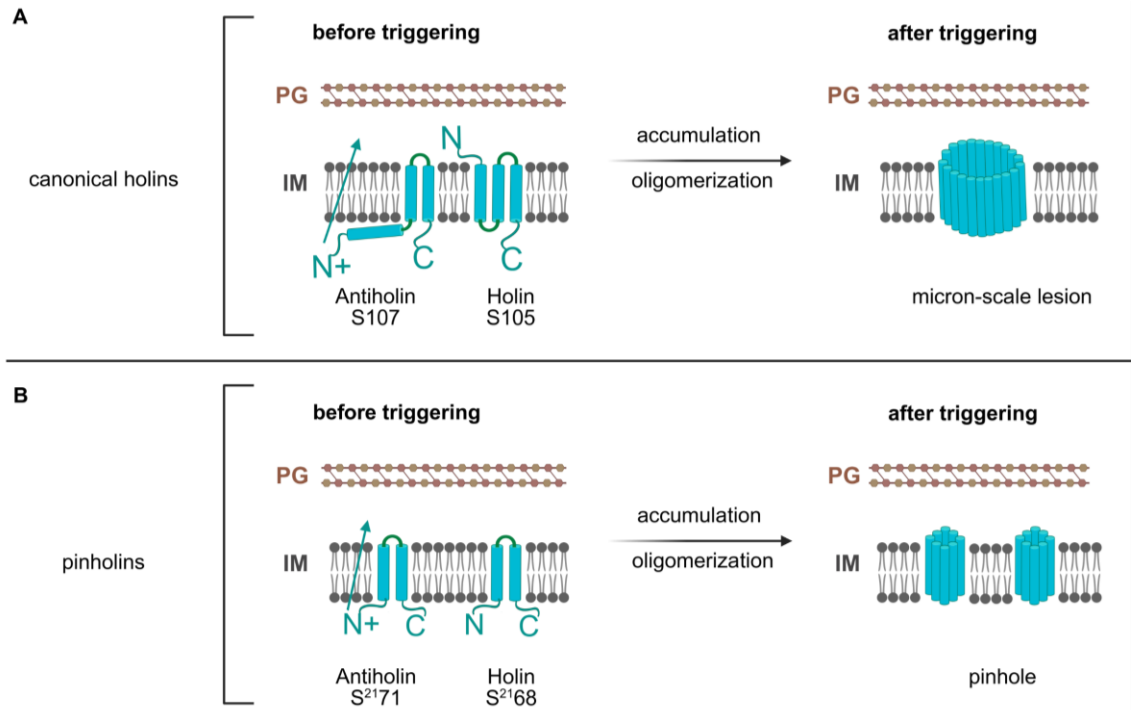

Figure 5: Holin structure. Schematic representation of the membrane topologies of two distinct classes of holin proteins: the canonical holin from bacteriophage λ (Panel A) and the pinholin from phage ϕ21 (Panel B). (**A**) The canonical holin S105 from phage λ features three transmembrane α-helices arranged in an N-out, C-in orientation. Its activity is negatively regulated by the antiholin S107. Upon a triggering signal, accompanied by the collapse of the proton motive force (PMF), the N-terminus of the holin undergoes a conformational change and flips into the periplasm (indicated by the blue arrow). This event facilitates the formation of large, micron-scale membrane holes. (**B**) The pinholin $S^{21}68$ from phage ϕ21 consists of two transmembrane α-helices with both N- and C-termini located in the cytoplasm (N-in, C-in orientation). It is negatively regulated by the antiholin $S^{21}71$. At the moment of triggering, the first transmembrane domain (TMD1) of $S^{21}71$ exits the membrane and relocates to the periplasm (blue arrow), resulting in the assembly of small, heptameric pinholes in the membrane [60,66,81].

1.3.2 Pinholin SAR endolysin pathway

This particular type of phage-mediated cell lysis is also initiated by the accumulation of the holins as dimers within the membrane (**Fig. 6A**). However, the structural characteristics of these proteins differ from the canonical holins. The so-called pinholins that are a part of this pathway are classified as class II holins and consequently possess two TMDs, exhibiting an N-in, C-in topology (**Fig. 5B**) [82,83]. These proteins

accumulate harmlessly with two TMDs in the bilayer, as the native topology is not capable of triggering. TMD1 is not essential for lesion formation and acts as a negative regulator of TMD2, which is the essential domain for hole formation [84]. The TMD1 domains of both holin molecules of the accumulated dimers must exit the bilayer to activate the complex and to proceed down a pathway to triggering [85,66,86]. These holins also reorganize into large, two-dimensional aggregates after reaching an allele-specific critical concentration - however, these are smaller and occur more frequently than in canonical holin lysis pathway (**Fig. 5B, 6B**) [82]. The aggregates self-organize into so-called pinholes, which represent a homoheptamer of pinholins with the hydrophilic face of TMD2 facing the lumen [81]. These pinholes have a diameter of under 2 nm, which is too small to allow most proteins to pass through [82,86]. Therefore, this type of phage-mediated cell lysis requires so-called SAR endolysins to be able to attack the peptidoglycan [87]. SAR endolysins (Signal Anchor Release endolysins) carry an N-terminal TMD, a signal anchor, which serves to engage the sec pathway of the host cell and then anchor the exported endolysin to the bilayer in a membrane potential-dependent fashion (**Fig. 6A**) [88,89]. It should be noted that this form is enzymatically inactive. It has been observed that some of the SAR domains can leave the membrane spontaneously; however, the enzymes are released instantaneously when the PMF breaks down (**Fig. 6B**) [36]. Subsequently, the enzymes fold into an enzymatically active form. In this process, the SAR domain plays a pivotal role in enzyme refolding. It facilitates structural stabilization through covalent disulfide bonds or non-covalent interactions with the enzyme's core [88–91]. Enzyme activation promotes the degradation of peptidoglycan. After the pinholins are triggered, the pinholes are formed and the SAR endolysins are released, the infected cells begin to shorten and become round, ultimately resulting in their rupture (**Fig. 6C**). This further difference to the canonical holin lysis pathway is probably indicative of the even distribution of endolysins and thus peptidoglycan degradation.

As previously outlined, TMD1 functions as an intrinsic intramolecular inhibitor of lysis when within the membrane. However, the presence of an antiholin within this lysis pathway has also been observed [83]. The antiholin is distinguished by the presence of an additional positively charged residue at its N-terminus, a feature that hinders the release of TMD1 (**Fig. 5B**). The holins also dimerize with the antiholins in this lysis pathway, thereby slowing down the lysis clock. The decrease in PMF also leads to a topological change of

TMD1 and thus converts the inactive holin-antiholin heterodimer into fully active molecules [81].

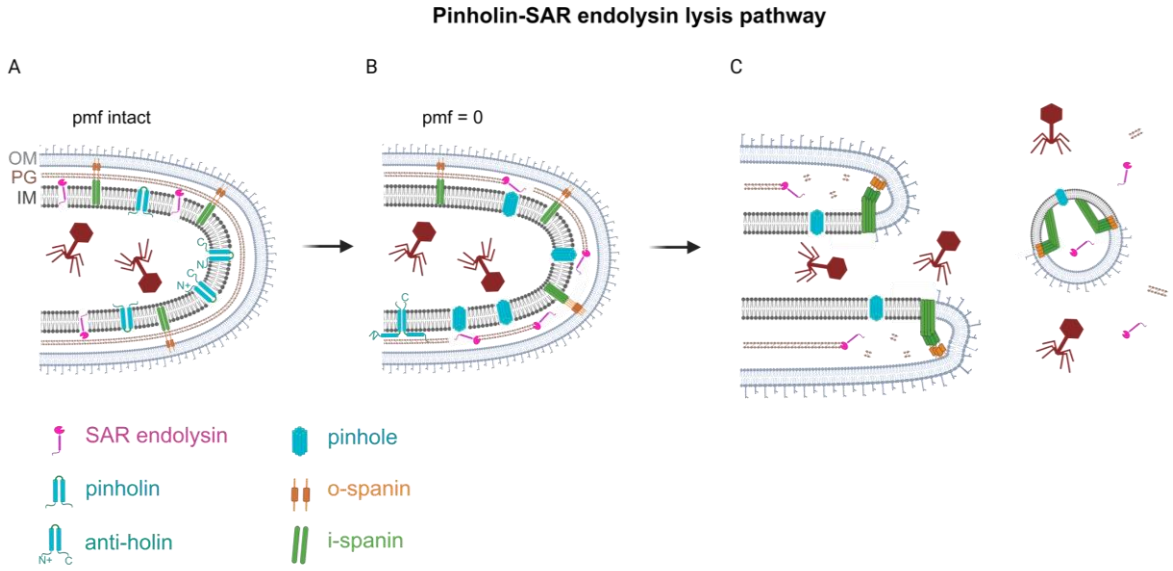

Figure 6: Phage lysis, the pinholin-SAR endolysin lysis pathway. Cartoon model of one of the two pathways of phage lysis of Gram-negative hosts exemplified by phage ϕ21 for the pinholin-SAR endolysin lysis pathway. During the expression of the late phage genes, the respective holins accumulate together with their antiholins in the inner membrane (**A**). In a similar manner, the endolysins have been observed to accumulate tethered to the membrane as SAR-endolysins during the pinholin lysis pathway (**A**). Once a critical holin concentration is attained, holin triggering results in small heptameric pinholes (**B**), which release the SAR endolysin from the inner membrane into the periplasm (**B**). The subsequent peptidoglycan degradation results in the activation of the spanins, which overcome the barrier of the outer membrane by fusing the inner and outer membrane and thus releasing the phage progeny (**C**) [54].

1.3.3 Spanin proteins

For a considerable period, it was hypothesized that the degradation of the peptidoglycan and the resultant instability of the cell would be sufficient to overcome the barrier of the outer membrane and cause the infected cell to lyse. However, scientific research in this field over the past two decades has shown that this hypothesis is incorrect. To disrupt the outer membrane to allow phage egress, most phages studied to date fuse the inner and outer membrane of the host cell, a process that is facilitated by spanin proteins. These proteins had previously been overlooked due to the fragility of the cells in the context of a shaker flask and their resulting destruction by shear forces [75,92,93]. To date, two different types of spanins have been identified: the so-called two-component spanins and the unimolecular

spanins (**Fig. 7**). Current *in silico* studies have identified over 500 two-component spanins and just over 50 unimolecular spanins in the NCBI reference sequence database [36,75,94–96]. Unimolecular spanins, also known as u-spanins, possess an outer membrane (OM) lipoprotein determinant and a C-terminal transmembrane domain (TMD) embedded in the inner membrane (IM) (**Fig. 7A**) [96]. Notably, these spanins are encoded as a single gene within the bacteriophage lysis cassette [95].

The two component spanins, such as the Rz and Rz1 proteins from phage λ, consist of a complex of an integral IM protein, the i-spanin, and an OM lipoprotein, the o-spanin, which spans the entire periplasm (**Fig. 7B**) [97,98]. There are three different ways known thus far of encoding o-spanin and i-spanin in the phage genome: the two genes encoding these proteins can be nested (λ), overlapped (P2) or separated (T4) [95]. Both spanin proteins are required for complete cell lysis. If either i-spanin or o-spanin is defective, cell lysis results in spherical cells lacking a cell wall and held together by the outer membrane [75]. The spanin complex assembles in the cell envelope during morphogenesis via C-terminal interactions. Recent studies have shown that Rz and Rz1 accumulate as covalent homodimers, stabilized by three intermolecular disulfide bonds: two within the Rz dimer and one within the Rz1 dimer. Consequently, the λ spanin complex is structurally a dimer composed of Rz_2:$Rz1_2$ [99]. During the early stages of lysis, these spanin complexes become trapped in the gaps of cross-linked peptidoglycan, rendering the PG layer a negative regulator of spanin activity [97,100]. Following holin triggering, the collapse of the proton motive force, caused by pore formation in the inner membrane, facilitates the release of endolysins. This, in turn, leads to the degradation of the peptidoglycan layer. Degradation of the peptidoglycan layer permits lateral diffusion of spanin complexes, allowing them to assemble into functional oligomers [101]. Conformational changes within these complexes generate the free energy required for outer membrane disruption [102]. The resulting oligomerized structures have been demonstrated to mediate membrane fusion by bringing the inner and outer membranes into close apposition [103–105].

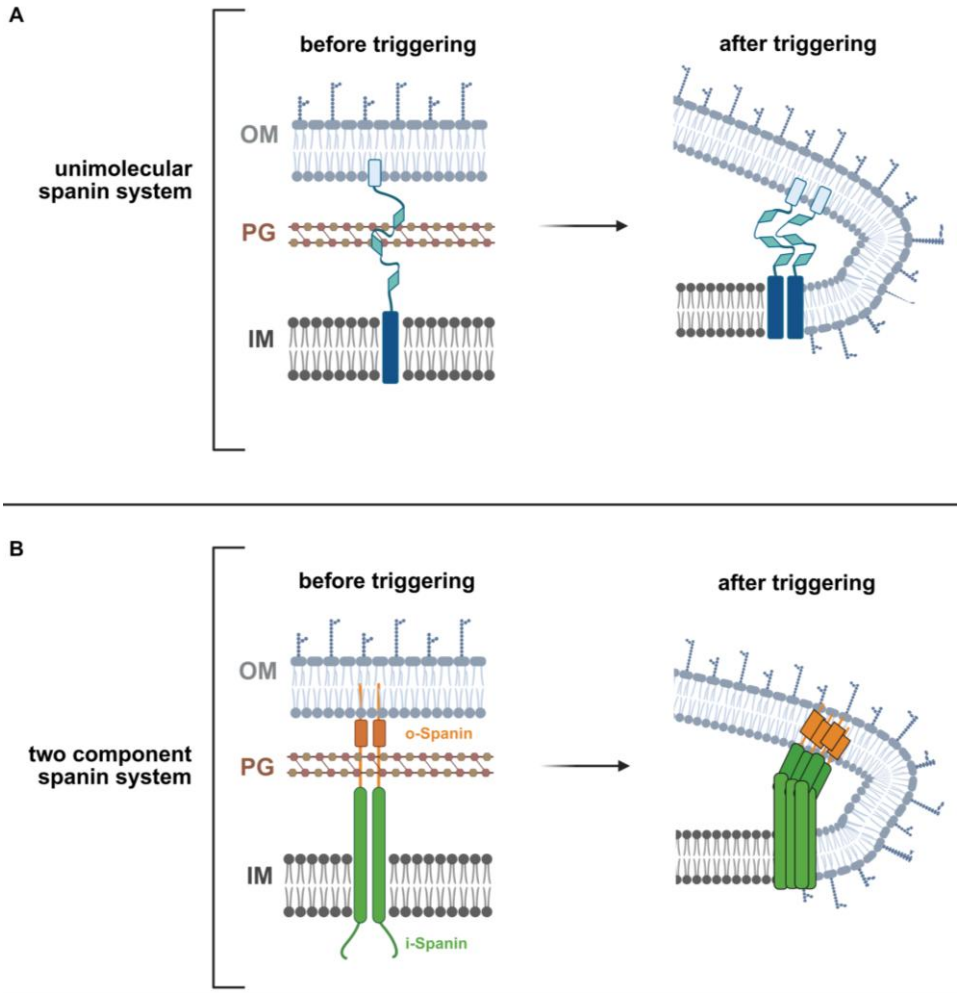

Figure 7: Spanin structure. Schematic illustration of the membrane topology of the two-component spanin prototype from phage λ and the unimolecular spanin (u-spanin) from phage T1. (**A**) The unimolecular spanin in T1 is composed of an N-terminus containing three fatty acyl chains (light blue) which attaches this part of the protein to the inner leaflet of the outer membrane. It is attached to the inner membrane via its C-terminal TMD (dark blue). The periplasmic domain of this u-spanin is predicted to be mainly extended beta sheets (turquoise diamonds) which connect the protein parts in the IM and OM through the PG meshwork. (**B**) In phage λ, the i-spanin is anchored in the inner membrane via an N-terminal transmembrane domain (green) and extends into the periplasm with a domain consisting of two α-helices connected by a linker region, likely forming a coiled-coil structure. The o-spanin is tethered to the inner leaflet of the outer membrane through three lipid modifications (orange square) and features a periplasmic segment (orange stick) that is predicted to be intrinsically disordered. The i- and o-spanins associate via their C-terminal regions to assemble into a spanin complex, bridging the IM and OM across the peptidoglycan layer [101,104,106].

Bacteriophage-encoded lysis proteins are currently being developed for various applications in medicine, the food industry, biotechnology, and pharmaceuticals [7,8,107–112]. For example, several research groups have demonstrated the potential for the use of spanins in the delivery of drugs and biochemicals into cells by means of membrane fusion [104].

1.4 Phage protein interactions with host cellular machinery

Phage-induced lysis represents a crucial and tightly regulated phase in the viral replication cycle. This event is preceded by an extensive remodelling of the host bacteriums metabolic and regulatory pathways. Such changes begin either immediately after infection or when the virus transitions from a lysogenic to a lytic life cycle. The genes involved in these early steps, commonly referred to as “early phage genes”, are among the first to be expressed. They typically encode for proteins that suppress the host's defence mechanisms, disrupt its gene regulation, and, quite often, arrest the bacterial cell cycle [113–115]. These combined actions establish a cellular environment favourable to efficient phage propagation.

In phage λ for example, expression of the Kil protein induces filamentation in host cells and inhibits cell division [116]. Interestingly, Kil also slows down the timing of lysis by about 30% [117]. This delay is thought to be due to Kil’s interaction with the bacterial protein FtsZ. By preventing FtsZ from polymerizing properly, Kil interferes with the formation of the Z-ring, which is essential for bacterial cytokinesis. Instead of forming a single, well-positioned division site, cells infected with λ exhibit a diffuse distribution of FtsZ or show misplaced rings. When Kil is overproduced, it appears to bind directly to FtsZ monomers, reducing their GTPase activity [117,118].

Another example of a phage encoded protein that interferes with the division machinery is the Gp04 protein from phage T4, which also targets FtsZ. Gp04 binds to FtsZ and disrupts Z-ring assembly, resulting in elongated, filamentous bacterial cells with multiple mispositioned Z-rings. This represents evidence of a breakdown in the spatial control of division [119,120].

Blocking bacterial division serves multiple strategic purposes for the phage. First, it helps to prevent the host from dividing too early, which could otherwise produce uninfected daughter cells [121]. Additionally, by halting division, the phage ensures that all of the host’s metabolic assets, including energy, nutrients, and biosynthetic capacity, remain devoted to viral replication [122,123]. Finally, inducing filamentous growth may provide more physical space for assembling and organizing large numbers of new phage particles [121,124].

1.5 Bacterial cell division

In order to better understand the importance of bacterial cell division for the life cycle of a phage, it is relevant to summarise the key factors of bacterial cell division at this point.

Bacterial cell division is orchestrated by the divisome, a highly sensitive and dynamic macromolecular complex made out of approximately a dozen proteins (**Fig. 8**) [125]. The included components are tightly regulated in both space and time throughout the cell cycle [126]. Their coordinated actions are essential for preserving cell wall integrity against the internal turgor pressure as well as ensuring that cytokinesis occurs only after DNA has been accurately replicated and segregated. At the heart of the divisome is FtsZ, a tubulin-like protein with GTPase activity. FtsZ is key to the early stages of divisome formation; it polymerizes to form the Z-ring, a structure that marks the future site of cell division [127]. This structure serves as a scaffold, guiding the assembly of additional division proteins and thereby establishing the cell's division plane [128–130].

To form the Z-ring, FtsZ assembles into polymers along the division plane using its polymerizing GTPase domain, which is one of its three conserved domains [131]. This domain, somewhat resembling tubulin, mediates filament formation through nucleotide binding. Upon assembly of FtsZ monomers into filaments, GTP hydrolysis leads to a conformational shift from a closed to an open state, resulting in a depolymerization and thereby contributing to the curved architecture of the Z-ring [132]. Recent studies have demonstrated that the FtsZ filament undergoes circumferential movement around the division plane, a process known as treadmilling [133]. While the individual monomers remain stationary within the filament, the movement occurs through a net addition of FtsZ subunits at one end of the filament [134].

FtsZ itself is not a membrane protein and cannot directly bind to the membrane. This interaction is mediated by membrane anchor proteins, such as FtsA and ZipA, which bind to the conserved C-terminal domain of FtsZ [135]. The absence of either anchor protein leads to defective cell division, ultimately resulting in lethality [136]. FtsA, a bacterial actin homologue, is a widely conserved membrane-binding protein that binds ATP with low affinity [137]. It localizes to the centre of the cell in an FtsZ-dependent manner and tethers FtsZ to the membrane through interactions with the C-terminus [138]. ZipA, present only in Gram-negative gammaproteobacteria, is an essential bitopic integral membrane protein, consisting of a large cytoplasmic domain connected to a single N-terminal transmembrane

domain by an extended linker [139]. ZipA shares a partially overlapping function with FtsA, since both proteins facilitate the binding of FtsZ to the membrane. However, ZipA interacts with the C-terminus of FtsZ through conserved residues distinct from those involved in binding FtsA [140]. The interaction of ZipA with FtsZ is also thought to contribute to the stabilisation of the Z-ring structure. Together, FtsZ, FtsA and ZipA form the proto-ring, which serves as the basis for subsequent protein recruitment [141]. The FtsE-FtsX complex attaches to this proto-ring and plays a crucial role in the recruitment of additional divisome components [142].

After a distinct delay, the second stage of divisome assembly, known as maturation, occurs just before constriction [143]. During this phase, a number of proteins, including FtsK, FtsQ, FtsL, FtsB, FtsW, PBP3, (FtsI)-PBP1B, and FtsN, are sequentially incorporated into the divisome [144]. FtsW and FtsI are important enzymes for peptidoglycan synthesis and are highly conserved in all bacterial species [145]. Their recruitment to the midcell depends on FtsK and the FtsQ-FtsL-FtsB complex, both of which require FtsA and ZipA for proper functioning [146]. Disruption of either of these proteins results in a lethal block to cell division. However, the division process can be restored in cells lacking FtsE or FtsX if they are cultured in a media with high osmotic pressure [145]. In addition to the essential divisome components, there are also non-essential proteins, such as the Zap proteins. Although their absence does not directly prevent cell division, these proteins, when functioning together, play an important role in ensuring the proper progression of normal cell division [147].

Once this stage of cell division is successfully completed, the constriction of the cell wall follows, which serves as the primary driving force behind cell division. The process of cell wall constriction is likely triggered by the arrival of the final divisome proteins that activate cytokinetic cell wall synthesis [148]. Given that the cell wall is crucial for maintaining cellular integrity, it is essential that this process proceeds without disruption. The cell wall is primarily composed of peptidoglycan (PG), which is a network of glycan strands interconnected by short peptide bridges [149,150]. In Gram-negative bacteria such as *E. coli*, the PG layer is typically a single, 3-6 nm thick layer. The enzymes responsible for synthesizing the glycan strands are glycosyltransferases (GTases), while transpeptidases (TPases) catalyse the crosslinking of peptide side chains. PG synthases are classified into three categories: bifunctional GTase/TPase enzymes (class A penicillin-binding proteins, PBPs), monofunctional TPases (class B PBPs) and

monofunctional GTases [151–153]. FtsW and FtsI serve as the primary GTase and TPase enzymes during bacterial cell division in *E.coli*, respectively [154,155]. The enzymes needed for PG synthesis require activation signals from previously recruited divisome proteins to initiate the constriction process [156,157]. It is also hypothesized that FtsZ contributes to the regulation of PG synthase activity through its treadmilling action [127]. However, PG synthesis is not solely regulated by the activation of FtsW and FtsI through intracellular divisome proteins. Constriction also necessitates activation signals from the OM lipoproteins LpoA and LpoB that act from outside the sacculus [158,159].

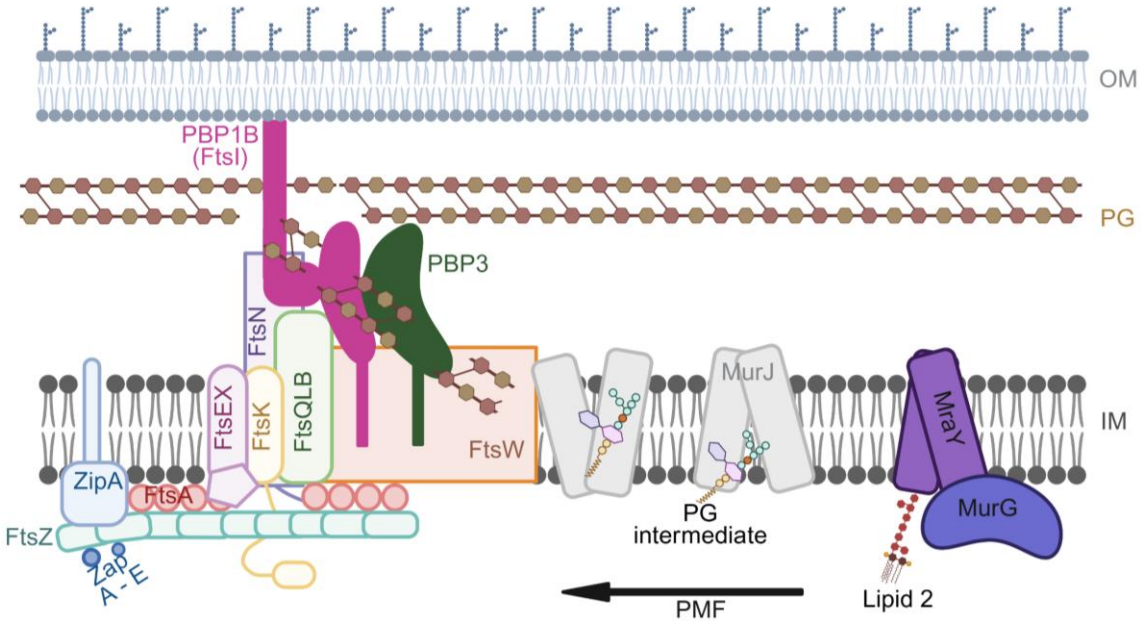

Figure 8: Bacterial divisiome during cell division. The schematic shows the essential members (with the exception of the Zap proteins) of the divisome multiprotein complexes for peptidoglycan synthesis during cell division in *E. coli* according to known localization patterns and interactions in the cell. The precise molecular architecture of the divisome and how they insert new material into the existing peptidoglycan layer are not yet known. The co-localization of MurJ with the divisome requires an active FtsW. MurJ requires the PMF in order to drive its conformational changes needed for its intended lipid transport mechanism - and by this the delivery of lipid II to the complex via FtsW. Lipid II is produced at the inner membrane by MraY and MurG. For simplicity, peptidoglycan hydrolases known to associate with each complex and to be required for their proper function, are not shown [146,160].

The process by which new material is incorporated into the existing PG has yet to be clarified. It is established that the PG precursor lipid II is synthesized at the inner leaflet of the cytoplasmic membrane and eventually translocated into the periplasmic space via the lipid II flippase FtsW [161,162]. FtsW has been shown to

interact with the two major PG synthases, PBP3 and PBP1B, and is essential for the recruitment of PBP3 to the divisome, likely acting in coordination with PBP1B [158,163]. Current evidence suggests that PBP1B and PBP3 constitute the principal enzymatic activities that drive septal peptidoglycan synthesis during cytokinesis. Moreover, it has been proposed that PBP3 plays a central role in regulating the spatial and temporal initiation of new PG synthesis, thereby ensuring precise coordination with the division machinery [158,164,165].

Several regulatory systems such as the Min system and the nucleoid occlusion system are essential for ensuring the correct spatial and temporal positioning of the divisome [166,167]. The Min system in *E. coli* consists of three proteins, MinC, MinD, and MinE, that work together to prevent the polymerization of FtsZ near the cell poles and thereby promoting accurate Z-ring assembly at midcell [168]. MinD is a deviant Walker-type ATPase that associates with the cytoplasmic membrane when bound to ATP [169]. Its membrane-associated partner, MinE, stimulates the hydrolysis of ATP, causing MinD to dissociate from the membrane [170]. Once MinD exchanges ADP for ATP, it can rebind to the membrane, initiating a new cycle. This dynamic interplay leads to the formation of oscillatory concentration gradients of Min proteins between the cell poles, eventually creating a bipolar gradient that restricts FtsZ assembly to the cell centre [171]. MinC, which interacts directly with two domains of FtsZ, acts as a strong inhibitor of FtsZ polymerization [172,173]. Through its association with MinD, MinC is also subject to an oscillatory movement and thereby contributing to the suppression of Z-ring formation at the poles, where MinD is predominantly localized [174]. In the absence of a functional Min system, cell division may still occur at midcell; however, division often takes place near the poles, leading to the formation of DNA-less minicells due to mispositioned septation [175].

The nucleoid occlusion system in *E. coli* involves the DNA-binding protein SlmA, which specifically associates with certain chromosomal regions that are located away from the replication terminus in the centre of the cell and closer to the replication origin (OriC) near the cell poles [176]. These binding interactions create a bipolar gradient of SlmA within the cell. In addition to its DNA-binding activity, SlmA interacts with FtsZ and thereby inhibiting its polymerization [177]. Through this dual functionality, SlmA prevents the assembly of the FtsZ ring in the vicinity of the nucleoid, especially in regions close to OriC, and thus contributes to the spatial regulation of cell division [178].

1.6 Model organism *Shewanella oneidensis* MR-1

Current research indicates that the genus *Shewanella* consists of over 70 species, with the majority inhabiting aquatic environments [179]. Several species have been identified as opportunistic pathogens in humans and aquatic animals [180]. *Shewanella* spp. are also known to adhere to diverse surfaces and form biofilms [181].

S. oneidensis MR-1 is a Gram-negative, facultatively aerobic gammaproteobacterium that serves as a key model organism in microbial research, because it is able to utilize a broad spectrum of terminal electron acceptors like manganese oxide under anaerobic conditions [182–186]. The genome of *S. oneidensis* MR-1 is made up of a 4.9 Mbp circular chromosome predicted to encode 4,318 proteins. Additionally, this bacterium carries a 161 kbp megaplasmid with 149 protein-coding genes [185,186]. *S. oneidensis* MR-1 exhibits a rod-shaped morphology, measuring 2-3 µm in length and 0.4-0.7 µm in diameter. It is motile, utilizing a single polar flagellum for swimming [187,188].

1.6.1 Phages of *S. oneidensis* MR-1

The genome of *S. oneidensis* MR-1 contains four prophages: λSo, MuSo1, MuSo2 [185,189,190] and CP4So [191]. Sequence analyses have shown that λSo and MuSo2 share homology with the *E. coli* phages λ (morphological group of siphoviruses) and Mu (morphological group of myoviruses), respectively. Both λSo and MuSo2 are capable of forming intact, infectious phage particles. In contrast, MuSo1 does not produce active particles, as shown by the absence of plaque formation, even when λSo and MuSo2 are deleted from the bacterial genome [189]. The fourth prophage, CP4So, is a P4-like cryptic element that can only be induced under specific conditions [191].

Prophages are known to carry genes that can provide beneficial traits to their bacterial hosts, such as enhanced resistance to antibiotics and environmental stressors [192–194]. This phenomenon is also observed in *S. oneidensis* MR-1, where the prophages λSo and MuSo2 play critical roles in biofilm development. These prophages significantly influence proper biofilm formation by mediating processes such as cell lysis, which may be necessary for the release of extracellular DNA and other factors involved in cell-cell and cell-surface interactions. While Mu-like phages primarily affect the early stages of biofilm development, λSo is the principal contributor to the formation of complex, three-

dimensional biofilm structures [189,195,196]. λSo is strongly induced in cells attaching to a surface, which is regulated by intracellular iron levels [189,195,197]. Elevated intracellular iron triggers the SOS response via RecA, which subsequently induces the lytic cycle of λSo.

The prophage λSo in *S. oneidensis* MR-1 has a genome size of 51 kbp and encodes 78 annotated genes [185,186]. It is integrated into a genomic region flanked by two genes of unknown function, which are conserved among closely related *Shewanella* species.

Although the genomes of *S. oneidensis* and its prophage λSo have been sequenced and annotated, and despite the growing volume of available phage genomic data, 23 genes within the λSo genome still encode proteins of unknown function [11].

1.7 Aim of this study

The aim of this study was to characterise selected gene products of the prophage λSo in greater detail, with a particular focus on their effects on the host cell following infection or prophage induction.

Special emphasis was placed on λSo-mediated cell lysis, in order to gain deeper insights at the protein level into this largely unexplored process.

2 Results

2.1 Analysis of the *Shewanella* prophage λSo

Research over the past few decades has revealed that phage genomes frequently contain gene clusters encoding rather small proteins, many of which lack identifiable structural homologues in existing databases [114]. These proteins are typically expressed immediately after infection or the initiation of the lytic cycle and are critical for the reprogramming of the host cell

One of the primary objectives of this study was to characterise the genome of phage λSo, with a particular focus on genes encoding proteins of unknown function. Prior research had identified two distinct gene clusters whose products are essential for the fitness of λSo[198]. The proteins encoded by these clusters are examined in greater detail in the following sections.

2.1.1 Characterization of the λSo lysis cluster

Previous studies by Binnenkade et al. identified a gene cluster spanning *SO_2966* to *SO_2974* as playing a key role in phage-mediated cell lysis in λSo. This cluster is made up of genes ranging from 162 to 2215 bp, encoding proteins between 53 and 737 amino acids in length (**Tbl. 1, Fig. 9A**). It has been demonstrated that a deletion of this gene cluster does not prevent the formation of phage particles; however, these particles are no longer capable of inducing host cell lysis [198].

Table 1: Lysis gene cluster

gene number	basepairs	amino acids	annotation
SO_2966	162	53	protein of unknown function
SO_2968	2215	737	Lambda phage terminase A
SO_2969	330	109	putative HNH nuclease YajD
SO_2970	360	119	protein of unknown function
SO_2971	270	89	putative holin S^{So}
SO_2972	628	208	protein of unknown function
SO_2973	513	170	putative endolysin R^{So}
SO_2974	264	87	pyridoxal phosphate dependent enzyme

Primary sequence based homology analyses using BLAST suggest that two of these genes, *SO_2971* and *SO_2973*, may encode a putative holin and endolysin, respectively. However, these functional assignments had not been proven experimentally thus far.

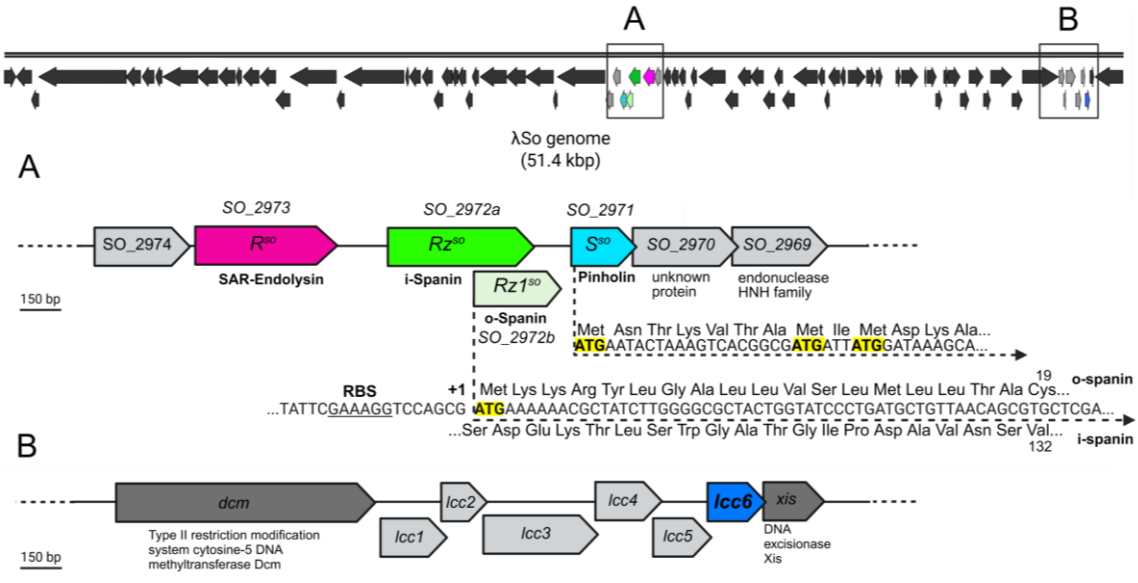

Figure 9: Genetic organization of *Shewanella* prophage λSo lysis genes. The upper panel displays the fully annotated genome of λSo. The predicted open-reading frames within the phage genome are represented as arrows indicating their transcriptional direction. The boxes labelled A and B show the position of the gene clusters involved in phage-induced cell lysis, which are displayed in the middle and lower panels in more detail. The deduced gene products are colour-coded according to their predicted function. (**A**) Genetic organization of the predicted lysis cluster (*SO_2971* to *SO_2973*). Genes encoding proteins directly involved in cell lysis are indicated as coloured arrows. The predicted translation start of the spanin component $Rz1^{So}$ within the +1 frame of the gene encoding spanin component Rz^{So} is highlighted in yellow; the upstream ribosome binding site is also indicated. The three alternative start sites of the pinholin-encoding gene s^{So} are accordingly highlighted in yellow. Bioinformatic predictions are based on NCBI BLASTP (National Library of Medicine) and PHAST analyses. (**B**) Gene organization of so-called λSo cluster C [*lcc1* (*SO_4794*) to *lcc6* (*SO_4975*)]. Predicted genes are indicated as arrows. *lcc6*, which is part of the lysis machinery, is coloured in blue, the other lcc genes are coloured in light-grey, and the neighbouring genes are shown in dark-grey. *dcm* encodes a DNA (cytosine-5-)-methyltransferase, and *xis* encodes the phage DNA excisionase Xis. Bioinformatic predictions are based on NCBI BLASTP (National Library of Medicine).

The homology analyses suggest that the gene product of *SO_2971* functions analogously to a pinholin, as the predicted protein possesses two transmembrane domains and a putative N-in/C-in topology (**Fig. S1**). Notably, the open reading frame contains two alternative translational start sites located six and eight amino acids downstream of the annotated start codon (**Fig. 9A**). Similar to the mechanism described for the *E. coli* phage

ϕ21 [84], these alternative start sites could give rise to distinct holin isoforms, potentially constituting a holin/antiholin regulatory system. Taken together, these features support the hypothesis that the *SO_2971* gene product serves as the key effector in initiating host cell lysis via depolarization of the cytoplasmic membrane. Accordingly, it will hereafter be referred to as λSo holin S (S^{So}).

The protein encoded by *SO_2973* represents a strong candidate for the putative endolysin, as structural predictions indicate the presence of an N-terminal SEC signal peptide, although a clearly defined proteolytic cleavage site following the signal sequence is missing (**Fig. S1**). This suggests that the protein likely belongs to the class of SAR endolysins, which are translocated into the periplasm but remain anchored to the cytoplasmic membrane via their uncleaved signal peptide. Release and activation of these endolysins is typically triggered by membrane depolarization, facilitated by pinholin-mediated pore formation. Accordingly, this protein will be referred to as λSo endolysin R (R^{So}).

Structure-based homology searches using the HHPred tool in the HAMMER database, which is focusing on predicted 3D structures rather than primary amino acid sequences, suggested that *SO_2972* may encode an additional key lysis-related protein: a putative spanin. Spanins are known to facilitate the final step of host cell lysis by disrupting the outer membrane, complementing the roles of holins and endolysins. The predicted structure of the *SO_2972* gene product is consistent with the cytoplasmic and periplasmic component of a canonical two-component spanin system [100,101]. Specifically, the protein is predicted to contain an N-terminal transmembrane domain (amino acids 9-31), followed by a long α-helical region (amino acids 32-110) (**Fig. 9B**). Further genetic analysis revealed additional features characteristic of known two-component spanin systems: an alternative open reading frame, designated *SO_2972b*, initiates within *SO_2972* in the +1 reading frame starting at nucleotide position 340 (**Fig. 9B**). A putative Shine-Dalgarno sequence (GAAAGG) is located 7 bp upstream of the predicted start codon. The *SO_2972b* ORF extends into the intergenic region between *SO_2972* and *SO_2971* and encodes a 95-amino-acid protein that contains a lipoprotein signal peptide. Using the SignalP-Tool, this peptide is predicted to be cleaved between residues 18 and 19, exposing an N-terminal cysteine required for lipid modification and anchoring to the outer membrane (**Fig. S1**). Consequently, these proteins are designated as λSo Spanin Rz and Rz1 (Rz^{So}, $Rz1^{So}$).

To gain deeper insight into the roles of these proteins during host cell lysis, bacterial strains were engineered with individual deletions of the genes encoding each respective protein. These experiments were conducted using a *S. oneidensis* background strain in which the two endogenous prophages, MuSo1 and MuSo2, had been removed. This was done to eliminate potential disruptive effects and ensure that any observed phenotypes could be attributed specifically to λSo. For clarity and simplicity, this strain will hereafter be referred to as the wild type (WT).

The engineered strains were subsequently characterised in greater detail using fluorescence microscopy, enabling a more precise assessment of phage infectivity, lytic activity, and potential morphological changes associated with the deletion of individual genes. For this experimental setup, exponentially growing cultures of *S. oneidensis* MR-1 harbouring the respective genetically modified lysogenic λSo prophages were treated with mitomycin C (MMC) to induce the lytic cycle. Mitomycin C is used to induce the lytic cycle in temperate phages (such as phage λ) because it specifically triggers DNA damage in the host bacterium. In *E. coli*, this process triggers the SOS response, which in turn activates RecA. RecA is responsible for cleaving the repressor protein CI of the λ phage. In the absence of the CI repressor, the phage DNA is activated for replication and the lytic cycle is triggered [199,200].

Following induction, cells were monitored using time-lapse phase-contrast microscopy to observe the dynamics of lysis. To verify phage protein expression and confirm phage particle assembly, the experiment was repeated using a *S. oneidensis* MR-1 background strain in which the gene product of *SO_2960*, which encodes a head-tail joining protein, was fused to the fluorescent protein Venus (**Fig. S2B, S2C**). Importantly, this fusion does not impair phage infectivity (**Fig. S2A**), allowing direct visualization of phage assembly processes in real time without functional disruption.

Following induction of λSo in wild-type cells, a pronounced elongation phase was observed, culminating in complete cell lysis approximately 180 minutes post-induction. In contrast, cells carrying the λSo variant with a deletion of the putative holin gene (Δs^{So}) exhibited no lysis (**Fig. 10B**). In these cells, the expression of proteins that are part of the phage particles was confirmed via fluorescence microscopy using the strain in which a structural protein was fused to a fluorophore (**Fig. 10A**). Despite this, no plaque-forming units were detected in the culture supernatant, although a certain part of the λSo genome

remained detectable within the cells via PCR (**Fig. 11A**). This suggests that λSo could be present in the cells without being lytically active. Complementation through ectopic expression of the deleted gene from a plasmid under the control of the putative late promotor of the λSo lysis cluster restored normal lysis (**Fig. S3, Fig. 7**).

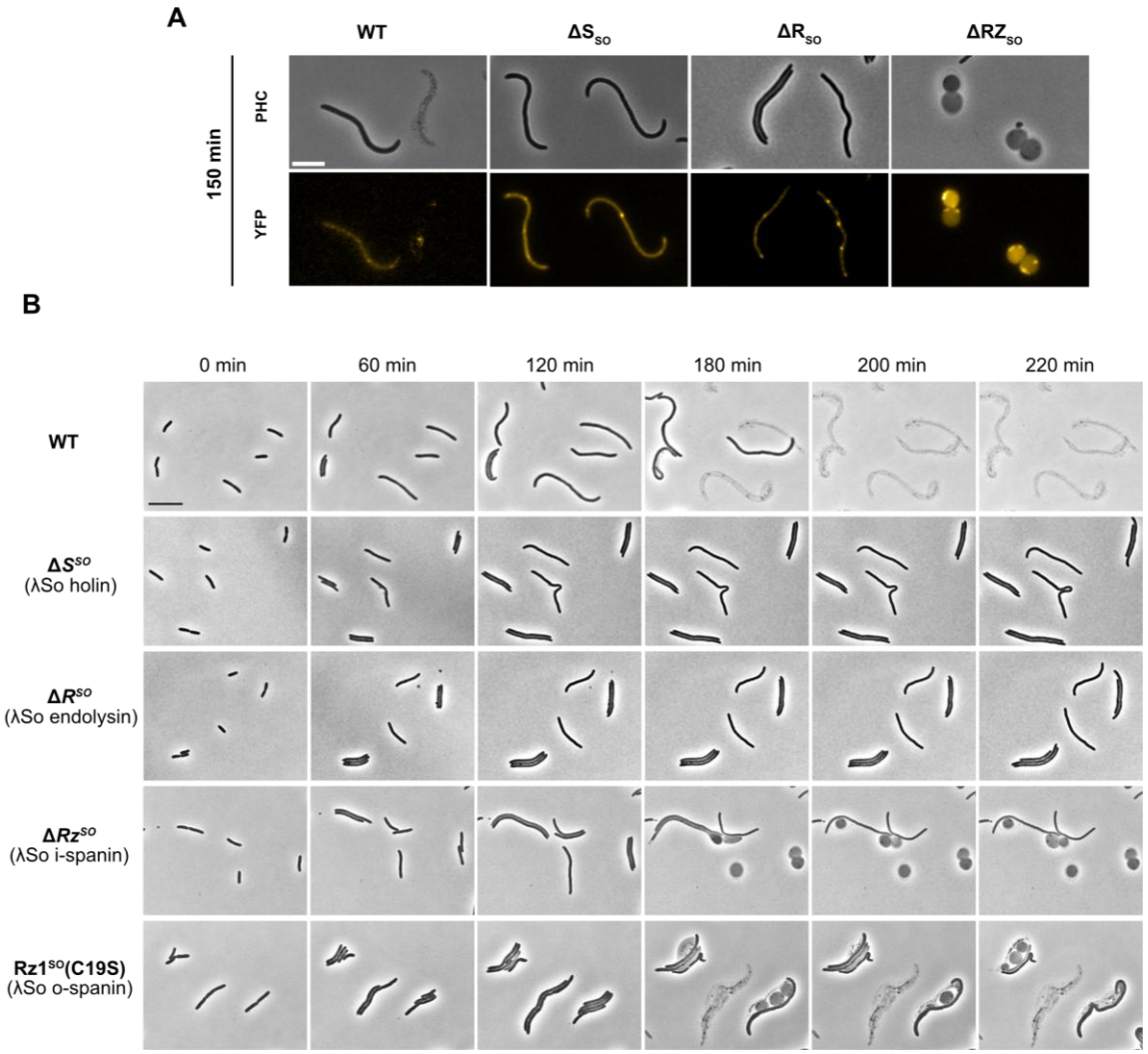

Figure 10: λSo-induced lysis of *S. oneidensis* MR-1 requires a pinholin, SAR endolysin and a spanin complex. (**A**) Microscopic images of *S. oneidensis SO_2960*-GGS-Venus cells (a strain, in which a head-tail-joining protein of λSo was fused to the fluorophore Venus) that bears deletions in the genes encoding for the pinholin (S^{So}), SAR endolysin (R^{So}) or i-spanin (Rz^{So}) as indicated. The time points subsequent to λSo induction by addition of mitomycin C (10 µg/mL) is 150 min. The images were taken in phase contrast and in the fluorescence channel of the fluorochrome YFP. The scale bar represents 5 µm. The liquid cultures were supplemented with 10 mM $MgCl_2$. (**B**) Micrographs display a time-lapse series of *S. oneidensis* strains in which the genes encoding for the pinholin (S^{So}), SAR endolysin (R^{So}), i-spanin (Rz^{So}) or o-spanin ($Rz1^{So}$) were deleted from the λSo genome as indicated. The time points subsequent to λSo induction by addition of mitomycin C (10 µg/mL) are indicated above. The scale bar represents 5 µm. The corresponding complementation strains are shown in Fig. S3.

To investigate the subcellular localisation of the holin protein, a recombinant construct for ectopic expression, in which the holin was fused to the green fluorescent protein (GFP), was constructed using a plasmid under the control of an inducible arabinose promoter. This plasmid was introduced into a background strain in which the gene for the holin was deleted. Successful expression of the fusion protein was confirmed by immunoblot analysis (**Fig. S4B**). Fluorescence microscopy of the corresponding cells revealed distinct foci, predominantly arranged in large clusters at the periphery of the cells (**Fig. S4A**). This spatial distribution strongly suggests that the holin localises to the cytoplasmic membrane. However, multiple bands were observed in the corresponding western blot, which may indicate the presence of degradation products of the fusion protein. These findings suggest that the stability of the GFP-holin fusion is limited under the conditions tested. Moreover, subsequent to the fusion of Holin and GFP, the phage particles proved to be incapable of accurate host cell lysis. Consequently, the outcomes of this experiment should be interpreted with caution and may be in need of optimisation.

To further investigate membrane integrity during phage induction, a membrane depolarization assay was conducted using $DiBAC_4(3)$ staining. Cells were stained with 1 mg/mL (wt/vol) $DiBAC_4(3)$ at a defined time point following λSo induction, and fluorescence intensity was measured using a TECAN plate reader. Four hours post-induction, a small but statistically significant reduction in depolarization was observed in Δs^{So} cells compared to the wild type (**Fig. 11B, Fig. S6**). These results provide further evidence supporting *SO_2971* as the functional pinholin in the λSo lysis system.

Cells carrying a deletion of the *SO_2973* gene, encoding the putative endolysin R^{So}, exhibited a comparable phenotype under microscopic observation: following phage induction, they underwent elongation but did not lyse, despite clear evidence of phage protein production (**Fig. 11**). Consistent with this, no plaque-forming units were detected in the culture supernatant (**Fig. 11A**). The lytic defect could be rescued by ectopic expression of the gene product of *SO_2973* from a plasmid, confirming the functional role of the encoded protein (**Fig. S3**). However, these cells showed a significant increase in membrane depolarisation. This observation suggests that in the absence of the putative endolysin, depolarization, which is presumably initiated by holin activity, can proceed, but lysis is blocked, allowing the accumulation of depolarized cells. Thus, the signal persists longer in the population than in wild-type cells, where it would normally be rapidly lost upon cell lysis.

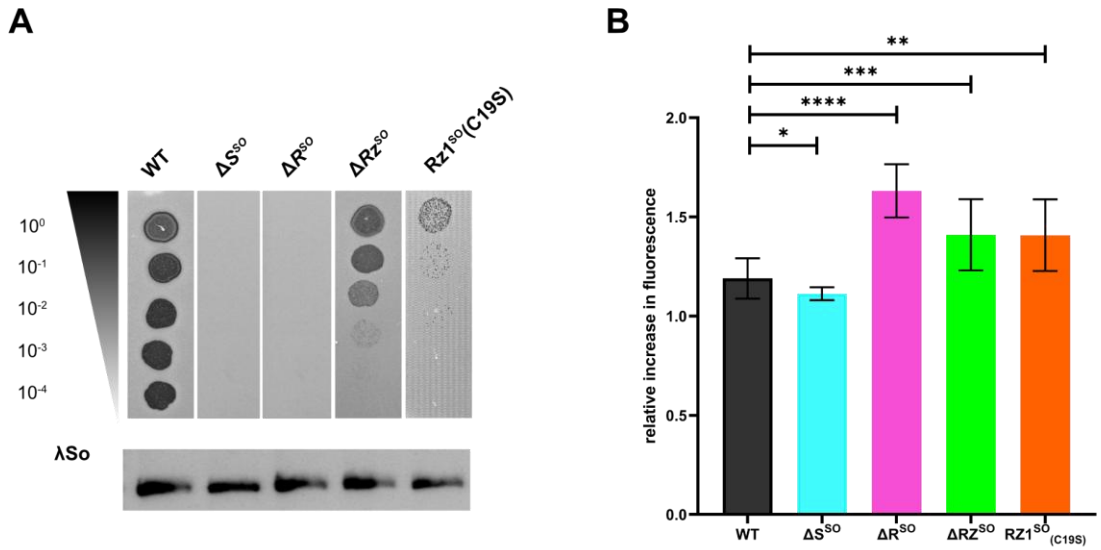

Figure 11: λSo-induced lysis of *S. oneidensis* MR-1 requires a pinholin, SAR endolysin and a spanin complex. (**A**) Lysis profiles of λSo mutants by spot test analysis. Upper panel: phage lysates of λSo mutants were spotted in different dilutions onto a bacterial lawn containing cells of an exponentially grown *S. oneidensis* host culture. Lower panel: as a control, PCR was performed with the phage lysate to determine the presence of λSo in the respective lysates. (**B**) Membrane depolarization assay on λSo mutants using DiBAC4(3). The cells were grown to exponential phase prior to λSo induction by mitomycin C phase and stained with $DiBAC_4(3)$ to visualize depolarization after 4 hours. Statistical significance was determined using a two-way ANOVA (analysis of variance) and is indicated by the P value. NS, not significant, *P value = P ≤ 0.05, **P value ≤ 0.01, ***P value ≤ 0.001, and ****P-value ≤ 0.0001.

Fluorescence microscopy images revealed relatively evenly distributed foci along the periphery of the cells (**Fig. S4A**), suggesting a uniform localisation of the *SO_2973*-encoded proteins within the cytoplasmic membrane. However, the correspondingly modified phage particles were unable to lyse the cells in the expected manner. This must be considered when evaluating the results. To assess the function of the putative spanin components, a deletion was performed targeting the gene *SO_2972a*, which encodes the predicted i-spanin Rz^{So} (**Fig. 9A**). This deletion also disrupted the overlapping gene *SO_2972b*. To specifically inactivate *SO_2972b* without affecting the Rz^{So} protein, a GTG-to-GTC substitution was introduced at position V132 in *SO_2972a*, resulting in a Cys19Ser change in *SO_2972b* that eliminates the cysteine required for lipid anchoring (**Fig. 9, S2**). Both resulting mutant strains displayed a striking phenotype in time-lapse microscopy: cells elongated normally after phage induction but, instead of undergoing lysis, a subset of both mutants rounded up into spherical forms (**Fig. 10**). When grown in planktonic shaking cultures, plaque-forming units were detected in the supernatant, but at levels three to four orders of magnitude lower than those of the wild type. Membrane depolarization

measurements using $DiBAC_4(3)$ and TECAN analysis revealed a signal comparable to that observed in the *SO_2973* deletion strain, indicating that depolarization occurs, but lysis is impaired. Fluorescence microscopy of the *SO_2972a*-GFP fusion protein revealed the presence of discrete, clustered foci localized along the cell periphery. In contrast, in a strain expressing a recombinant variant bearing the Cys19Ser mutation and thereby abolishing the function of the *SO_2972b* protein, a markedly altered distribution pattern was observed, characterised by uniform, non-clustered foci dispersed along the periphery of the cell.

Since the lysis proteins of phages infecting Gram-negative bacteria are often functionally interchangeable despite differences in their structures [107,201], the identified lysis proteins of λSo were ectopically expressed from a plasmid in *E. coli* MG1655. As demonstrated in Figure 13, the λSo lysis proteins were also capable of inducing cell lysis in *E. coli*. However, it should be noted that the duration of this process was significantly longer in this particular setup.

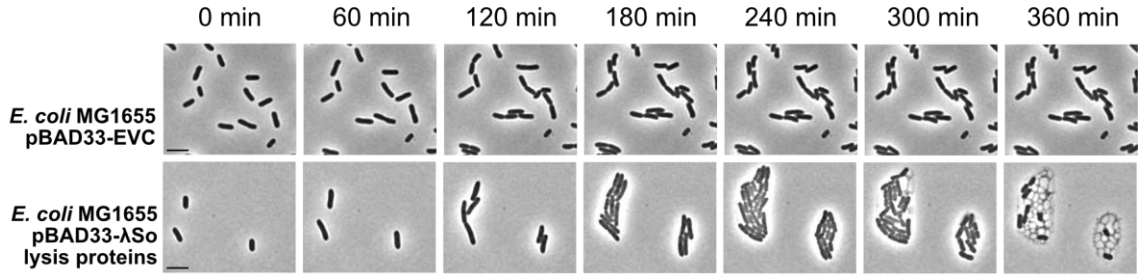

Figure 12: Proteins related to λSo cell lysis also cause cell lysis in *E. coli*. Time-lapse series of *E. coli* MG1655 in which the λSo pinholin, SAR-Endolysin, i-spanin and o-spanin were ectopically produced using the vector pBAD33. Cell cultures were supplemented with 0.2% arabinose to induce protein expression. The beginning of the time-lapse series (0 minutes) was defined as the time point at which arabinose was added to the respective cell culture. EVC resembles the empty vector control. The scale bar represents 5 µm.

2.1.1.1 Further characterization of the holin protein

To gain deeper insights into the mechanism of phage-mediated lysis in λSo, the gene *SO_2971* was subjected to detailed *in silico* analysis. This revealed the presence of two alternative translational start sites located six and eight amino acids downstream of the annotated start codon. These alternative start sites may give rise to shorter protein variants, potentially functioning as anti-holin.

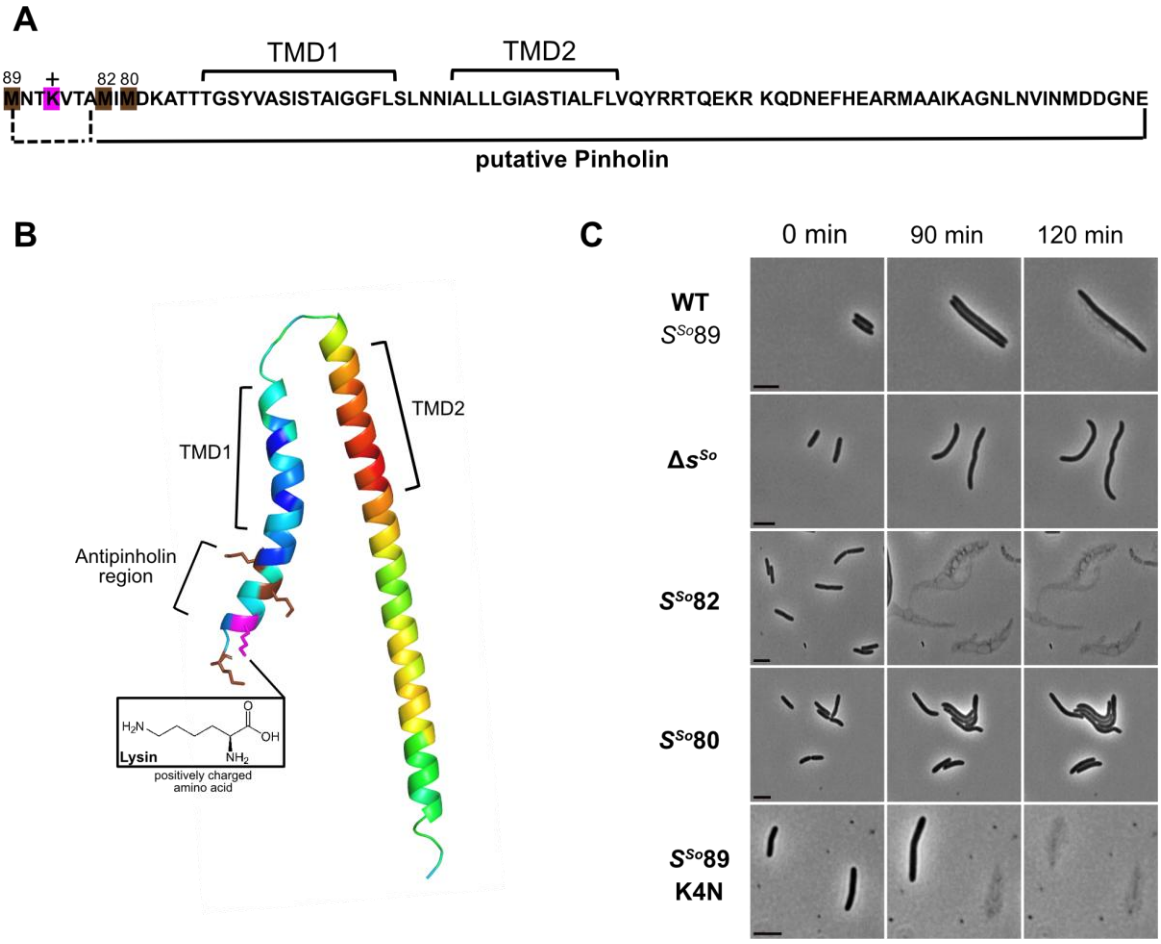

Figure 13: Alternative translational start sites encode a potential anti-pinholin. (**A**) Primary structure of the putative pinholin with corresponding predicted domains indicated. (**B**) 3D structures of the proteins of interest (λSo Holin) were predicted using Alphafold2 trough DeepMind´s Colab. The structures were visualised with Pymol. Certain protein domains are indicated using brackets. The structures are colour-coded by B-factor values. The respective amino acids that were modified are colour-coded as shown in the primary structure. (**C**) Micrographs display a time-lapse series of *S. oneidensis* strains in which the gene encoding for the pinholin (s^{So}) was deleted from the λSo genomes or modified as indicated. Cells were captured over a period of 120 minutes after being treated with 10 µg/ml MMC. The scale bar represents 2 µm.

To test this hypothesis, a series of targeted genetic modifications were introduced into *SO_2971*, including deletions, truncations, and point mutations. Specifically, the first eight codons ($S^{So}82$) and the first ten codons ($S^{So}80$) were removed to evaluate whether these N-terminal regions influence the timing of cell lysis, as assessed by fluorescence microscopy (**Fig 13A**). Additionally, a base substitution (K4N) was introduced, replacing the positively charged lysine at position 4 with asparagine, a neutral but polar amino acid (**Fig. 13A**). This mutation was designed to probe the role of the N-terminal charge in modulating holin function.

Following induction of the phage with MMC, wild-type cells exhibited pronounced filamentation, ending in cell lysis after approximately 120 minutes. As previously described, the Δs^{So} mutant showed comparable filamentation but failed to undergo lysis. The $S^{So}80$ strain, in which the gene was truncated at the second alternative start codon, displayed a similar non-lytic phenotype. In contrast, the $S^{So}82$ mutant, which carried a truncation at the first alternative start codon of the gene, underwent significantly earlier lysis with cell rupture beginning around 90 minutes post-induction. Similarly, the point mutant $S^{So}89$ (K4N), in which lysine at position 4 was substituted with asparagine, also exhibited premature lysis, resembling the phenotype of the $S^{So}82$ strain (**Fig. 13B**).

2.1.1.2 Further characterization of the spanin system

As previously noted, infectious plaque-forming phage particles were detected in the Δrz^{So} deletion strain, although at levels three to four orders of magnitude lower than those observed for the wild-type phage. Prior studies have demonstrated that spanins play a particularly critical role in phage egress under conditions that stabilize the outer membrane, such as in the presence of Mg^{2+} ions [202]. To investigate whether the spanin candidates identified in this study exhibit a similar dependency, both microscopic analyses and plaque assays were repeated for the Δrz^{So} strain under addition of 10 mM $MgCl_2$.

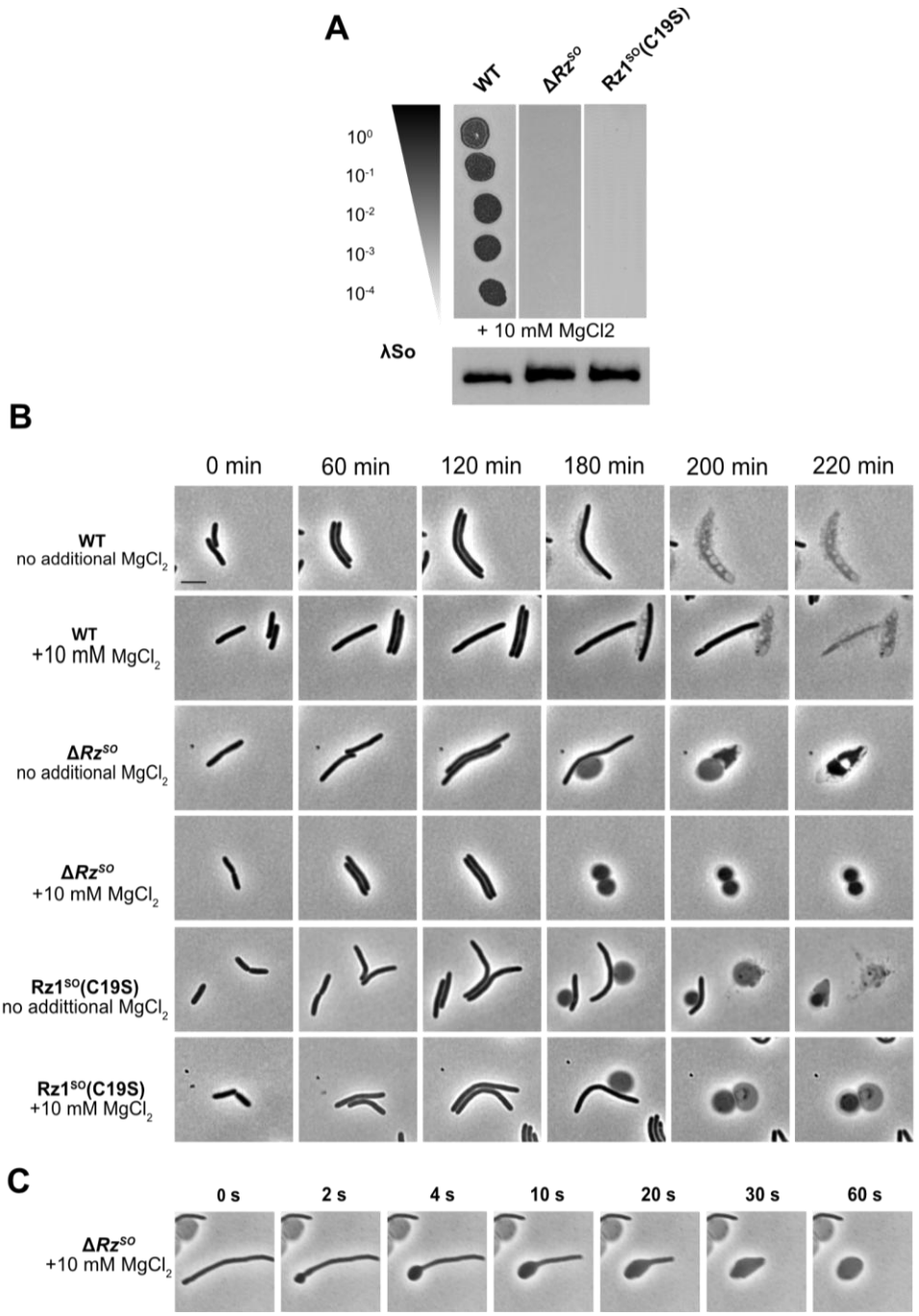

Figure 14: The spherical formation of the cells is due to the absence of *SO_2972* and is stabilized by the addition of $MgCl_2$. (**A**) Lysis profiles of λSo mutants after addition of divalent cations by spot test analysis. Upper panel: phage lysates of λSo mutants were spotted in different dilutions onto a bacterial lawn containing cells of an exponentially grown *S. oneidensis* host culture. Lower panel: as a control, PCR was performed with the phage lysate to determine the presence of λSo in the respective lysates. (**B**) Displayed are micrographs of a time-lapse series with *S. oneidensis* wild type and spanin-lacking (Δ*rz*^{So}; Rz1^{So} C19S) cells treated with and without 10 mM MgCl2 subsequent to phage induction using mitomycin C (10 µg/mL). The time points are indicated above; time point zero is defined as the start of induction. The scale bar represents 2 µm. (**C**) Morphology changes of cells lacking a spanin system after phage induction. Micrographs were taken after the onset of sphere formation. Full conversion into a sphere takes about 60 seconds. The scale bar represents 2 µm.

The membrane-stabilizing conditions induced by the presence of divalent cations prevented the detection of infectious phage particles in the supernatant of planktonic shaking cultures, as no plaques were formed, despite the presence of λSo DNA confirmed by PCR (**Fig. 14A**). Thus, the impaired cell lysis of the mutant phage is only observable under conditions lacking additional Mg^{2+}. Microscopic analyses further revealed that the spheres formed by Rz^{So}/$Rz1^{So}$ mutants were significantly more stable in the presence of Mg^{2+} and remained intact even 220 minutes post-induction with MMC (**Fig. 14B**). Moreover, the membrane-stabilizing conditions revealed that these morphological changes typically initiated at one pole of the elongated cell and progressed along its length within approximately one minute (**Fig. 14C**).

To further characterise the identified spanins, an *in silico* structural analysis was performed using AlphaFold2 and PyMOL. This analysis suggested that Rz^{So} and $Rz1^{So}$ most likely form dimers, which may assemble into a dimer of dimers (**Fig. 15A, Fig. S1, Tbl. S3**). The proteins appear to interact via their C-termini, while their N-termini are anchored in the inner membrane (Rz^{So}) or outer membrane ($Rz1^{So}$), respectively. The interaction between the dimers of the two spanins is predicted to induce a conformational change, potentially resulting in the "folding" of the Rz^{So} dimers, a process that could facilitate membrane fusion. Using PyMOL, a putative interaction interface between the proteins was identified. To experimentally validate the *in silico* predictions, recombinant protein versions were designed in which selected amino acid residues within the proposed interaction interface were substituted in order to disrupt the interaction and to assess the impact on the lysis phenotype (**Tbl. 2**, **Fig. S8**). The mutant phage's carrying the genes for these proteins were subsequently employed in plaque assays.

Table 2: Amino acid substitutions in Rz^{So} and $Rz1^{So}$

Rz^{So}	**$Rz1^{So}$**
T122S	C47Y
N129D	Y52F
C139R	S54N
N141D	K55R
C150R	K56R
	N57G
	C74S

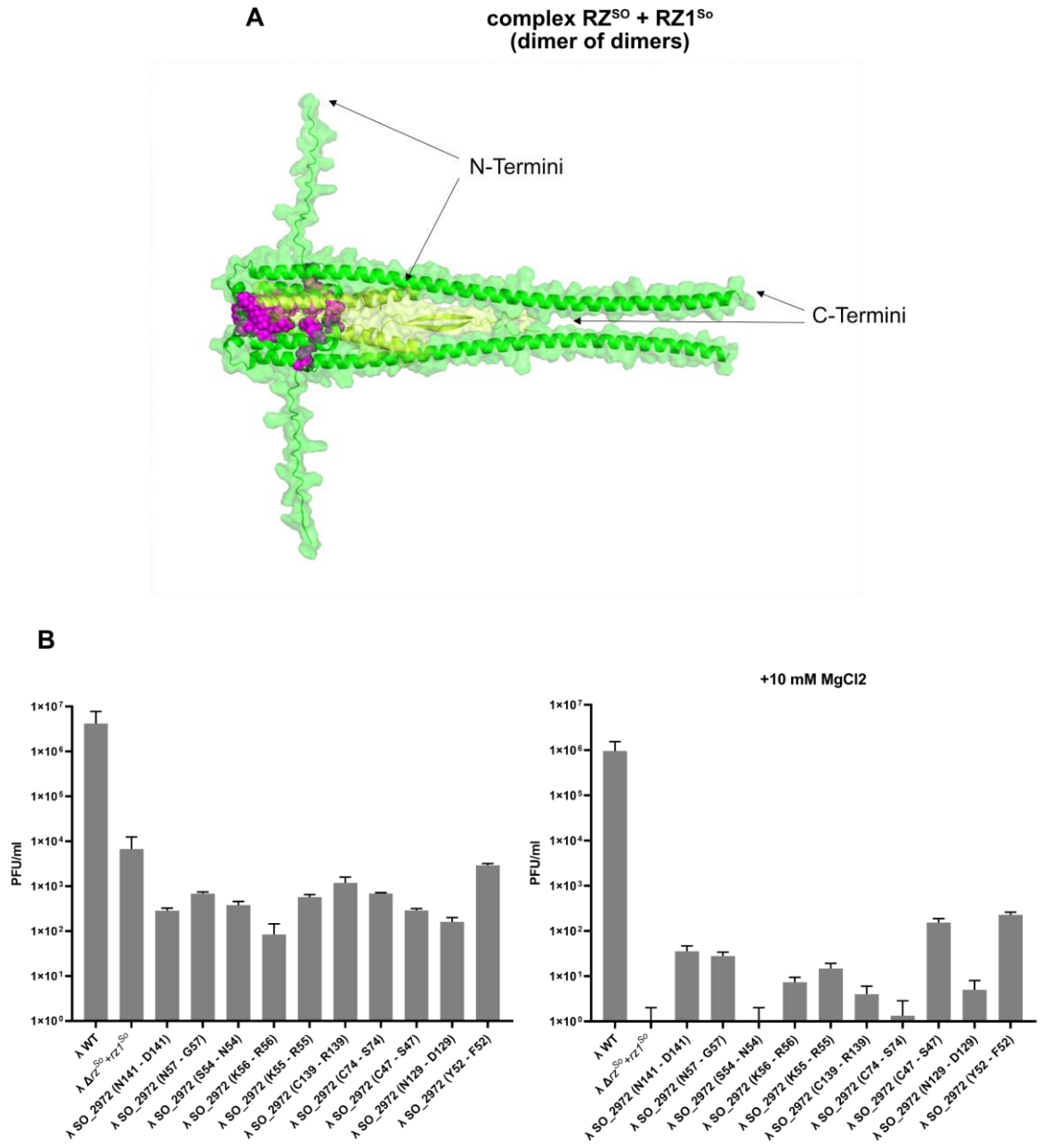

Figure 15: Structures of the λSo spanin complex: a dimer of dimers. (**A**) 3D structures of the protein complex of interest (λSo i-Spanin; λSo o-Spanin) were predicted using Alphafold2 trough DeepMind´s Colab. The structures were visualised with Pymol. N- and C-termini are indicated using arrows. The structures are colour-coded by respective protein (i-spanin green, o-spanin yellow). The hypothesised interaction surface of the i- and o-spanin proteins is shown in magenta. (**B**) Lysis profiles of λSo mutants by spot test analysis. Phage lysates of λSo mutants were spotted in different dilutions onto a bacterial lawn containing cells of an exponentially grown *S. oneidensis* host culture. Quantification of Lcc mutant plaque formation on *S. oneidensis* host cells. To determine the phage titer, the plaques were counted, and PFU/mL was calculated. Error bars represent the standard error of three independent experiments.

As shown in Figure 15B, the mutant phage's exhibited plaque forming units (PFU) levels comparable to those of the Δ*rz*^{So} phage under conditions lacking divalent cation supplementation. Notably, phages carrying the substitutions N141D and N129D in Rz^{So},

and K56R in $Rz1^{So}$ significantly reduced plaque formation compared to the control strain. Under membrane-stabilizing conditions, no plaques were detected for phage's harbouring proteins with substitutions at S54 and C74 in $Rz1^{So}$, a phenotype consistent with that of the Δrz^{So} phage. In contrast, all other introduced substitutions resulted in improved lysis relative to the control strain. The most pronounced increase in PFU under membrane-stabilizing conditions was observed for phage's carrying the C47Y and Y52F substitutions in $Rz1^{So}$ (**Fig. 15B)**.

2.1.1.3 Identification of a novel lysis component

To elucidate the effects of λSo on the host cell during infection or upon induction of the lytic cycle, RNA-seq analysis was performed on *Shewanella oneidensis* wild type strains lysogenized with λSo, as well as on a mutant strain in which the λSo gene cluster had been deleted ($\Delta\lambda$)[198]. The samples used for this approach were collected under standard growth conditions following induction of the SOS response via MMC treatment. The analysis revealed that, upon MMC addition, a gene cluster located near the end of the prophage genome was markedly upregulated. These genes ranked among the most highly expressed following induction. Notably, this cluster is situated upstream of the *int* and *xis* genes, which encode the integrase and excisionase enzymes, respectively.

This gene cluster, designated Lambda cluster C (Lcc) based on its genomic position downstream of two clusters named Cluster A and B, is made up of six genes (*SO_4794*, *SO_3007* - *SO_3010*, and *SO_4795*) (**Fig. 9B**). These genes range in size from 126 to 414 bp and encode proteins between 41 and 137 amino acids in length (**Tbl. 3**). The Lcc proteins lack any clear homologies to known domains, except Lcc4 and Lcc6, which are predicted to harbour a transmembrane domain (**Fig. S1**). Previous studies demonstrated that the deletion of the Lcc gene cluster leads to a pronounced reduction in the number of plaque-forming units (PFU), suggesting that, while the cluster is not strictly essential for phage viability, it is crucial for efficient and productive phage propagation.

Table 3: λ cluster C

gene number	basepairs	amino acids	annotation
SO_4794, lcc1	249	82	protein of unknown function
SO_3007, lcc2	126	41	protein of unknown function
SO_3008, lcc3	414	137	protein of unknown function
SO_3009, lcc4	276	91	protein of unknown function
SO_3010, lcc5	201	66	protein of unknown function
SO_4795, lcc6	198	65	protein of unknown function

To shed light on the role of the Lcc proteins in host cell takeover following infection or induction of the lytic cycle, individual gene deletion strains were generated and subjected to further functional analyses. A single deletion of *lcc1* could so far not be obtained. To assess the impact of each deletion on λSo infectivity, plaque assays were performed. For this purpose, phage lysates derived from the genetically modified λSo variants were prepared and applied at various dilutions to a *S. oneidensis* background strain in which the λSo integration site had been deleted. As a result, the phage was restricted to the lytic cycle, thereby allowing direct evaluation of lytic efficiency and infectivity.

Analysis of the single-gene deletion mutants of cluster C revealed that the observed reduction in PFU is specifically attributable to the deletion of *lcc6* (**Fig. 16A**). In contrast, deletion of *lcc2*, *lcc3*, *lcc4*, or *lcc5* had no significant impact on λSo proliferation under the tested conditions (**Fig. 16A**). Microscopic examination further demonstrated that Lcc6 plays an essential role in cell lysis, as cells carrying the Δ*lcc6* mutation elongated, but failed to lyse following induction of λSo with MMC in a way that is highly reminiscent to the phenotype of holin or endolysin mutants (**Fig. 16B, 17B**). This defect was successfully complemented by ectopic expression of Lcc6 from a plasmid. Notably, ectopic expression of Lcc6 alone in a *S. oneidensis* MR-1 background strain did not result in any observable changes in cell morphology (**Fig. 16C**).

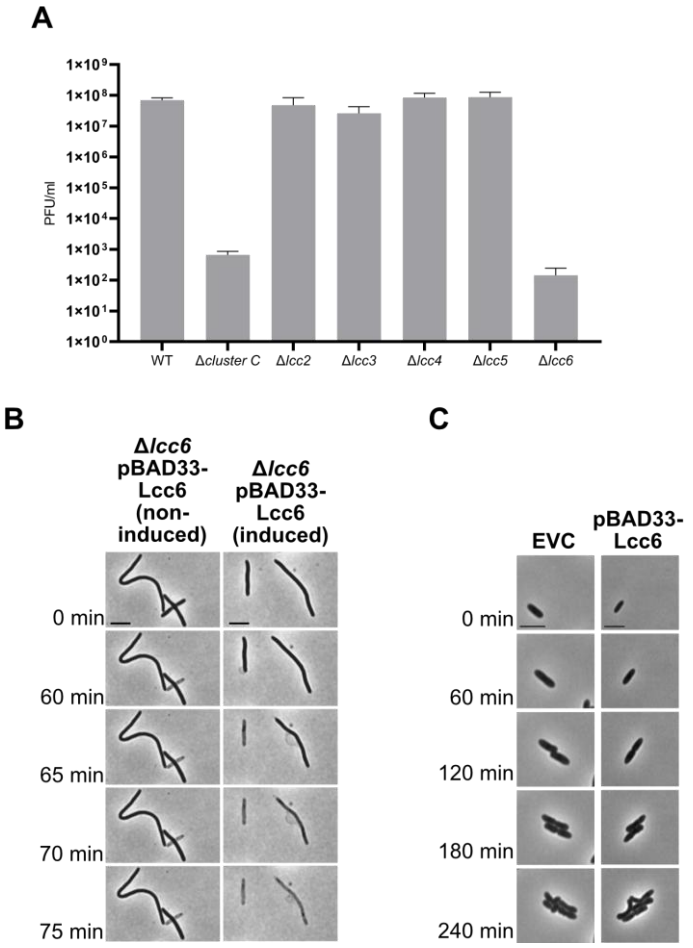

Figure 16: λSo-induced lysis of *S. oneidensis* MR-1 also requires a small transmembrane protein Lcc6. (**A**) Quantification of Lcc mutant plaque formation on *S. oneidensis* host cells. To determine the phage titer, the plaques were counted, and PFU/mL was calculated. Error bars represent the standard error of three independent experiments. (**B**) Displayed are micrographs of a time-lapse series of *S. oneidensis Δlcc6* mutant cells in which Lcc6 was produced after induction of the λSo lysis cassette. The cell culture was first treated with 10 µg/mL MMC for 180 minutes for induction of the lysis cassette and was then divided, with one supplemented with 0.2% arabinose to induce Lcc6 expression, while the other received no additional supplementation. After an incubation of 60 minutes, images were generated every 5 minutes for a total of 2 hours. The scale bar represents 2 µm. (**C**) Time-lapse series of *S. oneidensis MR-1* ΔλSo ΔMuSo1 ΔMuSo2 in which Lcc6 was ectopically produced using the vector pBAD33. Cell cultures were supplemented with 0.2% arabinose to induce protein expression. The beginning of the time-lapse series (0 minutes) was defined as the time point at which arabinose was added to the respective cell culture. EVC resembles the empty vector control. The scale bar represents 5 µm.

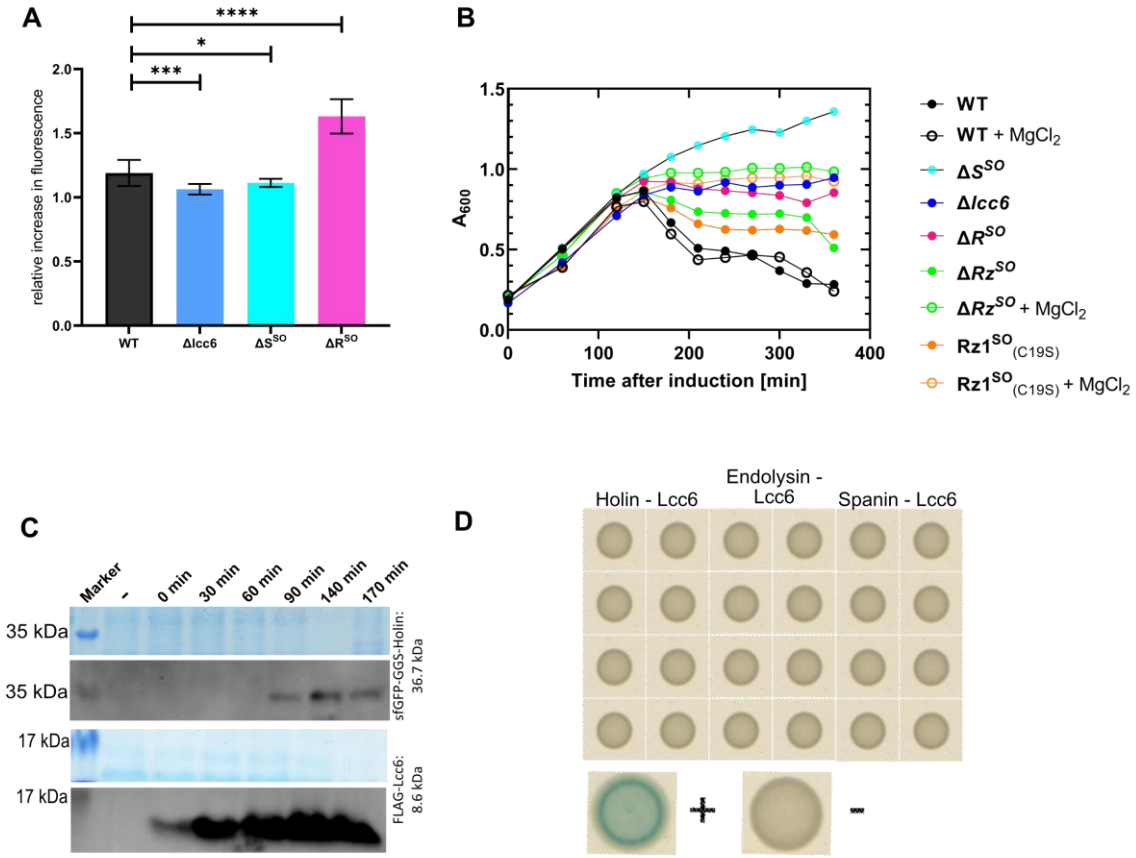

Figure 17: Lcc6 is required for λSo-induced cell lysis. (**A**) Membrane depolarization assay on λSo mutants using $DiBAC_4(3)$. The cells were grown to exponential phase prior to λSo induction by MMC and stained with $DiBAC_4(3)$ to visualize depolarization after the indicated time points. Statistical significance was determined using a two-way ANOVA (analysis of variance) and is indicated by the P value. NS, not significant, *P value = P ≤ 0.05, **P value ≤ 0.01, ***P value ≤ 0.001, and ****P-value ≤ 0.0001. (**B**) Lysis profiles of λSo mutants by bulk culture OD measurements. The respective λSo mutant cultures following inductions by MMC were incubated with constant shaking. Cultures to which 10 mM $MgCl_2$ was added are displayed by open symbols; those with no additional $MgCl_2$ are displayed by closed symbols. The shown data in this figure are representative of biological duplicates. (**C**) Visualization of the protein expression over time of the holin S^{So} fused to a sfGFP and Lcc6 fused to a single FLAG-Tag by western blot analysis. Time points are shown as minutes after induction of the phage with 10 µg/µL MMC. Polyclonal antibodies against GFP and 3xFLAG were used to detect the respective proteins. Sample normalization was achieved by adjusting cell suspensions to the same optical density at 600 nm (OD_{600}) and analysis of stained SDS-PAGE gels. The original data file of the cropped and reassembled western blot is displayed in Fig. S5. (**D**) Bacterial two hybrid analysis of Lcc6 with holin S^{So}, endolysin R^{So} and the i-spanin RZ^{So}. *E. coli* BTH101 was co-transformed with two-hybrid vector plasmids (put18/put18C, pKT25/pKNT25) expressing fusions of the protein of interest with the T18 and T25 domains, respectively. Transformants were spotted onto LB agar plates with IPTG and X-Gal and incubated at 30 °C for approximately 24 h. The plasmids put18C-zip and pKT25-zip were cotransformed as positive control (+). The negative control (-) contains the empty vectors put18c and pKT25. A blue colouring of the colonies (see positive control) shows a direct interaction of the hybrid proteins.

The positioning of the *lcc* genes directly upstream of *xis* suggests that Lcc expression occurs early during phage activation, whereas the expression of lysis genes such as the holin is expected to take place during later stages of the phage life cycle. To better understand the role of Lcc6 in phage-mediated cell lysis and to determine at which stage of the lysis process the protein might act, mutant strains were generated in which s^{So} and *lcc6* were chromosomally replaced by hybrid genes encoding N-terminally sfGFP-tagged holin or FLAG-tagged Lcc6. Although the resulting fusion proteins were non-functional, they allowed detection of the respective proteins by Western blotting. Following MMC induction, protein production was monitored, revealing that Lcc6 could be detected as early as 30 minutes post-induction, whereas holin expression was first observed after 90 minutes (**Fig. 17C**). As anticipated, Lcc6 is expressed early following λSo induction. This observation is further supported by the minimal membrane depolarization observed, which closely resembles the phenotype of holin deletion strains rather than that of endolysin deletion strains (**Fig. 17A**). However, no interaction between the proteins could be detected using a bacterial two-hybrid assay (**Fig. 17D**). These data indicate that Lcc6 is important for phage-induced cell lysis and suggest that the protein acts at the level of, or in concert with, holin rather than interacting with this protein or being directly involved in PG degradation or fusion of the inner and outer membrane after the bacterial cell wall has been removed (**Fig. 17B**).

2.1.1.4 Additional proteins needed for λSo Pinholin-SAR-Endolysin lysis

It has been demonstrated that phage-mediated cell lysis in λSo requires a greater number of proteins than the classical holin-endolysin-spanin system. This finding was supported by the results obtained from investigating the role of Lcc6. Consequently, additional uncharacterised proteins within the lysis cluster were investigated in greater detail. Deletion strains for each individual gene were constructed and subsequently analysed by microscopy and through the generation of lysis profiles. These analyses revealed that another gene product, encoded by *SO_2970*, appears to contribute to the lysis of *S. oneidensis* MR-1 cells by λSo. The protein encoded by *SO_2970* has a size of 119 amino acids and shows no homologies to known domains. The gene is located downstream of the putative pinholin and upstream of a protein predicted to belong to the HNH family of endonucleases (**Fig. 9**).

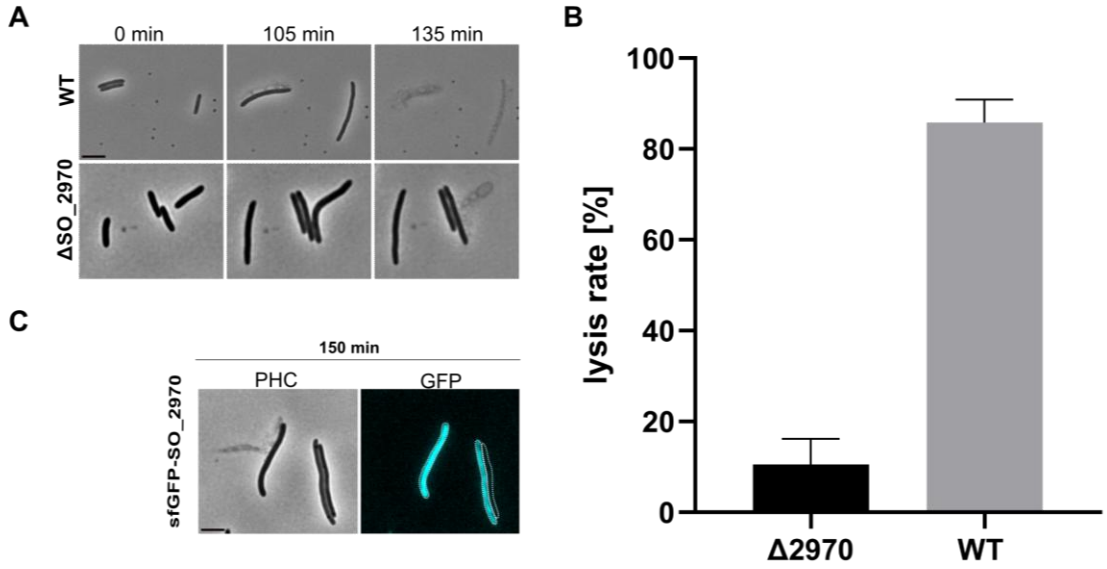

Figure 18: Deletion of SO_2970 leads to reduced lysis. (**A**) Time-lapse microscopy of *S. oneidensis* wild-type cells and *S. oneidensis* cells that carry a deletion of the gene *SO_2970* from the λSo genome. Timepoint 0 was taken 25 min after the addition of mitomycin C (10 µg/mL)). The size bar corresponds to 5 µm. (**B**) Lysis rate of the mutant compared to the wild type. Error bars represent the standard error of three independent experiments. (**C**) Microscopic images of *S. oneidensis* cells in which the protein encoded by *SO_2970* was fused to a fluorophore. The scale bar represents 5 µm.

Microscopic observations demonstrated clear differences in lysis between the wild type and the mutant (**Fig. 18A**). In the wild type strain, approximately 92% of the cells underwent lysis, whereas in the *SO_2970* deletion mutant, only around 19% of the cells lysed (**Fig. 18B**). *In silico* structural predictions using AlphaFold2 indicated that the protein lacks identifiable domains and is likely cytoplasmic (**Fig. S1**). This localization was further confirmed by a functional N-terminal sfGFP fusion to the *SO_2970* gene product (**Fig. 18C**).

2.1.2 Characterization of novel components in host takeover by λSo

In the analysis of the individual genes contained within cluster C, the focus was directed towards not only the deletions of the genes, but also the ectopic expression from a plasmid containing the individual genes, as well as the entire cluster. This was conducted in a *S. oneidensis* MR-1 ΔλSo ΔMuSo1 ΔMuSo2 background strain (data not shown).

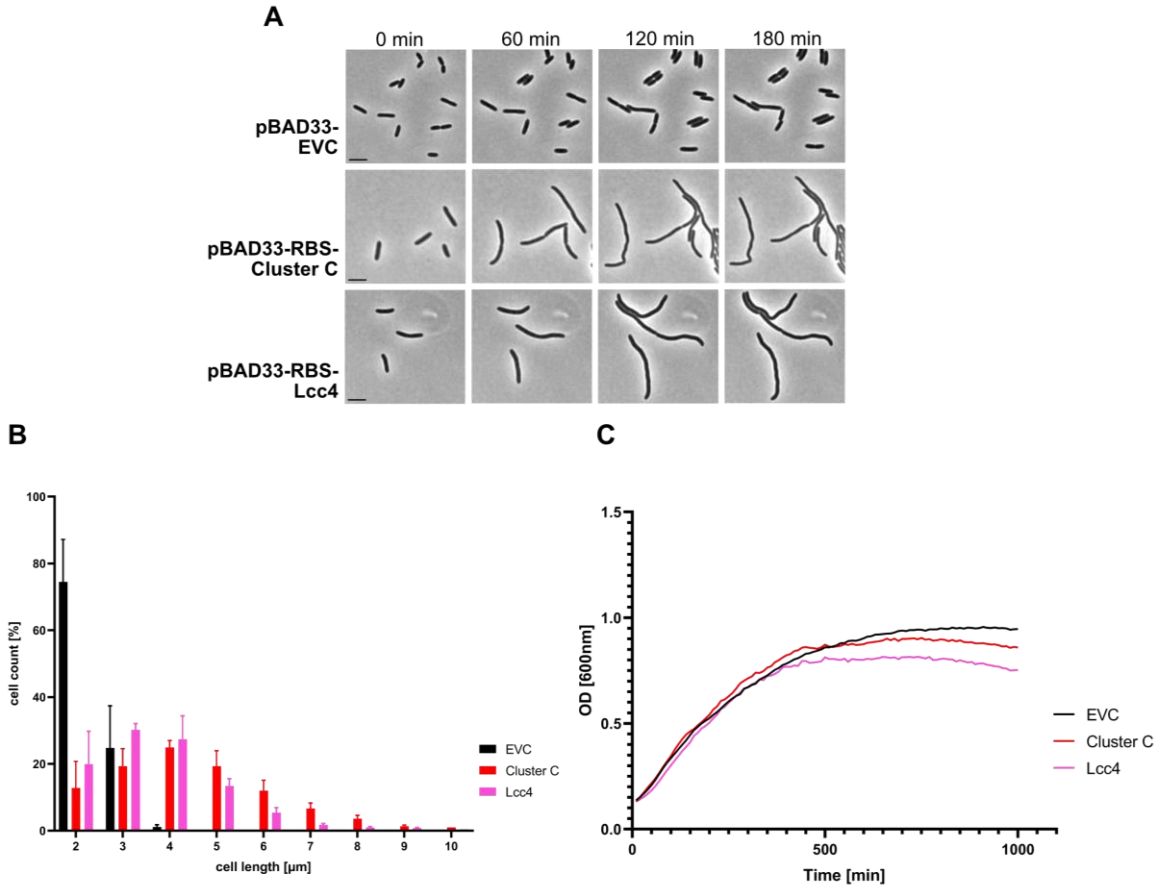

Figure 19: Ectopic production of Lcc4 leads to cell filamentation. (**A**) Time-lapse series of *S. oneidensis* MR-1 ΔλSo ΔMuSo1 ΔMuSo2 in which all proteins of cluster C as well as Lcc4 alone were ectopically produced using the vector pBAD33. Cell cultures were supplemented with 0.2% arabinose to induce protein expression. The beginning of the time-lapse series (0 minutes) was defined as the time point at which arabinose was added to the respective cell culture. EVC resembles the empty vector control. The scale bar represents 2 µm. (**B**) Quantification of cell length of *S. oneidensis* MR-1 after ectopic production of cluster C and Lcc4. Cell cultures were supplemented with 0.2% arabinose to induce protein expression. Pictures were taken two hours after arabinose was added to the respective cell culture. EVC resembles the empty vector control. 300 cells were analysed in each experiment using Bacstalk. Error bars represent the standard error of three independent experiments. (**C**) Growth deficiency of *S. oneidensis* MR-1 ΔλSo ΔMuSo1 ΔMuSo2 with ectopically produced Cluster C and Lcc4. The cultures following inductions by 0,2% arabinose were incubated with constant shaking. Optical density at 600nm was detected using the TECAN reader. The shown data in this figure are representative of biological duplicates.

It was found that overexpressing cluster C in the cells resulted in strong cell filamentation (**Fig. 19A**). In comparison with the wild type, these cells exhibited an average length of 4-6 µm, in contrast to the 2-3 µm observed in the wild type, and demonstrated the capacity to extend to lengths of up to 10 µm (**Fig. 19B**). Upon thorough examination of the ectopic expression of genes belonging to cluster C, it was evident that the observed phenotype was

attributable to the overproduction of Lcc4 (**Fig. 19A**). In the instance of Lcc4 being over-expressed individually, the cells demonstrated an average length of 4-5 µm. However, cells measuring up to 9 µm could also be detected.

Given that filamentation can significantly impact bacterial growth, the optical density (OD_{600}) of liquid cultures of the mutant strains was monitored over time using a TECAN plate reader. This allowed not only quantification of growth but also correlation with cell morphology. Cultures overexpressing the entire cluster C maintained the ability to grow; however, they failed to reach the OD_{600} values observed in the empty vector control (EVC) strain. Overexpression of Lcc4 alone resulted in an even more pronounced growth defect (**Fig. 19C**). These findings indicate that Lcc4 may influence bacterial cell division, as its ectopic production leads to pronounced cell filamentation and impaired culture growth - hallmark indicators of disrupted or inhibited cell division processes [203].

To determine whether the observed phenotype is specific to λSo and its native host *S. oneidensis* MR-1, or if it is transferable to other Gram-negative species, as is the case for the lysis proteins, the plasmids encoding either cluster C or *lcc4* alone were introduced into *E. coli* MG1655. No filamentation or associated growth phenotype was observed under these conditions (**Fig. 20A-C**). The observed phenotype resulting from the ectopic expression of cluster C, particularly Lcc4, appears to be species-specific and dependent on host-specific components present in *S. oneidensis* MR-1, the natural host of λSo.

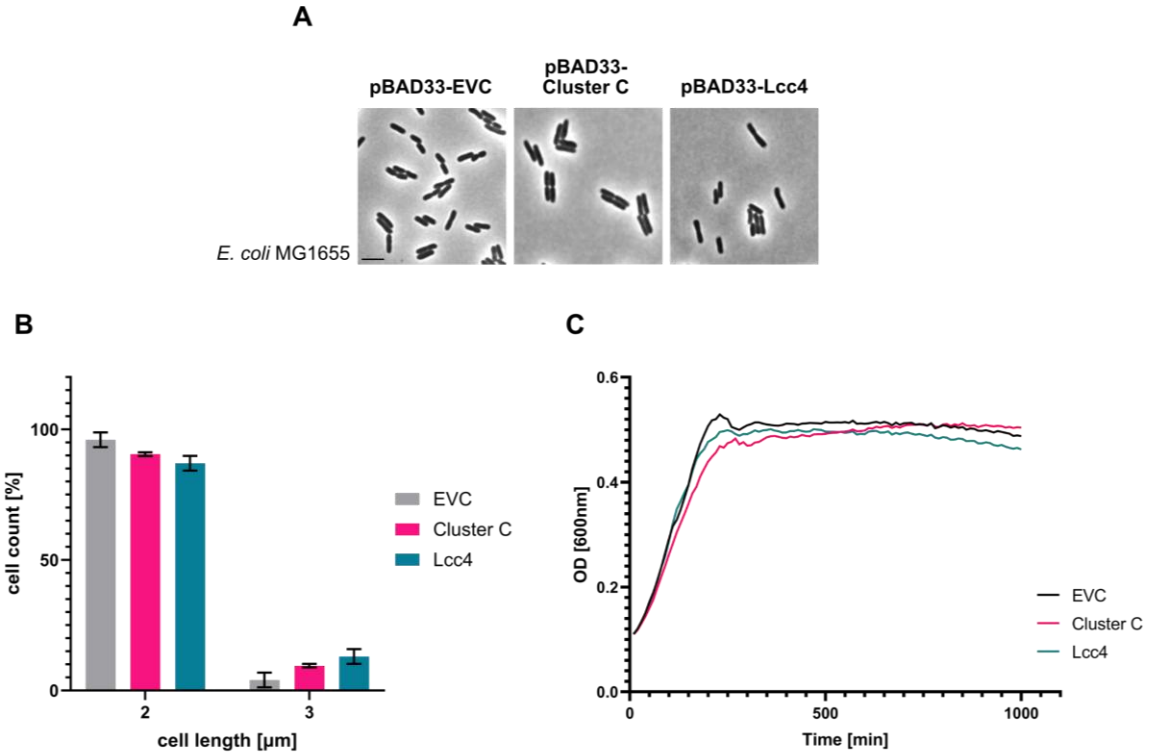

Figure 20: Ectopic production of Lcc4 in *E coli* does not lead to filamentation. (**A**) Micrograph of *E. coli* MG1655 cells in which all proteins of the λSo cluster C as well as Lcc4 alone were ectopically produced using the vector pBAD33. Cell cultures were supplemented with 0.2% arabinose to induce protein expression. The pictures were taken two hours after arabinose was added to the respective cell culture. EVC resembles the empty vector control. The scale bar represents 2 µm. (**B**) Quantification of cell length of *E. coli* MG1655 after ectopic production of cluster C and Lcc4. Cell cultures were supplemented with 0.2% arabinose to induce protein expression. Pictures were taken two hours after arabinose was added to the respective cell culture. EVC resembles the empty vector control. 300 cells were analysed in each experiment using Bacstalk. Error bars represent the standard error of three independent experiments. (**C**) Growth deficiency of *E. coli* MG1655 with ectopically produced cluster C. The *E. coli* cultures following inductions by 0,2% arabinose were incubated with constant shaking. Optical density at 600 nm was detected using the TECAN reader. The shown data in this figure are representative of biological duplicates.

A variety of experimental approaches exist for investigating the function of previously uncharacterised proteins [204]. When functional integrity is maintained, the incorporation of affinity tags - such as hexa-histidine, FLAG, or fluorophore labels - enables the use of techniques like pull-down assays, affinity chromatography, and other interaction-based methods to study potential binding partners.

In this study, Lcc4 was tagged with a triple FLAG epitope to facilitate experimental handling and downstream analyses. The tagged recombinant protein was subsequently ectopically expressed via plasmid-based expression, and the resulting strains were examined using fluorescence microscopy and Western blotting.

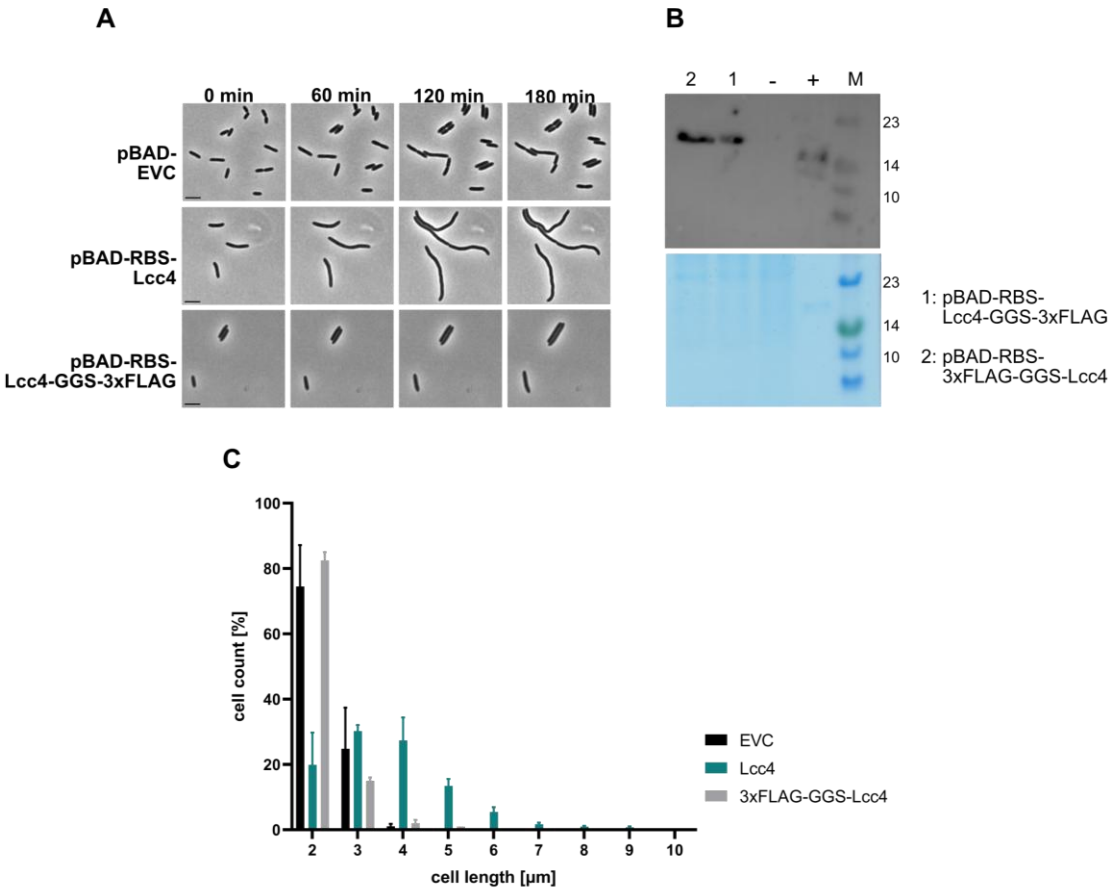

Figure 21: A tripple FLAG-Tag interferes with the function of Lcc4. (**A**) Time-lapse series of *S. oneidensis* MR-1 ΔλSo ΔMuSo1 ΔMuSo2 in which Lcc4 fused to a 3xFLAG-Tag was ectopically produced using the vector pBAD33. Cell cultures were supplemented with 0.2% arabinose to induce protein expression. The beginning of the time-lapse series (0 minutes) was defined as the time point at which arabinose was added to the respective cell culture. EVC resembles the empty vector control. The scale bar represents 2 µm. (**B**) Visualization of the protein expression over time of Lcc4 fused to a triple FLAG-Tag by western blot analysis. Polyclonal antibodies against 3xFLAG were used to detect the respective proteins. Sample normalization was achieved by adjusting cell suspensions to the same optical density at 600 nm (OD_{600}) and analysis of stained SDS-PAGE gels. The original data file of the cropped and reassembled western blot is displayed in Fig. S8. (**C**) Quantification of cell length of *S. oneidensis* MR-1 after ectopic production of Lcc4 fused to a 3xFLAG-Tag. Cell cultures were supplemented with 0.2% arabinose to induce protein expression. Pictures were taken two hours after arabinose was added to the respective cell culture. EVC resembles the empty vector control. 300 cells were analysed in each experiment using Bacstalk. Error bars represent the standard error of three independent experiments.

As shown in Figure 21B, the fusion proteins are uniformly expressed, with no observable differences between N-terminal and C-terminal tagging. However, fluorescence microscopy reveals that fusing the Lcc4 protein with a triple FLAG epitope compromises its function, as the filamentation phenotype typically induced by ectopic expression of native Lcc4 is no longer evident in the tagged variants (**Fig. 21A**). Only minimal elongation was observed (**Fig. 21C**); however, this phenotype was markedly less

pronounced than that of the native control strain. Consequently, these modified proteins were excluded from further experiments to avoid artefactual results due to potential disruption of native protein topology.

2.1.2.1 Identification of possible interaction partner of Lcc4

Lcc4 is a 91-amino acid protein featuring a predicted transmembrane domain spanning residues 35 to 57 (**Fig. S1**). Topology analysis using DeepTMHMM suggests an N-in/C-in orientation within the membrane. To gain insights into the potential function of Lcc4, particularly its role in bacterial cell division, comprehensive *in silico* analyses were performed using AlphaFold2 and PyMOL.

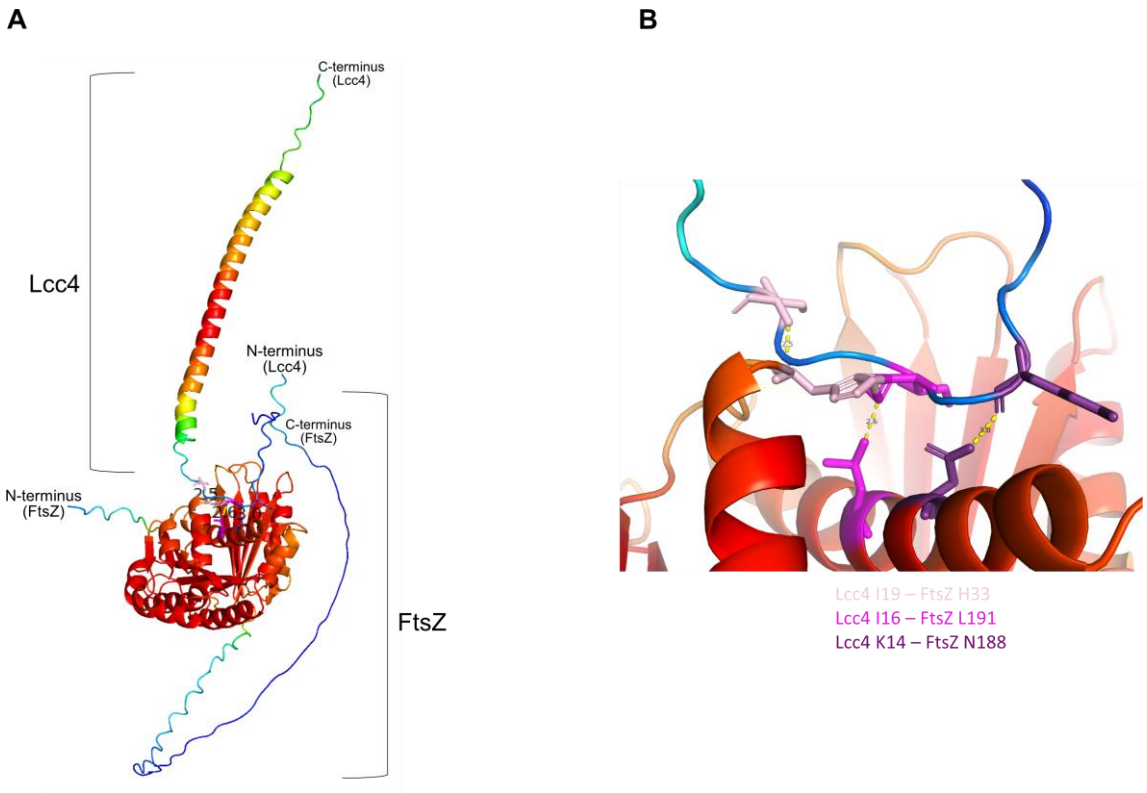

Figure 22: Structure of the hypothesized protein complex of FtsZ and Lcc4 as predicted by AlphaFold. (**A**) 3D structures of the proteins of interest were predicted using Alphafold2 trough DeepMind´s Colab. The structures were visualized with Pymol. Certain protein domains are indicated using brackets. The structures are colour-coded by B-factor values / atomic displacement parameter. (**B**) The respective amino acids that are part of the interaction surface are colour-coded as stated.

In these analyses, Lcc4 was modelled as an oligomer in complex with various known cell division proteins, allowing for the identification of potential interaction partners based on structural predictions derived from primary sequence information. Through these *in silico* analyses, two potential interaction partners for Lcc4 were identified: FtsZ and ZipA (**Fig. 22, 23A**). The predicted interaction interfaces were visualized using PyMOL, and key residues potentially involved in the protein-protein interactions were highlighted (**Fig. 22, 23B**).

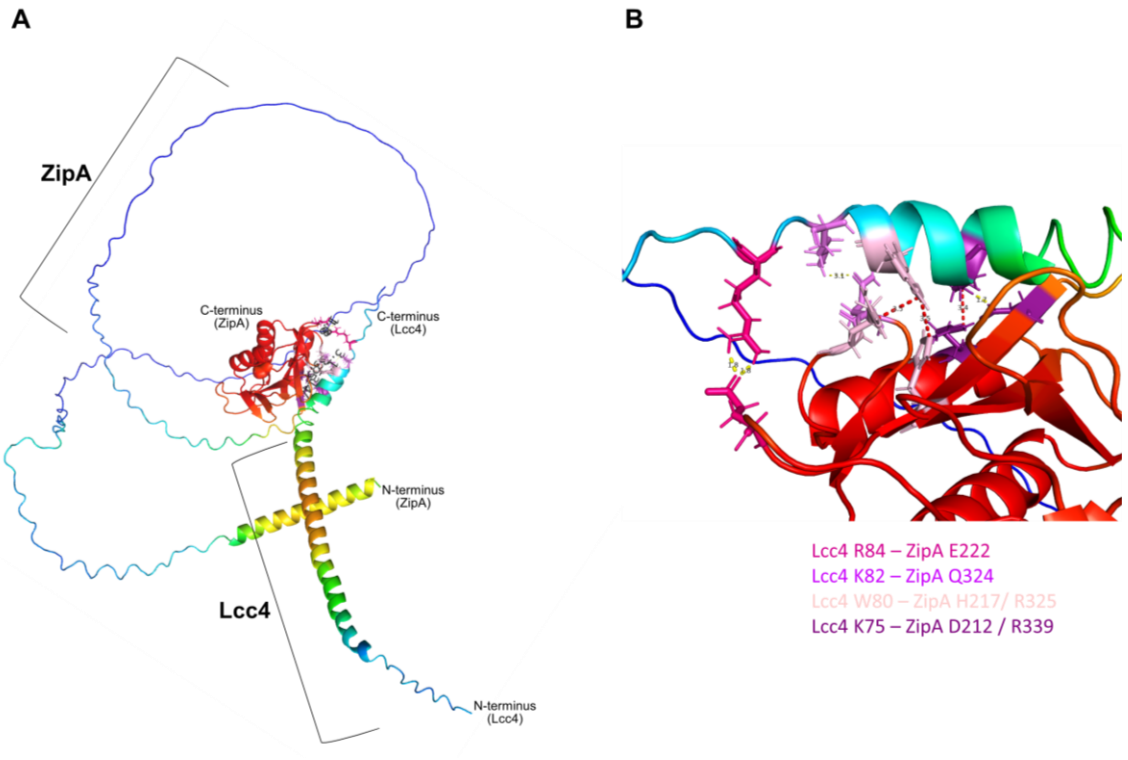

Figure 23: Structure of the hypothesized protein complex of ZipA and Lcc4 as predicted by AlphaFold. (**A**) 3D structures of the proteins of interest were predicted using Alphafold2 trough DeepMind´s Colab. The structures were visualized with Pymol. Certain protein domains are indicated using brackets. The structures are colour-coded by B-factor values / atomic displacement parameter. (**B**) The respective amino acids that are part of the interaction surface are colour-coded as stated.

To assess the reliability of these structural predictions, site-directed mutagenesis was performed on the candidate interaction residues (**Tbl. 4**). The resulting recombinant Lcc4 variants were ectopically expressed from a plasmid in the respective *S. oneidensis* background strain, and their phenotypes were subsequently examined via microscopy and optical density measurements to evaluate the effects on cell morphology and growth.

Table 4: possible interaction residues of Lcc4 and certain cell division proteins

Lcc4	FtsZ	ZipA
K14 - R14	N188	
I16 - L16	L191	
I19 - L19	H33	
K75 - R75		D212 / R339
W80 - Y80		H217 / R325
K82 - R82		Q324
R84 - K84		E222

FtsZ and ZipA are essential components of the bacterial cell division machinery, rendering their genomic modification or deletion using conventional genetic techniques not achievable. Therefore, site-directed substitutions were first introduced into the predicted interaction residues of Lcc4 (**Tbl. 4**). To ensure a controlled experimental context and to prevent potential interference from endogenous phage-encoded factors, the modified Lcc4 variants were ectopically expressed from a plasmid in a background strain in which the λSo sequence had been deleted. This approach allowed for the functional analysis of the Lcc4 variants in isolation from possible interactions with the native phage protein.

The substitution of lysine at position 14 in Lcc4, predicted to interact with asparagine 188 of FtsZ, as well as lysines at positions 82 and 75 in Lcc4, predicted to interact with aspartic acid 212 and glutamine 324 of ZipA, respectively, did not result in a substantial alteration of the filamentation phenotype upon ectopic expression from plasmid pBAD33 (**Fig. 24A**). Only the K14 substitution led to a modest reduction in filamentation relative to the control strain overexpressing native Lcc4. In this mutant, the cells exhibited an average length of 4-5 µm and demonstrated markedly reduced growth compared to the background strain (**Fig. 24B, C**).

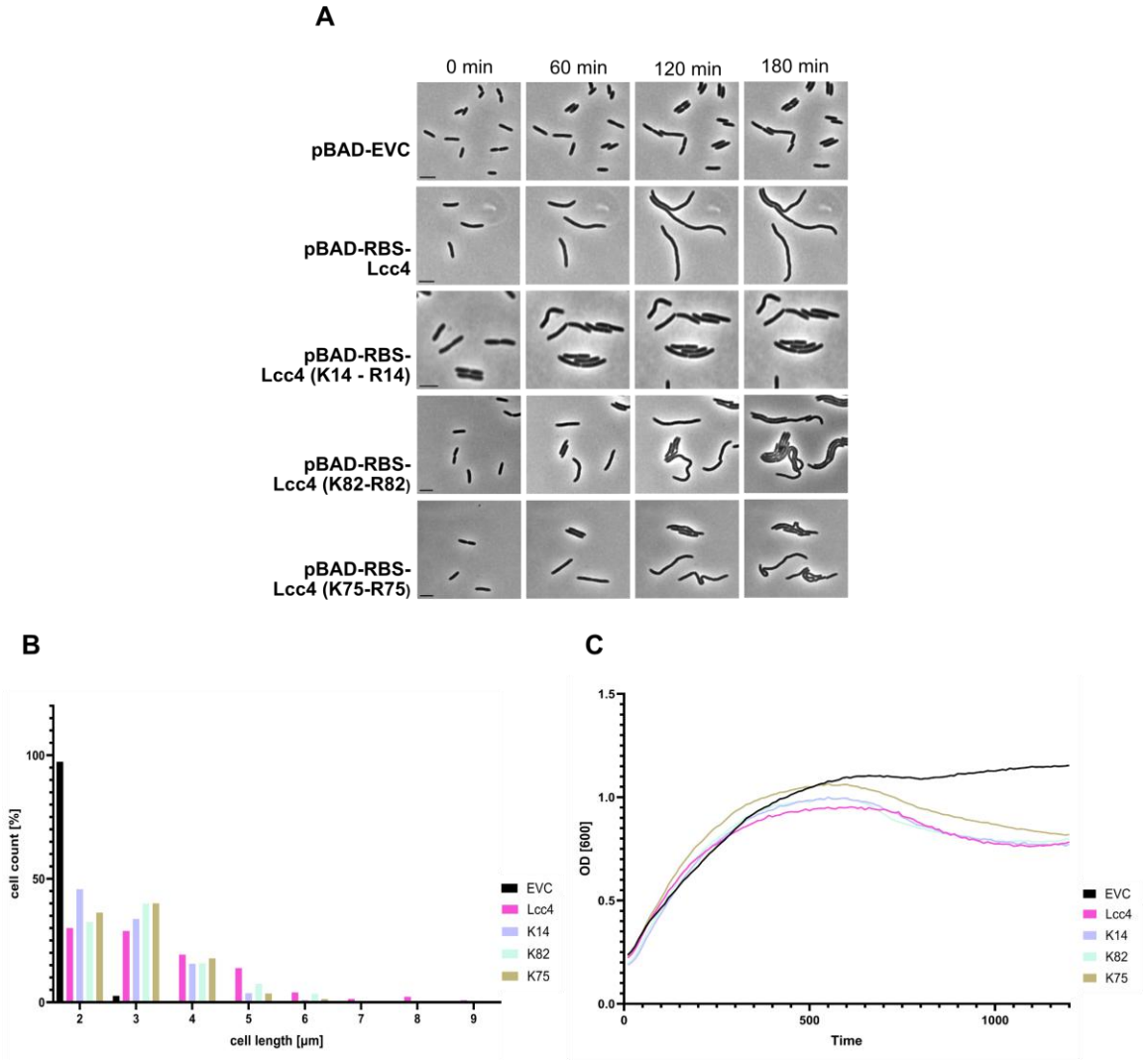

Figure 24: Ectopic production of Lcc4 carrying defined amino acid substitutions leads to cell filamentation. (**A**) Time-lapse series of *S. oneidensis* MR-1 ΔλSo ΔMuSo1 ΔMuSo2 in which Lcc4 as well as correspondingly labelled modifications of this proteins were ectopically produced using the vector pBAD33. Cell cultures were supplemented with 0.2% arabinose to induce protein expression. The beginning of the time-lapse series (0 minutes) was defined as the time point at which arabinose was added to the respective cell culture. EVC resembles the empty vector control. The scale bar represents 2 µm. (**B**) Quantification of cell length of *S. oneidensis* MR-1 ΔλSo ΔMuSo1 ΔMuSo2 after ectopic production of Lcc4 and modified Lcc4. Cell cultures were supplemented with 0.2% arabinose to induce protein expression. Pictures were taken two hours after arabinose was added to the respective cell culture. EVC resembles the empty vector control. 300 cells were analysed in each experiment using Bacstalk. Error bars represent the standard error of three independent experiments. (C) Growth deficiency of *S. oneidensis* MR-1 ΔλSo ΔMuSo1 ΔMuSo2 with ectopically produced Lcc4 and it´s mutants. The cultures were incubated with constant shaking following inductions by 0,2% arabinose. Optical density at 600nm was detected using the TECAN reader. The shown data in this figure are representative of biological duplicates.

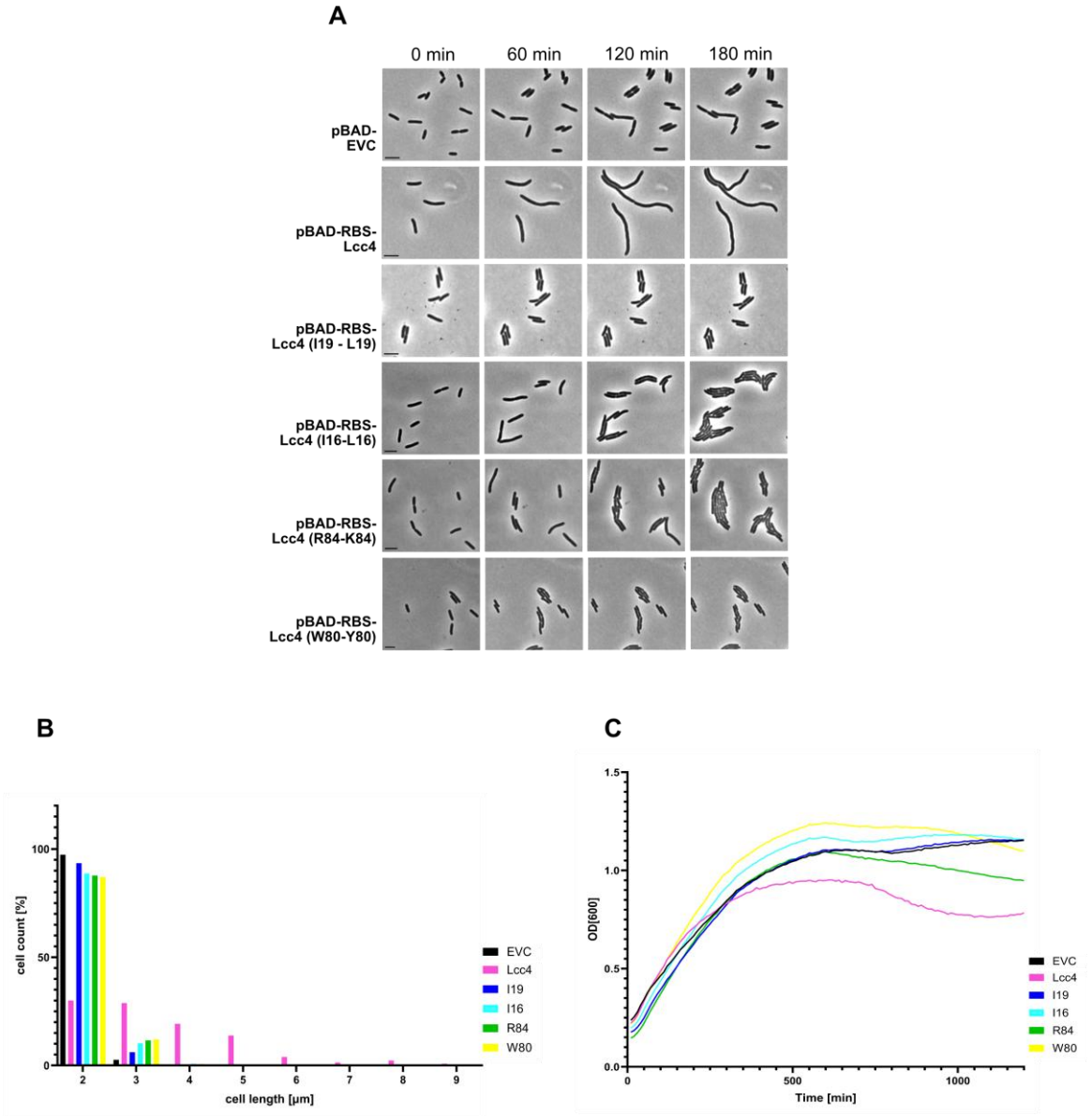

Figure 25: Ectopic production of Lcc4 carrying defined amino acid substitutions leads to no cell filamentation, diminishing the previously observed phenotype. (**A**) Time-lapse series of *S. oneidensis* MR-1 ΔλSo ΔMuSo1 ΔMuSo2 in which Lcc4 as well as correspondingly labelled modifications of this proteins were ectopically produced using the vector pBAD33. Cell cultures were supplemented with 0.2% arabinose to induce protein expression. The beginning of the time-lapse series (0 minutes) was defined as the time point at which arabinose was added to the respective cell culture. EVC resembles the empty vector control. The scale bar represents 2 µm. (**B**) Quantification of cell length of *S. oneidensis* MR-1 after ectopic production of Lcc4 and modified Lcc4. Cell cultures were supplemented with 0.2% arabinose to induce protein expression. Pictures were taken two hours after arabinose was added to the respective cell culture. EVC resembles the empty vector control. 300 cells were analysed in each experiment using Bacstalk. Error bars represent the standard error of three independent experiments. (**C**) Growth deficiency of *S. oneidensis* MR-1 ΔλSo ΔMuSo1 ΔMuSo2 with ectopically produced Lcc4 and it´s mutants. The cultures were incubated with constant shaking following inductions by 0,2% arabinose. Optical density at 600nm was detected using the TECAN reader. The shown data in this figure are representative of biological duplicates.

The substitution of isoleucine residues at positions 16 and 19 in Lcc4, predicted to interact with histidine 33 and leucine 192 in FtsZ, as well as arginine 84 and tryptophan 80, predicted to interact with glutamic acid 222 and histidine 217 in ZipA, resulted in a markedly altered filamentation phenotype (**Fig. 25A**). Upon ectopic expression of the accordingly modified Lcc4 variants, filamentation was no longer observed. Quantitative analysis of microscopic images using BacStalk revealed an average cell length of 2-3 µm, comparable to wild type morphology (**Fig. 25B**). Additionally, assessment of cellular growth via optical density measurements in liquid culture showed no significant impairment in these strains. Notably, the strain expressing Lcc4 R84K exhibited a decline in growth after approximately 8 hours relative to the control strain *S. oneidensis* MR-1 ΔλSo ΔMuSo1 ΔMuSo2 carrying the empty vector control (pBAD33-EVC). In contrast, the strain expressing Lcc4 W80Y demonstrated improved growth compared to the control (**Fig. 25C**). The data obtained from these experiments support the hypothesis that Lcc4 interacts with both FtsZ and ZipA. The predicted interaction interface between Lcc4 and FtsZ likely involves isoleucine residues at positions 16 and 19 in Lcc4 and histidine 33 and leucine 192 in FtsZ. Similarly, the interaction with ZipA appears to involve arginine 84 and tryptophan 80 in Lcc4, along with glutamic acid 222 and histidine 217 in ZipA.

As established in previous investigations, expression of Lcc4 does not induce filamentation in *E. coli*. To further explore the underlying molecular basis of this observation, the FtsZ proteins of *E. coli* and *S. oneidensis* MR-1 were subjected to comparative structural and sequence analyses. In addition to three-dimensional structure predictions generated using AlphaFold2, a comparative analysis of the primary amino acid sequences was conducted employing BLAST and Clustal Omega.

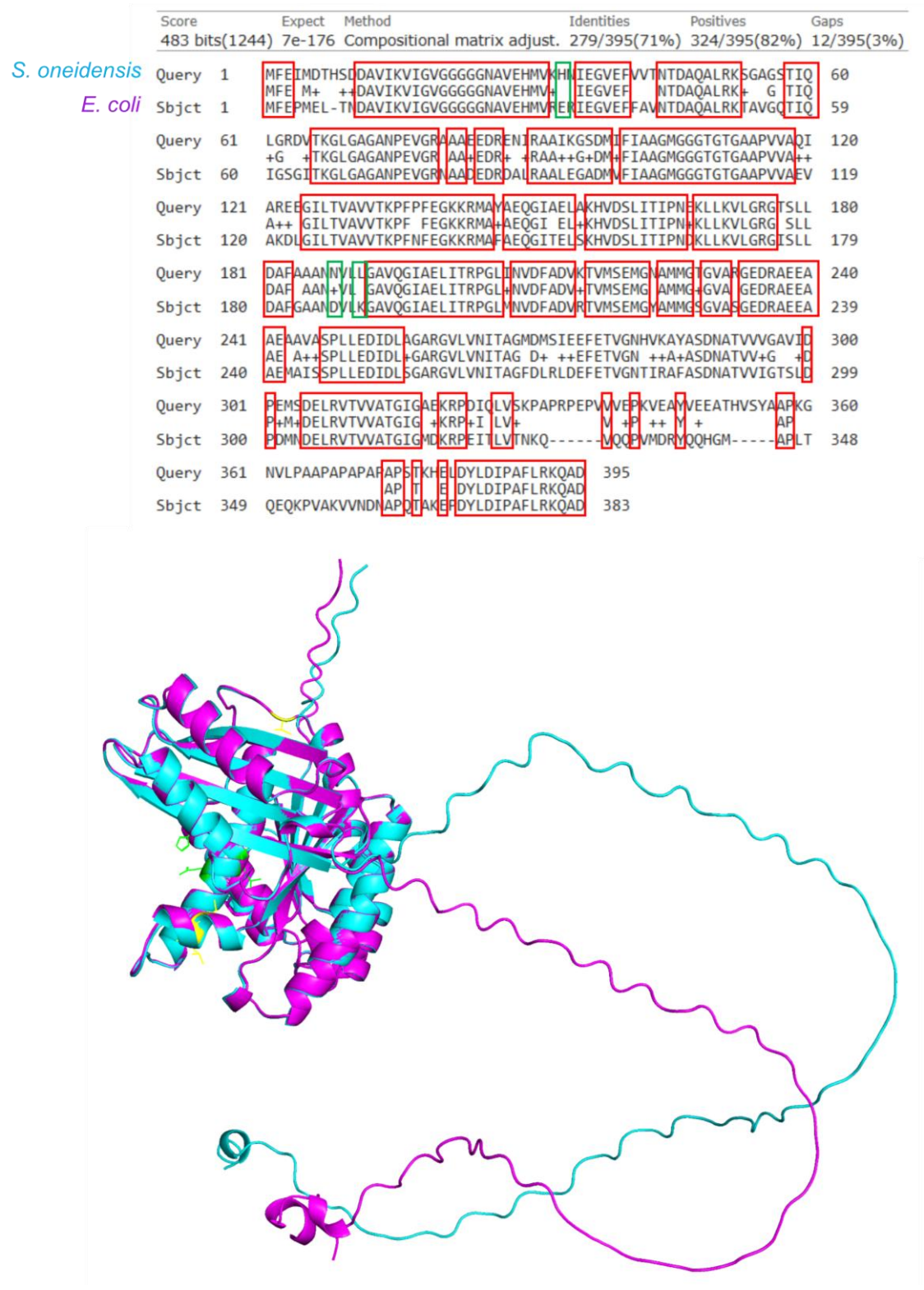

Figure 26: Alignment of the predicted structures of FtsZ of *S. oneidensis* MR-1 und *E.coli* MG1655. 3D structures of the proteins of interest were predicted using Alphafold2 trough DeepMind´s Colab. The structures were visualized with Pymol. FtsZ of *S. oneidensis* MR-1 is shown in blue, FtsZ of *E. coli* MG1655 is shown in magenta. The predicted interaction surface of FtsZ of *S. oneidensis* MR-1 with Lcc4 is shown in green. The conserved amino acids of both proteins are indicated in the primary structure using red brackets.

These analyses revealed a 71% sequence identity between the two FtsZ homologs (**Fig. 26**). However, critical differences were identified at specific residues previously postulated to be involved in the interaction interface with Lcc4. Notably, the leucine residue at position 191 in *S. oneidensis* FtsZ, which is hypothesised to interact with isoleucine 16 of Lcc4, is replaced by a lysine in *E. coli*. Similarly, histidine at position 33, presumed to engage with isoleucine 19 of Lcc4, is substituted by a glutamic acid in the *E. coli* homolog. Additionally, asparagine 188, which did not exhibit detectable interaction in the experimental system, corresponds to an aspartic acid in *E. coli* (**Fig. 26**). These findings provide compelling support for the hypothesis that these specific amino acid residues are critical determinants mediating the interaction between FtsZ from *S. oneidensis* MR-1 and the phage-encoded Lcc4 protein of λSo. The lack of filamentation phenotype in *E. coli* is thus likely attributable to these sequence divergences at key interaction sites.

Previous studies in *S. oneidensis* MR-1 demonstrated that elevated iron uptake can induce DNA damage, which is subsequently detected by the recombinase protein RecA. RecA facilitates the autocatalytic cleavage of the phage repressor CI, thereby triggering phage induction [195]. Given that the activation of phage λSo is strongly dependent on the SOS response, it was of particular interest to investigate whether this regulatory pathway also influences the phenotype associated with Lcc4 expression. To address this, Lcc4 was ectopically expressed from a plasmid in a strain background lacking the *sulA* gene. SulA is a well-characterised component of the bacterial SOS response and is upregulated in response to DNA damage [205]. Its primary function is to inhibit cell division, thereby affording the cell time to initiate DNA repair [206]. Mechanistically, SulA exerts its effect by binding directly to the tubulin-like cell division protein FtsZ, which is essential for the assembly of the Z-ring and the progression of cytokinesis [207]. This interaction inhibits both the polymerisation and GTPase activity of FtsZ, effectively halting Z-ring formation and blocking cell division. Importantly, this inhibition is reversible: upon completion of DNA repair, SulA is degraded by the Lon protease complex, thereby restoring normal FtsZ function and cell division.

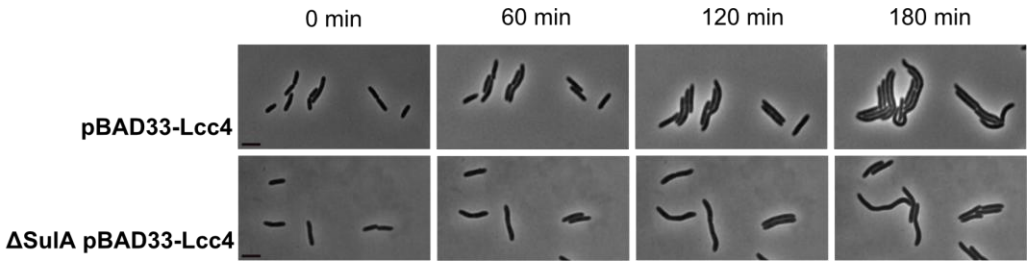

Figure 27: The SOS-response protein SulA is not involved in the cell filamentation caused by Lcc4. Time-lapse series of *S. oneidensis* MR-1 ΔλSo ΔMuSo1 ΔMuSo2 and *S. oneidensis* MR-1 ΔλSo ΔMuSo1 ΔMuSo2 Δ*sulA* in which Lcc4 was ectopically produced using the vector pBAD33. Cell cultures were supplemented with 0.2% arabinose to induce protein expression. The beginning of the time-lapse series (0 minutes) was defined as the time point at which arabinose was added to the respective cell culture. The scale bar represents 2 µm.

The aim of this experiment was to determine whether the filamentation phenotype induced by Lcc4 is mediated via SulA. As shown in Figure 27, deletion of *sulA* had no observable effect on the cell elongation phenotype resulting from Lcc4 expression. Cells lacking SulA exhibited filamentation comparable to those of the control strain in which *sulA* was intact. These findings suggest that the Lcc4-induced inhibition of cell division occurs independently of SulA, indicating a distinct, SulA-independent mechanism of action.

2.1.2.2 Characterization of the interaction between Lcc4 and FtsZ

As previous findings in this study suggest a potential direct interaction between Lcc4 and FtsZ, this part of the project aims to investigate this interaction in greater detail.

The process of bacterial cell division, particularly the role of FtsZ, has been extensively studied, and several research groups have successfully visualized FtsZ ring formation through the ectopic expression of fluorescently labelled FtsZ alongside its native counterpart [89,134]. Building on this methodology, the current investigation employed a similar approach, utilizing the ectopic expression of fluorescence-tagged FtsZ to visualize Z-ring formation and assess the influence of Lcc4 on this process.

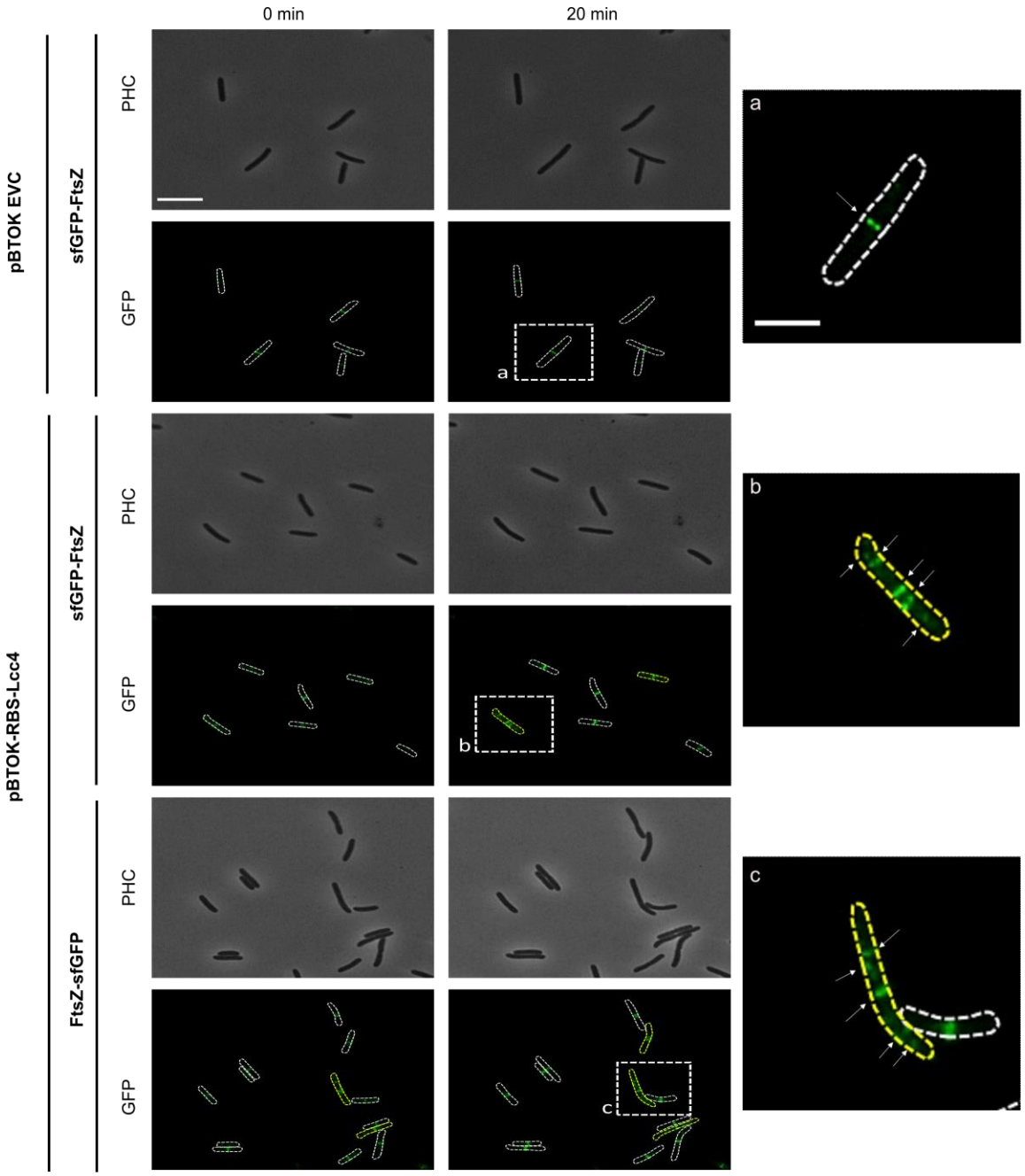

Figure 28: Coexpression of FtsZ with Lcc4 leads to a diffuse localisation of FtsZ. Time-lapse series of *S. oneidensis* MR-1 ΔλSo ΔMuSo1 ΔMuSo2 in which Lcc4 was ectopically produced using pBTOK. A pBTOK empty vector (pBTOK EVC) was used for comparison. In addition, FtsZ was expressed with sfGFP using pBAD33. Induction of sfGFP-FtsZ was performed for 60 min by addition of 0.2 % L-arabinose prior to the induction of Lcc4 with 0.2 µg/ml anhydrotetracycline (AHT). The beginning of the time-lapse series (0 minutes) was defined as the time point at which AHT was added to the respective cell culture. The time-lapse images were taken in phase contrast and in the GFP fluorescence channel. Cells showing a FtsZ localisation deviating from the empty vector control were highlighted in the fluorescence images with a yellow cell border. Figures a to c show selected cells of the empty vector control and Lcc4 overexpression in the GFP fluorescence signal for improved comparability. The visible FtsZ foci are marked with arrows. The scales are 5 µm.

In this experimental setup, Lcc4 was ectopically expressed from a separate vector than FtsZ to allow for independent regulation of the two proteins. The *S. oneidensis* MR-1 ΔλSo ΔMuSo1 ΔMuSo2 strain served as the background. To visualize FtsZ dynamics, both N-terminal and C-terminal fluorescent fusions of FtsZ were constructed, and their expression was verified via Western blotting (**Fig. S5**). The resulting strains were then analysed by fluorescence microscopy to assess Z-ring formation and its potential modulation upon co-expression of Lcc4.

As illustrated in Figure 28, cells ectopically expressing only the FtsZ-sfGFP fusion exhibited a single, well-defined Z-ring centrally positioned within the cell (**Fig. 28a**). 60 minutes after induction with arabinose, a mild filamentation phenotype was observed; however, cell division still occurred. This phenotype was consistent for both N- and C-terminal FtsZ fusions. In contrast, co-expression of Lcc4 from plasmid pBTOK resulted in a range of aberrant phenotypes. These included cells with multiple, mislocalized Z-rings (**Fig. 28b**), cells displaying diffuse cytoplasmic FtsZ signal without clear ring formation (**Fig. 28c**), and a subset of cells still exhibiting a single central Z-ring (**Fig. 28c**).

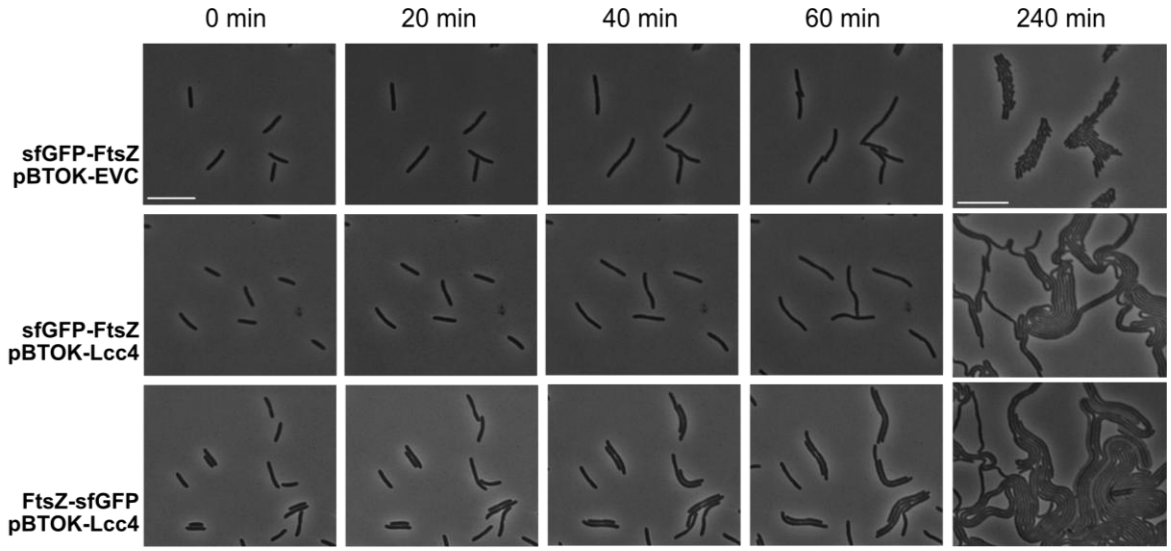

Figure 29: Coexpression of FtsZ with Lcc4 leads to a strong filamentation of the cells. Time-lapse series of *S. oneidensis* MR-1 ΔλSo ΔMuSo1 ΔMuSo2 in which Lcc4 was ectopically produced using pBTOK. A pBTOK empty vector (pBTOK EVC) was used for comparison. Induction of Lcc4 was performed with 0.2 µg/ml anhydrotetracycline (AHT). The beginning of the time-lapse series (0 minutes) was defined as the time point at which AHT was added to the respective cell culture. The scales are 5 µm.

Notably, the co-expression of both proteins led to a pronounced filamentation phenotype, with cells largely losing the ability to undergo regular division (**Fig. 29**). These data further support the hypothesis that Lcc4 interacts with FtsZ, as its co-expression leads to altered Z-ring localization and assembly, ultimately disrupting normal cell division.

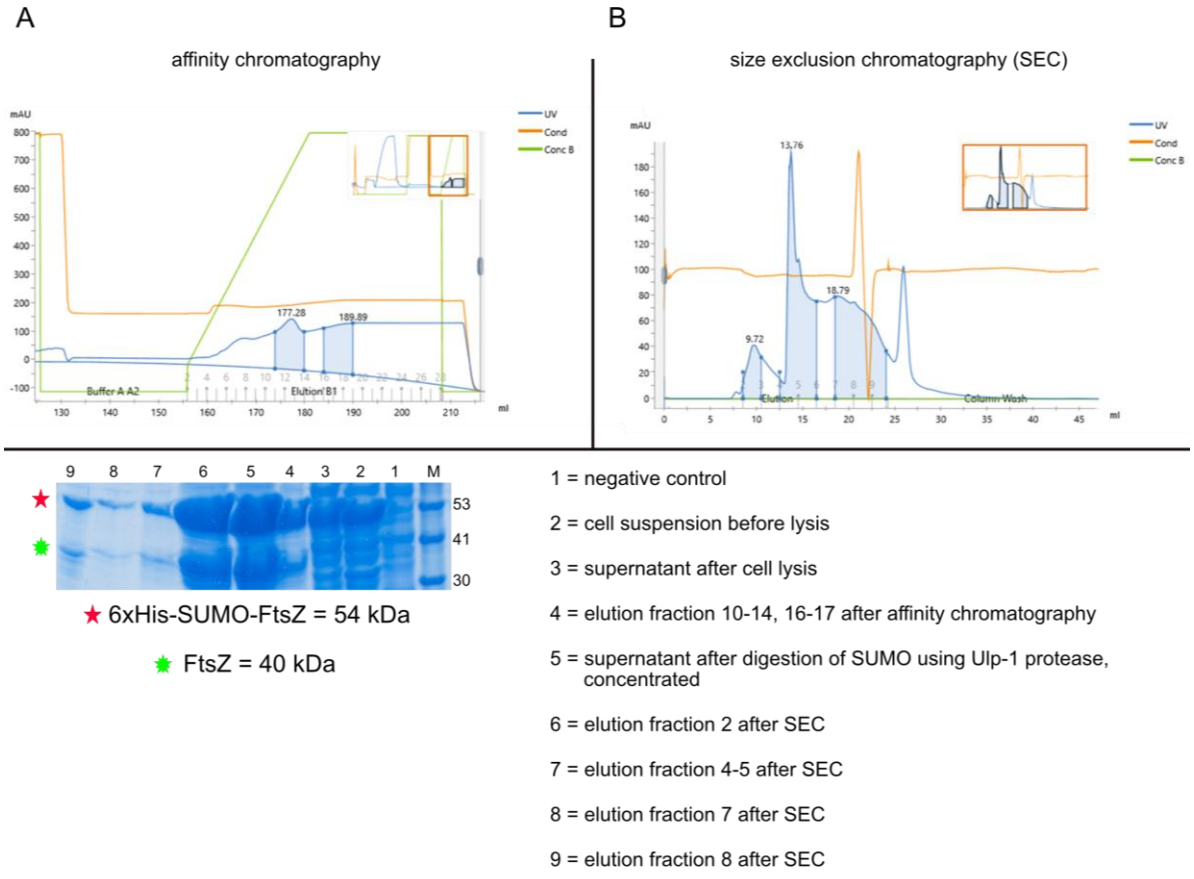

Figure 30: Purification of FtsZ using affinity- and size exclusion chromatography. Displayed in panel A and B are the elution profiles of the affinity as well as the size exclusion chromatography using the Äkta system. For the affinity chromatography, the proteins were eluted using a linear imidazol gradient (displayed in green). (lower panel) Visualization of the protein expression of FtsZ fused to a Hexa-Histidin-Tag as well as a SUMO-cleavage-side during the purification process by SDS page polyacrylamide analysis. The original data file of the cropped and reassembled western blot is displayed in Fig. S10.

As the functionality of Lcc4 is already compromised by the addition of small affinity tags such as a FLAG tag (**Fig. 21**), experimental approaches like pulldown assays, using Lcc4 as bait, could not be pursued due to the high risk of generating misleading results stemming from loss of native Lcc4 function. Nevertheless, given the accumulating evidence suggesting an interaction between Lcc4 and FtsZ, FtsZ was purified in the course

of this study using affinity and size exclusion chromatography, enabling subsequent *in vitro* interaction studies with this key division protein.

For this purpose, FtsZ was engineered to include an N-terminal hexa-histidine tag followed by a SUMO protease cleavage site, and was ectopically produced in *E. coli* ROSETTA cells using a pET-based expression plasmid [208]. This design facilitated efficient purification under native conditions and allowed for subsequent removal of the affinity tag to preserve the native structure and function of FtsZ for down-stream interaction assays [208,209]. The expression of the respective proteins was verified by western blot analysis prior to their use in subsequent experiments (**Fig. S9**).

Figure 29 illustrates the purification profiles of the target proteins. Initially, proteins were extracted from the cell lysate using affinity chromatography via a hexa-histidine tag. Subsequent purification was performed by size exclusion chromatography (SEC) (**Fig 30 A, B**). The individual fractions from the SEC, reflecting protein content as indicated by peak height, were analysed by SDS-PAGE (**Fig 30B, lower panel**). To monitor potential protein loss throughout the process, samples from each purification step were included as controls. As shown in the lower panel of Figure 27, the highest protein content was observed in lane 6 (fraction 2); however, this fraction also displayed a high level of non-specific bands (**Fig. S10**), suggesting the presence of contaminants. In contrast, lane 7 (fractions 4-5) exhibited a lower overall protein concentration but significantly reduced non-specific background. Consequently, proteins from fractions 4 and 5 were selected for downstream applications to minimize contamination with degradation products or unwanted proteins.

Certain phage proteins are known to interact with FtsZ and disrupt host cell division [210]. For instance, the Kil protein from phage λ, a temperate phage infecting *E. coli*, interferes with FtsZ polymerization, leading to the formation of multiple oligomeric species of varying sizes [118]. To investigate whether Lcc4 exerts a similar effect on FtsZ polymerization in *S. oneidensis* MR-1, a filamentation assay was conducted to compare the sedimentation behaviour of long FtsZ filaments with that of shorter oligomers or monomers.

Due to structural constraints preventing affinity purification of full-length Lcc4, a synthetic peptide comprising the N-terminal 26 amino acids of Lcc4 was used. This

peptide was custom-synthesized by GenScript Biotech (Netherlands) BV for the experiment.

Table 5: synthetic peptide

	Primary amino acid sequence
Lcc4	MFEFTEDKKGLRPKYIGTIKHNGIRRTLMVLMTLPTILAVICLNF FMFLVYVIMAFWLILLGTFKLLAGMFQAKTWEVWHKPRQVHD DSK
Lcc4-derived peptide	MFEFTEDKKGLRPKYIGTIKHNGIRR

For this experimental setup, FtsZ was incubated with GTP, either alone or in combination with the respective test protein, for approximately one hour at room temperature. Following incubation, the samples were subjected to ultracentrifugation to pellet any FtsZ filaments that had formed. Both the resulting supernatants and pellets were subsequently analysed by SDS-PAGE to assess the distribution of FtsZ between polymerized and soluble forms. To enable accurate assessment of FtsZ distribution, aliquots of the reaction mixtures were also analysed by SDS-PAGE prior to centrifugation, alongside the post-centrifugation samples. Additionally, purified FtsZ and the synthetic Lcc4 peptide were each run individually as controls.

As shown in Figure 31, the protein distribution, which is reflected by the intensity of the SDS-PAGE bands, changes upon centrifugation. Prior to centrifugation, the protein concentrations in both experimental setups, FtsZ with Lcc4 (approach 1) and FtsZ with GTP (approach 2), were comparable. Following centrifugation, a distinct shift in FtsZ distribution is observed: in approach 1, a greater proportion of FtsZ remains in the supernatant, whereas in approach 2, FtsZ is predominantly found in the pellet, indicating filament formation. The synthetic Lcc4 peptide is detected exclusively in the supernatant, consistent with its significantly lower sedimentation coefficient compared to FtsZ, rendering it unsedimentable under the applied centrifugation conditions.

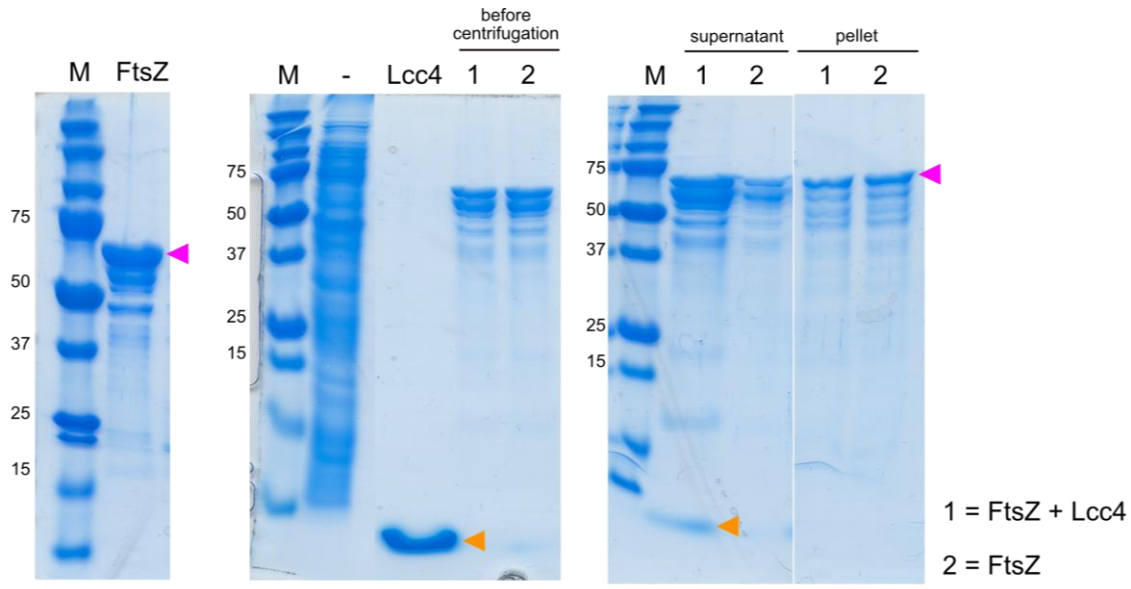

Figure 31: Addition of a Lcc4-derived peptide to FtsZ leads to a change in its polymerization properties. Sedimentation assay in the presence of the Lcc4-derived peptide. FtsZ (indicated in magenta) was incubated for 15 min together with 1 mM GTP, then mixed with the Lcc4 peptide (indicated in orange) and incubated for another 60 min. Alternatively, FtsZ was mixed with the Lcc4 peptide prior to addition of GTP. FtsZ polymers were collected by ultracentrifugation and analysed via SDS page gel electrophoresis. FtsZ and Lcc4 bands are shown from Coomassie-stained gels of supernatant and pellet samples, following sedimentation of FtsZ assembly reactions in the presence of GTP. The peptide inhibits in vitro FtsZ assembly as assayed by sedimentation of bundled FtsZ polymer bundles.

3 Discussion

3.1 Analysis of the *Shewanella* phage λSo

Phages are the most abundant biological entities on Earth and exert a major influence on the dynamics and evolution of their bacterial hosts through their parasitic lifestyle [108,211]. Phage-mediated lysis of bacterial cells is a critical process across all ecosystems, significantly influencing microbial population structures and serving as a key factor in phage fitness [74]. Phage-mediated lysis is a highly regulated and temporally coordinated process that works through three distinct stages in Gram-negative bacteria, which are typically orchestrated by canonical holins or pinholins, endolysins or SAR endolysins, and either the i-spanin/o-spanin complex or the u-spanin [36]. Additional proteins often contribute to the efficiency and regulation of these steps [212–214]. The genes encoding these lysis-related proteins are usually organized in clusters located directly downstream of a single late promoter [202]. However, lysis is not the only critical step in the phage life cycle; the reprogramming of the host cell into a production platform for the assembly of phage particles is equally important. Consequently, a large portion of the phage genome is dedicated to genes encoding proteins involved in this process [185,215]. Notably, some of these proteins are incorporated into the virions themselves, allowing them to exert their function immediately upon infection [216,217].

The model used in this study, *Shewanella phag*e λSo, is an active prophage in *S. oneidensis* MR-1. As a temperate phage with lytic capabilities, λSo can apply significant influence on host cell physiology. Interestingly, it enhances biofilm formation in *S. oneidensis* and actively suppresses the activity of other prophages present within the host genome [189,190,195,198]. The induction of the lytic cycle in λSo is dependent on the host's SOS response and is mediated by the RecA protein. This protein enables the transition from lysogeny to lysis in response to cellular stress or DNA damage through the degradation of the λ CI regulator [218,219].

In this study, the lysis process mediated by phage λSo was examined in detail, leading to the identification of several previously uncharacterised lysis components essential for effective host cell lysis by this phage. Furthermore, a previously uncharacterised protein

from a six-gene cluster encoding small proteins was investigated in greater detail. This protein was found to play a role in modulating host cell division during the early stages of host takeover by the phage.

3.1.1 λSo uses a pinholin-SAR-endolysin lysis pathway

Previous research has demonstrated that λSo significantly influences biofilm formation in *S. oneidensis* MR-1, primarily through cell lysis and the subsequent release of extracellular DNA (eDNA). This eDNA is an important structural component of the biofilm matrix and contributes to its stability [189]. In this study, a genomic region encompassing *SO_2966* to *SO_2974* - originally annotated in *S. oneidensis* MR-1 and predicted to encode, among other genes, a putative holin and lysozyme - was deleted (**Tbl. S1, 2**) [185]. The resulting mutant strains exhibited reduced eDNA release, suggesting that this gene cluster plays a role in λSo-mediated cell lysis and thereby impacts biofilm architecture.

In the course of this study, the genes within this region were subjected to more detailed characterization. Upon closer examination, it became evident that the initial annotation of the holin gene was incorrect. Through homology-based and structural analyses of the gene products encoded by neighbouring loci, the true holin-encoding gene was identified as *SO_2971*, hereafter referred to as λSo holin S (S^{So}) (**Tbl. S2, Fig. S1**). These structural insights further support the hypothesis that the λSo holin functions as a pinholin, given its two transmembrane domains, which are distinct from the three typically found in canonical holins [62,86,220] (**Fig S1**). Due to their distinct structural features, pinholins do not create large, micron-scale lesions in the cytoplasmic membrane as canonical holins do. Instead, they assemble into small, heptameric pores known as pinholes. While these pores are sufficient to dissipate the PMF, they are too small to permit the passage of large enzymes such as endolysins. Consequently, pinholin-mediated lysis relies on a specialized class of endolysins known as SAR-endolysins [85,88,221]. These enzymes are translocated to the periplasm immediately after synthesis but remain inactive in a membrane-bound state. This membrane association is mediated by an N-terminal transmembrane domain that anchors the enzyme to the inner membrane [222]. Upon pinhole formation and subsequent PMF collapse, SAR-endolysins are released from the membrane, undergo conformational activation, and initiate peptidoglycan degradation, ultimately driving cell lysis. Consistent with this mechanism, the putative λSo endolysin, which is

encoded by *SO_2973* and now designated λSo endolysin R (R^{So}), exhibits high homology to known SAR-endolysins and contains an N-terminal signal/transmembrane anchor domain characteristic of this class. Structural analyses and homology-based comparisons therefore support the model that λSo-mediated proton motive force collapse and subsequent cell wall degradation are facilitated by a functional pinholin/SAR-endolysin pair.

Using light and fluorescence microscopy, it was demonstrated that phage-mediated cell lysis was abolished upon deletion of the genes encoding either the holin or the endolysin, despite continued production of phage particles. No plaque-forming, infectious phage could be recovered from the supernatant of liquid cultures lacking these genes. Additionally, membrane depolarization was assessed using $DiBAC_4(3)$, revealing a modest but statistically significant reduction in depolarization following deletion of the holin gene. Given the role of holins in triggering membrane depolarization, a more pronounced effect was anticipated. The relatively subtle change observed may be attributed to the inability to temporally synchronize lysis events across the bacterial population, highlighting the asynchronous nature of phage-induced lysis. In contrast, cells of the strain lacking the endolysin-encoding gene exhibited a significant increase in membrane depolarization. As the initial step of lysis - membrane depolarization mediated by pinholins - can still occur in these cells, the observed increase likely reflects the accumulation of depolarized but structurally intact cells. In the absence of cell wall degradation, these cells do not lyse immediately, allowing the depolarization signal to persist. Notably, in phages encoding SAR-endolysins, such as phage P1, endolysin release and incorrect lysis can occur even without holin-mediated membrane depolarization [35,90]. However, under the conditions tested, no lysis was observed in λSo holin mutants, even after prolonged incubation. Whether this is due to persistent membrane anchoring of the λSo endolysin and a failure to release remains an open question and requires further investigation.

Fluorescence microscopy revealed a clustered, membrane-associated localization pattern for the GFP-tagged holin protein. Numerous small foci were apparent, likely reflecting the inherent tendency of holins to form clusters. Additionally, the appearance of larger foci suggests the possible formation of higher-order aggregates in localized membrane regions. However, these observations should be interpreted with caution, as western blot analysis of the holin-GFP fusion protein revealed degradation products, potentially complicating the assessment of its subcellular distribution. In contrast, the GFP-tagged

endolysin exhibited a uniform membrane-associated localization, consistent with the expected distribution of SAR endolysins within the periplasm, anchored to the cytoplasmic membrane. Nonetheless, the corresponding protein band on the western blot was faint, indicating low expression or instability of the fusion construct. Thus, further optimization of expression and construct design is necessary to ensure accurate interpretation of the localization of the endolysin proteins.

3.1.2 The λSo lysis system requires a two component spanin system

Extensive research over the past two decades has established that the presence of holins and endolysins alone is not sufficient to achieve complete cell lysis. A third component, a protein or protein complex, is required to mediate the final disruption of the outer membrane [93,97,223]. A large proportion of phages utilise so-called spanins, which are phage-encoded lysis proteins essential for breaching the outer membrane barrier [101]. Known spanins exist as either single- or two-component systems that all share the common feature of interacting with the outer membrane via a lipid anchor [102]. In Gram-negative bacteria, this is typically achieved through a signal sequence followed by one or more cysteine residues, to which the lipid moiety is covalently attached [224,225]. In addition, spanins often possess a C-terminal transmembrane domain, effectively linking the inner and outer membranes and providing the structural framework required to mediate membrane fusion during the final step of lysis [104].

In *E. coli* phage λ, the genes encoding Rz (i-spanin) and Rz1 (o-spanin) are intimately nested [34,92]. This spanin complex is composed of a dimer consisting of i-spanin and o-spanin dimers [102,103]. The biological activity of this complex depends on cysteine residues at positions 152 and 29 in the i-spanin and o-spanin, respectively. These cysteines mediate homotypic, homodimeric interactions - i.e., i-spanin with i-spanin and o-spanin with o-spanin, rather than forming a heterodimeric complex between i-spanin and o-spanin [94,100]. This specific mode of interaction is essential for proper spanin function and successful completion of the final step of phage-mediated lysis, which involves disruption of the outer membrane [102,103].

In the initial annotation of *S. oneidensis* MR-1, no gene resembling that of a spanin was identified, as the primary amino acid sequences of the genes within the putative lysis cluster lacked detectable similarity to known spanins. However, using a candidate-based approach

focused on predicted 3D protein structures rather than primary sequence homology, a spanin system was identified [226]. This system comprises the inner membrane component Rz^{So} and the outer membrane component $Rz1^{So}$. Notably, as in *E. coli* phage λ, the genes encoding Rz^{So} and $Rz1^{So}$ are nested, with *rz1*^{So} initiating within the 3′-end of *rz*^{So} and extending toward the gene encoding the pinholin S^{So}. This genomic arrangement spans a region previously annotated as non-coding and suggests that these four genes, encoding holin (S^{So}), endolysin (R^{So}), and the spanin pair (Rz^{So}/$Rz1^{So}$), form a single, continuous lysis operon.

Protein structure predictions generated by AlphaFold2 further support this identification. The predicted structure of Rz^{So} reveals a long α-helix anchored at the N-terminus in the cytoplasmic membrane, followed by a bend and a shorter second α-helix (**Fig. S1**). This structural configuration is strikingly similar to that of the canonical two-component spanin system of *E. coli* phage λ, reinforcing the functional assignment of Rz^{So}/$Rz1^{So}$ as a λSo spanin complex. Additionally, Rz^{So} contains a stretch of residues near its C-terminus that lacks a defined secondary structure. Within this unstructured region, cysteine residues at positions 139 and 150 may facilitate *in vivo* dimerization through disulfide bond formation, potentially contributing to spanin complex assembly and stability. In the case of $Rz1^{So}$, the mature protein begins - following removal of the signal peptide - with a conserved N-terminal cysteine likely involved in lipid modification for outer membrane anchoring. This is followed by an unstructured region and a distinctive C-terminal α-helix, a feature absent in the Rz1 of *E. coli* λ. Notably, unlike $Rz1^{Ec}$, which contains a proline-rich segment critical for membrane fusion, $Rz1^{So}$ lacks such a motif. However, it contains two cysteine residues at positions 47 and 74, suggesting the potential for homodimerization, in contrast to the single cysteine present in $Rz1^{Ec}$. Thus, while the general mechanism of membrane fusion is likely conserved between the two systems, the domains and residues of λSo required for spanin complex formation are different from known spanin proteins.

Microscopic analysis revealed a distinct phenotype associated with deletion of the putative spanin genes: upon induction of λSo, cells lacking these genes failed to undergo complete lysis and instead formed spheroplast-like structures. This phenotype can be attributed to the function of pinholins, which disrupt the proton motive force and lead to the formation of pinholes, thereby triggering the release of SAR-endolysins that degrade the peptidoglycan layer. However, in the absence of spanins, fusion of the inner and outer

membranes is impeded, and the intact outer membrane is mostly sufficient to preserve cellular integrity, preventing regular, full lysis. This distinctive phenotype is particularly pronounced under outer membrane-stabilizing conditions, such as in the presence of divalent cations like Mg^{2+}, which further support the integrity of the outer membrane and make the formation of spheroplasts readily observable. Supporting this, membrane depolarization assays indicated that both holin and endolysin remain functional in these cells. The slightly reduced depolarization signal observed in the Δ*rz*^{So} strain, compared to the Δ*r*^{So} strain, may be due to the increased fragility of the spanin-deficient cells, potentially leading to partial cell loss during measurement and an under evaluation of the depolarization signal.

In silico analyses using AlphaFold2 predicted that Rz^{So} and Rz1^{So}, similar to the spanins of *E. coli* phage λ [102], likely form a dimer composed of homodimers. To experimentally assess this predicted interaction, targeted amino acid substitutions were introduced into Rz^{So} and Rz1^{So}. These modified proteins were then expressed ectopically from a pBBR1-based plasmid under the control of the putative lysis cluster promoter in a Δ*rz*^{So}+*rz1*^{So} background strain, as genomic modification of the spanin genes proved technically challenging (**Fig. S7**). Substitutions introduced within the predicted interaction interface of the spanin proteins revealed that residues N129 and C139 in Rz^{So}, as well as S54 and C74 in Rz1^{So}, play critical roles in the stability of the oligomeric complex. Under outer membrane-stabilizing conditions, substitutions at S54 and C74 in Rz1^{So} abolished cell lysis entirely, showing a phenotype closely resembling that of the Δ*rz*^{So}+*rz1*^{So} mutant. This indicates that these mutations likely disrupt spanin function completely. For other substitution variants, plaque formation was still observed, although at significantly reduced levels compared to the wild type strain, suggesting a partial impairment of spanin functionality. Residues C139 in Rz^{So} and C74 in Rz1^{So} may therefore represent functional homologs of the cysteine residues found in *E. coli* Rz and Rz1, which are essential for the dimer-dimer interactions required to form the functional spanin dimer. The interaction that ultimately leads to phage-mediated cell lysis thus appears to be mediated primarily by the cysteines in the respective C-termini of the proteins. It is assumed that the complex of spanins undergoes a conformational change after the degradation of the peptidoglycan and the following release of the complex, which may result in a folding of the Rz^{So} dimers and thereby providing the necessary free energy [104].

This process then brings the inner and outer membranes into close proximity, facilitating their fusion (**Fig. 32**).

However, under standard conditions, the plaque-forming units (PFU) of the mutants used in the experiment to obtain this data more closely resembled those of the $\Delta rz^{So}+rz1^{So}$ background than the wild type, warranting cautious interpretation of these results. Further optimization of the experimental setup is required to confirm the functional relevance of these substitutions.

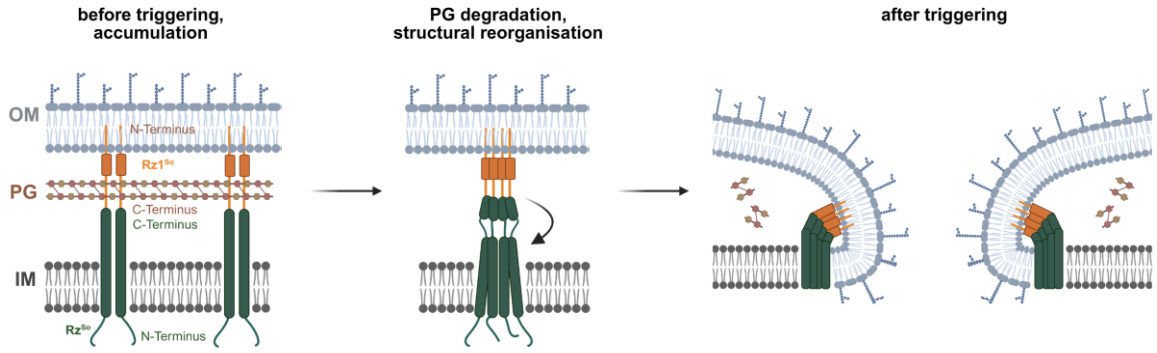

Figure 32: Schematic representation of the function of the λSo spanin complex. The i-spanin is anchored in the inner membrane via an N-terminal transmembrane domain (dark green) and extends into the periplasm. The o-spanin is bound to the inner leaflet of the outer membrane and features a periplasmic segment (orange). The i- and o-spanins associate via their C-terminal regions across the peptidoglycan layer. In the event of PG degradation, the spanin proteins oligomerize into a dimer of dimers. It is hypothesised that this complex will undergo a conformational change, which will result in a reorganisation of the complex. It is the final step in phage-mediated lysis that brings the IM and OM together, resulting in their fusion.

Although the lysis mechanism characterised here appears to differ from that of *E. coli* phage λ, the core lysis proteins are functionally conserved - emphasizing the principle that structure dictates function. Accordingly, the lysis system from *S. oneidensis* phage λSo is fully functional in other Gram-negative bacteria such as *E.coli* as well.

3.1.3 The λSo holin encodes its own inhibitor

Several holin systems, including both canonical holins and pinholins, have been extensively characterised. A well-studied example is the pinholin of phage ϕ21, encoded by the s^{21} gene. This gene possesses a unique feature: it contains two translation start sites

(positions 23 and 32), resulting in the production of two isoforms, called $S^{21}71$, the full-length pinholin, and $S^{21}68$, a slightly truncated variant lacking three N-terminal residues [83,84,221]. Both isoforms contain two transmembrane domains (TMs), with TM1 functioning as a regulatory domain and TM2 forming the pore structure. The shorter isoform, $S^{21}68$, acts as the active lysis effector. Its TM1 can be externalized into the periplasm upon triggering, facilitating the assembly of monoheptameric pinholes that enable proton leakage and membrane depolarization. In contrast, $S^{21}71$ possesses an additional positively charged residue on the cytoplasmic side of the N-terminus, which inhibits TM1 externalization. As a result, $S^{21}71$ functions as an antiholin by forming inactive membrane-embedded heterodimers with $S^{21}68$ [221,227,228]. Upon disruption of the PMF, the antiholin can undergo a conformational reorganization, enabling it to transition into an active holin form. This structural shift allows the formation of functional holin-holin pairs, contributing to the assembly of pore complexes and the progression of membrane depolarization and lysis. The balance and temporal accumulation of the two isoforms regulate the precise timing of lysis initiation.

Given that the gene encoding the λSo pinholin contains not one but two alternative translational start sites, it was hypothesized that this could give rise to three isoforms: the full-length $S^{So}89$, as well as the shorter variants $S^{So}82$ and $S^{So}80$. Notably, $S^{So}89$, like $S^{21}71$ from phage ϕ21, contains an additional positively charged lysine residue at position 4 near its N-terminus (**Fig. 33**). Based on this similarity, it was proposed that $S^{So}89$ may function as an antiholin, potentially regulating lysis timing by inhibiting one or both of the shorter, active isoforms through the formation of non-functional heterodimers. To experimentally validate this hypothesis, targeted truncations of the s^{So} gene were constructed to enable the controlled expression of individual isoforms. Additionally, site-directed mutagenesis was used to substitute the lysine residue at position 4 in the full-length $S^{So}89$ isoform. This modification aimed to determine whether this positively charged residue is critical for the proposed antiholin function.

Light microscopy analysis revealed that strains expressing the $S^{So}82$ variant of the holin gene exhibited premature cell lysis compared to the control, indicating enhanced pinholin activity. A similar lysis phenotype was observed in the strain where lysine at position 4 of the full-length $S^{So}89$ isoform was substituted with asparagine, supporting the role of this residue in antiholin function. In contrast, no detectable lysis occurred in cells expressing only the $S^{So}80$ isoform, a phenotype comparable to that of the Δs^{So} deletion

strain. These findings strongly suggest that the isoform encoded by $S^{So}82$ functions as the active holin. Deletion of the first eight amino acids appears to prevent the formation of antiholin/holin heterodimers, allowing only holin-holin homodimerization. This unimpeded assembly likely promotes the formation of holin aggregates and subsequent pore formation, thereby eliminating the regulatory delay normally imposed by the antiholin. The current findings also support the hypothesis that substitution of lysine at position 4 in the full-length $S^{So}89$ isoform (K4N) results in a complete loss of antipinholin function, as evidenced by significantly accelerated cell lysis. TMD1, the first transmembrane domain of $S^{So}89$, is normally anchored in the membrane by this positively charged lysine at the cytoplasmic end of the N-terminus (**Fig. 33**). Removal of this charge, as in the K4N variant, likely facilitates the extrusion of TMD1 into the periplasm, thereby enabling premature pinhole formation and initiating lysis earlier than in the wild type. Under normal conditions, the antipinholin delays this conformational change, thereby regulating the timing of lysis.

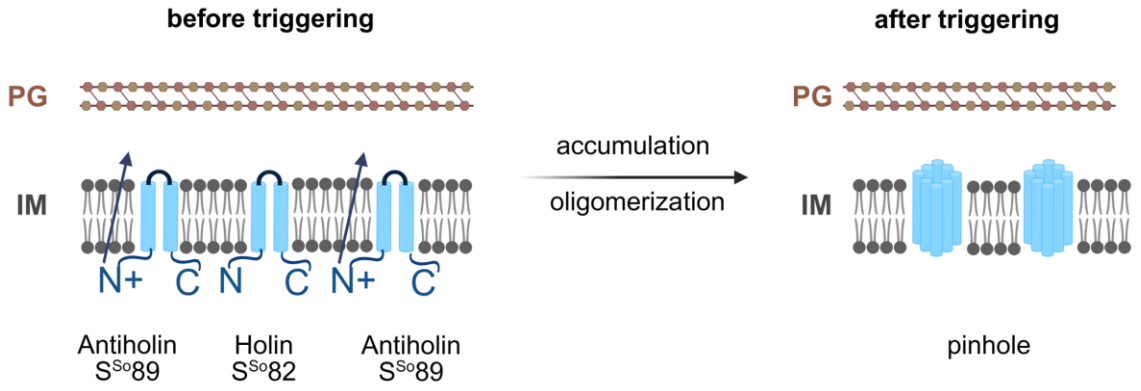

Figure 33: Schematic representation of the membrane topologies of the holin and antiholin proteins of λSo. The pinholin $S^{So}82$ consists of two transmembrane α-helices with both N- and C-termini located in the cytoplasm (N-in, C-in orientation). It is negatively regulated by the antiholin $S^{So}89$ at a possible ratio of 2.5:1. At the moment of triggering, the first transmembrane domain of $S^{So}89$ exits the membrane and relocates to the periplasm (dark blue arrow), resulting in the assembly of small, heptameric pinholes in the membrane.

These results demonstrate that in λSo, both the active holin and its inhibitor, the antipinholin, are encoded within a single gene via alternative translation start sites. To determine the functional ratio of holin to antipinholin required for proper lysis timing, additional experiments are needed. Based on analogous systems, such as the spanin

complex in *E.coli* phage λ, a ratio of approximately 2.5:1 may be optimal for controlled lysis [97,102,103].

3.1.4 λSo lysis requires at least two more proteins for sufficient lysis

Several publications have demonstrated that the lysis systems of certain bacteriophages exhibit a complexity that extends well beyond the canonical components responsible for membrane depolarisation, peptidoglycan degradation, and membrane fusion [229,230]. Although the lysis system of *S. oneidensis* MR-1, comprising holin, endolysin, and the spanin complex, is sufficient to induce cell lysis when expressed in *E. coli*, evidence suggests that in its native host, *S. oneidensis*, additional proteins may be required to ensure a correctly timed and efficient lysis process. In the course of this study, two additional proteins were identified that play a critical role in the phage-mediated lysis process of λSo.

RNA-seq analysis was carried out using samples following induction of the λSo lytic cycle. This identified a previously uncharacterised protein, Lcc6, which appears to play a critical role in phage-mediated lysis and overall phage fitness (unpublished). Deletion of the *lcc6* gene led to a marked reduction in lytic activity, whereas ectopic overexpression of Lcc6 in the absence of phage induction had no discernible impact on cell morphology or growth. These findings indicate that Lcc6 is not a standalone lytic factor but likely functions together with other λSo-encoded proteins. Despite its functional relevance, no direct interactions between Lcc6 and canonical lysis proteins (holin, endolysin, spanin) could be detected. Notably, *lcc6* is among the most highly expressed genes following induction and encodes a 65-amino-acid protein with a predicted N-terminal transmembrane domain. Its expression starts well before that of the holin protein, and membrane depolarisation profiles in Δ*lcc6* strains mirror those observed in Δs^{So} strains, pointing to a role of Lcc6 in the early stages of lysis. Moreover, the absence of cell rounding in Δ*lcc6* strains following phage induction suggests that Lcc6 does not participate in the spanin-mediated membrane fusion step, further supporting its function upstream of this terminal phase of lysis. Lcc6 may play a role in initiating pinholin assembly, potentially by promoting antiholin removal or directly facilitating pore complex formation. However, direct experimental evidence supporting such a mechanism is currently lacking, and the precise impact of Lcc6 on the timing and progression of cell lysis remains to be clarified.

Another protein was identified through detailed characterisation of the genes comprising the λSo lysis cluster. The gene product of *SO_2970* appears to play a role in efficient cell lysis, as deletion of this gene led to a significant reduction in the lysis rate: in contrast to wild-type cells, only approximately 19% of observed cells underwent lysis in the Δ*SO_2970* strain following λSo induction. Furthermore, no cell rounding was observed following induction of λ Δ*SO_2970*, suggesting that the deletion of *SO_2970* disrupts the lysis process at an earlier stage. The gene *SO_2970* encodes a 119 amino-acid cytoplasmic protein. While its exact role in phage-mediated lysis remains unclear, its involvement is evident, and further investigation will be required to elucidate the mechanism of action.

3.1.5 Conclusion

Prior to the actual triggering event during the late phase of λSo gene expression, the pinholins (S^{So}), classified as class II holins with two transmembrane domains and an N-in, C-in topology, accumulate in the cytoplasmic membrane in an inactive state alongside their corresponding antiholins. The antiholins share structural similarity with the holin proteins but possess an additional positively charged residue at the N-terminus, which stabilises TMD1 within the membrane and thereby prevents premature activation. By forming heterodimers with holins, antiholins play a fundamental role in ensuring precise timing of lysis. Simultaneously, SAR endolysins (R^{So}) are transported into the periplasm, where they remain membrane-anchored in an inactive state. The spanin complex, which consists of the i-spanins (Rz^{So}) and the o-spanins ($Rz1^{So}$), also accumulates harmlessly in the periplasm, where its components are restrained by the intact peptidoglycan layer. In parallel, two additional phage proteins - Lcc6, a membrane-bound protein with an N-terminal transmembrane domain, and gene product (GP) 2970, a cytoplasmic protein - also accumulate in their respective compartments, potentially contributing to the early stages of the lysis process (**Fig. 34A**).

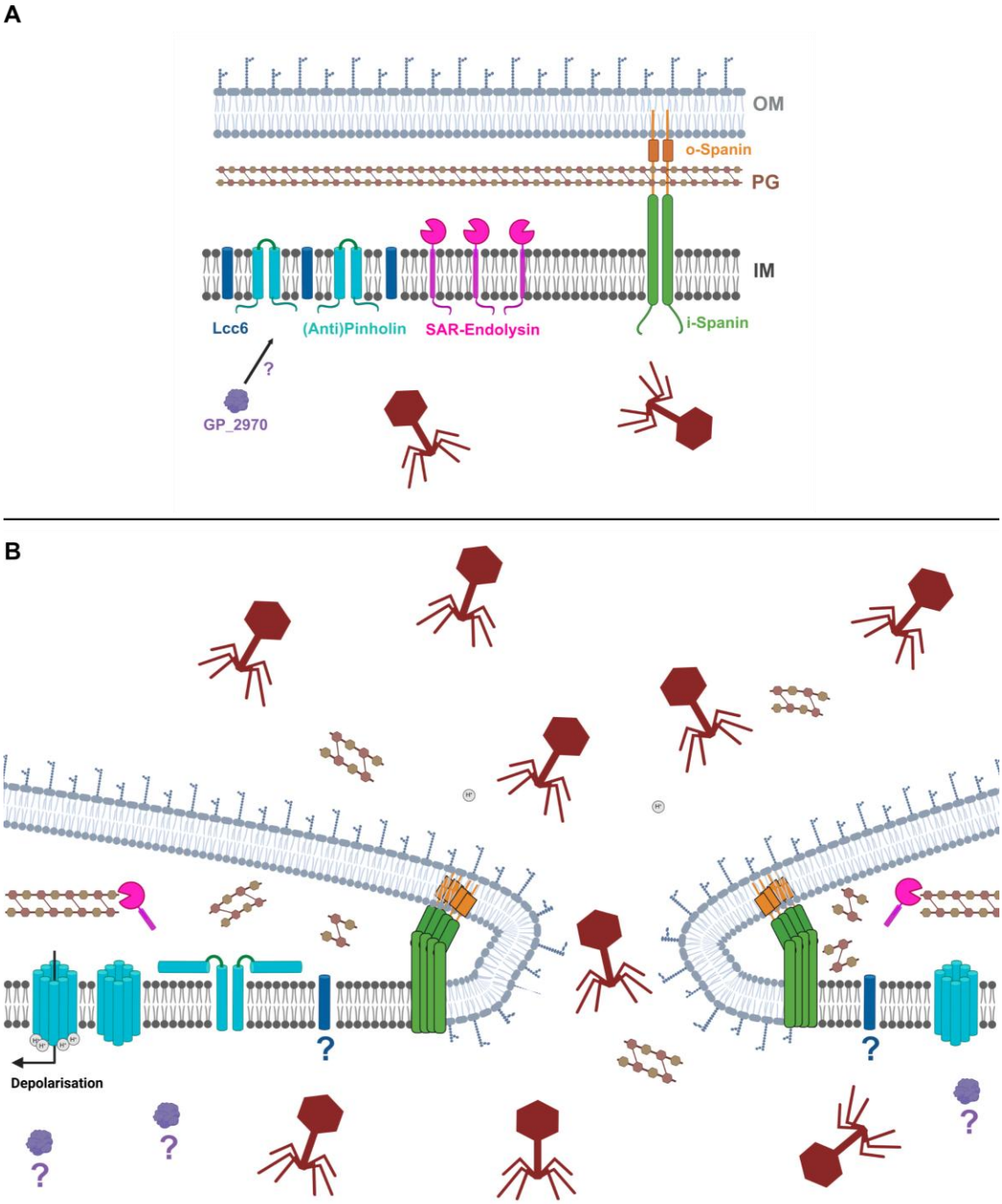

Figure 34: Cartoon model of λSo mediated phage lysis of its host *Shewanella oneidensis* MR-1. (**A**) In the late phase of the lytic cycle, lysis proteins accumulate in their respective compartments: pinholin-antiholin heterodimers localise in the inner membrane; SAR endolysin is tethered to the membrane in the periplasm; and the spanin complex accumulates but remains inactive due to the intact peptidoglycan. The accessory proteins Lcc6 (membrane-bound) and GP2970 (cytoplasmic) also accumulate. (**B**) Holin activation, triggered by PMF collapse, forms pinholes that release SAR endolysin into the periplasm, where it becomes enzymatically active and degrades peptidoglycan. This degradation activates spanin-mediated fusion of the inner and outer membranes, allowing phage progeny release. Lcc6 and GP2970 are essential for efficient lysis, though their precise roles remain to be elucidated.

A trigger event, which is typically the collapse of the proton motive force upon reaching an allele-specific threshold concentration of holins, induces a topological rearrangement of the first transmembrane domain of the pinholin. This restructuring converts previously inactive holin-antiholin heterodimers into fully active holin molecules, as activation requires the translocation of both TMD1 domains from the bilayer. While the precise mechanism remains unresolved, the membrane-associated phage protein Lcc6 may facilitate this transition. Similarly, the cytoplasmic protein encoded by *SO_2970* could also contribute to this early lysis step. The holins then reorganise into two-dimensional aggregates that form small membrane disruptions known as pinholes, typically less than 2 nm in diameter. The dissipation of the PMF simultaneously triggers the release of SAR endolysins from the inner membrane, where they fold into their catalytically active forms and initiate peptidoglycan degradation. As the peptidoglycan layer is dismantled, the spanin complex reorganises into functional dimer of dimers. This structural rearrangement promotes the fusion of the inner and outer membranes, completing the lysis process and allowing phage progeny to be released from the host cell to initiate new infections (**Fig. 34B**).

The lysis system of λSo shares key features with the well-characterised pinholin-SAR-endolysin pathway of phage ϕ21; however, it also includes novel components that appear to be critical for efficient phage-mediated lysis in its native host, *S. oneidensis* MR-1. Further in-depth investigation is required to elucidate the specific roles of these additional factors and to gain a more comprehensive understanding of the molecular mechanisms underlying this complex lysis process.

3.2 Identification of novel host effector proteins in λSo

Bacterial cell division is a critical and highly regulated phase in the cellular life cycle, requiring the coordinated duplication and segregation of the genome, as well as the controlled remodelling of the cell envelope [126,141,231–233]. The cell's shape and mechanical integrity are determined by the peptidoglycan cell wall, which surrounds the cytoplasmic membrane and protects the cell from osmotic lysis due to high internal turgor pressure [234,235]. To divide successfully, the cell must not only accurately identify the division site and recruit essential division proteins, but also initiate and tightly regulate peptidoglycan synthesis at this location [236]. In most bacteria, the spatial organisation of the

division machinery, which is commonly referred to as the divisome, is orchestrated by FtsZ. FtsZ is a tubulin-like GTPase that serves as the bacterial counterpart to the eukaryotic tubulin [134]. FtsZ polymerises into a dynamic ring structure at the respective division site, known as the Z-ring, where it serves as a scaffold for the recruitment of downstream division proteins and coordinates the progression of cytokinesis [127].

To secure resources exclusively for themselves, prevent daughter cell formation, and create space for accumulating phage progeny, many bacteriophages produce specific proteins that interfere with the tightly regulated process of bacterial cell division [210]. This interference typically results in filamentation and ultimately cell death. For instance, the Kil protein of phage λ in *E. coli* interacts directly with FtsZ, inhibiting its protofilament formation in a ZipA-dependent manner [116,117]. Similarly, GP0.4 of phage T7 disrupts cell division by binding to FtsZ and preventing its polymerisation into functional protofilaments [120,237].

3.2.1 λSo protein Lcc4 inhibits the cell division machinery

Analysis of the λSo genome revealed the presence of three distinct gene clusters, named clusters A, B, and C, which encode proteins of unknown function [198]. RNA-seq data showed that genes within cluster C are among the most highly expressed immediately following induction of the λSo lytic cycle (unpublished). This cluster is made up of six genes (*lcc1* - *lcc6*), all of which encode small proteins with no identifiable homology to any known protein domains, leaving their functions currently uncharacterised.

In this study, it was demonstrated that one gene from cluster C, *lcc4*, encodes a protein that interferes with the host cell cycle and thereby contributes significantly to phage fitness. Lcc4 is a 91 amino acid protein predicted to be a transmembrane protein, and possibly adopting an N-in/C -in membrane topology. Deletion of *lcc4* alone does not produce any discernible effect on phage infectivity, indicating that this gene is not essential for successful infection under the tested conditions (**Fig. 16A**). When *lcc4* was ectopically expressed from a plasmid in a strain lacking the λSo prophage, the cells exhibited a pronounced filamentation phenotype: instead of the average length of 2-3 µm, the cells elongated to an average of 5-7 µm. Additionally, Lcc4 expression was associated with markedly reduced cellular growth. These findings support the hypothesis

that Lcc4 disrupts normal cell division, likely by interfering with the divisome and thereby preventing proper cytokinesis, which causes unchecked elongation. To enable functional investigation of Lcc4 in the subsequent course of the study, a recombinant variant of the protein carrying a FLAG tag was expressed. However, following induction, only minimal filamentation was observed. Numerous other recombinant protein versions were investigated, but any modification of the protein resulted in a loss of the corresponding phenotype (data not shown). This suggests that even small affinity tags may disrupt Lcc4 function: potentially by interfering with binding interfaces for interaction partners or by altering the protein's structural conformation in a manner that impairs its activity.

It was also determined that the protein Lcc4, along with all proteins encoded by the cluster C genes, exhibit host-specific functionality in *S. oneidensis* MR-1 infected by λSo. When ectopically expressed from a plasmid in *E. coli*, these proteins fail to induce any observable change in cell length, indicating their activity is restricted to the native host context. Structural comparison of FtsZ from *S. oneidensis* and *E. coli* reveals a sequence identity of approximately 71%; however, the residues predicted to mediate the interaction between FtsZ and Lcc4 in *S. oneidensis* are not conserved in the *E. coli* homolog. This lack of conservation at the putative interaction interface likely impairs the ability of Lcc4 to associate functionally with *E. coli* FtsZ. Consequently, this may explain why ectopic expression of recombinant Lcc4 in *E. coli* does not result in a filamentation phenotype, underlining the importance of the specific amino acid identities at the interaction site for mediating functional effects.

It was further demonstrated that cell filamentation in *S. oneidensis* MR-1 upon ectopic expression of Lcc4 is independent of the cell division inhibitor SulA and, by extension, largely independent of the SOS response - aside from its role in phage λSo induction. A deletion of the *sulA* gene had no detectable impact on the filamentation phenotype. Cells expressing Lcc4 in the *sulA*-deficient background displayed elongation comparable to that observed in the wild type control strain. These results indicate that the Lcc4-induced block in cell division operates via a SulA-independent mechanism.

Given the pronounced cell elongation observed upon plasmid-based expression of Lcc4, a potential interference with the bacterial cell division machinery was hypothesized. To explore this, structural predictions were performed using AlphaFold2. This analysis focused on potential interactions between Lcc4 and key division proteins. The results

obtained suggested possible interactions between Lcc4 and the proteins FtsZ and ZipA. The predicted complex structures were further examined using PyMOL, enabling the identification of putative interaction interfaces. Guided by these models, recombinant Lcc4 variants were generated, in which selected amino acids at the predicted interfaces with FtsZ or ZipA were substituted. The substitutions were designed to be as conservative as possible to minimize alterations to preserve overall protein integrity. The advantage of employing conservative amino acid substitutions lies in preserving the electrostatic environment and maintaining structural similarity between residues, thereby minimizing disruptions to protein folding [204,238,239]. This strategy allows for subtle perturbations rather than complete disruption of the system, enabling a more precise investigation into which molecular features of a residue, such as charge, size, or polarity, are critical for function. Using this approach, it was determined that residues isoleucine at position 16 and 19 in Lcc4 are important for interaction with FtsZ, while arginine at position 84 and tryptophane at position 80 are involved in the interaction with ZipA. Isoleucine residues are commonly enriched at protein-protein interfaces, where they contribute to the formation of a hydrophobic core that excludes water molecules and stabilises the interaction predominantly through van der Waals forces. Arginine, on the other hand, often mediates electrostatic interactions or forms salt bridges at the interface, particularly in the presence of oppositely charged residues. Tryptophan can further contribute to interface stability through aromatic stacking interactions or by engaging with the protein backbone via its indole ring, and thereby enhancing binding specificity and affinity. At the established positions, the specific identity of the amino acids appears to be critical: evidenced not only by the absence of a filamentation phenotype in this experimental setup, but also by the fact that these residues are not conserved in *E. coli* FtsZ. This dual observation provides further support for the hypothesis that these particular residues constitute part of the functional interaction surface between Lcc4 and FtsZ in *S. oneidensis* MR-1.

In following experiments, other residues predicted to contribute to these interactions, but which did not show functional relevance under conservative substitutions, could be subjected to more disruptive mutations, such as charge-altering substitutions. This approach could assess whether electrostatic properties rather than side-chain identity drive the interaction.

To investigate the potential impact of Lcc4 on the subcellular localisation of FtsZ based on the predicted interaction between the two proteins, the spatial behaviour of FtsZ was analysed in the presence of ectopically expressed Lcc4. For this purpose, a fluorescently tagged variant of FtsZ was expressed from a plasmid in a background strain that retained the native *ftsZ* gene. This ensured that both native and tagged FtsZ were present, allowing normal divisome function to be largely preserved while enabling visualisation of FtsZ ring formation. Lcc4 was expressed from a separate plasmid under an inducible promoter to allow independent control of its expression. Microscopic analysis revealed that Lcc4 significantly alters the localisation pattern of FtsZ. In the presence of Lcc4, FtsZ no longer formed well-defined rings at the midcell as it was observed in the control strain. Instead, FtsZ exhibited either a diffuse cytoplasmic distribution or appeared as abnormally localised rings outside of the division plane. This disruption could be attributed to direct interference by Lcc4 with FtsZ polymerisation dynamics. This would be analogous to the action of the Kil protein from bacteriophage λ, which inhibits cell division in *E. coli* by targeting FtsZ [116,117]. Alternatively, the observed delocalisation of FtsZ may result from an interaction between Lcc4 and ZipA, potentially impairing the membrane anchoring and spatial stabilisation of the FtsZ ring. ZipA plays a central role in tethering FtsZ filaments to the cytoplasmic membrane and maintaining their correct positioning at midcell [139,140]. Disruption of ZipA function by Lcc4 would therefore compromise the structural integrity of the divisome, leading to the formation of mislocalised or unstable Z-Rings. While FtsZ is still able to polymerise and associate with the membrane in the absence of ZipA primarily through interaction with FtsA, these alternative assemblies lack full stability and functional coordination [136]. As a consequence, recruitment of essential downstream division proteins is hindered, resulting in a failure of septum formation and ultimately in a characteristic filamentous phenotype [149,240–242]. In the present study, microscopy revealed both extensive filamentation and the presence of correctly positioned as well as atypically localised Z-Rings upon Lcc4 expression. These observations are strongly pointing to an inhibitory effect of Lcc4 on ZipA function. Both mechanisms remain plausible and may contribute to the perturbation of cell division observed upon Lcc4 expression. To conclusively determine the molecular mechanism by which Lcc4 affects FtsZ dynamics - whether through direct interaction, ZipA inhibition or an alternative pathway - further targeted experiments will be necessary.

Recombinant FtsZ was purified to facilitate subsequent experiments such as interaction assays, as purification of Lcc4 was not possible due to its loss of function when fused to affinity tags. For FtsZ, a strategy employing a C-terminal hexa-histidine tag in combination with a SUMO (Small Ubiquitin-like Modifier) fusion system was used. The SUMO tag is known to enhance the solubility and proper folding of recombinant proteins in heterologous expression systems [209]. Importantly, cleavage at the SUMO-specific protease site leaves no additional residues on the target protein, thereby yielding native FtsZ in its unmodified form, which is essential for maintaining its functional integrity in downstream applications [243]. The bands observed in the first elution fraction of the size exclusion chromatography that do not correspond to the expected molecular weight of the target protein are likely due to protein aggregates and aggregated degradation products. This interpretation is supported by the presence of both bands at the expected molecular weight and additional bands corresponding to significantly smaller polypeptides (**Fig. S10**). Notably, this fraction eluted well before the anticipated elution volume for proteins with molecular weights of approximately 54 or 40 kDa, indicating the presence of high-molecular-weight species. The following sample preparation for SDS-PAGE, which includes denaturation, likely dissociated these aggregates into their individual components, thereby revealing a mixture of intact protein and degradation products on the gel. These findings are consistent with aggregation-related behaviour commonly observed during recombinant protein expression and purification.

A synthetic peptide consisting of the first 26 amino acids of Lcc4 was ordered from GenScript Biotech (Netherlands) BV to allow experiments with purified recombinant FtsZ that specifically assess its interaction with Lcc4. This N-terminal region of Lcc4 was selected based on structural predictions which indicate that this part of the protein mediates the interaction with FtsZ. By using this defined peptide segment, it was possible to isolate and examine the interaction independently of the full-length Lcc4 protein, whose purification is impossible due to a loss of function upon tagging.

The Kil protein encoded by bacteriophage λ inhibits the formation of FtsZ protofilaments through a direct interaction with FtsZ in a ZipA-dependent manner. This interference leads to the generation of multiple oligomeric FtsZ species of varying sizes. All of these oligomers are consistently smaller than the characteristic 15S species corresponding to the narrow distribution of FtsZ-GTP protofilaments typically observed in the absence of Kil [118]. Accordingly, recombinant FtsZ and the synthetic Lcc4 peptide were subjected to a

filamentation assay adapted from the protocol established by Corrales-Guerrero et al., with the aim of investigating the polymerisation dynamics of FtsZ in the presence of GTP and/or Lcc4 [244]. This approach was chosen to assess whether Lcc4 influences FtsZ filament formation under defined in vitro conditions. Equimolar concentrations of the proteins were combined in an appropriate buffer systems. This step was followed by incubation under defined conditions after the addition of the respective components. To assess filament formation, the samples were subsequently ultracentrifuged to separate polymerised FtsZ (pellet) from the unpolymerized fraction (supernatant). The analysis revealed a marked shift in FtsZ distribution upon addition of Lcc4: a higher proportion of FtsZ was retained in the supernatant compared to the control condition characterised by GTP addition alone. This observation indicates that Lcc4 interferes with FtsZ polymerisation, likely by impairing filament formation, and thereby reduces the extent of FtsZ filamentation under the tested conditions. As FtsZ is known to form protofilaments *in vitro* upon the addition of GTP, it was anticipated that in the control, the majority of FtsZ would sediment during ultracentrifugation with little to no protein remaining in the supernatant [131,245–247]. However, this expected distribution was not observed. One possible explanation lies in the intrinsic dynamic instability of FtsZ polymers, which has been shown to be Ca^{2+}-dependent *in vitro* [248]. This dynamic behaviour may contribute to incomplete or unstable polymer formation under the given conditions. Nonetheless, the experimental procedure calls for further optimisation, particularly with respect to buffer composition, as polymerisation efficiency and filament stability are influenced by factors such as Ca^{2+} concentration and pH. Additionally, enhancing the purity of the recombinant FtsZ protein may reduce variability and improve interpretability. The current results must therefore be interpreted with caution and verified under refined experimental conditions.

3.2.2 Conclusion

Following infection of *S. oneidensis* MR-1 by phage λSo or upon induction of the lytic cycle, the phage initiates a coordinated takeover of various host cellular processes to optimise conditions for viral replication. Among the phage-encoded factors involved in this process is Lcc4, a transmembrane protein that interferes with the host cell's divisome machinery, thereby disrupting normal cell division. As a result, the infected host cell undergoes extensive filamentation, continuing to grow in length without dividing. This filamentous state benefits the phage by maximising intracellular space for virion

assembly, preventing the formation of uninfected daughter cells and allowing more efficient exploitation of the host's metabolic resources.

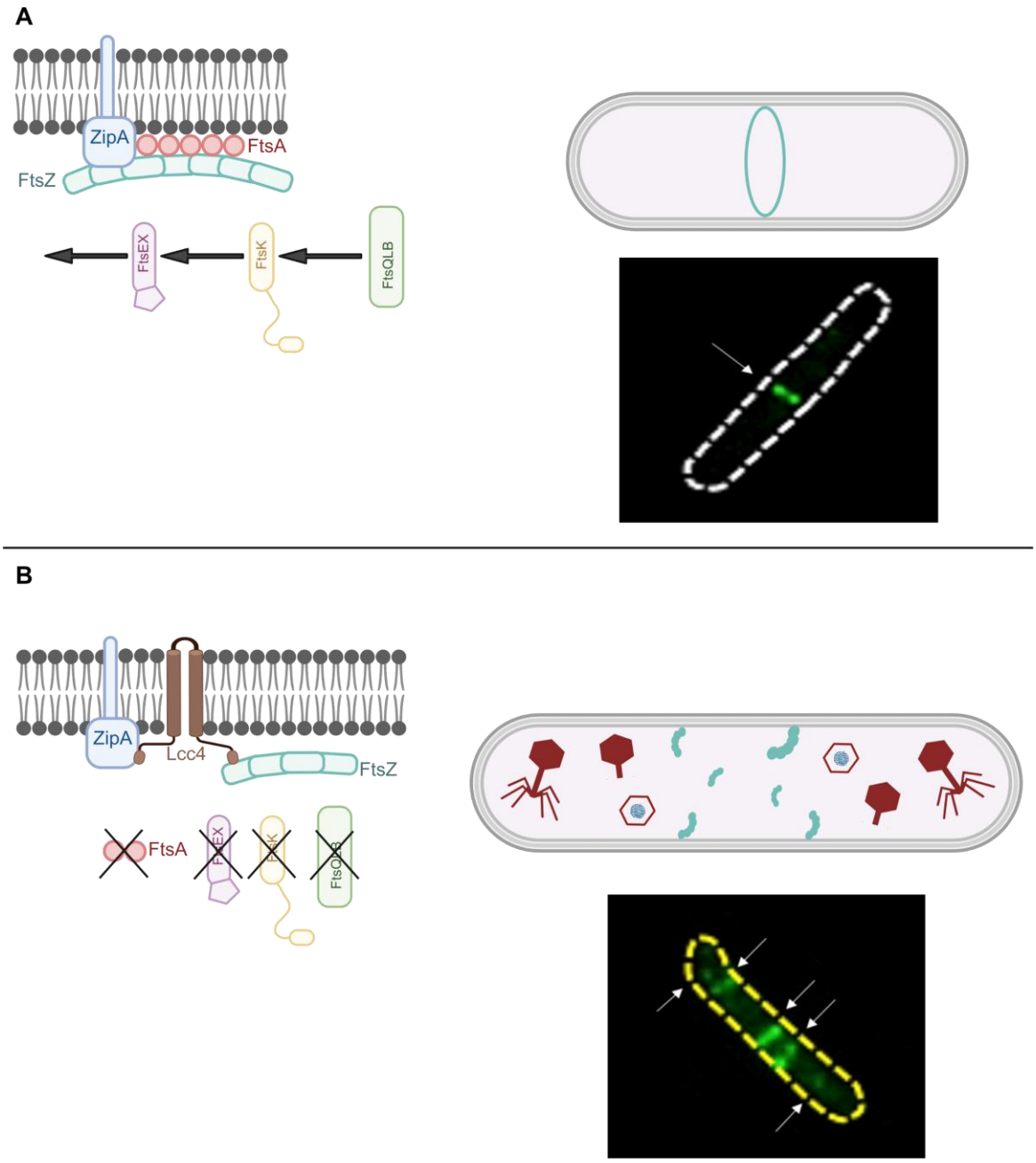

Figure 35: Lcc4 blocks cell division. Proposed model of Lcc4-mediated inhibition of cell division. As a highly expressed cluster C gene product post-λSo induction, Lcc4 localizes to the membrane, potentially at midcell, where it disrupts FtsZ ring formation. Fluorescence microscopy reveals diffuse and mispositioned FtsZ structures, suggesting impaired ring closure. This effect likely arises from direct interaction with FtsZ and interference with FtsZ-ZipA binding.

The precise molecular mechanism by which Lcc4 interferes with bacterial cell division remains to be fully understood. However, the findings in this study suggest that Lcc4 interacts with the key divisome components FtsZ and ZipA. Specifically, isoleucine residues at positions 16 and 19 appear to be critical for the interaction with FtsZ, while arginine at position 84 and tryptophan at position 80 are essential for the interaction with ZipA. The structural integrity of Lcc4 is evidently crucial for its function, as even minor modifications, such as the addition of affinity tags, abolish the characteristic filamentation phenotype. Despite a 71% sequence identity between the FtsZ proteins of *S. oneidensis* MR-1 and *E. coli*, no cell elongation phenotype is observed in *E. coli* upon ectopic expression of recombinant Lcc4. This suggests that specific, non-conserved residues are required for a functional interaction, underscoring the high degree of specificity in the molecular interface between Lcc4 and its divisome targets.

A possible mechanism by which Lcc4 inhibits cell division may proceed as follows: Upon infection of *S. oneidensis* MR-1 by λSo or upon induction of the phage's lytic cycle, Lcc4 is expressed early and integrated into the cytoplasmic membrane, adopting an N-in/C-in topology. Once inserted into the membrane, Lcc4 interacts with key components of the divisome, specifically FtsZ and/or ZipA. The interaction with FtsZ is mediated through the N-terminal region of Lcc4, while interaction with ZipA occurs via its C-terminal region. In the case of FtsZ, Lcc4 is proposed to obstruct the surface region required for FtsZ-FtsZ interactions, thereby impairing protofilament formation (**Fig. S12**). This disruption prevents proper Z-ring assembly, eliminating the cytoskeletal scaffold necessary for progression of cell division and leading to a filamentous phenotype as cells continue to elongate without dividing. Simultaneously, the interaction between Lcc4 and ZipA may block the binding site on ZipA responsible for recruiting FtsZ to the membrane (**Fig. S12**). Although membrane attachment of FtsZ via FtsA may still occur under these conditions, the absence of functional ZipA anchoring results in mislocalised and unstable FtsZ rings. This in turn leads to abnormally spatial organisation of the Z-rings and further disrupts the assembly of the divisome (**Fig. 35**). It remains to be determined whether both mechanisms operate in parallel or whether one predominates *in vivo*. Nonetheless, both provide plausible molecular explanations for the observed inhibition of cell division by Lcc4.

3.3 Outlook

The results presented in this study on the phage-mediated lysis of *Shewanella oneidensis* MR-1 by λSo show that the process follows the classical pinholin-SAR endolysin pathway, whereby a two-component spanin system is used. However, complete and efficient lysis appears to require additional, as yet uncharacterised, phage-encoded factors. In this context, the small transmembrane protein Lcc6 has been shown to be a modulator of early lysis phases. The elucidation of the exact molecular mechanisms by which Lcc6 exerts its effect is an important starting point for future research. In particular, interaction-based methodologies such as co-immunoprecipitation could provide valuable insights into potential protein partners or regulatory complexes involving Lcc6.

Similarly, for the gene product of the gene *SO_2970*, the next priority for investigation should include temporal expression profiling and the assessment of membrane depolarisation dynamics following induction of a λSo mutant deficient in this gene. These analyses will help to clarify its role within the lytic cascade.

Another notable observation is the temporally uncoupled expression of Lcc6 and the holin protein, suggesting a finely tuned regulatory mechanism orchestrated by phage-encoded transcriptional controls. Investigation of this regulatory architecture by promoter dissection or RNA seq-based transcriptomic analyses during the phage-induced SOS response may reveal novel transcriptional regulators that are critical for the precise timing of lysis initiation.

Moreover, the identification of functional homologues of Lcc6 in non-model or previously uncharacterised phages could deepen the understanding of the evolutionary diversity and mechanistic plasticity of phage-encoded lytic strategies.

In addition to its role in lysis, this study has also shown that Lcc4, another small phage-encoded transmembrane protein, specifically targets and disrupts the bacterial cell division machinery, in particular by impairing the function and subcellular localisation of FtsZ. These results provide a robust foundation for further research into phage-mediated inhibition of host cell division.

A logical progression of this work would involve the biophysical characterisation of Lcc4 interactions with FtsZ and ZipA. The successful purification of recombinant ZipA using

the same protocol as for FtsZ (**Fig. S11**) permits a range of interaction studies, including biolayer interferometry, *in vivo* cross-linking, and co-immunoprecipitation assays. Employing synthetic constructs of Lcc4 that retain the C-terminal region may further elucidate its interaction domains and complex formation dynamics. Advanced structural techniques such as cryo-electron microscopy and nuclear magnetic resonance (NMR) spectroscopy could offer high-resolution insights into the architecture and binding interfaces of these protein complexes.

Finally, it would be of great interest to determine whether analogue mechanisms exist in other temperate phages and whether Lcc4-like proteins represent conserved evolutionary strategies to modulate bacterial cytokinesis. In the long term, such studies could not only improve our fundamental understanding of host-phage interactions, but also yield new molecular tools for the precision control of bacterial cell division, with far-reaching implications for synthetic biology and the synthetic biology industry.

4 Materials & Methods

4.1 Materials

The reagents generally used in this study were purchased from Carl-Roth (Germany), Merck (Germany) Sigma-Aldrich (Germany), Thermo Fisher Scientific (USA) and new England Biolabs (NEB, USA).

A detailed list of materials is given below.

Table 6: Composition of media used in this study

Medium	composition	
Luria-Miller (Lysogeny Broth) LB medium	Trypton Yeast extract NaCl	10 g/L 5 g/L 10 g/L

Table 7: Antibiotics and other additives used in this study

Antibiotic or additive	Stock concentration	Final concentration	Solvent
Chloramphenicol	10 mg/ml	10 µg/ml	96 % (v/v) EtOH
Ampicillin-sodium salt	100 mg/ml	100 µg/ml	$_{dd}H_2O$
Kanamycinsulfate	50 mg/ml	50 µg/ml	$_{dd}H_2O$
L-Arabinose	20 % (w/v)	0,2 % (w/v)	$_{dd}H_2O$
DAP (Meso-diaminopimelic acid)	60 mM	300 µM	$_{dd}H_2O$
Sucrose	80 % (w/v)	10 % (w/v)	$_{dd}H_2O$
IPTG (isopropyl-β-D- thiogalactopyranoside)	1 M	1 mM	$_{dd}H_2O$

Table 8: Kits used in this study

Kit	Application
E.Z.N.A PCR Cleanup Kit (Omega Bio-Tek, USA)	PCR purification
E.Z.N.A Plasmid DNA Mini Kit (Omega Bio-Tek, USA)	Plasmid preparation
E.Z.N.A Gel Extraction Kit (Omega Bio-Tek, USA)	DNA extraction from agarose gels
E.Z.N.A Bacterial DNA Kit (Omega Bio-Tek, USA)	Chromosomal DNA extraction

Table 9: Antibodies used in this study

Antibody	Dilution
Monoclonal Anti-FLAG M2, HRP coupled (Sigma-Aldrich, Germany)	1 : 1000
6xHis-Antibody, HRP coupled (Thermo Fisher Scientific, USA)	1 : 5000

Table 10: Further chemical components and their application in this study

Component	Application
Western Lightning® Plus-ECL (PerkinElmer, USA)	Western Blot (HRP conjugate)
CDP-Star (Sigma-Aldrich, Germany)	Western Blot (AP conjugate)
GeneRuler ™ 1 kb DNA Ladder (Life Technologies, USA)	Ladder (agarose gel electrophoresis)
BLUeye Prestained Protein Ladder (GeneDireX Inc., USA)	Ladder (SDS page)

Table 11: Enzymes and their application in this study

Enzyme	Application
EcoRV (Fast Digest - Thermo Fisher Scientific, USA)	Linearization of pNPTS
SmaI (Fast Digest - Thermo Fisher Scientific, USA)	Linearization of pBAD33
BamHI (Fast Digest - Thermo Fisher Scientific, USA)	Linearization of pBT146 and BACTH plasmids
XhoI (Fast Digest - Thermo Fisher Scientific, USA)	Linearization of pET24c
LguI (Fast Digest - Thermo Fisher Scientific, USA)	Linearization of pET24c
Phusion DNA polymerase (in house production)	PCR
Taq polymerase (in house production)	PCR

Table 12: Buffers and relevant solutions used in this study

Acrylamide gels	composition	
4x lower buffer, pH 8.8	SDS Tris HCl	0.4 % 1.5 M
4x upper buffer, pH 6.8	SDS Tris HCl	0.4% 0.5 M
Acrylamide / bisacrylamide solution 37.5 Rotiphorese (Carl-Roth, Germany)		30 %
APS in $_{dd}H_2O$		10 % (w/v)
SDS-solution in $_{dd}H_2O$		10 % (w/v)
10x SDS-PAGE running buffer, pH 8.3	Tris-Base Glycine SDS	250 mM 1.92 M 0.25 % (w/v)
2x SDS-PAGE sample buffer, pH 6.8	Tris SDS Glycerol β-mercaptoethanol Bromphenolblue	125 mM 4 % 20 % 10 % 0.02 %
Coomassie staining solution	Coomassie Methanol Acetic acid $_{dd}H_2O$	0.1 % (w/v) 200 mL 50 mL 250 mL
Fixing solution	Ethanol Acetic acid $_{dd}H_2O$	25 % 5 % 70 %

Western Blot	composition	
10x Western Buffer	Tris-Base Glycine	0.25 M 1.92 M
1x Western Transfer Buffer	10x Western Transfer Buffer Methanol $_{dd}H_2O$	100 mL 100mL Add to 1 L
10x PBS, pH 7.4	NaCl KCl	80 g 2 g

	Na_2HPO_4 x 2 H_2O	17.8 g
	KH_2PO_4	2.4 g
	$_{dd}H_2O$	Add to 1 L
1x PBS-T	10x PBS	100 mL
	Tween 20	1 mL
	$_{dd}H_2O$	Add to 1 L
Blocking solution	Milk powder	5 % in PBS-T
Antibody solution	Milk powder	2,5 % in PBS-T

Agarose gel electrophoresis	composition	
1x TBE buffer, pH 8.0	Tris-Base	89 mM
	Boric acid	89 mM
	EDTA	1 mM
6x Agarose gel electrophoresis loading buffer	Xylene cyanole	0.5 % (w/v)
	Bromphenol blue	0.5 % (w/v)
	Glycerine	30 % (w/v)

Chromatography	composition	
Lysis Buffer Ulp-1, pH 8.0	NaH_2PO_4	50 mM
	NaCl	300 mM
	Imidazole	20 mM
	PMSF	100 µg/ml
	DNAse 1	10 U/ml
Buffer A Ulp-1, pH 8.0	NaH_2PO_4	50 mM
	NaCl	300 mM
	Imidazole	20 mM
	β-Mercapthoethanol	1mM
Buffer B Ulp-1, pH 8.0	NaH_2PO_4	50 mM
	NaCl	300 mM
	Imidazole	250 mM
	β-Mercapthoethanol	1mM
Dialysis Buffer 1 Ulp-1, pH 8.0	Tris-HCl	50 mM
	NaCl	150 mM
	Glycerol	10 % (w/v)
Dialysis Buffer 2 Ulp-1, pH 8.0	Tris-HCl	50 mM
	NaCl	150 mM
	Glycerol	50 % (w/v)
Lysis/Wash 1 Buffer FtsZ/ZipA, pH 8.0	Tris-HCl	50 mM
	KCl	200 mM
	Imidazol	20 mM
	Glycerol	10 %
	DNAse	20 ng/mL
	RNAse 1	20 ng/mL
	PMSF (for 1st IMAC only)	100 µg/ml
	DTT	1 mM
	$MgCl_2$	2 mM
Wash Buffer 2 FtsZ/ZipA, pH 8.0	Tris-HCl	50 mM
	KCl	1000 mM
	Imidazol	20 mM
	Glycerol	10 %
	PMSF	100 µg/ml
	DTT	1 mM
	$MgCl_2$	2 mM
Elution Buffer FtsZ/ZipA, pH 8.0	Tris-HCl	50 mM
	KCl	200 mM
	Imidazol	300 mM
	Glycerol	10 %

	PMSF (for 1st IMAC only)	100 µg/ml
	DTT	1 mM
	$MgCl_2$	2 mM
SEC Buffer FtsZ/ZipA, pH 8.0	Tris-HCl	50 mM
	KCl	200 mM
	Glycerol	10 %
	DTT	0.7 mM
	$MgCl_2$	2 mM
Dialysis Buffer FtsZ/ZipA, pH 7.4	HEPES-KOH	50 mM
	KCl	50 mM
	DTT	1 mM
	Glycerol	10 %
	$MgCl_2$	2 mM

Further solutions	composition	
5x isothermal reaction buffer, pH 7.5	PEG 8000	25 % (w/v)
	Tris-HCl	500 mM
	$MgCl_2$	50 mM
	DTT	50 mM
	NAD	5 mM
	dNTP´s	1 mM each
	$_{dd}H_2O$	Add to 1 mL
Gibson Assembly master mix	5x Isothermal reaction buffer	320 µL
	Taq DNA ligase	160 µL (40 u/µL)
	T5 exonuclease	0.64 µL
	Phusion DNA polymerase	20 µL (2 u/µL)
	$_{dd}H_2O$	699.36 µL
P buffer, 7.4	HEPES / NaOH	200mM
	KCl	200mM
	$MgCl_2$	50mM

Table 13: Laboratory equipment and its use in this study

Equipment	Usage
Mastercycler nexus gradient (Eppendorf, Germany)	PCR cycler
NanoDrop 1000 Spectrophotometer (PEQLAB, Germany)	Spectrophotometer
Leica DMI6000 B microscope (Leica AG, Germany)	Fluorescence microscopy
Intas Photo imager (INTAS science imaging, Germany)	Chemiluminescence imaging
TE77 ECL Semi-Dry transfer Unit (Amersham bioscience Corp., UK)	Blotting
Tecan INFINITE M NANO+ (Tecan, CH)	Microplate reader (growth curves)
Äkta pure 25 (Cytiva, USA)	Chromatography

Table 14: Bacterial strains used in this study

Name	Species	Strain	Genotype	Plasmid	Source of reference
Shewanella	*oneidensis*				
S79	*Shewanella oneidensis*	MR-1	Wild type		Venkateswaran et al., 1999 [249]
S1427	*Shewanella oneidensis*	MR-1	ΔMuSo1 ΔMuSo2		Kreinebaum et al., 2020 [250]
S5013	*Shewanella oneidensis*	MR-1	ΔMuSo1 ΔMuSo2 ΔSO_4794-4795 (cluster C)		Hager 2017, unpublished

Name	Species	Strain	Genotype	Plasmid	Source of reference
S5625	*Shewanella oneidensis*	MR-1	ΔMuSo1 ΔMuSo2 ΔSO_3007		this work
S5626	*Shewanella oneidensis*	MR-1	ΔMuSo1 ΔMuSo2 ΔSO_3008		this work
S5627	*Shewanella oneidensis*	MR-1	ΔMuSo1 ΔMuSo2 ΔSO_3009		this work
S5628	*Shewanella oneidensis*	MR-1	ΔMuSo1 ΔMuSo2 ΔSO_3010		this work
S5629	*Shewanella oneidensis*	MR-1	ΔMuSo1 ΔMuSo2 ΔSO_4795		this work
S5635	*Shewanella oneidensis*	MR-1	ΔMuSo1 ΔMuSo2 SO_4795 3xFLAG		this work
S5430	*Shewanella oneidensis*	MR-1	ΔλSo ΔMuSo1 ΔMuSo2	pBAD33-RBS-SO_4794-4795	this work
S5642	*Shewanella oneidensis*	MR-1	ΔλSo ΔMuSo1 ΔMuSo2	pBAD33-RBS-SO_3009	this work
S6610	*Shewanella oneidensis*	MR-1	ΔλSo ΔMuSo1 ΔMuSo2		Kreinebaum et al., 2020 [250]
S8433	*Shewanella oneidensis*	MR-1	ΔMuSo1 ΔMuSo2 SO_2960-GGS-Venus		Kühn, unpublished
S8843	*Shewanella oneidensis*	MR-1	ΔMuSo1 ΔMuSo2 Δ*SO_2970*		this work
S8790	*Shewanella oneidensis*	MR-1	ΔMuSo1 ΔMuSo2	pBAD33 sfGFP-SO_4215	this work
S8911	*Shewanella oneidensis*	MR-1	ΔMuSo1 ΔMuSo2	pBTOK-SO_3009 pBAD33-SO_4215-sfGFP	this work
S8915	*Shewanella oneidensis*	MR-1	ΔMuSo1 ΔMuSo2	pBTOK-SO_3009 pBAD33-sfGFP-SO_4215	this work
S8972	*Shewanella oneidensis*	MR-1	ΔMuSo1 ΔMuSo2 Δ*SO_2973*		this work
S8975	*Shewanella oneidensis*	MR-1	ΔMuSo1 ΔMuSo2 Δ*SO_2972*		this work
S9603	*Shewanella oneidensis*	MR-1	ΔMuSo1 ΔMuSo2 SO_2971-GGS-sfGFP		this work
S9006	*Shewanella oneidensis*	MR-1	ΔMuSo1 ΔMuSo2 Δ*SO_2971*		this work
S9296	*Shewanella oneidensis*	MR-1	ΔλSo ΔMuSo1 ΔMuSo2	pBAD33-EVC	this work
S9297	*Shewanella oneidensis*	MR-1	ΔλSo ΔMuSo1 ΔMuSo2	pBAD33-RBS-SO_3009-GGS-FLAG	this work
S9347	*Shewanella oneidensis*	MR-1	ΔMuSo1 ΔMuSo2 ZapA-GGS-Venus	pBAD-33-RBS-SO_4795	this work
S9489	*Shewanella oneidensis*	MR-1	ΔMuSo1 ΔMuSo2 Δ*SO_2973*	pBAD33-sfGFP-SO_2973	this work
S9491	*Shewanella oneidensis*	MR-1	ΔMuSo1 ΔMuSo2 SO_2960-GGS-Venus Δ*SO_3009*	pBAD33-RBS-sfGFP-SO_4215	this work
S9492	*Shewanella oneidensis*	MR-1	ΔMuSo1 ΔMuSo2 SO_2960-GGS-Venus Δ*SO_3009*	pBAD33-RBS-SO_4215-sfGFP	this work
S9496	*Shewanella oneidensis*	MR-1	ΔMuSo1 ΔMuSo2 Δ*SO_2972*::*SO_2972* (V132 GTG-GTC)		this work

Name	Species	Strain	Genotype	Plasmid	Source of reference
S9497	*Shewanella oneidensis*	MR-1	ΔMuSo1 ΔMuSo2 Δ*SO_2972::SO_2972* (D113 GTG-GTC)		this work
S9516	*Shewanella oneidensis*	MR-1	ΔMuSo1 ΔMuSo2 SO_2960-GGS-Venus Δ*SO_2971*	pBAD33-SO_2971-sfGFP	this work
S9517	*Shewanella oneidensis*	MR-1	ΔMuSo1 ΔMuSo2 SO_2960-GGS-Venus Δ*SO_2972*	pBAD33 sfGFP-SO_2972 (V132 GTG-GTC)	this work
S9519	*Shewanella oneidensis*	MR-1	ΔMuSo1 ΔMuSo2 SO_2960-GGS-Venus Δ*SO_2973*	pBAD33-SO_2973-mCherry	this work
S9584	*Shewanella oneidensis*	MR-1	ΔMuSo1 ΔMuSo2 SO_2960-GGS-Venus Δ*SO_2971*	pBAD33 sfGFP-SO_2972	this work
S9617	*Shewanella oneidensis*	MR-1	ΔMuSoI ΔMuSoII Δ*SO_2972* pBBR1-λSo predicted lysis cluster late promotor-RBS-SO_2972a+b		this work
S9618	*Shewanella oneidensis*	MR-1	ΔMuSoI ΔMuSoII Δ*SO_2973* pBBR1-λSo predicted lysis cluster late promotor-RBS-SO_2973		this work
S9623	*Shewanella oneidensis*	MR-1	ΔMuSoI ΔMuSoII Δ*SO_2972* pBBR1-λSo predicted lysis cluster late promotor-RBS-SO_2972b		this work
S9638	*Shewanella oneidensis*	MR-1	ΔλSo ΔMuSo1 ΔMuSo2	pBAD33-SO_2973	this work
S9639	*Shewanella oneidensis*	MR-1	ΔλSo ΔMuSo1 ΔMuSo2	pBAD33-SO_2972	this work
S9661	*Shewanella oneidensis*	MR-1	ΔλSo ΔMuSo1 ΔMuSo2	pBAD33-SO_2971	this work
S9664	*Shewanella oneidensis*	MR-1	ΔMuSo1 ΔMuSo2 Δ*SO_2972::2972* (K55 AAG-AGG)		this work
S9665	*Shewanella oneidensis*	MR-1	ΔMuSo1 ΔMuSo2 Δ*SO_2972::2972* (C139 TGT-TGC)		this work
S9666	*Shewanella oneidensis*	MR-1	ΔMuSo1 ΔMuSo2 Δ*SO_2972::2972* (N57 AAC-AGC)		this work
S9667	*Shewanella oneidensis*	MR-1	ΔMuSo1 ΔMuSo2 Δ*SO_2972::2972* (K56 AAA-AGA)		this work
S9668	*Shewanella oneidensis*	MR-1	ΔMuSo1 ΔMuSo2 Δ*SO_2972::2972* (I124 ATC-CTC)		this work
S9673	*Shewanella oneidensis*	MR-1	ΔMuSo1 ΔMuSo2 Δ*SO_2972::2972* (C74 TGC-TCC)		this work
S9675	*Shewanella oneidensis*	MR-1	ΔMuSo1 ΔMuSo2 Δ*SO_2972::2972* (S54 AGC-AAC)		this work

Name	Species	Strain	Genotype	Plasmid	Source of reference
S9726	*Shewanella oneidensis*	MR-1	Δλ ΔMuSo1 ΔMuSo2	pBAD33-RBS-SO_2972	this work
S9727	*Shewanella oneidensis*	MR-1	Δλ ΔMuSo1 ΔMuSo2	pBAD33-RBS-SO_2972.1	this work
S9783	*Shewanella oneidensis*	MR-1	Δλ ΔMuSo1 ΔMuSo2	pBAD33-RBS-SO_3009 (K14-R14))	this work
S9829	*Shewanella oneidensis*	MR-1	ΔMuSo1 ΔMuSo2 SO_2971 (ΔMNTKVTAMI)		this work
S9864	*Shewanella oneidensis*	MR-1	ΔMuSo1 ΔMuSo2 SO_2960-GGS-Venus SO_2971 (ΔMNTKVTAMI)		this work
S9865	*Shewanella oneidensis*	MR-1	ΔMuSo1 ΔMuSo2 SO_2960-GGS-Venus SO_2971 (K4N)		this work
S9867	*Shewanella oneidensis*	MR-1	ΔMuSo1 ΔMuSo2 ΔSO_2970		this work
S9868	*Shewanella oneidensis*	MR-1	ΔMuSo1 ΔMuSo2 ΔURLC		this work
S9877	*Shewanella oneidensis*	MR-1	ΔMuSo1 ΔMuSo2 SO_2971 (ΔMNTKVTA)		this work
S9878	*Shewanella oneidensis*	MR-1	ΔMuSo1 ΔMuSo2 sfGFP-URLC		this work
S9879	*Shewanella oneidensis*	MR-1	ΔMuSo1 ΔMuSo2 SO_2960-GGS-Venus ΔSO_2970		this work
S9894	*Shewanella oneidensis*	MR-1	ΔMuSo1 ΔMuSo2 SO_2960-GGS-Venus SO_2971 (ΔMNTKVTA)		this work
S9898	*Shewanella oneidensis*	MR-1	ΔMuSo1 ΔMuSo2 ΔSO_2970		this work
S9919	*Shewanella oneidensis*	MR-1	ΔMuSo1 ΔMuSo2 Δ2972	pBBR1 MCS2-λSoPLys-RBS-SO_2972 (N141 - D141)	this work
S9920	*Shewanella oneidensis*	MR-1	ΔMuSo1 ΔMuSo2 Δ2972	pBBR1 MCS2-λSoPLys-RBS-SO_2972 (T122 - S122)	this work
S9921	*Shewanella oneidensis*	MR-1	ΔMuSo1 ΔMuSo2 Δ2972	pBBR1 MCS2-λSoPLys-RBS-SO_2972 (N57 - G57)	this work
S9922	*Shewanella oneidensis*	MR-1	ΔMuSo1 ΔMuSo2 Δ2972	pBBR1 MCS2-λSoPLys-RBS-SO_2972 (S54 - N54)	this work
S9923	*Shewanella oneidensis*	MR-1	ΔMuSo1 ΔMuSo2 Δ2972	pBBR1 MCS2-λSoPLys-RBS-SO_2972 (K56 - R56)	this work
S9924	*Shewanella oneidensis*	MR-1	ΔMuSo1 ΔMuSo2 Δ2972	pBBR1 MCS2-λSoPLys-RBS-	this work

Name	Species	Strain	Genotype	Plasmid	Source of reference
				SO_2972 (K55 - R55)	
S9925	*Shewanella oneidensis*	MR-1	ΔMuSo1 ΔMuSo2 Δ2972	pBBR1 MCS2-λSoPLys-RBS-SO_2972 (C139 - R139)	this work
S9926	*Shewanella oneidensis*	MR-1	ΔMuSo1 ΔMuSo2 Δ2972	pBBR1 MCS2-λSoPLys-RBS-SO_2972 (C74 - S74)	this work
S9927	*Shewanella oneidensis*	MR-1	ΔMuSo1 ΔMuSo2 Δ2972	pBBR1 MCS2-λSoPLys-RBS-SO_2972 (C47 - Y47)	this work
S9928	*Shewanella oneidensis*	MR-1	ΔMuSo1 ΔMuSo2 Δ2972	pBBR1 MCS2-λSoPLys-RBS-SO_2972 (C150 - R150)	this work
S9929	*Shewanella oneidensis*	MR-1	ΔMuSo1 ΔMuSo2 Δ2972	pBBR1 MCS2-λSoPLysr-RBS-SO_2972 (N129 - D129)	this work
S9930	*Shewanella oneidensis*	MR-1	ΔMuSo1 ΔMuSo2 Δ2972	pBBR1 MCS2-λSoPLys-RBS-SO_2972 (Y52 - F52)	this work
S9933	*Shewanella oneidensis*	MR-1	ΔλSo ΔMuSo1 ΔMuSo2	pBAD33-RBS-Lcc6	this work
S9938	*Shewanella oneidensis*	MR-1	ΔMuSo1 ΔMuSo2 URLC sfGFP		this work
S9939	*Shewanella oneidensis*	MR-1	ΔMuSo1 ΔMuSo2 SO_2960-GGS-Venus ΔURLC		this work
S9940	*Shewanella oneidensis*	MR-1	ΔMuSo1 ΔMuSo2 SO_2960-GGS-Venus ΔURLC		this work
S9948	*Shewanella oneidensis*	MR-1	ΔMuSo1 ΔMuSo2 SO_2971 (K4N)		this work
S9970	*Shewanella oneidensis*	MR-1	ΔMuSo1 ΔMuSo2 Δ2972	pBBR1 MCS2-λSoPLys-RBS-SO_2972 (V49-A49)	this work
S9971	*Shewanella oneidensis*	MR-1	ΔMuSo1 ΔMuSo2 Δ2972	pBBR1 MCS2-λSoPLysr-RBS-SO_2972 (I124-L124)	this work
S9971	*Shewanella oneidensis*	MR-1	ΔMuSo1 ΔMuSo2 Δ2972	pBBR1 MCS2-λSoPLys-RBS-SO_2972 (I124-L124)	this work
S9898	*Shewanella oneidensis*	MR-1	ΔMuSo1 ΔMuSo2 ΔSO_2970	pBBR1 MCS2-λSoPLys-RBS-SO_2970-sfGFP	this work
S10075	*Shewanella oneidensis*	MR-1	ΔλSo ΔMuSo1 ΔMuSo2	pBAD33-RBS-SO_3009 (I19-L19)	this work

Name	Species	Strain	Genotype	Plasmid	Source of reference
S10075	*Shewanella oneidensis*	MR-1	ΔλSo ΔMuSo1 ΔMuSo2	pBAD33-RBS-SO_3009 (I16-L16)	this work
S10076	*Shewanella oneidensis*	MR-1	ΔλSo ΔMuSo1 ΔMuSo2	pBAD33-RBS-SO_3009 (R84-K84)	this work
S10077	*Shewanella oneidensis*	MR-1	ΔλSo ΔMuSo1 ΔMuSo2	pBAD33-RBS-SO_3009 (K82-R82)	this work
S10078	*Shewanella oneidensis*	MR-1	ΔλSo ΔMuSo1 ΔMuSo2	pBAD33-RBS-SO_3009 (W80-Y80)	this work
S10079	*Shewanella oneidensis*	MR-1	ΔλSo ΔMuSo1 ΔMuSo2	pBAD33-RBS-SO_3009 (K75-R75)	this work
S10080	*Shewanella oneidensis*	MR-1	ΔλSo ΔMuSo1 ΔMuSo2	pBAD33-RBS-SO_3009 (K20-R20)	this work
S10081	*Shewanella oneidensis*	MR-1	ΔλSo ΔMuSo1 ΔMuSo2	pBAD33-RBS-SO_3009 (N22-Q22)	this work
S10082	*Shewanella oneidensis*	MR-1	ΔλSo ΔMuSo1 ΔMuSo2	pBAD33-RBS-SO_3009 (R12-K12)	this work

Name	Species	Strain	Genotype	Plasmid	Source of reference
Esche-richia	*coli*				
	Escherichia coli	DH5α λpir	recA1 gyrA (lacIZYA-argF) (80d lac [lacZ] M15) pir RK6, cloning strain		Miller and Mekalanos, 1988 [251]
	Escherichia coli	WM 3064	thrB1004 pro thi rpsL hsdS lacZ ΔM15 RP4-1360 Δ(ara-BAD) 567ΔdapA 1341::[erm pir(wt)], conjugation strain for Shewanella		W. Metcalf, University of Illinois, Ur-bana-Cham-paign
	Escherichia coli	BTH 101	F-, cya-99, araD139, galE15, galK16, rpsL1 (Str r), hsdR2, mcrA1, mcrB1		Euromedex, France
	Escherichia coli	BL21 (DE3)	*fhuA2 [lon] ompT gal (λ DE3) [dcm] ΔhsdS λ DE3 = λ sBamHIo ΔEcoRI-B int::(lacI::PlacUV5::T7 gene1) i21 Δnin5*		NEB
	Escherichia coli	Rosetta	F^- ompT $hsdS_B(r_B^- m_B^-)$ gal dcm (DE3) pRARE		Merck
E5439	*Escherichia coli*	MG 1655		pBAD33-RBS-Cluster C	this work
E5440	*Escherichia coli*	MG 1655		pBAD33-EVC	this work

E9784	*Escherichia coli*	MG 1655		pBAD33- λSoPLys -RBS-SO_2971-SO_2973	this work
E9785	*Escherichia coli*	MG 1655		pBAD33- λSoPLys -RBS-SO_2970-SO_2973	this work
E9786	*Escherichia coli*	MG 1655		pBAD33-RBS-SO_3009	this work
E9787	*Escherichia coli*	MG 1655		pBAD33-RBS-SO_4795	this work

Table 15: Plasmids used in this study

Plasmids	Description	Source of reference
pNPTS138-R6KT	mobRP4+ ori-R6K sacB, suicide plasmid for in frame deletions or insertions in S. putrefaciens and *S. oneidensis*, Kmr	Lassak et al., 2010 [252]
pBAD33	expression vector with pBAD promoter of the araBAD (arabinose) operon and the gene encoding the positive and negative regulator of this promoter, araC	Guzman et al., 1995 [253]
pBBR1MCS-2	broad host range vector, mob, Kmr	Kovach et al., 1995 [254]
pET SUMO/CAT	Expression Vector carrying an N-terminal 6xHis-Tag sequence followed by a SUMO cleavage site, Amp	Invitrogen
pNPTS138-R6KT		
pNPTS138-R6KT Δ*4794-4795*	λSO cluster C in frame deletion vector	Hager 2017, unpublished
pNPTS138-R6KT Δ*SO_3007*	*lcc2* in frame deletion vector	this work
pNPTS138-R6KT Δ*SO_3008*	*lcc3* in frame deletion vector	this work
pNPTS138-R6KT Δ*SO_3009*	*lcc4* in frame deletion vector	this work
pNPTS138-R6KT Δ*SO_3010*	*lcc5* in frame deletion vector	this work
pNPTS138-R6KT Δ*SO_4795*	*lcc6* in frame deletion vector	this work
pNPTS138-R6KT Δ*SO_2971*	holin in frame deletion vector	this work
pNPTS138-R6KT Δ*SO_2972*	spanin in frame deletion vector	this work
pNPTS138-R6KT Δ*SO_2973*	endolysin in frame deletion vector	this work
pNPTS138-R6KT *SO_2971*	complementation vector of holin in-frame deletion	this work
pNPTS138-R6KT SO_2972	complementation vector of spanin in-frame deletion	this work
pNPTS138-R6KT SO_2973	complementation vector of endolysin in-frame deletion	this work
pNPTS138-R6KT *SO_2972* (V132 GTG-GTC)	spanin $Rz1^{SO}$ Cys19Ser substitution	this work
pNPTS Holin (ΔMNTKVTA)		this work
pNPTS Holin KO		this work
pNPTS Holin (ΔMNTKVTAMI)		this work
pNPTS *SO_2970* KO		this work
pNPTS URLC KO		this work
pNPTS URLC sfGFP		this work
pNPTS sfGFP URLC		this work
pNPTS Holin (K4N)		this work

Plasmids	Description	Source of reference
pBBR1 MCS2		
pBBR1 MCS2-λSoPLys-RBS-*SO_2972* (N141 - D141)	complementation vector of spanin in-frame deletion carrying a markerless in-frame substitution of Lys14 to Arg in the spanin protein	this work
pBBR1 MCS2-λSoPLys-RBS-*SO_2972* (T122 - S122)	complementation vector of spanin in-frame deletion carrying a markerless in-frame substitution of Thr122 to Ser in the spanin protein	this work
pBBR1 MCS2-λSoPLys-RBS-*SO_2972* (N57 - G57)	complementation vector of spanin in-frame deletion carrying a markerless in-frame substitution of Asn57 to Gly in the spanin protein	this work
pBBR1 MCS2-λSoPLys-RBS-*SO_2972* (S54 - N54)	complementation vector of spanin in-frame deletion carrying a markerless in-frame substitution of Ser54 to Asn in the spanin protein	this work
pBBR1 MCS2-λSoPLys-RBS-*SO_2972* (K56 - R56)	complementation vector of spanin in-frame deletion carrying a markerless in-frame substitution of Lys56 to Arg in the spanin protein	this work
pBBR1 MCS2-λSoPLys-RBS-*SO_2972* (K55 - R55)	complementation vector of spanin in-frame deletion carrying a markerless in-frame substitution of Lys55 to Arg in the spanin protein	this work
pBBR1 MCS2-λSoPLys-RBS-*SO_2972* (C139 - R139)	complementation vector of spanin in-frame deletion carrying a markerless in-frame substitution of Cys139 to Arg in the spanin protein	this work
pBBR1 MCS2-λSoPLys-RBS-*SO_2972* (C74 - S74)	complementation vector of spanin in-frame deletion carrying a markerless in-frame substitution of Cys74 to Ser in the spanin protein	this work
pBBR1 MCS2-λSoPLys-RBS-*SO_2972* (C47 - Y47)	complementation vector of spanin in-frame deletion carrying a markerless in-frame substitution of Cys47 to Tyr in the spanin protein	this work
pBBR1 MCS2-λSoPLys-RBS-*SO_2972* (C150 - R150)	complementation vector of spanin in-frame deletion carrying a markerless in-frame substitution of Cys150 to Arg in the spanin protein	this work
pBBR1 MCS2-λSoPLysr-RBS-*SO_2972* (N129 - D129)	complementation vector of spanin in-frame deletion carrying a markerless in-frame substitution of Asn129 tp Asp in the spanin protein	this work
pBBR1 MCS2-λSoPLys-RBS-*SO_2972* (Y52 - F52)	complementation vector of spanin in-frame deletion carrying a markerless in-frame substitution of Tyr52 to Phe in the spanin protein	this work
pBBR1 MCS2-λSoPLys-RBS-*SO_2972* (V49-A49)	complementation vector of spanin in-frame deletion carrying a markerless in-frame substitution of Val49 to Ala in the spanin protein	this work
pBBR1 MCS2-λSoPLysr-RBS-*SO_2972* (I124-L124)	complementation vector of spanin in-frame deletion carrying a markerless in-frame substitution of Ile124 to Leu in the spanin protein	this work
pBBR1 MCS2-λSoPLys-RBS-*SO_2972* (I124-L124)	complementation vector of spanin in-frame deletion carrying a markerless in-frame substitution of Ile124 to Leu in the spanin protein	this work
pBBR1 MCS2-λSoPLys-RBS-*SO_2970*-sfGFP	complementation vector of SO_2970 in-frame deletion fused to a GFP	this work
pBAD33		
pBAD33-RBS-cluster C	complementation vector of cluster C in-frame deletion	this work
pBAD33-RBS-Lcc4	complementation vector of Lcc4 in-frame deletion	this work
pBAD33-RBS-Lcc6	complementation vector of Lcc6 in-frame deletion	this work

Plasmids	Description	Source of reference
pBAD33-RBS-*SO_3009*-GGS-FLAG	C-terminal FLAG tag of Lcc4 (*SO_3009*)	this work
pBAD33-RBS-*SO_3009* (K14-R14)	markerless in-frame substitution of Lys14 to Arg in the Lcc4 protein	this work
pBAD33-RBS-SO_3009 (I19-L19)	markerless in-frame substitution of Ile19 to Leu in the Lcc4 protein	this work
pBAD33-RBS- Lcc4 (I16-L16)	markerless in-frame substitution of Ile16 to Leu in the Lcc4 protein	this work
pBAD33-RBS- Lcc4 (R84-K84)	markerless in-frame substitution of Arg84 to Lys in the Lcc4 protein	this work
pBAD33-RBS- Lcc4 (K82-R82)	markerless in-frame substitution of Lys82 to Arg in the Lcc4 protein	this work
pBAD33-RBS- Lcc4 (W80-Y80)	markerless in-frame substitution of Trp80 to Tyr in the Lcc4 protein	this work
pBAD33-RBS- Lcc4 (K75-R75)	markerless in-frame substitution of Lys75 to Arg in the Lcc4 protein	this work
pBAD33-RBS- Lcc4 (K20-R20)	markerless in-frame substitution of Lys20 to Arg in the Lcc4 protein	this work
pBAD33-RBS- Lcc4 (N22-Q22)	markerless in-frame substitution of Asn22 to Gln in the Lcc4 protein	this work
pBAD33-RBS- Lcc4 (R12-K12)	markerless in-frame substitution of Arg12 to Lys in the Lcc4 protein	this work
pBAD33-RBS-*SO_2972*	complementation vector of spanin Rz^{SO} in-frame deletion	this work
pBAD33-RBS-*SO_2972.1*	complementation vector of spanin $Rz1^{SO}$ in-frame deletion	this work
pBAD33-RBS-sfGFP-*SO_4215*	N-terminal sfGFP tag of FtsZ (*SO_4215*)	this work
pBAD33-RBS-*SO_4215*-sfGFP	C-terminal sfGFP tag of FtsZ (*SO_4215*)	this work
pBTOK-Lcc4	complementation vector of Lcc4 in-frame deletion	this work
pBAD33-sfGFP-*SO_2973*	N-terminal sfGFP tag of endolysin R^{So} (SO_2973)	this work
pBAD33-*SO_2971*-sfGFP	C-terminal sfGFP tag of holin S^{So} (*SO_2971*)	this work
pBAD33 sfGFP-*SO_2972*	N-terminal sfGFP tag of spanin Rz^{So} (SO_2972)	this work
pBAD33 sfGFP-*SO_2972* (V132 GTG-GTC)	N-terminal sfGFP tag of spanin Rz^{So} (*SO_2972*) carrying a amino acid substitution	this work
pBAD33-*SO_2973*-mCherry	C-terminal mCherry tag of endolysin R^{So} (*SO_2973*)	this work
Bacterial Two Hybrid		
pKT25-*SO_2973*	fusion of endolysin R^{So} (*SO_2973*) used for Bacterial Two Hybrid	this work
pKNT25-*SO_2973*	fusion of endolysin R^{So} (*SO_2973*) used for Bacterial Two Hybrid	this work
pUT18-*SO_2973*	fusion of endolysin R^{So} (*SO_2973*) used for Bacterial Two Hybrid	this work
pUT18c-*SO_2973*	fusion of endolysin R^{So} (*SO_2973*) used for Bacterial Two Hybrid	this work
pKT25-*SO_2971*	fusion of holin S^{So} (*SO_2971*) used for Bacterial Two Hybrid	this work
pKNT25-*SO_2971*	fusion of holin S^{So} (*SO_2971*) used for Bacterial Two Hybrid	this work
pUT18-*SO_2971*	fusion of holin S^{So} (*SO_2971*) used for Bacterial Two Hybrid	this work
pUT18c-*SO_2971*	fusion of holin S^{So} (*SO_2971*) used for Bacterial Two Hybrid	this work
pKT25-*SO_2972*	fusion of spanin Rz^{So} (*SO_2972*) used for Bacterial Two Hybrid	this work

Plasmids	Description	Source of reference
pKNT25-*SO_2972*	fusion of spanin Rz^{So} (*SO_2972*) used for Bacterial Two Hybrid	this work
pUT18-*SO_2972*	fusion of spanin Rz^{So} (*SO_2972*) used for Bacterial Two Hybrid	this work
pUT18c-*SO_2972*	fusion of spanin Rz^{So} (*SO_2972*) used for Bacterial Two Hybrid	this work
pKT25-*SO_4795*	fusion of Lcc6 (*SO_4795*) used for Bacterial Two Hybrid	this work
pKNT25-*SO_4795*	fusion of Lcc6 (*SO_4795*) used for Bacterial Two Hybrid	this work
pUT18-*SO_4795*	fusion of Lcc6 (*SO_4795*) used for Bacterial Two Hybrid	this work
Protein Purification		
pET-6xHis-SUMO-*SO_4215*	fusion of FtsZ (*SO_4215*) used for protein purification	this work
pET-6xHis-SUMO-*SO_2897*	fusion of ZipA (*SO_2897*) used for protein purification	this work

Table 16: Oligonucleotides used in this study

ID	Primer name	Sequence 5′→ 3′
ST340	Check Lcc fwd	agggcgaaccctatcaaatcatcgatatc
ST341	Check Lcc rev	cgcagcctaccacaacgtagttg
ST342	Lcc4 down fwd	tctgcaggat gccaatccccaacgcctttg
ST343	Lcc4 down rev	tgagtgatgtttgag ccaaggcaggtgcatgatgactc
ST344	Lcc4 up fwd	atgcacctgccttgg ctcaaacatcactcaccaccctagc
ST345	Lcc4 up rev	ggatccagat cgccatgccacgcaaacaag
ST342	Lcc4 down fwd	tctgcaggat gccaatccccaacgcctttg
ST343	Lcc4 down rev	tgagtgatgtttgag ccaaggcaggtgcatgatgactc
ST344	Lcc4 up fwd	atgcacctgccttgg ctcaaacatcactcaccaccctagc
ST345	Lcc4 up rev	ggatccagat cgccatgccacgcaaacaag
ST354	Lcc4-GGS-FLAG fwd	ctcggtacccaggagggaaaat atgtttgagtttactgaagataaaaaaggtttaagacctaagt
ST355	Lcc4-GGS-FLAG rev	gaggatcccctcacttgtcgtcgtcgtccttgtagtccgagccgcc tttagagtcatcatgcacctgccttg
ST378	Spanin up fwd	gcttctctgcagga taacgattttgccattgaagataacgacgac
ST379	Spanin up rev D113	tattcgaaaggtccagcgac gaaaaaacgctatcttggggcgct
ST380	Spanin down fwd D113	ccccaagatagcgttttttc gtcgctggacctttcgaatacctga
ST381	Spanin down rev	ttcgtggatccagat ccgtcgctggctatgactgc
ST382	Spanin up rev V132	ctgatgctgttaacagcgtc ctcgagcagtccgccagatgt
ST383	Spanin down fwd V132	catctggcggactgctcgag gacgctgttaacagcatcagggatac
ST519	Holin up	tcgagctcggtacccaggagggaaaat atgaatactaaagtcacggcgatgattatgga
ST520	Holin down	ctctagaggatcccc ttattcatttccgtcatccatattgattacgtttaggtt
ST521	Endolysin up	tcgagctcggtacccaggagggaaaat atgcgcaataaggtattagtcacaggcc
ST522	Endolysin down	ctctagaggatcccc ttaattgagagcatcgaggcagtcgc
ST523	Spanin RZ up	tcgagctcggtacccaggagggaaaat atgctctcgacaatatcaagtaaaatcattgcg
ST524	Spanin RZ down	ctctagaggatcccc tcagaaagatcttggtttttcttgctggaatacg
ST525	RZ1 up	tcgagctcggtacccaggagggaaaat atgaaaaaacgctatcttggggcgc
ST526	RZ1 down	ctctagaggatcccc ttactcggtagacagtttcgatttttgctct
ST527	Spanin RZ+RZ1 down fwd	ctttctgaaggagggaaaat atgaaaaaacgctatcttggggcg
ST528	Lysis cluster down	gtcgactctagaggatcccc ttattcatttccgtcatccatattgattacgtttaggtt
ST535	late promotor up	cgggctgcaggaatt aacaaaatgatttacccaagccttatgttttactatcct
ST536	late promotor down	taccttattgcgcatattttccctcct agatgccccaaaacaaaaagcccc
ST537	Lysis cluster up	tgttttggggcatctaggagggaaaat atgcgcaataaggtattagtcacaggcc

ID	Primer name	Sequence 5´→ 3´
ST538	Lysis cluster + 2970 down	gcttgatatcgaatt tcatagctcaccggagccgt
ST539	Lysis cluster down	gcttgatatcgaatt ttattcatttccgtcatccatattgattacgtttaggtt
ST573	late promotor fwd	tcccccgggctgcaggaatt aacaaaatgatttacccaagccttatgttttactatcct
ST574	late promotor rev	gagagcatattttccctcct agatgccccaaaacaaaaagcccc
ST575	Spanin up fwd	gggcatctaggagggaaaat atgctctcgacaatatcaagtaaaatcattgcg
ST576	C150 up rev	gttccttgggcggaaaaacg tactgaatcttggttacggtaacggttcg
ST577	C150 down fwd	gtaaccaagattcagtacgt ttttccgcccaaggaactgataggc
ST578	Spanin down rev	gataagcttgatatcgaatt ttactcggtagacagtttcgatttttgctct
ST579	N141 up rev	tcttggttacggtaacggtc cgcacatctggcggactgc
ST580	N141 down fwd	agtccgccagatgtgcggac cgttaccgtaaccaagattcagtatgtttttcc
ST581	C139 up rev	ttacggtaacggttcgcacg tctggcggactgctcgag
ST582	C139 down fwd	tcgagcagtccgccagacgt gcgaaccgttaccgtaaccaagattc
ST583	N129 up rev	gactgctcgagcacgctgtc aacagcatcagggataccagtagcg
ST584	N129 down fwd	gtatccctgatgctgttgac agcgtgctcgagcagtcc
ST585	I124 up rev	ctgttaacagcatcagggag accagtagcgccccaagatagc
ST586	I124 down fwd	cttggggcgctactggtctc cctgatgctgttaacagcgtgctcg
ST587	T122 up rev	acagcatcagggataccaga agcgccccaagatagcgttttttc
ST588	T122 down fwd	cgctatcttggggcgcttct ggtatccctgatgctgttaacagcgt
ST589	W119 up rev	gggataccagtagcgcccccc agatagcgtttttcatcgctggacct
ST590	W119 down fwd	atgaaaaaacgctatctggg ggcgctactggtatccctgatgc
ST591	C47 up rev	gaatacggcggaacgatgta atggcctatcagttccttgggcg
ST592	C47 down fwd	aggaactgataggccattac atcgttccgccgtattccagca
ST593	V49 up rev	ttgctggaatacggcgggagc gatgcaatggcctatcagttccttggg
ST594	V49 down fwd	tgataggccattgcatcgct ccgccgtattccagcaagaaaaac
ST595	Y52 up rev	tggtttttcttgctggaaaa cggcggaacgatgcaatggc
ST596	Y52 down fwd	attgcatcgttccgccgttt tccagcaagaaaaaccaagatctttctgaatacac
ST597	S54 up rev	gatcttggtttttcttgttg gaatacggcggaacgatgcaatgg
ST598	S54 down rev	atcgttccgccgtattccaa caagaaaaaccaagatctttctgaatacaccaactc
ST599	K55 up rev	gaaagatcttggtttttcct gctggaatacggcggaacgatg
ST600	K55 down fwd	ttccgccgtattccagcagg aaaaaccaagatctttctgaatacaccaactcgt
ST601	K56 up rev	tcagaaagatcttggtttct cttgctggaatacggcggaacg
ST602	K56 down rev	cgccgtattccagcaagaga aaccaagatctttctgaatacaccaactcgt
ST603	N57 up rev	tggtgtattcagaaagatcttggct tttcttgctggaatacggcggaac
ST604	N57 down fwd	cgtattccagcaagaaaagc caagatctttctgaatacaccaactcgttgatga
ST605	C74 up rev	gatagccaatcgagatcgga tagagaaattactttcatcaacgagttggtgtattcag
ST606	C74 down fwd	tgaaagtaatttctctatcc gatctcgattggctatcgctagaaaaatggatta
ST629	Lcc4 fwd	cgaattcgagctcggtacccaggagggaaaat atgtttgagtttactgaagataaaaaaggtttaagac-ctaagtatctt ggcacaatcaaacataacgg
ST630	Lcc4 rev	gtcgactctagaggatcccc tcatttagagtcatcatgcacctgcctt
ST631	Lcc4 fwd	cgaattcgagctcggtacccaggagggaaaatatgtttgagtttactgaaga-taaaaaaggtttaagacctaagtatattg
ST632	Lcc4 rev	gtcgactctagaggatcccc tcatttagagtcatcatgcacctg ctttggcttatgccatacttccc
ST633	Lcc4 rev	gtcgactctagaggatcccc tcatttagagtcatcatgcacctgccttggcctatgccatacttcccatgttt
ST634	Lcc4 rev	gtcgactctagaggatccccctcatttagagtcatcatgcacctgccttggcttatgata-tacttcccatgttttagcct
ST635	Lcc4 rev	gtcgactctagaggatcccc tcatttagagtcatcatg cacctgccttggcttatgccatacttcc catgttctagcctgaaacataccagcca
ST636	Lcc4 fwd	cgaattcgagctcggtacccaggagggaaaatatgtttgagtttactgaaga-taaaaaaggtttaagacctaagtat attggcacaatcagacataacggcattagaagaac
ST637	Lcc4 fwd	cgaattcgagctcggtacccaggagggaaaatatgtttgagtttactgaaga-taaaaaaggtttaagacctaagtatattggcacaatcaaacatcaaggcattagaagaactttaat
ST638	Lcc4 fwd	cgaattcgagctcggtacccaggagggaaaatatgtttgagtttactgaaga-taaaaaaggtttaaaacctaagtatattggcacaat
ST639	His-SUMO-FtsZ fwd	acagagaacagattggtggt tttgagatcatggacactcactcagacga
ST640	His-SUMO-FtsZ rev	gctttgttagcagccggatc ttagtcagcttgcttacgcaaaaatgct
ST641	check pTB146 fwd	atgccggccacgatgcg
ST642	FtsZ check rev	accttgctcagcataagccatacgc

ID	Primer name	Sequence 5´→ 3´
ST643	FtsZ check fwd	gcacctgttgtggcacaaattgc
ST644	check pTB146 rev	cccaaggggttatgctagttattgctcag
ST645	SUMO-ZipA fwd	acagagaacagattggtggt gaagatttgcaactagttttgttcgttttaggc
ST646	SUMO-ZipA rev	gctttgttagcagccggatc ttaggcgttggcgcgaatacg
KH 001	Lcc4 K14 up fwd	cgaattcgagctcggtacccaggagggaaaatatgtttgagtttactgaaga-taaaaaaggtttaagacctaggtatattggcacaatcaaacat
KH 002	Lcc4 K14 down rev	gtcgactctagaggatcccctcatttagagtcatcatgcacctgcctt
KH 003	Lcc4 I19 up fwd	cgaattcgagctcggtacccaggagggaaaat atgtttgagtttactgaagataaaaaaggtttaagac-ctaagtatattggcacactcaaacataacggcattagaag
KH 004	Lcc4 I 19 down rev	gtcgactctagaggatcccctcatttagagtcatcatgcacctgcctt
KH 005	Holin up fwd	gcttctctgcaggat tgcggcggtgataatatttttttgctga
KH 006	Holin up rev	agctctacaaaggatcctaa atgaataaagtcgtcgttatcttcaatggcaaaatc
KH 007	sfGFP fwd	acgacgactttattcattta ggatcctttgtagagctcatccatgcc
KH 008	sfGFP rev	atgacggaaatgaaggctcg agcaaaggagaagaactttt cactggagt
KH 009	Holin down fwd	tcttctcctttgctcgagcc ttcatttccgtcatccatattgattacgtttaggt
KH 010	Holin down rev	ttcgtggatccagat ctattaaatgcaaatttggataaatctgagcttgccc
KH 011	Holin up fwd	gcttctctgcaggat gattggtcgcctttgtgggggg
KH 012	Holin up rev	tctacaaaggatccggctcg aatactaaagtcacggcgatgattatggataaagc
KH 013	sfGFP fwd	gtgactttagtattcgagcc ggatcctttgtagagctcatccatgcc
KH 014	sfFGP rev	gtaatcggaggccaaacatg agcaaaggagaagaactttt cactggagtt
KH 015	Holin down fwd	agttcttctcctttgctcat gtttggcctccgattactcggtagac
KH 016	Holin down rev	ttcgtggatccagat gcccgttcagagctgcaaaaaaatttatc
KH 017	RZ up fwd	gcttctctgcaggat gtaccagtggcactaatttcttttctccattg
KH 018	RZ up rev	tctacaaaggatccggctcg ctctcgacaatatcaagtaaaatcattgcgttacttatc
KH 019	sfGFP fwd	gatattgtcgagagcgagcc ggatcctttgtagagctcatccatgcc
KH 020	sfGFP rev	aaatttaggcgttaaaaatg agcaaaggagaagaactttt cactggagt
KH 021	RZ down fwd	agttcttctcctttgctcat ttttaacgcctaaatttgccagaaaaaaaggtct
KH 022	RZ down rev	ttcgtggatccagat aggcgaaaccactaccccaattaacg
KH 023	RZ1 up fwd	gcttctctgcaggat ggttagcgcttgcattgactctattaaatcg
KH 024	RZ1 up rev	tggatgagttatacaaataa tcggaggccaaacatgaatactaaagtcac
KH 025	mCherry fwd	tcatgtttggcctccgatta tttgtataactcatccataccaccagtcgaatg
KH 026	mCherry rev	aactgtctaccgagggctcg gtttccaaaggggaagaggacaatatg
KH 027	RZ1 down fwd	tccccttggaaaccgagcc ctcggtagacagtttcgatttttgctctg
KH 028	RZ1 down rev	ttcgtggatccagat tcgattggacgtatcaatacggtattggc
KH 029	Endolysin up fwd	gcttctctgcaggat tttcatcgctggacctttcgaatacct
KH 030	Endolysin up rev	tggatgagttatacaaataa ttttgtgcaagttactgataattagagttttttatctttgtttgg
KH 031	mCherry fwd	cagtaacttgcacaaaatta tttgtataactcatccataccaccagtcgaatgt
KH 032	mCherry rev	tcgatgctctcaatggctcg gtttccaaaggggaagaggacaatatgg
KH 033	Endolysin down fwd	tccccttggaaaccgagcc attgagagcatcgaggcagtcgc
KH 034	Endolysin down rev	ttcgtggatccagat agaaactcatgggcagtatttgagagtgatg
IO066	chk Lambda fw	cgt tca act tcg tta gac gga tg
IO067	chk Lambda rv	gcg gat ttc agt gtt tcc aga g
IO062	chk SO_4794-4795 fw	ctt aat cgt aga taa ctt tgc ggg cgg tg
IO063	chk SO_4794-4795 rv	gta cat gaa aga ctc atg tac aag atg gag aaa g
IO031	EcoRV_KO_SO4974_US_fw	gcg aat tcg tgg atc cag atg ctt aag caa tgg tac gcc a
IO032	OL_KO_SO4974_US_rv	gtt ggc aat ggg ttg ttt agc cac cct tag ctg ttt gct c
IO033	OL_KO_SO4974_DS_fw	gag caa aca gct aag ggt ggc taa aca acc cat tgc caa c
IO034	EcoRV_KO_SO4974_DS_rv	gcc aag ctt ctc tgc agg atg ttc atg ctg cct cct atg c
IO035	EcoRV_KO_SO3007_US_fw	gcg aat tcg tgg atc cag atc aca cta tca cca cca atg a
IO036	OL_KO_SO3007_US_rv	gcg ttt agt tgt aat cac ttc ttc atg ctt cct cct ttt g
IO037	OL_KO_SO3007_DS_fw	caa aag gag gaa gca tga aga agt gat tac aac taa acg ca
IO038	EcoRV_KO_SO3007_DS_rv	gcc aag ctt ctc tgc agg atc att aaa gtt ctt cta atg ccg t

ID	Primer name	Sequence 5´→ 3´
IO039	EcoRV_KO_SO3008_US_fw	gcg aat tcg tgg atc cag atc ctg aat aca tca tca aca act
IO040	OL_KO_SO3008_US_rv	agt aaa ctc aaa cat cac tca atc act tac ctt cct ttg cc
IO041	OL_KO_SO3008_DS_fw	gca aag gaa ggt aag tga ttg agt gat gtt tga gtt tac tga
IO042	EcoRV_KO_SO3008_DS_rv	gcc aag ctt ctc tgc agg atc atg tga ata aaa tcc aaa tta gcg
IO047	EcoRV_KO_SO3010_US_fw	gcg aat tcg tgg atc cag atc aaa gta tat cta gaa act gca gc
IO048	OL_KO_SO3010_US_rv	gat gaa aaa cgt gtt cat gaa gtc atc atg cac ctg cct t
IO049	OL_KO_SO3010_DS_fw	aag gca ggt gca tga tga ctt cat gaa cac gtt ttt cat ct
IO050	EcoRV_KO_SO3010_DS_rv	gcc aag ctt ctc tgc agg atc ata tcg aat ttg gtg gca g
IO051	EcoRV_KO_SO4795_US_fw	gcg aat tcg tgg atc cag atg ata ttg ctg atc aaa tgg ct
IO052	OL_KO_SO4795_US_rv	ttc ttg ctg aaa cat tat gcg ttc atg atg cac ctg cct t
IO053	OL_KO_SO4795_DS_fw	aag gca ggt gca tca tga acg cat aat gtt tca gca aga aat
IO054	EcoRV_KO_SO4795_DS_rv	gcc aag ctt ctc tgc agg atc aat taa tac gtg ggc taa gc
DF 001	Holin KO up fwd	gcttctctgcaggatgcggcggtgataatatttttttgctgaca
DF 002	Holin KO up rev	ccaaacatgaatactaatgaataaagtcgtcgttatcttcaatggcaaaatc
DF 003	Holin KO down fwd	acgactttattcattagtattcatgtttggcctccgattactcg
DF 004	Holin KO down rev	ttcgtggatccagatgagctgcaaaaaaatttatcctcggtgact
DF 005	Endolysin KO up fwd	gcttctctgcaggattggacctttcgaatacctgagttaactctttg
DF 006	Endolysin KO up rev	taaatcatgcgcaatctcaattaattttgtgcaagttactgataattagagttttttatctttgt
DF 007	Endolysin KO down fwd	acaaaattaattgagattgcgcatgatttacttaccaatccttgga
DF 008	Endolysin KO down rev	ttcgtggatccagatgagaaactcatgggcagtatttgagagtgat
DF 013	SO_2972 KO up fwd	gcttctctgcaggatacccaatcagcaggtaccagtgg
DF 014	SO_2972 KO up rev	aaaatgctctcgacatctttctgaatacaccaactcgttgatgaaagt
DF 015	SO_2972 KO down fwd	gtgtattcagaaagatgtcgagagcatttttaacgcctaaatttgc
DF 016	SO_2972 KO down rev	ttcgtggatccagattaccccaattaacgcacttaaaaccgc
DF 037	FtsZ-sfGFP up fwd	tcgagctcggtacccaggagggaaaatatgtttgagatcatggacactcactcagacg
DF 038	FtsZ-sfGFP up rev	tttgctcgagccgccgtcagcttgcttacgcaaaaatgctg
DF 039	FtsZ-sfGFP down fwd	gctgacggcggctcgagcaaaggagaagaacttttcactggagt
DF 040	FtsZ-sfGFP down rev	gtcgactctagaggatcccctcaggatcctttgtagagctcatccatgcc
DF 049	check-Holin KO fwd	cctttgtgggggatcttgtggtcc
DF 050	check-Holin KO rev	gcgctattaaatgcaaatttggataaatctgagctt
DF 051	check-Endolysin KO fwd	agtagcgccccaagatagcgttt
DF 052	check-Endolysin KO rev	tggcgaagtaagtaatcgagagaatctcct
DF 054	check-SO_2972 KO fwd	gcaactcgagcttgaatccatttggattagt
DF 055	check-SO_2972 KO rev	ggtacatgcaaagaccaaggaaagatgagtg
DF 100	pKT25 SO_2972 fwd	gactctagaggatcctctcgacaatatcaagtaaaatcattgcgttacttatcg
DF 101	pKT25 SO_2972 rev	aggtacccggggatcgaaagatcttggtttttcttgctggaatacgg
DF 102	put18;put18c;pKNT25 SO_2972 fwd	cgactctagagctctcgacaatatcaagtaaaatcattgcgttacttatcg
DF 103	put18;put18c;pKNT25 SO_2972 rev	ggtacccggggaaagatcttggtttttcttgctggaatacgg
DF 110	Holin Knock-in fwd	gcttctctgcaggatgcgctattaaatgcaaatttggataaatctgagct
DF 111	Holin Knock-in rev	ttcgtggatccagatcctttgtgggggatcttgtggtcc
DF 112	Endolysin Knock-in fwd	gcttctctgcaggattggcgaagtaagtaatcgagagaatctcct
DF 113	Endolysin Knock-in rev	ttcgtggatccagatagtagcgccccaagatagcgtt
DF 114	SO_2972 Knock-in fwd	gcttctctgcaggatgcagatggacggccagtaaagctaggcg
DF 115	SO_2972 Knock-in rev	ttcgtggatccagatatgttgggtatgcggcatttaatgca
DF 156	pNPTS SO_2991 KO (A17) up fwd	gcttctctgcaggattggcatgcaggatttgagctatggg
DF 157	pNPTS SO_2991 KO (A17) up rev	tactgccgatgtagcaaaaatccttttaattattttcaattattcca

ID	Primer name	Sequence 5′→ 3′
DF 158	pNPTS SO_2991 KO (A17) down fwd	attaaaaggatttttgctacatcggcagtaacaat
DF 159	pNPTS SO_2991 KO (A17) down rev	ttcgtggatccagattttgctttaaactgtcaactgt
DF 160	pNPTS SO_2991 KO (1-A70) up fwd	gcttctctgcaggataatagcatgctgccagtact
DF 161	pNPTS SO_2991 KO (1-A70) up rev	ccttgttatttaagccgcgagcgcatcgtttacgt
DF 162	pNPTS SO_2991 KO (1-A70) down fwd	aacgatgcgctcgcggcttaaataacaaggagtcgt
DF 163	pNPTS SO_2991 KO (1-A70) down rev	ttcgtggatccagatcgatggctggataatcacgc
DF 164	pNPTS SO_2991 KO (A70-141) up fwd	gcttctctgcaggattggcatgcaggatttgagct
DF 165	pNPTS SO_2991 KO (A70-141) up rev	atctaactttgccgcaaaaatccttttaattattttcaattattcca
DF 166	pNPTS SO_2991 KO (A70-141) down fwd	attaaaaggatttttgcggcaaagttagataccgc
DF 167	pNPTS SO_2991 KO (A70-141) down rev	ttcgtggatccagatagtcagactctatgcagaaag
DF 168	pNPTS SO_2938 KO (G17) up fwd	gcttctctgcaggataaatctcaccttcgggtttg
DF 169	pNPTS SO_2938 KO (G17) up rev	atccccgccaccaccaaaatcctcacgaaatttttctaat
DF 170	pNPTS SO_2938 KO (G17) down fwd	tttcgtgaggattttggtggtggcggggatgatga
DF 171	pNPTS SO_2938 KO (G17) down rev	ttcgtggatccagatagtagttatttactgataacgttca
DF 172	pNPTS SO_2938 KO (1-Q90) up fwd	gcttctctgcaggatattttgtcacctcgcattct
DF 173	pNPTS SO_2938 KO (1-Q90) up rev	aacttcccacagtagttgctctatgccatttgaatat
DF 174	pNPTS SO_2938 KO (1-Q90) down fwd	aatggcatagagcaactactgtgggaagttaccca
DF 175	pNPTS SO_2938 KO (1-Q90) down rev	ttcgtggatccagatatgtgatccttgatggcaca
DF 176	pNPTS SO_2938 KO (Q90-181) up fwd	gcttctctgcaggataaatctcaccttcgggtttg
DF 177	pNPTS SO_2938 KO (Q90-181) up rev	aatggtgatgtccgcaaaatcctcacgaaatttttctaat
DF 178	pNPTS SO_2938 KO (Q90-181) down fwd	tttcgtgaggattttgcggacatcaccattaaatc
DF 179	pNPTS SO_2938 KO (Q90-181) down rev	ttcgtggatccagattagattctgaatacgcaggaa
DF 180	RBS-Holin(M1-E89)-GGS-sfGFP up fwd	tcgagctcggtacccaggagggaaaatatgaatactaaagtcacggcgatgattatggataaagc
DF 181	RBS-Holin(M1-E89)-GGS-sfGFP up rev	tttgctcgagccgccttcatttccgtcatccatattgattacgtttaggt
DF 182	RBS-Holin(M1-E89)-GGS-sfGFP down fwd	aatgaaggcggctcgagcaaaggagaagaactttttcactggagt
DF 183	RBS-Holin(M1-E89)-GGS-sfGFP down rev	ctctagaggatcccctcaggatcctttgtagagctcatccatgcc
DF 184	RBS-Endolysin-GGS-mCherry up fwd	tcgagctcggtacccaggagggaaaatatgcgcaataaggtattagtcacaggcctga
DF 185	RBS-Endolysin-GGS-mCherry up rev	cctttggaaaccgagccgccattgagagcatcgaggcagtcgc
DF 186	RBS-Endolysin-GGS-mCherry down fwd	ctcaatggcggctcggtttccaaaggggaagaggacaatatgg

ID	Primer name	Sequence 5´→ 3´
DF 187	RBS-Endolysin-GGS-mCherry down rev	ctctagaggatcccctcatttgtataactcatccataccaccagtcgaatg
DF 200	RBS-sfGFP-RzRz1 up fwd	tcgagctcggtacccaggagggaaaatatgagcaaaggagaagaacttttcactggagt
DF 201	RBS-sfGFP-RzRz1 up rev	cgagagcgagccgccggatcctttgtagagctcatccatgcc
DF 202	RBS-sfGFP-RzRz1 down up	ggatccggcggctcgctctcgacaatatcaagtaaaatcattgcgttactt
DF 203	RBS-sfGFP-RzRz1 down rev	ctctagaggatcccccttactcggtagacagtttcgatttttgctct
DF204	Holin (-1.ATG) up fwd	gccaagcttctctgcaggatggctgatggcgttggtttggg
DF205	Holin (-1.ATG) up rev	cgagtaatcggaggccaaacatgattatggataaagcaacgacaactggaagc
DF206	Holin (-1.ATG) down fwd	gttgctttatccataatcgtttggcctccgattactcggtagac
DF207	Holin (-1.ATG) down rev	gcgaattcgtggatccagatcagttttatgcaaaaccgcgaaatgagac
DF208	Holin (-2.ATG) up fwd	gccaagcttctctgcaggatccaagtggctgatggcgttgg
DF209	Holin (-2.ATG) up rev	cgagtaatcggaggccaaacatggataaagcaacgacaactggaagct
DF210	Holin (-2.ATG) down fwd	gttgtcgttgctttatccatgtttggcctccgattactcggtagac
DF211	Holin (-2.ATG) down rev	gcgaattcgtggatccagatcagttttatgcaaaaccgcgaaatgagac
DF227	SO_2970-GGS-sfGFP up fwd	gccaagcttctctgcaggattagctttttccatgcggctttggct
DF228	SO_2970-GGS-sfGFP up rev	agctctacaaaggatcctgaatgagccaaccaagctggcg
DF229	SO_2970-GGS-sfGFP mid fwd	cgccagcttggttggctcattcaggatcctttgtagagctcatccatgc
DF230	SO_2970-GGS-sfGFP mid rev	ccggtgagctaggcggctcgagcaaaggagaagaactttcactggagt
DF231	SO_2970-GGS-sfGFP down fwd	tctcctttgctcgagccgcctagctcaccggagccgtcca
DF232	SO_2970-GGS-sfGFP down rev	gcgaattcgtggatccagatcatgaatactaaagtcacggcgatgattatgga
DF224	Holin K4N up fwd	gccaagcttctctgcaggatcagtaatggccgcggttagcg
DF225	Holin K4N up rev	cgagtaatcggaggccaaacatgaatactaacgtcacggcgatgattatgga
DF226	Holin K4N down fwd	gccgtgacgttagtattcatgtttggcctccgattactcggtagac
DF226	Holin K4N down fwd	gcgaattcgtggatccagatcagttttatgcaaaaccgcgaaatgagac

4.2 Microbiological methods

4.2.1 Cultivation of bacterial strains

All bacterial strains used in this study are summarised in Table 14. *S. oneidensis* cells were incubated in LB medium at room temperature (RT) or 30°C and *E. coli* cells in LB medium at 37°C (unless otherwise stated). The media for *E. coli* WM 3064 [2,6-diaminoheptanedioic acid (DAP)-auxotrophic] were supplemented with DAP at a final concentration of 300 µM. Selective media were supplemented with 50 µg/mL Kanamycin, 10 µg/mL Chloramphenicol, 100 µg/ml ampicillin or 10 mM $MgCl_2$. To induce protein production from pBAD33-, pTB146- or pBTOK-based constructs, the corresponding cultures were supplemented with 0.2 % arabinose or 0.5 µM IPTG or 200 ng/ml AHT, respectively. For long term storage of the respective bacterial strains, those strains were grown to an OD_{600} of 1 and supplemented with DMSO to a final concentration of 10% (v/v). The strains were frozen using liquid nitrogen and stored at -70°C.

4.2.2 Conjugation of *S. oneidensis* MR-1 cells

Conjugation of *S. oneidensis* was performed to transfer pNPTS into the cells. Plasmids were introduced in *S. oneidensis* by mating, using *E. coli* WM3064 as a donor strain. After overnight cultivation of recipient and donor strain, 2 ml of the culture was centrifuged (1 min, 13,000 rpm) and washed three times in LB medium. Both pellets were unified in 250 µl LB medium and spotted as three drops on a LB-agar plate containing 300 µM DAP. After incubation for 12 h at 30 °C, colonies were suspended in 2 ml LB, washed three times in LB and plated on LB-agar plates supplemented with the respective antibiotics for selection. Kanamycin resistant colonies were cultured overnight in LB without antibiotics and plated on LB agar plates containing 10 % (w/v) sucrose to select for double crossover events. Subsequently, cells were restreaked in parallel on LB and LB kanamycin plates to screen for kanamycin-sensitive colonies. In-frame deletions or insertions were confirmed by colony PCR. For complementation, the genes of interest were cloned into vector pBAD33 and expressed from the L-arabinose-inducible promoter of the plasmid. The genes encoding the endolysin (R) and the spanins (Rz and Rz1) were placed behind the intergenic region between *SO_2974* and *SO_2975*, which was hypothesized to harbour

a promoter region responsible for the expression of lysis genes on the broad-host range plasmid pBBR1MCS-2 (pBBR1-λSoPLys).

4.2.3 Electroporation

Electroporation was used to introduce pBAD33 plasmids into *S. oneidensis* MR-1. 2 ml of the respective *S. oneidensis* culture (OD_{600}) was centrifuged for 3min at 8,000 rpm. The obtained pellet was resuspended in 1 ml cold sorbitol (1 M) and centrifuged again (cells have to be kept cold from this point onwards). The supernatant was removed completely and the cell pellet was resuspended in 50 µl fresh sorbitol. Approximately 100 ng of the plasmid in question was added to the cells. The solution was then transferred to a fresh, cold electroporation cuvette and electroporation was performed by applying a pulse of 2.5 kV for 4-5 ms. After this, 1 mL of LB was added and the cells were incubated for 1-2 h at 30°C to be able to regenerate. The mixture was then centrifuged and the bacterial pellet was resuspended in 100 µl LB, followed by plating on LB agar plates containing chloramphenicol, which were incubated at 30°C for 1-2 days.

4.2.4 Induction and cultivation of phages

To derive λSo from the respective *S. oneidensis* strain, the phages were induced either through addition of 10 µg/mL mitomycin C to an exponentially growing liquid culture of the corresponding strains or an incubation of the culture at 30°C at 40 rpm for ~48 hours (unless otherwise stated) [199]. To prepare the phage lysate, the entire cell material was then pelleted in a centrifuge at 13,000 rpm for 15 minutes or 3,500 rpm for 5 minutes at room temperature, which was followed by a filtration of the supernatant using a 0.25-µm filter. To determine the PFU per milliliter of the phage lysate, a plaque assay was performed. Working stocks were stored at 4°C.

4.2.5 Determination of phage lysis profiles

To verify the ability of phage-induced host lysis, spot test and bulk culture OD measurements were performed. For spot test analysis, phage lysates were isolated from the corresponding bacterial strains which were incubated for 48 hours (30°C) by centrifugation (5,000 rpm, 5 minutes); 1.5 mL of an exponential growing bacteria

suspension lacking the λSo genome was inoculated in 30 mL 0.5% soft-agar supplemented with or without 10 mM MgCl2 (30) and spread on LB plates; 3 µL of individual phage lysates was spotted onto the surface of the plates. The lysing properties of the phages were displayed by forming clear zones on the bacterial lawn.

For bulk culture OD measurements, overnight cultures of the corresponding bacterial strains were adjusted to an OD600 of 0.2 in 250-mL erlenmeyer flasks with 15 mL of LB. The flasks were incubated at 30°C with constant shaking at 180 rpm with or without membrane-stabilizing conditions. After induction of λSo mutants with MMC, the optical density was determined for a total of 6 hours. For the first two time points, measurements at 60-minute intervals were conducted, following regular 30-minute intervals until the end of the experiment. The data were plotted using GraphPad Prism 10 (GraphPad Software).

4.2.6 Microscopy

Samples for all microscopy images were harvested from the appropriate exponential growing *S. oneidensis* or *E. coli* cultures. Microscopy images were acquired by a DMI6000 B inverse microscope (Leica) equipped with a pco.edge sCMOS camera (PCO) and an HC PL APO 100×/1.40 oil PH3 phase contrast objective utilizing the VisiView software (Visitron Systems GmbH). Images were subsequently analysed and edited using the ImageJ-based Fiji tool [255], PowerPoint 2019 (Microsoft Corporation), AffinityDesigner 1.7v and Bacstalk [256].

4.2.7 Determination of cell length

The protein production was induced using 0,2% arabinose in exponentially growing planktonic cultures of the respective strains and incubated for 2 ½ hours. All cell suspensions were adjusted to an OD_{600} of 0.3 and 4 µl of each suspension was placed on an agar pad. Image acquisition was carried out using a DMI6000 B inverse microscope (Leica) equipped with a pco.edge sCMOS camera (PCO) and an HC PL APO 100×/1.40 oil PH3 phase contrast objective utilizing the VisiView software (Visitron Systems GmbH). Cell lengths were determined of at least 300 cells per strain using Bacstalk from duplicates in two independent experiments [256].

4.2.8 One-step growth experiment

To determine the latent period and burst size of λSo, a one-step growth experiment was performed [257]. Briefly, 20 mL of cell culture of *S. oneidensis* ΔλSo ΔMuSo1 ΔMuSo2 was prepared in LB medium and incubated at RT. On the following day, 160 mL of LB medium was mixed with 1.6 mL of the grown culture and left to stand on the shaker at 32°C up to an OD600 of ~0.4. The entire preparation was then divided into 3 × 50 mL samples and centrifuged at 6,000 rpm for 15 minutes at 4°C. The supernatant was removed, and the pellets were each divided into 500 µL LB medium. Lambda phage solution (1.21·109 PFU/mL) was added to the bacteria at dilutions of 1:50, 1:500, and 1:5,000. The phages were allowed to adsorb for 1 minute. After adsorption, free phage particles were removed by centrifugation. The pellet was resuspended in 1 mL LB medium. The preparations were each added to 99 mL LB medium and incubated at RT and 120 rpm. At 5-minute intervals, 250-µL samples were taken, mixed with 5 mL of soft agar [0.3% (wt/vol)], and poured over an LB plate. Resulting plaques were quantified following overnight incubation at 30°C. The burst size was calculated by dividing the average phage titer at the plateau phase by the average phage titer along the latent phase.

4.2.9 Bacterial Two Hybrid Assay

The Bacterial Two-Hybrid (BACT) system is a method with which protein-protein interactions can be detected [258]. For this purpose, 20 µl of chemically competent *E. coli* BTH 101 were transformed with 1 µl of the corresponding plasmids by heat shock. Regeneration was carried out by adding 900 µl of LB medium for 1 h at 30 °C. The entire transformation mixture was then transferred to test tubes containing 5 ml LB medium, supplemented with 50 µg/ml kanamycin and 100 µg/ml ampicillin as selection markers. The incubation was carried out overnight at 30 °C. On the following day, 10 µl of the overnight cultures were plated onto LB agar plates containing 50 µg/ml kanamycin, 100 µg/ml ampicillin, 50 µg/ml X-Gal and 1mM IPTG in duplicates. Bacteria expressing interacting hybrid proteins show clearly visible blue colonies. Cells that do not have interacting hybrid proteins show a white colouration of the colonies in the presence of X-Gal. The addition of IPTG enables the increased expression of β-galactosidase.

4.2.10 Measurement of planktonic growth

Cell cultures with set OD_{600} were inoculated into a transparent, flat bottom 96-well plate (Sarstedt, Germany) to generate growth curves. Each well was filled with 250 µl of the respective culture. The plate was inserted into a microplate reader (INFINITE M NANO+, Tecan, CH) and incubated at 30°C under constant shaking. The OD_{600} was measured every 10 min for set period of time. Growth curves were generated with Microsoft Excel and GraphPad Prism 10 (GraphPad Software) using the obtained data points. All experiments were conducted in biological triplicates.

4.2.11 Membrane depolarization assay

Bis-(1,3-dibutylbarbituric acid) trimethine oxonol [$DiBAC_4(3)$; Molecular Probes] was used for staining of depolarized cells [259]. A 10 mg/mL (wt/vol) stock solution was prepared in DMSO. Working solutions [200 mg/mL (wt/vol) in water and 0.5% Tween20] were prepared freshly. About 500 mL liquid culture aliquots was collected by centrifugation (13,000 rpm, 3 minutes). All steps were performed at room temperature. Pellets were resuspended in 200 mL PBS and stained with DiBAC4(3) at a final concentration of 1 mg/mL (wt/vol) for 20 minutes in the dark. After three steps of washing with 200 mL PBS, cells were resuspended in 200 mL PBS and evaluated using the TECAN plate reader. The used bis-oxonal has an excitation maximum of 490 nm and an emission maximum of 516 nm. The data were plotted using GraphPad Prism 10 (GraphPad Software).

4.3 Molecular biological methods

4.3.1 Polymerase chain reaction

The polymerase chain reaction (PCR) was used to amplify DNA fragments required for cloning and verification of genomic mutations. The starter oligonucleotides were designed using Benchling (Biology Software, https://benchling.com). This tool searches for DNA regions with ~ 50% GC-content, 60°C melting temperature and more than 18 bp in length. The DNA was then synthesized by Microsynth AG (Balgach, Switzerland) using a method that is based on chain-termination sequencing by Sanger [260]. The Phusion polymerase was

used to amplify DNA fragments for cloning, since this polymerase has proof reading activity [261]. To verify genomic mutations, the Taq-polymerase was used. For difficult samples with strong secondary structures DMSO was added to a final concentration of 2.5 % to linearize the DNA. The exact program for each polymerase is described in tables 17 and 18. Consecutively, the PCR product was analyzed in agarose gels and purified either with the DNA probe purification kit (Omega Biotek, Norcross) or gel extraction kit (Omega Biotek, Norcross). The procedure was done according to manufacturer information.

Table 17: PCR programm

Cycle	Temperature	Time
1	95 °C (Taq) 98 °C (Phusion)	5 min 30 sec
30	95 °C (Taq) 98 °C (Phusion)	30 sec 30 sec
	56 - 60 °C	30 sec
	72 °C	diverse
1	72 °C	10 min

Table 18: Composition of the PCR reagents

Component	Taq PCR	Phusion PCR
$_{dd}H_2O$	19,. µL	36.65 µL
Reaction buffer	2.5 µL	10 µL
dNTP´s	0.5 µL	1.5 µL
fwd Primer (50 µM)	0.3 µL	0.3 µL
rev Primer (50 µM)	0.3 µL	0.3 µL
Polymerase	1 µL	0.25 µL
Template	1 µL	1 µL
Total Volume	25 µL	50 µL

4.3.2 Agarose gel electrophoresis

DNA probes were supplemented with 5x loading dye (50 % (v/v) glycerine, 0.25 % (w/v) bromphenol blue added to 1 x TAE) and separated by size in 1 % agarose gels prepared in 0.5 x TAE (0.175 % acetic acid, 20 mM Tris base, 0.5 mM EDTA) and 0.005 % EtBr. DNA fragments were visualised using a 2 UV-Transilluminator (UVP, USA).

4.3.3 In vitro digestion of DNA

Plasmids required for cloning were linearised using restriction enzyme digestion. The fast digest enzymes and buffer by Thermo Scientific were used for these reactions and the procedure was done according to manufacturer information (Thermo Fisher Scientific, USA).

4.3.4 Plasmid and strain constructions

Plasmids and corresponding oligonucleotides used in this study are summarized in Tables 15 and 16. For DNA preparations, the appropriate enzymes (Fermentas, St. Leon-Rot, Germany) and kits (VWR International GmbH, Darmstadt, Germany) were used. Gene deletion and insertion strains were generated by sequential double homologous recombination using the suicide plasmid pNPTS-R6K as described earlier [252]. Briefly, substitution fragments were constructed by combining approximately 500-bp fragments of the up- and downstream regions of the designated gene. For gene deletions, a few codons (typically around six) of the corresponding reading frame were kept. Single or multiple nucleotide substitutions were done by inserting a modified gene fragment into the corresponding gene deletion. Plasmids were constructed using standard Gibson assembly protocols [262] and transferred into *Shewanella* cells by electroporation or conjugative mating with *E. coli* WM3064. To isolate plasmids, the corresponding *E. coli* strains with the plasmid to be isolated were inoculated in LB medium with the respective antibiotic and incubated overnight at 37°C with shaking (180 rpm). Subsequently, 6 - 8 mL of the culture were harvested and the plasmid was isolated using a kit ‘E.Z.N.A Plasmid DNA mini Kit I’ according to the manufacturer's instructions.

4.3.5 Gibson Assembly

The Gibson assembly describes a method in which nucleic acid fragments previously synthesised by PCR are joined together isothermally [262–264]. In this work, the Gibson assembly was used to generate plasmids. Among other things, this required the aforementioned PCR products, a linearised vector and the Gibson master mix. The master mix contained a 5'-exonuclease, a DNA polymerase and a DNA ligase. The previously cut vector and DNA fragments were required in equimolar quantities. These were added to the

Gibson Assembly-Master Mix and incubated at 50°C for one hour. Since both the PCR fragments and the linear vector contain regions that serve as recognition sequences for certain restriction enzymes and are therefore homologous to each other, the fragments can be incorporated into the linear vector. The polymerase fills the gaps trough insertion of fitting nucleotides, whereupon the ligase closes the strand breaks. This is resulting in a circular vector with containing the insert of interest.

4.4 Biochemical methods

4.4.1 SDS- Page and Western blotting

Protein fusions were tested for stability and expression using western blot analysis. Cells were grown in liquid culture until exponential phase to generate lysates. At an OD_{600} of 0.5 the cells of the appropriate strains were either treated with 10 µg/µL MMC to induce λSo or treated with 0.2% Arabinose / 0,5 µM IPTG / 200 ng/ml AHT to induce protein production and harvested by centrifugation at different time points. Cells corresponding to an OD_{600} of 10 were resuspended in sample buffer, heated at 99°C for 5 minutes, and stored at −20°C [265]. 10 µL of the sample was resolved by SDS-PAGE using 12.5% polyacrylamide gels. Subsequently, proteins were transferred to nitrocellulose Immobilon-P membrane (Milli-pore, Schwalbach) by semidry transfer. Polyclonal antibodies against GFP, hexa-Histidin and 3xFLAG were used to detect proteins fused to sfGFP, 6xHis or 3xFLAG. Respective antibodies harboured a horseradish peroxidase (HRP) fusion, and SuperSignal West Pico chemiluminescent substrate (Thermo Scientific, Schwerte, Germany) was used to generate a luminescence signal. The signal was then detected using a Fusion-SL chemiluminescence imager (Peqlab, Erlangen, Germany). All blots and gels shown derive from the same experiments and were processed in parallel.

4.4.2 Protein isolation

For isolation using affinity chromatography, the protein in question was fused with a Hexa-Histidin-Tag as well as a SUMO-cleavage side (for FtsZ and ZipA), using the expression vector pTB146, from which the protein expression can be induced by addition of IPTG to the medium [266]. The corresponding *E. coli* Rosetta or BL21 strain were

inoculated in 1.5 L liquid culture with 10 µg/mL Chloramphenicol as well as 100 µg/ml ampicillin and incubated at 30°C until OD600 of 0.6 [267]. The vector based protein expression was induced with 0.5 mM IPTG - the cell culture was then further incubated for 3 hours. The cells were harvested using centrifugation for 15 min at 6,500 rpm. The obtained pellet was washed with 100 ml of Lysis Buffer then stored until further use at -80°C.

For further experimental procedure the cells were thawed on ice in the corresponding lysis buffer. The pellet was resuspend gently; the cells were lysed using a French press (two passages at 16,000 psi) at 4°C. The suspension was centrifuged for 30 min at 16,500 rpm and 4°C to remove cell debris and unlysed cells. The supernatant was filtered using a 0.22 µm syringe filter and applied to the Äkta system for further chromatography.

A affinity chromatography NiNTA column (HisTrapHP 5 ml, GE Healthcare) was connected to the ÄKTA PURE25 system (GE healthcare), as well as a 150 ml superloop (GE healthcare), which was filled with protein buffer. The sample was injected into the superloop by the use of an external peristaltic pump before the run was started. The first step of the program was to wash the column with 5 column volumes (CV) of water (5 ml/min), followed by equilibration with 5 CV of protein buffer supplemented with 20 mM imidazole (5 ml/min). The sample was applied with a slower rate (1 ml/min) to assure binding of the protein of interest to the NiNTA column (HisTrapHP 5 ml, GE Healthcare). After this step is finished, the unspecific proteins are removed by washing with 10 CV with 5 ml/min of protein buffer, supplemented with 10% of elution buffer. The elution buffer consists of the corresponding protein buffer supplemented with 600 mM imidazole. The proteins were eluted with 3 CV of a linear gradient of lysis buffer with 10% elution buffer to 100% elution buffer (3 ml/min). This step was followed by 3 CV of 100% elution buffer, to assure removal of proteins. Following this, the column was washed with 5 CV of water (5 ml/min) and 5 CV of 20% ethanol (5 ml/min).

6xHis-SUMO-FtsZ was set in a overnight dialysis against at least 2 L of Dialysis/SEC Buffer. This was followed by a collection of the protein from dialysis bag and an addition of 0.7 mM DTT as well as 10 U His-Ulp1 protease. This was incubated for 3 h at 4°C. The protein mixture was purified again using affinity chromatography with a NiNTA column (HisTrapHP 5 ml, GE Healthcare). In this step, the column was washed with 10 CV Wash Buffer after the flow through; the proteins were eluted using a gradient with

5 CV elution Buffer. In the Flowthrough and beginning of Washing the cleaved FtsZ appears. In the gradient step the His-SUMO tag and the His-Ulp1 come off the column.

The obtained proteins were stored at -20°C after snap freezing in liquid nitrogen or they were immediately further purified by using size exclusion chromatography (SEC).

For SEC, four different columns were used depending on the sample volume and protein size. The Superdex 200 (GE Healthcare) and Superdex200 increase (GE Healthcare) columns were used for volumes up to 500 µl and 600 kDa; the Superdex200 PG column (GE Healthcare) was used for volumes up to 2 ml and 600 kDa and the Superpose 6 column (GE Healthcare) was used for volumes up to 2 ml and 5,000 kDa. The SEC method was not only used for protein purification but also for analysis of the aggregation state. For this, proteins were first purified by affinity chromatography and SEC as described above. Following, the superdex 200 increase column (GE healthcare) was used for analysis. The high molecular weight calibration kit (GE healthcare) was used to obtain a calibration curve. This kit consists of blue dextran to determine the void volume of the column and several globular proteins for calibration. The used flow rate was 200 µl/min and the sample size was 200 µl, which is according to manufacturer information for analytical runs. The obtained elution volumes were used to create a calibration curve by plotting the elution volume against a logarithmic scale of the molecular weight of the calibration proteins. The proteins of interest were analysed with SEC by using the same flow rate and sample size and the obtained formula for the calibration curve was used to calculate the molecular weight of the eluted protein. The protein was further analysed by SDS-PAGE to obtain data about the aggregation state. The FtsZ protein was set in a dialysis bag once again embed in 2 L of Dialysis Buffer 2 and left overnight at 4°C. The obtained proteins were stored at -80°C after snap freezing in liquid nitrogen

4.4.3 Sedimentation assay

A sedimentation assay was performed to investigate the filamentation properties of FtsZ with the addition of a proteins of interest [244]. Purified FtsZ (3 µM) was pre-incubated for 15 min with addition of 1 mM ATPγS and 2mM GTP. After this pre-incubation the protein of interest (3 µM) was added and further incubated for another 15 - 60 min. To sediment possible FtsZ polymers, the mixtures were centrifuged for 15 min at 385,900 × g and 25°C using a Beckman MLA-130 rotor in a Beckman TL-100 ultracentrifuge (Beckman Coulter,

USA). After immediate removal of the supernatants, the pellets were dissolved in 250 µL of SDS sample buffer and incubated for 5 min at 95 °C. Samples (10 µL) were loaded onto a 10% SDS-polyacrylamide gel, and proteins were visualized with Coomassie brilliant blue after electrophoresis.

4.4.4 Bioinformatic approaches

The gene map of the λSo genome was generated using the SnapGene 7.0 software (snapgene.com). The sequence of the potential spanin proteins was identified and characterised based on a prediction of protein domains using SMART, SignalP and Deep-Coil [268–270]. Topological prediction and classification of transmembrane proteins were carried out using the DeepTMHMM database [271]. ProtParam was used for the calculation of physical and chemical parameters of proteins [272]. The structure of all mentioned proteins of λSo and *S. oneidensis* were predicted using Alphafold2 [273]. Bioinformatic predictions of the genetic organization of cluster C and the lysis cluster are based on PHAST analysis as well as the NCBI BLASTP database [274]. The obtained data were then analyzed using Pymol (The PyMOL Molecular Graphics System, Version 2.0 Schrödinger, LLC) and the included APBS electrostatics tool [275,276]. A comparison of the primary structure of two proteins of interest was carried out using clustalOmega [277]. The NCBI and Pfam database were accessed to obtain the amino acid sequences of other phage lysis proteins. The collected data was statistically analysed using Prism software (GraphPad Soft-ware, Inc., San Diego, USA) [278]. The test for normal distribution was carried out using an unpaired T-test. The Mann-Whitney test was used to determine differences between two groups [279]. A significance value of $p \leq 0.05$ was considered statistically significant.

Appendix

A Figures

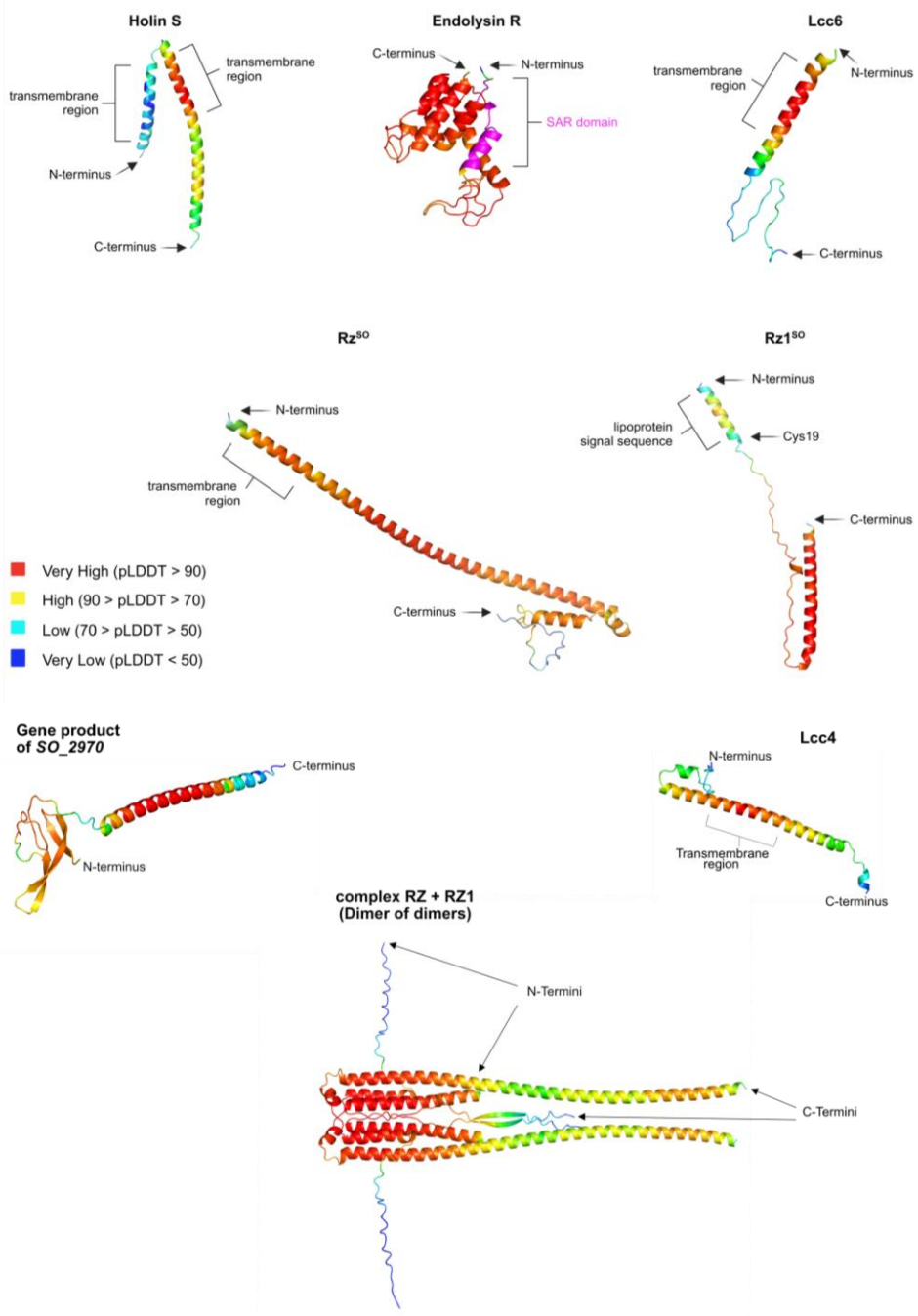

Figure S1: Structures of the λSo lysis proteins as predicted by AlphaFold. 3D structures of the proteins of interest (λSo Holin; λSo Endolysin; λSo lcc6; λSo i-Spanin; λSo o-Spanin) were predicted using Alphafold2 trough DeepMind´s Colab. The structures were visualized with Pymol. N- and C-termini are indicated using arrows, certain protein domains are indicated using brackets. The structures are colour-coded by B-factor values.

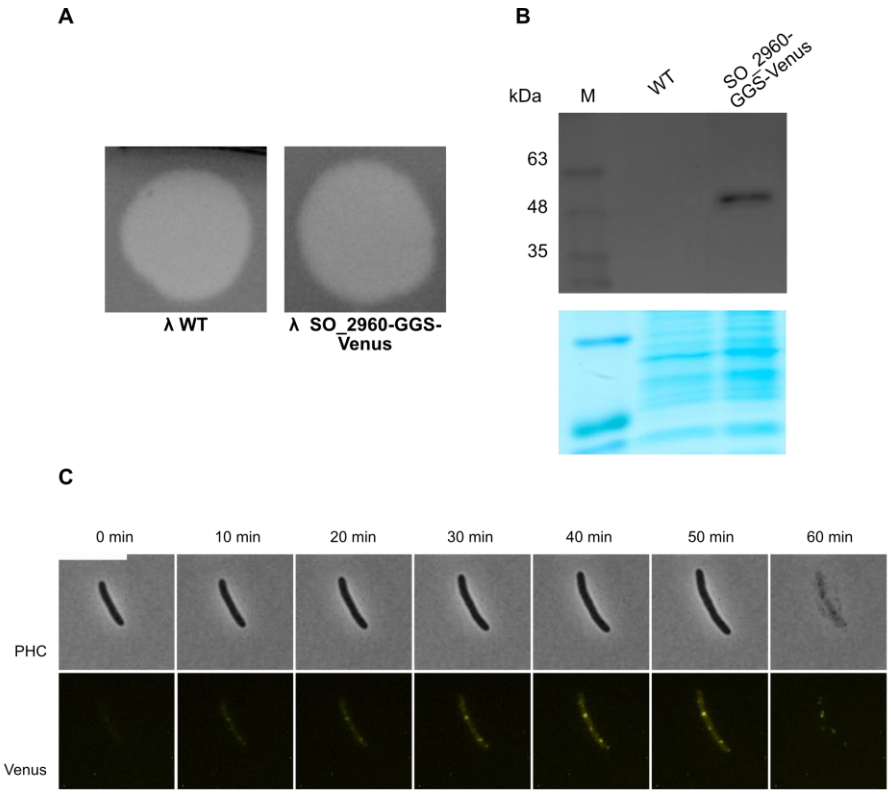

Figure S2: λSO phage particles carrying a SO_2960-Venus-fusion are infectious. (**A**) A spot test was carried out to test the infectivity of the phage lysates. The lysates were dripped onto an LB plate containing *S. oneidenis* Δλ ΔMuSo2 cells. Shown is a representative replicate of replicate of 3 biological replicates. (**B**) A stable protein fusion could be detected in the Western blot. The Venus fusions were detected using an anti-GFP antibody. The Coomassie Brilliant Blue coloured SDS gel serves as a loading control. The unlabelled background strain ΔMuSo1 ΔMuSo2 served as a negative control (labelled here as WT). (**C**) The time-lapse image under the fluorescence microscope shows the production of fluorescent *SO_2960* phage particles and a subsequent subsequent cell lysis of *S. oneidenis* Δλ ΔMuSo2 cells. The *SO_2960*-Venus phage lysate was used in the ratio of an MOI 2. The cells and lysate were incubated for 20 min at 30°C. Subsequently the course of infection was photographed under a fluorescence microscope every 10 min over a period of 3 h. The scale corresponds to 5 µm.

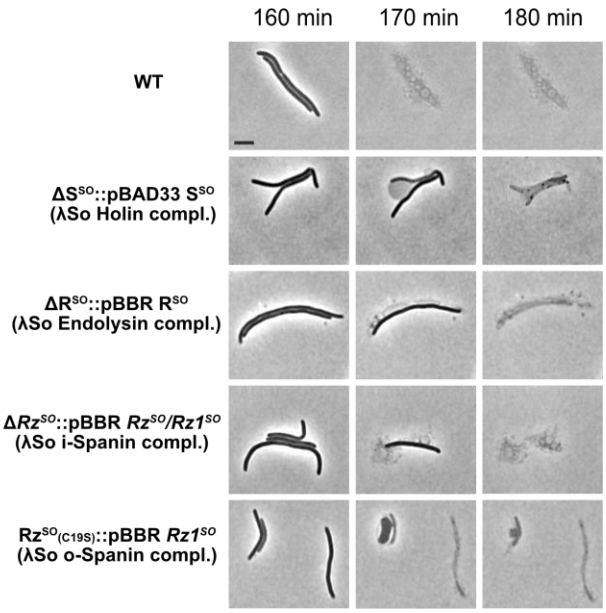

Figure S3: Complementation of λSo lysis mutants. Micrographs of a time-lapse series of *S. oneidensis* wild type and complementations of lysis-defective cells treated with 10 µg/ml MMC. Spanin complementation cells were supplemented with 10 mM $MgCl_2$. The time points are indicated above; time point zero is defined as the start of induction. The scale bar represents 2 µm.

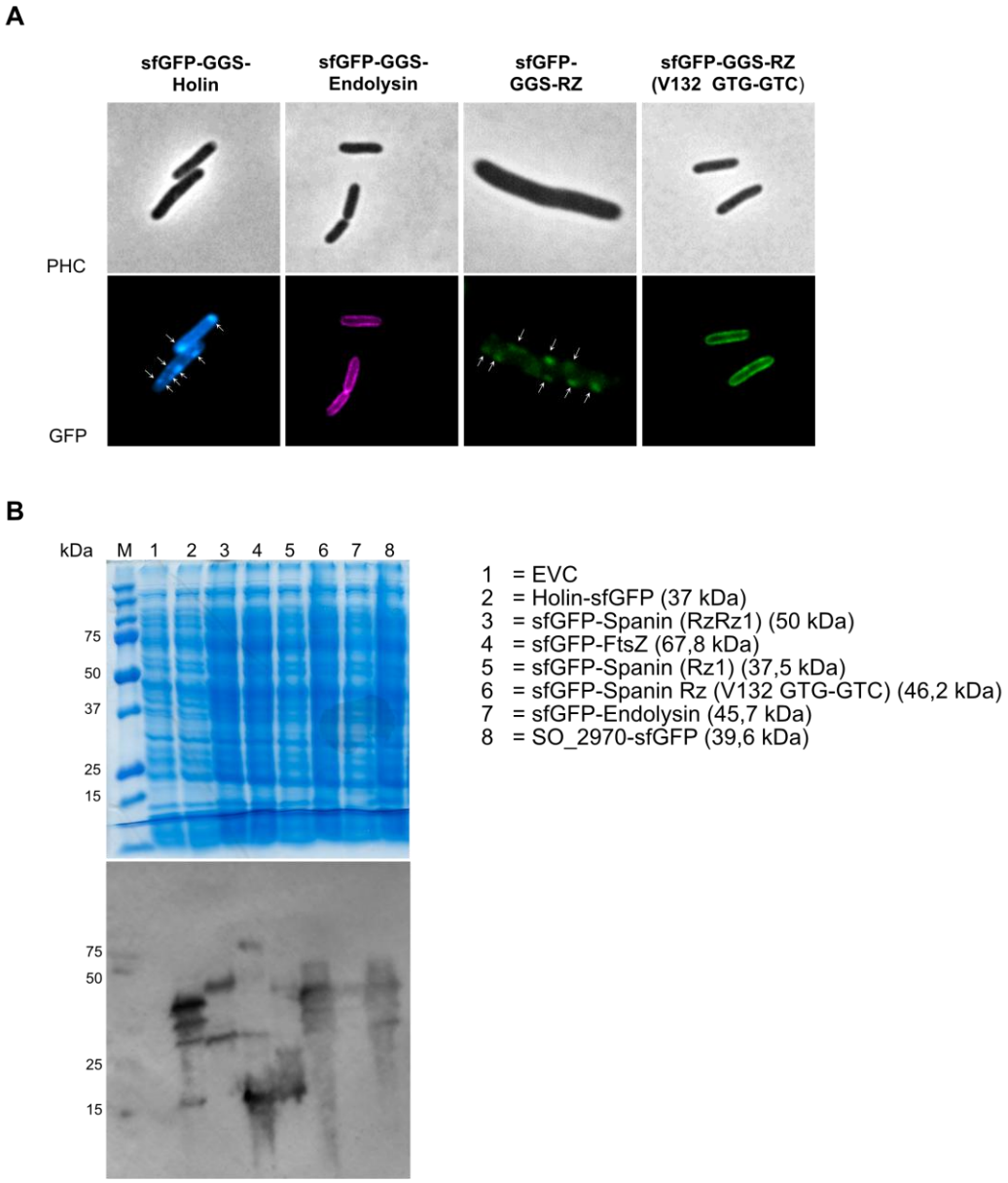

Figure S4: Localisation of the λSo lysis proteins. (**A**) Fluorescence micrographs of *S. oneidensis* MR-1 ΔMuSo1 ΔMuSo2 with fluorescently labelled holin S^{SO}, endolysin R^{SO}, spanin Rz^{SO} as well as spanin proteins carrying a substitution at V132. The fusion proteins sfGFP-holin and sfGFP-spanin show a specific localization, which is indicated above using arrows. The GFP-labelled lysis proteins were expressed using pBAD33. The images were taken 90 min (30 °C, 180 rpm) after induction with 0.2 % L-arabinose in phase contrast and in the fluorescence channel of the fluorophore GFP. (**B**) Visualization of the protein expression of different proteins fused to a sfGFP by western blot analysis. Samples were taken 3 hours after induction of the protein expression with 0,2% arabinose (for pBAD33) or 10 µg/ml MMC (pbbr1). Polyclonal antibodies against GFP were used to detect the respective proteins. Sample normalization was achieved by adjusting cell suspensions to the same optical density at 600 nm (OD_{600}) and analysis of stained SDS-PAGE gels.

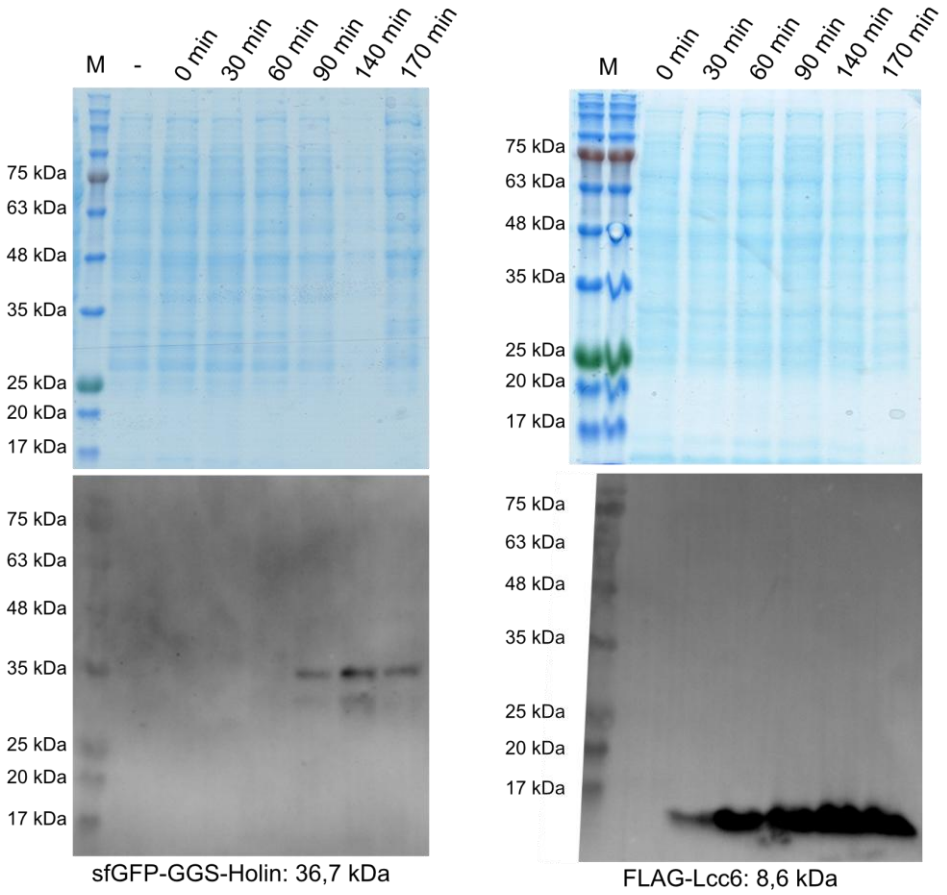

Figure S5: Lcc6 is required for λSo-induced cell lysis. Visualization of the protein expression over time of Holin S^{SO} fused to a sfGFP and Lcc6 fused to a single FLAG-Tag by western blot analysis. Time points are shown as minutes after induction of the phage with 10 µg/µL MMC. Polyclonal antibodies against GFP and 3xFLAG were used to detect the respective proteins. Sample normalization was achieved by adjusting cell suspensions to the same optical density at 600 nm (OD600) and analysis of stained SDS-PAGE gels.

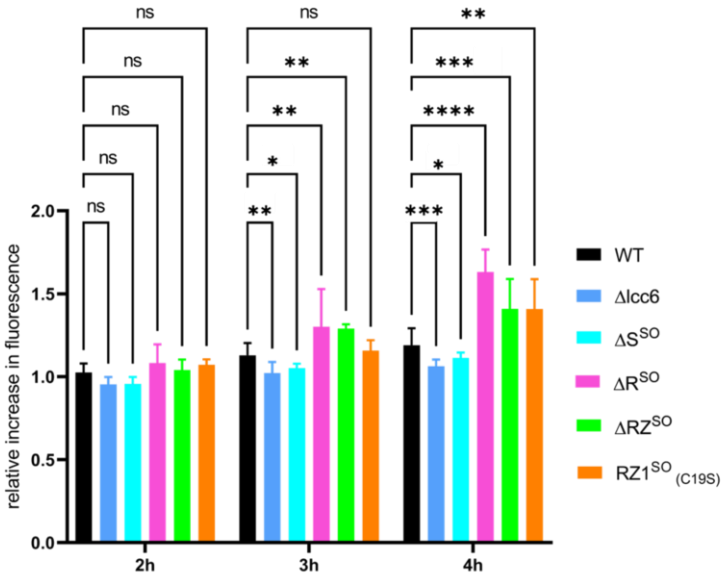

Figure S7: Membrane depolarization assay on λSo mutants using DiBAC$_4$(3). The cells were grown to exponential phase prior to λSo induction by mitomycin C phase and stained with DiBAC$_4$(3) to visualize depolarization after the indicated time points. Statistical significance was determined using a two-way ANOVA (analysis of variance) and is indicated by the P value. NS, not significant,*P value = P ≤ 0.05, **P value ≤ 0.01, ***P value ≤ 0.001, and ****P-value ≤ 0.0001.

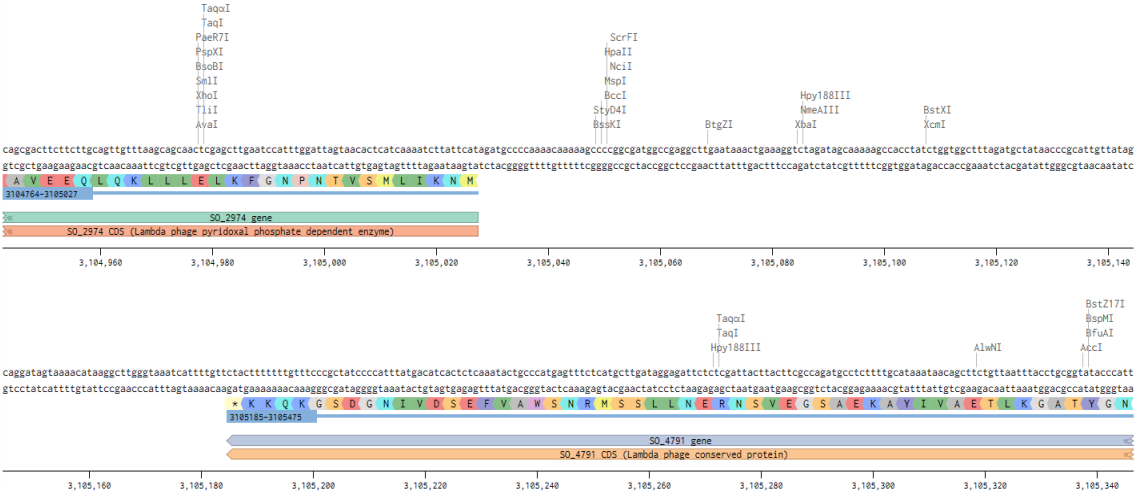

Figure S7: intergenic region of gene *SO_2974* and *SO_2975*. The vector used was pBBR1-MCS2. The predicted promotor is suspected to be localized in the intergenic region of gene *SO_2974* and *SO_2975* (157bp).

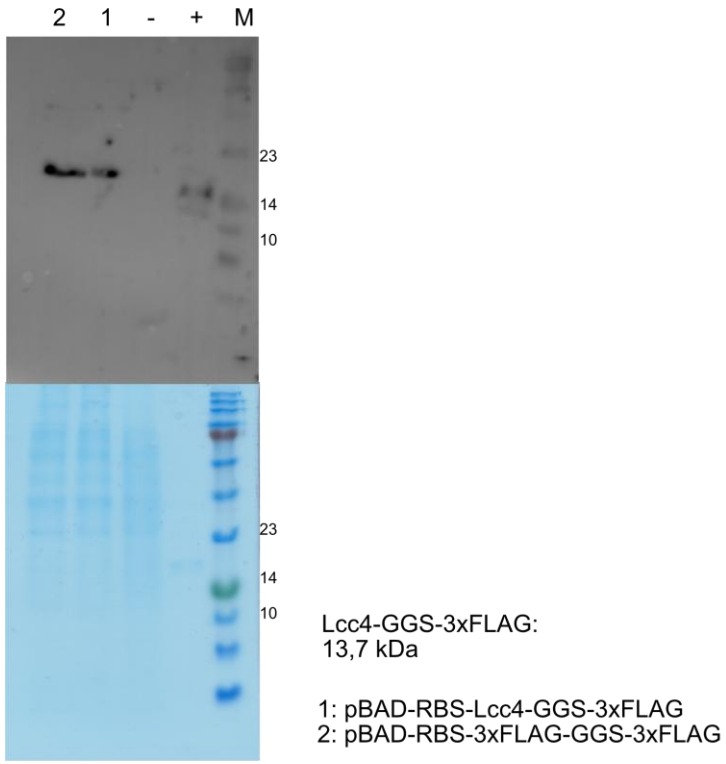

Figure S8: A tripple FLAG-Tag interferes with the function of Lcc4. Visualization of the protein expression over time of Lcc4 fused to a triple FLAG-Tag by western blot analysis. Polyclonal antibodies against 3xFLAG were used to detect the respective proteins. Sample normalization was achieved by adjusting cell suspensions to the same optical density at 600 nm (OD600) and analysis of stained SDS-PAGE gels.

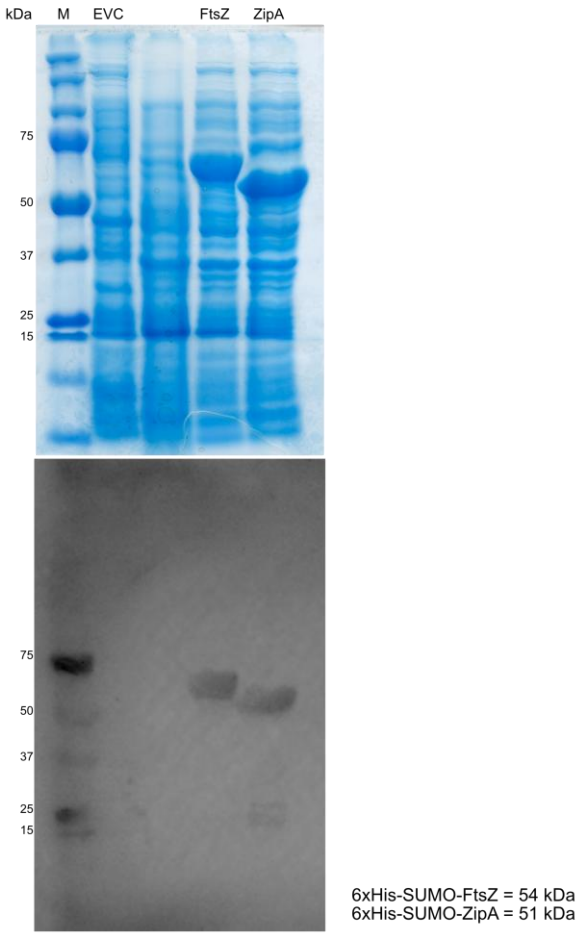

Figure S9: Purification of FtsZ and ZipA. Visualization of the protein expression of FtsZ as well as ZipA fused to a fused to a Hexa-Histidin-Tag as well as a SUMO-cleavage-side by western blot analysis. Polyclonal antibodies against 6cHis were used to detect the respective proteins. Sample normalization was achieved by adjusting cell suspensions to the same optical density at 600 nm (OD_{600}) and analysis of stained SDS-PAGE gels

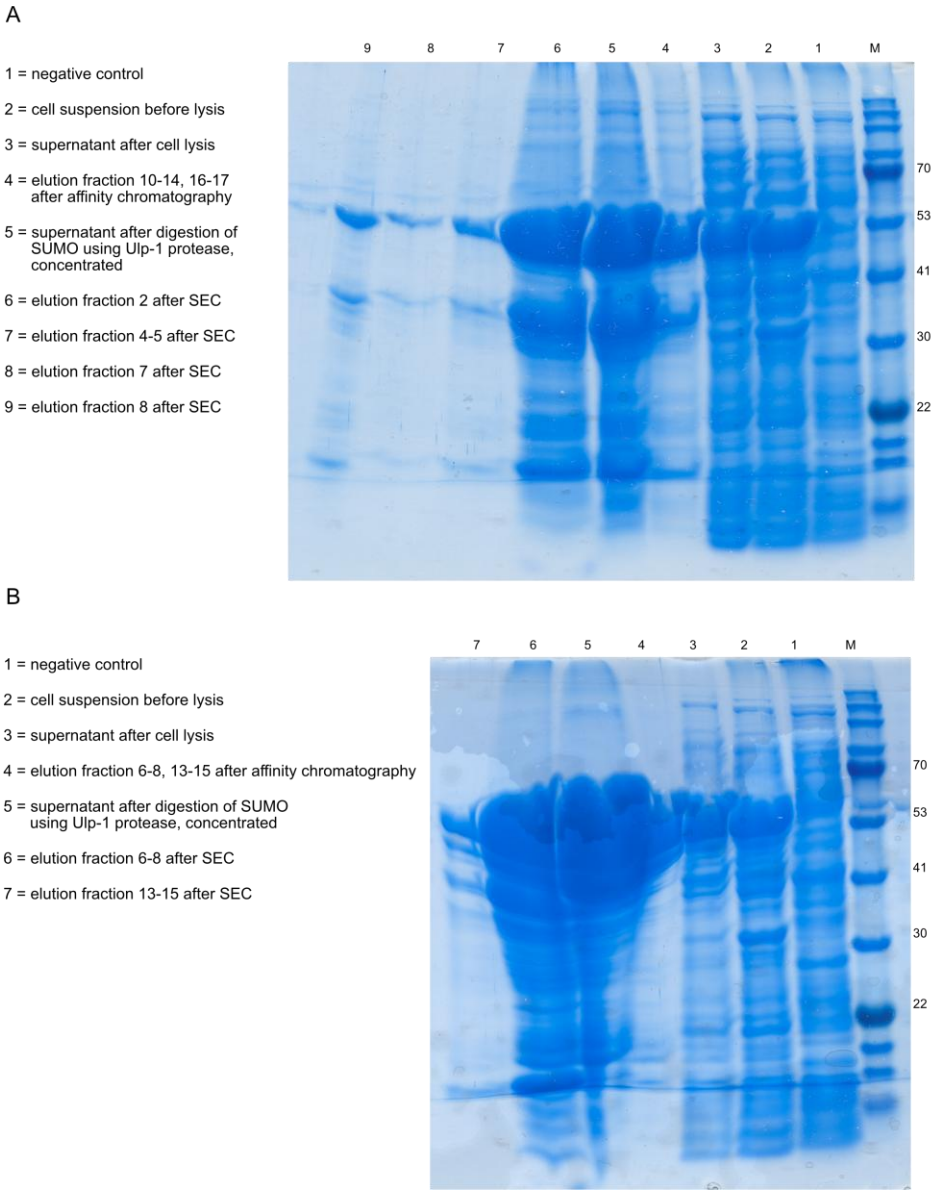

Figure S10: Purification of FtsZ and ZipA. Visualization of the protein expression of FtsZ as well as ZipA fused to a Hexa-Histidin-Tag as well as a SUMO-cleavage-side during the purification process by SDS page polyacrylamide analysis.

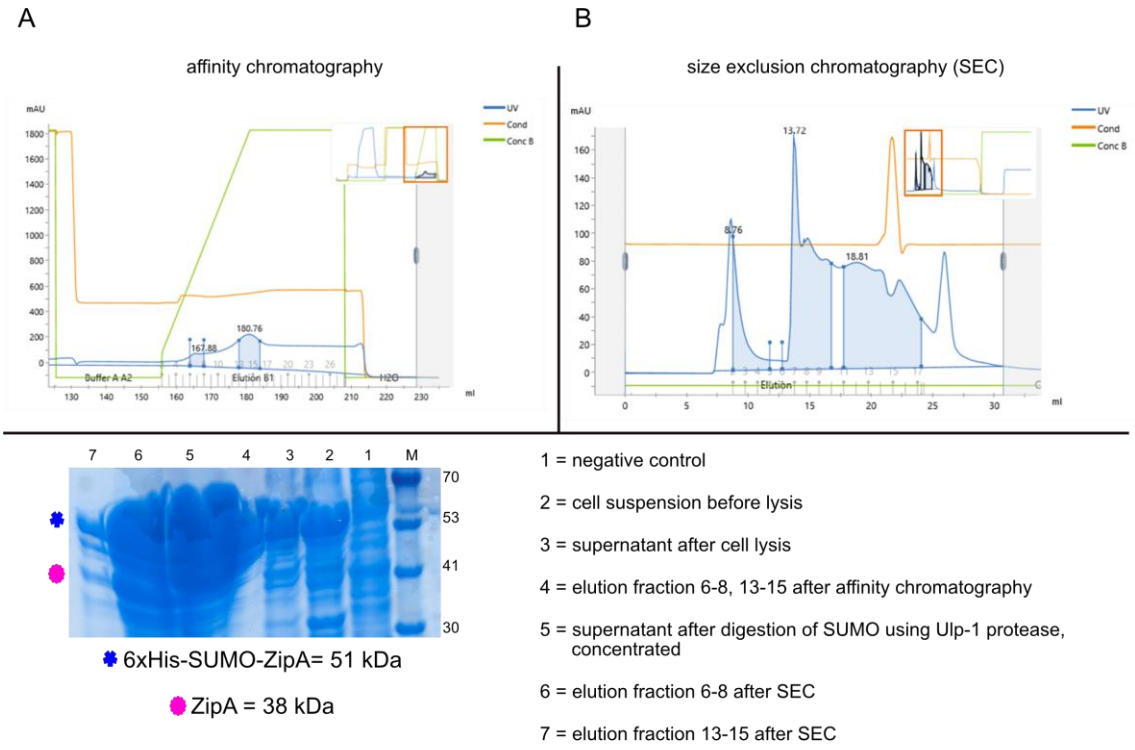

Figure S11: Purification of ZipA using affinity- and size exclusion chromatography. Displayed in panel A and B are the elution profiles of the affinity as well as the size exclusion chromatography using the Äkta system. For the affinity chromatography, the proteins were eluted using a linear imidazol gradient (displayed in green). (lower panel) Visualization of the protein expression of ZipA fused to a Hexa-Histidin-Tag as well as a SUMO-cleavage-side during the purification process by SDS page polyacrylamide analysis. The original data file of the cropped and reassembled western blot is displayed in S10.

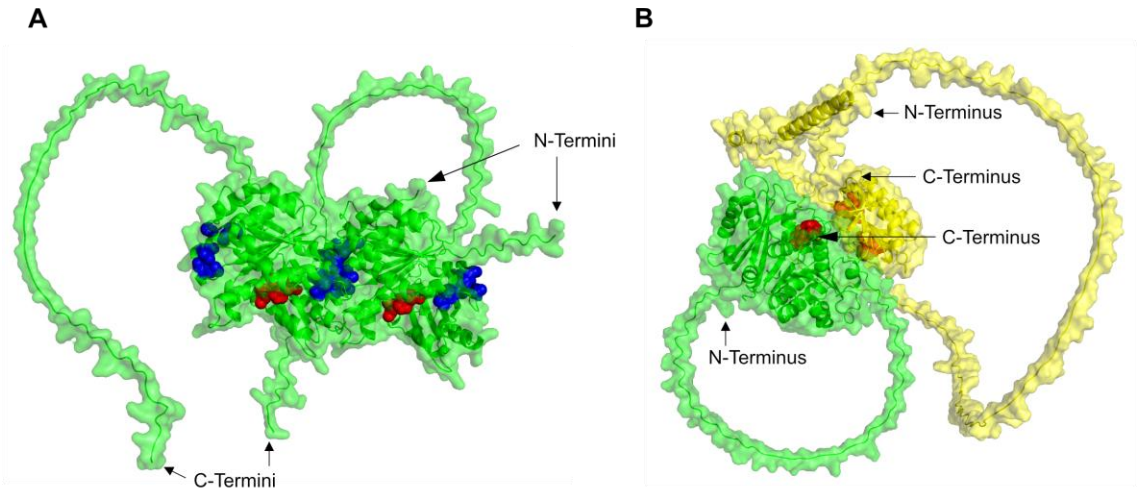

Figure S12: Structure of the hypothesized protein complexes of an FtsZ oligomer as well as FtsZ and ZipA predicted by AlphaFold. 3D structures of the proteins of interest were predicted using Alphafold2 trough DeepMind´s Colab. The structures were visualized with Pymol. The respective amino acids that are part of the interaction surface are color coded as stated. (**A**) Predicted interaction between FtsZ and FtsZ. The possible interaction surface with Lcc4 is shown in red. The amino acid residues important for interaction between the two FtsZ monomers are colored in blue. (**B**) Possible interaction between FtsZ and ZipA. FtsZ is shown in green, ZipA in yellow. The predicted interaction surface of each protein with Lcc4 is shown in red.

B Tables

Table S1: λSO gene numbers old and new annotations

gene number (new)	gene number (old)	trivial name
SO_RS13625	*SO_2938*	Lambda phage encoded lipoprotein
SO_RS13630	*SO_2939*	Lambda phage uncharacterised protein
not annotated	*SO_4790*	Lambda phage uncharacterised protein
SO_RS13635	*SO_2940*	*j* gene (tail fibre protein)
SO_RS13640	*SO_2941*	*i* gene (tail assembly protein)
SO_RS13645	*SO_2942*	phage transcriptional regulator
SO_RS23090	*SO_2944*	structural protein
SO_RS13660	*SO_2945*	tail fibre protein
SO_RS13665	*SO_2946*	protein with carbohydrate-binding module
SO_RS13670	*SO_2947*	Lambda phage protein of known function
SO_RS13675	*SO_2948*	*k* gene (tail assembly protein)
SO_RS13680	*SO_2949*	*l* gene (minor tail protein)
SO_RS13685	*SO_2950*	Lambda phage uncharacterised protein
SO_RS13690	*SO_2951*	Lambda phage protein of known function
SO_RS13695	*SO_2952*	*m* gene (minor tail protein)
SO_RS13700	*SO_2953*	*h* gene (tail length tape measure protein H)
SO_RS23020	*SO_2954*	Lambda phage uncharacterised protein
SO_RS13705	*SO_2955*	*g* gene (minor tail protein G)
SO_RS13710	*SO_2956*	*v* gene (major tail protein V)
SO_RS13715	*SO_2957*	Lambda phage protein of known function DUF3168
SO_RS13720	*SO_2958*	HK97-gp10 family
SO_RS13725	*SO_2959*	Lambda phage uncharacterised protein
SO_RS13730	*SO_2960*	head-tail joining protein
SO_RS13735	*SO_2961*	head-tail connector protein HK97-gp6 family
SO_RS13740	*SO_2962*	helical domain protein
SO_RS13745	*SO_2963*	major capsid protein
SO_RS13750	*SO_2964*	head maturationn protease
SO_RS13755	*SO_2965*	*b* gene (phage portal protein B)
SO_RS23025	*SO_2966*	Lambda phage uncharacterised protein
SO_RS13760	*SO_2968*	*a* gene (terminase A)
SO_RS13765	*SO_2969*	endonuclease HNH family
SO_RS13770	*SO_2970*	Lambda phage uncharacterised protein
SO_RS13775	*SO_2971*	*s* gene Holin
not annotated	*SO_2972*	*rz1* Spanin
SO_RS13780	*SO_2972*	*rz* Spanin
SO_RS13785	*SO_2973*	*r* gene Endolysin
SO_RS13790	*SO_2974*	pyridoxal phosphate dependent enzyme
SO_RS13795	*SO_4791*	Lambda phage conserved protein
SO_RS13800	*SO_2975*	Lambda phage uncharacterised protein
SO_RS13805	*SO_2976*	Lambda phage uncharacterised protein

not annotated	*SO_4792*	Lambda phage uncharacterised protein
SO_RS13810	*SO_2977*	Lambda phage uncharacterised protein
SO_RS13815	*SO_2978*	Integrase
SO_RS13820	*SO_2979*	Lambda phage uncharacterised protein
SO_RS13825	*SO_2980*	Lambda phage protein
SO_RS13830	*SO_2981*	Lambda phage uncharacterised protein
SO_RS13835	*SO_2982*	Lambda phage uncharacterised protein
SO_RS13840	*SO_2983*	Lambda phage uncharacterised protein
SO_RS13845	*SO_2984*	*p* gene (replication protein P)
SO_RS13850	*SO_2985*	*o* gene (replication protein O)
SO_RS13855	*SO_2986*	Lambda phage uncharacterised protein
SO_RS13860	*SO_2987*	Lambda phage uncharacterised protein
SO_RS13865	*SO_2988*	*cII* gene (regulatory protein cII)
SO_RS13870	*SO_2989*	*cro* gene (transcriptional repressor of early genes Cro)
SO_RS13875	*SO_2990*	*cI* gene (lytic gene repressor CI)
SO_RS13880	*SO_2991*	Lipoprotein
SO_RS13885	*SO_2992*	Lambda phage protein of unknown function
SO_RS13890	*SO_4793*	Lambda phage uncharacterised protein
SO_RS13895	*SO_2993*	type II DNA modification methyltransferase
SO_RS13900	*SO_2995*	Lambda phage uncharacterised protein
SO_RS13905	*SO_2997*	Lambda phage uncharacterised protein
SO_RS13910	*SO_2998*	Lambda phage uncharacterised protein
SO_RS23035	*SO_2999*	Lambda phage uncharacterised protein DUF1317
SO_RS13915	*SO_3000*	Lambda phage uncharacterised protein
SO_RS13920	*SO_3001*	Lambda phage uncharacterised protein
SO_RS13925	*SO_3002*	Lambda phage uncharacterised protein
SO_RS13930	*SO_3003*	Lambda phage uncharacterised protein
SO_RS13935	*SO_3004*	*dam* gene (type II restriction-modification system DNA N-6-adenine-methytransferase)
SO_RS13940	*SO_3005*	Lambda phage uncharacterised protein
SO_RS13945	*SO_3006*	*dcm* gene (type II restriction modification system cytosine-5 DNA methyl-transferase Dcm
not annotated	*SO_4794*	*lcc1*
SO_RS23415	*SO_3007*	*lcc2*
SO_RS13950	*SO_3008*	*lcc3*
SO_RS13955	*SO_3009*	*lcc4*
SO_RS13960	*SO_3010*	*lcc5*
SO_RS13965	*SO_4795*	*lcc6*
SO_RS13970	*SO_3012*	*xis* gene (DNA excisionase X)
SO_RS13975	*SO_3013*	*int* gene (Integrase Int)

Table S2: New annotations of genes

	old	new
endonuclease	SO_2969	SO_RS13765
	SO_2970	SO_RS13770
holin	SO_2971	SO_RS13775
spanin	SO_2972	SO_RS13780
endolysin	SO_2973	SO_RS13785
	SO_2974	SO_RS13790
dcm	SO_3006	SO_RS13945
cluster C	SO_4794-SO_4795	?-SO_RS13965
lcc1	SO_4794	not annotated
lcc2	SO_3007	SO_RS23415
lcc3	SO_3008	SO_RS13950
lcc4	SO_3009	SO_RS13955
lcc5	SO_3010	SO_RS13960
lcc6	SO_4795	SO_RS13965
xis	SO_3012	SO_RS13970
int	SO_3013	SO_RS13975

Table S3: Confidence metrics of the oligomer of the λSo spanins

Homooligomers					
	Rz dimer	Rz trimer	Rz tetramer	Rz pentamer	Rz hexamer
Mean pLDDT:	64.5656	58.0492	59.2988	42.1578	44.2286
pTM:	0.4834	0.4968	0.4578	0.3172	0.3099
ipTM:	0.4686	0.4833	0.4295	0.2673	0.2645
Heterooligomers					
	Rz trimer + Rz1 dimer	Rz dimer + Rz1 dimer	Rz trimer + Rz1 dimer without signal peptide		
Mean pLDDT:	64.5656	69.3300	60.7036		
pTM:	0.4834	0.6223	0.518		
ipTM:	0.4686	0.6060	0.4747		

References

1. Dion, M. B., Oechslin, F. & Moineau, S. Phage diversity, genomics and phylogeny. *Nat. Rev. Microbiol.* **18**, 125–138 (2020).
2. Whitman, W. B., Coleman, D. C. & Wiebe, W. J. Prokaryotes: The unseen majority. *Proc. Natl. Acad. Sci.* **95**, 6578–6583 (1998).
3. Clokie, M. R. J., Millard, A. D., Letarov, A. V. & Heaphy, S. Phages in nature. *Bacteriophage* (2011).
4. Bergh, Ø., BØrsheim, K. Y., Bratbak, G. & Heldal, M. High abundance of viruses found in aquatic environments. *Nature* **340**, 467–468 (1989).
5. Brüssow, H., Canchaya, C. & Hardt, W.-D. Phages and the Evolution of Bacterial Pathogens: from Genomic Rearrangements to Lysogenic Conversion. *Microbiol. Mol. Biol. Rev.* **68**, 560–602 (2004).
6. Haerter, J. O., Mitarai, N. & Sneppen, K. Phage and bacteria support mutual diversity in a narrowing staircase of coexistence. *ISME J.* **8**, 2317–2326 (2014).
7. Chan, B. K., Abedon, S. T. & Loc-Carrillo, C. Phage Cocktails and the Future of Phage Therapy. *Future Microbiol.* **8**, 769–783 (2013).
8. Schmelcher, M. & Loessner, M. J. Application of bacteriophages for detection of foodborne pathogens. *Bacteriophage* **4**, e28137 (2014).
9. Zhu, Y., Shang, J., Peng, C. & Sun, Y. Phage family classification under Caudoviricetes: A review of current tools using the latest ICTV classification framework. *Front. Microbiol.* **13**, 1032186 (2022).
10. Zerbini, F. M. *et al.* Changes to virus taxonomy and the ICTV Statutes ratified by the International Committee on Taxonomy of Viruses (2023). *Arch. Virol.* **168**, 175 (2023).

11. Pope, W. H. *et al.* Whole genome comparison of a large collection of mycobacteriophages reveals a continuum of phage genetic diversity. *eLife* **4**, e06416 (2015).
12. Székely, A. J. & Breitbart, M. Single-stranded DNA phages: from early molecular biology tools to recent revolutions in environmental microbiology. *FEMS Microbiol. Lett.* **363**, fnw027 (2016).
13. Santamaría, R. I., Bustos, P., Van Cauwenberghe, J. & González, V. Hidden diversity of double-stranded DNA phages in symbiotic *Rhizobium* species. *Philos. Trans. R. Soc. B Biol. Sci.* **377**, 20200468 (2022).
14. Nguyen, H. M. *et al.* RNA and Single-Stranded DNA Phages: Unveiling the Promise from the Underexplored World of Viruses. *Int. J. Mol. Sci.* **24**, 17029 (2023).
15. Hatfull, G. F. & Hendrix, R. W. Bacteriophages and their genomes. *Curr. Opin. Virol.* **1**, 298–303 (2011).
16. Salmond, G. P. C. & Fineran, P. C. A century of the phage: past, present and future. *Nat. Rev. Microbiol.* **13**, 777–786 (2015).
17. Hay, I. D. & Lithgow, T. Filamentous phages: masters of a microbial sharing economy. *EMBO Rep.* **20**, e47427 (2019).
18. Zinke, M., Schröder, G. F. & Lange, A. Major tail proteins of bacteriophages of the order Caudovirales. *J. Biol. Chem.* **298**, 101472 (2022).
19. Ackermann, H.-W. Tailed Bacteriophages: The order Caudovirales. *Adv. Virus Res.* (1998) doi:10.1016/s0065-3527(08)60785-x.
20. Ge, X. & Wang, J. Structural mechanism of bacteriophage lambda tail's interaction with the bacterial receptor. *Nat. Commun.* **15**, 4185 (2024).
21. Bertozzi Silva, J., Storms, Z. & Sauvageau, D. Host receptors for bacteriophage adsorption. *FEMS Microbiol. Lett.* **363**, fnw002 (2016).

22. Trifonova, T. S. *et al.* [DNA mapping in the capsid of giant bacteriophage phiEL (Caudovirales: Myoviridae: Elvirus) by analytical electron microscopy]. *Vopr. Virusol.* **66**, 434–441 (2022).

23. Ackermann, H.-W. 5500 Phages examined in the electron microscope. *Arch. Virol.* **152**, 227–243 (2007).

24. Fokine, A. & Rossmann, M. G. Molecular architecture of tailed double-stranded DNA phages. *Bacteriophage* **4**, e28281 (2014).

25. Aksyuk, A. A. & Rossmann, M. G. Bacteriophage Assembly. *Viruses* **3**, 172–203 (2011).

26. Lhuillier, S. *et al.* Structure of bacteriophage SPP1 head-to-tail connection reveals mechanism for viral DNA gating. *PNAS* (2009) doi:106 (21) 8507-8512.

27. Maffei, E. *et al.* Systematic exploration of Escherichia coli phage–host interactions with the BASEL phage collection. *PLoS Biol.* (2021) doi:10.1371/journal.pbio.3001424.

28. Gong, Q. *et al.* Novel Host Recognition Mechanism of the K1 Capsule-Specific Phage of *Escherichia coli* : Capsular Polysaccharide as the First Receptor and Lipopolysaccharide as the Secondary Receptor. *J. Virol.* **95**, e00920-21 (2021).

29. Ackerman, H. W.; Dubow, M. S. *Viruses of Prokaryotes: General Properties of Bacteriophages*. (CRC Press, 1987).

30. Tomasz Olszak, Agnieszka Latka, Bartosz Roszniowski, Miguel A. Valvano, & Zuzanna Drulis-Kawa. Phage Life Cycles Behind Bacterial Biodiversity. *Curr. Med. Chem.* **24**, 3987–4001 (2017).

31. Lwoff, A. Lysogeny. *Bacteriol. Rev.* (1953) doi:10.1128/br.17.4.269-337.1953.

32. Floor, E. Interaction of morphogenetic genes of bacteriophage T4. *J. Mol. Biol.* **47**, 293–306 (1970).

33. Ackermann, H.-W. & Krisch, H. M. A catalogue of T4-type bacteriophages. *Arch. Virol.* **142**, 2329–2345 (1997).

34. Zhang, M., Zhang, T., Yu, M., Chen, Y.-L. & Jin, M. The Life Cycle Transitions of Temperate Phages: Regulating Factors and Potential Ecological Implications. *Viruses* **14**, 1904 (2022).

35. Young, R., Wang, I.-N. & Roof, W. D. Phages will out: strategies of host cell lysis. *Trends Microbiol.* **8**, 120–128 (2000).

36. Cahill, J. & Young, R. Phage Lysis: Multiple Genes for Multiple Barriers. in *Advances in Virus Research* vol. 103 33–70 (Elsevier, 2019).

37. Roughgarden, J. Lytic/Lysogenic Transition as a Life-History Switch. *Virus Evol.* **10**, veae028 (2024).

38. Herskowitz, I. & Hagen, D. The Lysis-Lysogeny decision of phage λ: explicit programming and responsiveness. *Annual Review of Genetics* vol. 14 399–445 (1980).

39. Zamora-Caballero, S. *et al.* Antagonistic interactions between phage and host factors control arbitrium lysis–lysogeny decision. *Nat. Microbiol.* **9**, 161–172 (2024).

40. Brady, A. *et al.* Molecular Basis of Lysis–Lysogeny Decisions in Gram-Positive Phages. *Annu. Rev. Microbiol.* **75**, 563–581 (2021).

41. Erez, Z. *et al.* Communication between viruses guides lysis–lysogeny decisions. *Nature* **541**, 488–493 (2017).

42. Aframian, N. *et al.* Dormant phages communicate via arbitrium to control exit from lysogeny. *Nat. Microbiol.* **7**, 145–153 (2021).

43. Kumar, A., Das, B. & Kumar, N. Vibrio Pathogenicity Island-1: The Master Determinant of Cholera Pathogenesis. *Front. Cell. Infect. Microbiol.* **10**, 561296 (2020).

44. Argov, T. *et al.* Temperate bacteriophages as regulators of host behavior. *Curr. Opin. Microbiol.* **38**, 81–87 (2017).

45. Wang, X. *et al.* Cryptic prophages help bacteria cope with adverse environments. *Nat. Commun.* **1**, 147 (2010).

46. Lally, P. *et al.* A Cryptic Prophage Transcription Factor Drives Phenotypic Changes via Host Gene Regulation. Preprint at https://doi.org/10.1101/2024.09.21.614188 (2024).

47. Ragunathan, P. T., Ng Kwan Lim, E., Ma, X., Massé, E. & Vanderpool, C. K. Mechanisms of Regulation of Cryptic Prophage-Encoded Gene Products in Escherichia coli. *J. Bacteriol.* **205**, e00129-23 (2023).

48. Strathern, A. & Herskowitz, I. Defective prophage in Escherichia coli K12 strains. *Virology* **67**, 136–143 (1975).

49. Lindqvist, B. H. Mechanisms of Genome Propagation and Helper Exploitation by Satellite Phage P4. *Microbiol Rev* **57**, (1993).

50. Lang, A. S., Zhaxybayeva, O. & Beatty, J. T. Gene transfer agents: phage-like elements of genetic exchange. *Nat. Rev. Microbiol.* **10**, 472–482 (2012).

51. Erez, Z. *et al.* Communication between viruses guides lysis–lysogeny decisions. *Nature* **541**, 488–493 (2017).

52. Cenens, W., Makumi, A., Mebrhatu, M. T., Lavigne, R. & Aertsen, A. Phage–host interactions during pseudolysogeny: Lessons from the Pid/ dgo interaction. *Bacteriophage* **3**, e25029 (2013).

53. Mäntynen, S., Laanto, E., Oksanen, H. M., Poranen, M. M. & Díaz-Muñoz, S. L. Black box of phage–bacterium interactions: exploring alternative phage infection strategies. *Open Biol.* **11**, 210188 (2021).

54. Young, R. Phage lysis: do we have the hole story yet? *Curr. Opin. Microbiol.* **16**, 790–797 (2013).

55. Abeysekera, G. S., Love, M. J., Manners, S. H., Billington, C. & Dobson, R. C. J. Bacteriophage-encoded lethal membrane disruptors: Advances in understanding and potential applications. *Front. Microbiol.* **13**, 1044143 (2022).

56. Young, R. Phage lysis: Three steps, three choices, one outcome. *J. Microbiol.* **52**, 243–258 (2014).

57. Chang, C. Y., Nam, K. & Young, R. S gene expression and the timing of lysis by bacteriophage lambda. *J. Bacteriol.* **177**, 3283–3294 (1995).

58. To, K. H., Dewey, J., Weaver, J., Park, T. & Young, R. Functional Analysis of a Class I Holin, P2 Y. *J. Bacteriol.* **195**, 1346–1355 (2013).

59. Reddy, B. L. & Saier, M. H. Topological and phylogenetic analyses of bacterial holin families and superfamilies. *Biochim. Biophys. Acta BBA - Biomembr.* **1828**, 2654–2671 (2013).

60. Wang, I.-N., Smith, D. L. & Young, R. Holins: The Protein Clocks of Bacteriophage Infections. *Annu. Rev. Microbiol.* **54**, 799–825 (2000).

61. Savva, C. G. *et al.* Stable micron-scale holes are a general feature of canonical holins. *Mol. Microbiol.* **91**, 57–65 (2014).

62. Dewey, J. S. *et al.* Micron-scale holes terminate the phage infection cycle. *Proc. Natl. Acad. Sci.* **107**, 2219–2223 (2010).

63. Bläsi, U., Chang, C. Y., Zagotta, M. T., Nam, K. B. & Young, R. The lethal lambda S gene encodes its own inhibitor. *EMBO J.* **9**, 981–989 (1990).

64. Ramanculov, E. & Young, R. Functional analysis of the phage T4 holin in a λ context. *Mol. Genet. Genomics* **265**, 345–353 (2001).

65. Young, R. & Bläsi, U. Holins: form and function in bacteriophage lysis. *FEMS Microbiol. Rev.* **17**, 191–205 (1995).

66. Park, T., Struck, D. K., Deaton, J. F. & Young, R. Topological dynamics of holins in programmed bacterial lysis. *PNAS* doi:10.1073/pnas.0600943103.

67. Lella, M., Kamilla, S., Jain, V. & Mahalakshmi, R. Molecular Mechanism of Holin Transmembrane Domain I in Pore Formation and Bacterial Cell Death. *ACS Chem. Biol.* **11**, 910–920 (2016).

68. Groman, N. B. & Suzuki, G. Quantitative study of endolysin synthesis during reproduction of Lambda phages. *J. Bacteriol.* **86**, 187–194 (1963).

69. Biefikowska-Szewczyk, K., Lipiflska, B. & Taylor, A. The R Gene Product of Bacteriophage Lambda is the Murein Transglycosylase. *Mol. Gen. Genet. MGG* doi:10.1007/BF00271205.

70. Groman, N. B. & Suzuki, G. Relation of endolysin to lysis by lambda bacteriophages. *J. Bacteriol.* **84**, 596–597 (1962).

71. White, R. *et al.* Holin triggering in real time. *Proc. Natl. Acad. Sci.* **108**, 798–803 (2011).

72. Young, R. & Bläsi, U. Holins: form and function in bacteriophage lysis. *FEMS Microbiol. Rev.* **17**, 191–205 (1995).

73. Bläsi, U., Fraisl, P., Chang, C., Zhang, N. & Young, R. The C-terminal sequence of the lambda holin constitutes a cytoplasmic regulatory domain. *J. Bacteriol.* **181**, 2922—2929 (1999).

74. Wang, I.-N. Lysis Timing and Bacteriophage Fitness. *Genetics* **172**, 17–26 (2006).

75. Berry, J., Rajaure, M., Pang, T. & Young, R. The Spanin Complex Is Essential for Lambda Lysis. *J. Bacteriol.* **194**, 5667–5674 (2012).

76. Bonovich, M. T. & Young, R. Dual start motif in two lambdoid S genes unrelated to lambda S. *J. Bacteriol.* **173**, 2897–2905 (1991).

77. Bläsi, U., Nam, K., Hartz, D., Gold, L. & Young, R. Dual translational initiation sites control function of the lambda S gene. *EMBO J.* **8**, 3501–3510 (1989).

78. Bläsi, U. & Young, R. Two beginnings for a single purpose: the dual-start holins in the regulation of phage lysis. *Mol. Microbiol.* **21**, 675–682 (1996).

79. Steiner, M. & Bläsi, U. Charged amino-terminal amino acids affect the lethal capacity of Lambda lysis proteins S107 and S105. *Mol. Microbiol.* **8**, 525–533 (1993).

80. Gründling, A., Smith, D. L., Bläsi, U. & Young, R. Dimerization between the Holin and Holin Inhibitor of Phage λ. *J. Bacteriol.* **182**, 6075–6081 (2000).

81. Pang, T., Savva, C. G., Fleming, K. G., Struck, D. K. & Young, R. Structure of the lethal phage pinhole. *Proc. Natl. Acad. Sci.* **106**, 18966–18971 (2009).

82. Pang, T., Fleming, T. C., Pogliano, K. & Young, R. Visualization of pinholin lesions in vivo. *Proc. Natl. Acad. Sci.* **110**, (2013).

83. Barenboim, M., Chang, C., Dib Hajj, F. & Young, R. Characterization of the dual start motif of a class II holin gene. *Mol. Microbiol.* **32**, 715–727 (1999).

84. Pang, T., Park, T. & Young, R. Mutational analysis of the S ^{21} pinholin. *Mol. Microbiol.* **76**, 68–77 (2010).

85. Park, T., Struck, D. K., Dankenbring, C. A. & Young, R. The Pinholin of Lambdoid Phage 21: Control of Lysis by Membrane Depolarization. *J. Bacteriol.* **189**, 9135–9139 (2007).

86. Pang, T., Park, T. & Young, R. Mapping the pinhole formation pathway of S ^{21}. *Mol. Microbiol.* **78**, 710–719 (2010).

87. Oliveira, H. *et al.* Molecular Aspects and Comparative Genomics of Bacteriophage Endolysins. *J. Virol.* **87**, 4558–4570 (2013).

88. Xu, M., Struck, D. K., Deaton, J., Wang, I.-N. & Young, R. A signal-arrest-release sequence mediates export and control of the phage P1 endolysin. *Proc. Natl. Acad. Sci.* **101**, 6415–6420 (2004).

89. Sun, Q. *et al.* Regulation of a muralytic enzyme by dynamic membrane topology. *Nat. Struct. Mol. Biol.* **16**, 1192–1194 (2009).

90. Xu, M. *et al.* Disulfide Isomerization After Membrane Release of Its SAR Domain Activates P1 Lysozyme. *Science* **307**, 113–117 (2005).

91. Kuty, G. F., Xu, M., Struck, D. K., Summer, E. J. & Young, R. Regulation of a Phage Endolysin by Disulfide Caging. *J. Bacteriol.* **192**, 5682–5687 (2010).

92. Zhang, N. Complementation and characterization of the nested Rz and Rz1 reading frames in the genome of bacteriophage k.

93. Holt, A. *et al.* Phage-encoded cationic antimicrobial peptide required for lysis. *J. Bacteriol.* **204**, JB0021421 (2021).

94. Cahill, J. *et al.* Suppressor Analysis of the Fusogenic Lambda Spanins. *J. Virol.* **91**, e00413-17 (2017).

95. Kongari, R., Snowden, J., Berry, J. D. & Young, R. Localization and Regulation of the T1 Unimolecular Spanin. *J. Virol.* **92**, e00380-18 (2018).

96. Kongari, R., Snowden, J., Berry, J. D. & Young, R. Localization and Regulation of the T1 Unimolecular Spanin. *J. Virol.* **92**, (2018).

97. Berry, J., Rajaure, M., Pang, T. & Young, R. The Spanin Complex Is Essential for Lambda Lysis. *J. Bacteriol.* **194**, 5667–5674 (2012).

98. Kongari, R. *et al.* Phage spanins: diversity, topological dynamics and gene convergence. *BMC Bioinformatics* **19**, 326 (2018).

99. Berry, J. D., Rajaure, M. & Young, R. Spanin function requires subunit homodimerization through intermolecular disulfide bonds. *Mol. Microbiol.* **88**, 35–47 (2013).

100. Cahill, J. *et al.* Genetic Analysis of the Lambda Spanins Rz and Rz1: Identification of Functional Domains. *G3 GenesGenomesGenetics* **7**, 741–753 (2017).

101. Berry, J., Summer, E. J., Struck, D. K. & Young, R. The final step in the phage infection cycle: the Rz and Rz1 lysis proteins link the inner and outer membranes. *Mol. Microbiol.* **70**, 341–351 (2008).

102. Berry, J., Savva, C., Holzenburg, A. & Young, R. The lambda spanin components Rz and Rz1 undergo tertiary and quaternary rearrangements upon complex formation. *Protein Sci.* **19**, 1967–1977 (2010).

103. Berry, J. D., Rajaure, M. & Young, R. Spanin function requires subunit homodimerization through intermolecular disulfide bonds. *Mol. Microbiol.* **88**, 35–47 (2013).

104. Rajaure, M., Berry, J., Kongari, R., Cahill, J. & Young, R. Membrane fusion during phage lysis. *Proc. Natl. Acad. Sci.* **112**, 5497–5502 (2015).

105. Bryl, K., Keôdzierska, S., Laskowska, M. & Taylor, A. Membrane fusion by proline-rich Rz1 lipoprotein, the bacteriophage λ *Rz1* gene product. *Eur. J. Biochem.* **267**, 794–799 (2000).

106. Kongari, R. *et al.* Phage spanins: diversity, topological dynamics and gene convergence. *BMC Bioinformatics* **19**, 326 (2018).

107. Lukacik, P. *et al.* Structural engineering of a phage lysin that targets Gram-negative pathogens. *Proc. Natl. Acad. Sci.* **109**, 9857–9862 (2012).

108. Klimenko, A. I., Matushkin, Y. G., Kolchanov, N. A. & Lashin, S. A. Bacteriophages affect evolution of bacterial communities in spatially distributed habitats: a simulation study. *BMC Microbiol.* **16**, S10 (2016).

109. Ofir, G. & Sorek, R. Contemporary Phage Biology: From Classic Models to New Insights. *Cell* **172**, 1260–1270 (2018).

110. Choi, W.-J. *et al.* Synthetic Fertilizer and Livestock Manure Differently Affect Δ15N in the Agricultural Landscape: A Review. *Agric Ecosyst Env.* **237**, 1 (2017).

111. Drulis-Kawa, Z., Majkowska-Skrobek, G. & Maciejewska, B. Bacteriophages and phage-derived proteins--application approaches. *Curr. Med. Chem.* **22**, 1757–1773 (2015).

112. Samir, S. Molecular Machinery of the Triad Holin, Endolysin, and Spanin: Key Players Orchestrating Bacteriophage-Induced Cell Lysis and their Therapeutic Applications. *Protein Pept. Lett.* **31**, 85–96 (2024).

113. Bulssico, J., PapukashvilI, I., Espinosa, L., Gandon, S. & Ansaldi, M. Phage-antibiotic synergy: Cell filamentation is a key driver of successful phage predation. *PLOS Pathog.* **19**, e1011602 (2023).

114. Beggs, G. A. & Bassler, B. L. Phage small proteins play large roles in phage–bacterial interactions. *Curr. Opin. Microbiol.* **80**, 102519 (2024).

115. Howard-Varona, C. *et al.* Phage-specific metabolic reprogramming of virocells. *ISME J.* **14**, 881–895 (2020).

116. Reisinger, G. Lambda kil-mediated lysis requires the phage context. *Virology* **Volume 193**, (1993).

117. Haeusser, D. P. *et al.* The Kil Peptide of Bacteriophage λ Blocks Escherichia coli Cytokinesis via ZipA-Dependent Inhibition of FtsZ Assembly. *PLoS Genet.* **10**, e1004217 (2014).

118. Hernández-Rocamora, V. M., Alfonso, C., Margolin, W., Zorrilla, S. & Rivas, G. Evidence That Bacteriophage λ Kil Peptide Inhibits Bacterial Cell Division by Disrupting FtsZ Protofilaments and Sequestering Protein Subunits. *J. Biol. Chem.* **290**, 20325–20335 (2015).

119. Studier, F. W. Bacteriophage T7: Genetic and biochemical analysis of this simple phage gives information about basic genetic processes. *Science* **176**, 367–376 (1972).

120. Kiro, R. *et al.* Gene product 0.4 increases bacteriophage T7 competitiveness by inhibiting host cell division. *Proc. Natl. Acad. Sci.* **110**, 19549–19554 (2013).

121. Dhanoa, G. K., Kushnir, I., Qimron, U., Roper, D. I. & Sagona, A. P. Investigating the effect of bacteriophages on bacterial FtsZ localisation. *Front. Cell. Infect. Microbiol.* **12**, 863712 (2022).

122. Heller, D. M., Tavag, M. & Hochschild, A. CbtA toxin of Escherichia coli inhibits cell division and cell elongation via direct and independent interactions with FtsZ and MreB. *PLOS Genet.* **13**, e1007007 (2017).

123. Boeckh, C., Bade, E. G., Delins, H. & Reeve, J. N. Inhibition of bacterial segregation by early functions of phage Mu and association of replication protein B with the inner cell membrane. *Mol. Gen. Genet. MGG* **202**, 461–466 (1986).

124. Stewart, C. R., Deery, W. J., Egan, E. S. K., Myles, B. & Petti, A. A. The product of SPO1 gene 56 inhibits host cell division during infection of Bacillus subtilis by bacteriophage SPO1. *Virology* **447**, 249–253 (2013).

125. Söderström, B. & Daley, D. O. The bacterial divisome: more than a ring? *Curr. Genet.* **63**, 161–164 (2017).

126. Cameron, T. A. & Margolin, W. Insights into the assembly and regulation of the bacterial divisome. *Nat. Rev. Microbiol.* **22**, 33–45 (2024).

127. Barrows, J. M. & Goley, E. D. FtsZ dynamics in bacterial division: What, how, and why? *Curr. Opin. Cell Biol.* **68**, 163–172 (2021).

128. Löwe, J. & Amos, L. A. Crystal structure of the bacterial cell-division protein FtsZ. *Nature* **391**, 203–206 (1998).

129. Lutkenhaus, J. FtsZ ring in bacterial cytokinesis. *Mol. Microbiol.* **9**, 403–409 (1993).

130. Morrison, J. J. & Camberg, J. L. Building the Bacterial Divisome at the Septum. *Subcell. Biochem.* **104**, 49–71 (2024).

131. Fujita, J. *et al.* Structures of a FtsZ single protofilament and a double-helical tube in complex with a monobody. *Nat. Commun.* **14**, 4073 (2023).

132. Huang, K.-H., Durand-Heredia, J. & Janakiraman, A. FtsZ Ring Stability: of Bundles, Tubules, Crosslinks, and Curves. *J. Bacteriol.* **195**, 1859–1868 (2013).

133. Adams, D. W. & Errington, J. Bacterial cell division: assembly, maintenance and disassembly of the Z ring. *Nat. Rev. Microbiol.* **7**, 642–653 (2009).

134. Erickson, H. P., Anderson, D. E. & Osawa, M. FtsZ in Bacterial Cytokinesis: Cytoskeleton and Force Generator All in One. *Microbiol. Mol. Biol. Rev.* **74**, 504–528 (2010).

135. Vega, D. E. & Margolin, W. Direct Interaction between the Two Z Ring Membrane Anchors FtsA and ZipA. *J. Bacteriol.* **201**, (2019).

136. Naha, A., Haeusser, D. P. & Margolin, W. Anchors: A way for FtsZ filaments to stay membrane bound. *Mol. Microbiol.* **120**, 525–538 (2023).

137. Martos, A. *et al.* Isolation, Characterization and Lipid-Binding Properties of the Recalcitrant FtsA Division Protein from Escherichia coli. *PLoS ONE* **7**, e39829 (2012).

138. Pichoff, S., Shen, B., Sullivan, B. & Lutkenhaus, J. FtsA mutants impaired for self-interaction bypass ZipA suggesting a model in which FtsA's self-interaction competes with its ability to recruit downstream division proteins. *Mol. Microbiol.* **83**, 151–167 (2012).

139. Cameron, T. A., Vega, D. E., Yu, C., Xiao, H. & Margolin, W. ZipA Uses a Two-Pronged FtsZ-Binding Mechanism Necessary for Cell Division. *mBio* **12**, e02529-21 (2021).

140. Kuchibhatla, A., Bhattacharya, A. & Panda, D. ZipA Binds to FtsZ with High Affinity and Enhances the Stability of FtsZ Protofilaments. *PLoS ONE* **6**, e28262 (2011).

141. Mahone, C. R. & Goley, E. D. Bacterial cell division at a glance. *J. Cell Sci.* **133**, jcs237057 (2020).

142. Alcorlo, M., Martínez-Caballero, S., Molina, R. & Hermoso, J. A. Regulation of Lytic Machineries by the FtsEX Complex in the Bacterial Divisome. in *Macromolecular Protein Complexes IV: Structure and Function* (eds. Harris, J. R. & Marles-Wright, J.) (2022). doi:10.1007/978-3-031-00793-4_9.

143. Aarsman, M. E. G. *et al.* Maturation of the Escherichia coli divisome occurs in two steps. *Mol. Microbiol.* **55**, 1631–1645 (2005).

144. Bramhill, D. Bacterial cell division. *Annu. Rev. Cell Dev. Biol.* (1997) doi:0.1146/annurev.cellbio.13.1.395.

145. De Leeuw, E. *et al.* Molecular characterization of *Escherichia coli* FtsE and FtsX. *Mol. Microbiol.* **31**, 983–993 (1999).

146. Galinier, A., Delan-Forino, C., Foulquier, E., Lakhal, H. & Pompeo, F. Recent Advances in Peptidoglycan Synthesis and Regulation in Bacteria. *Biomolecules* **13**, 720 (2023).

147. Pazos, M. & Peters, K. Peptidoglycan. in *Bacterial Cell Walls and Membranes* (ed. Kuhn, A.) (2019). doi:10.1007/978-3-030-18768-2_5.

148. Männik, J., Pichoff, S., Lutkenhaus, J. & Männik, J. Cell Cycle-Dependent Recruitment of FtsN to the Divisome in Escherichia coli. *mBio* **13**, e02017-22 (2022).

149. Typas, A., Banzhaf, M., Gross, C. A. & Vollmer, W. From the regulation of peptidoglycan synthesis to bacterial growth and morphology. *Nat. Rev. Microbiol.* **10**, 123–136 (2012).

150. Rohs, P. D. A. & Bernhardt, T. G. Growth and Division of the Peptidoglycan Matrix. *Annu. Rev. Microbiol.* **75**, 315–336 (2021).

151. Spratt, B. G. Distinct penicillin binding proteins involved in the division, elongation, and shape of Escherichia coli K12. *Proc. Natl. Acad. Sci.* **72**, 2999–3003 (1975).

152. Hernández-Rocamora, V. M. *et al.* Real-time monitoring of peptidoglycan synthesis by membrane-reconstituted penicillin-binding proteins. *eLife* **10**, e61525 (2021).

153. Mueller, E. A. & Levin, P. A. Bacterial Cell Wall Quality Control during Environmental Stress. *mBio* (2029) doi:10.1128/mBio.02456-20.

154. Taguchi, A. *et al.* FtsW is a peptidoglycan polymerase that is functional only in complex with its cognate penicillin-binding protein. *Nat. Microbiol.* **4**, 587–594 (2019).

155. Boyle, D. S., Khattar, M. M., Addinall, S. G., Lutkenhaus, J. & Donachie, W. D. ftsW is an essential cell-division gene in Escherichia coli. *Mol. Microbiol.* **24**, 1263–1273 (1997).

156. Rohs, P. D. A. *et al.* A central role for PBP2 in the activation of peptidoglycan polymerization by the bacterial cell elongation machinery. *PLOS Genet.* **14**, e1007726 (2018).

157. Tsang, M.-J., Yakhnina, A. A. & Bernhardt, T. G. NlpD links cell wall remodeling and outer membrane invagination during cytokinesis in Escherichia coli. *PLOS Genet.* **13**, e1006888 (2017).

158. Egan, A. J. F. *et al.* Outer-membrane lipoprotein LpoB spans the periplasm to stimulate the peptidoglycan synthase PBP1B. *Proc. Natl. Acad. Sci.* **111**, 8197–8202 (2014).

159. Jean, N. L. *et al.* Elongated structure of the outer-membrane activator of peptidoglycan synthesis LpoA: implications for PBP1A stimulation. *Struct. Lond. Engl. 1993* **22**, 1047–1054 (2014).

160. Huang, K.-H., Durand-Heredia, J. & Janakiraman, A. FtsZ Ring Stability: of Bundles, Tubules, Crosslinks, and Curves. *J. Bacteriol.* **195**, 1859–1868 (2013).

161. Barreteau, H., Blanot, D., Mengin-Lecreulx, D. & Touzé, T. Lipid Intermediates in Bacterial Peptidoglycan Biosynthesis. in *Biogenesis of Fatty Acids, Lipids and Membranes* (ed. Geiger, O.) (2017). doi:10.1007/978-3-319-43676-0_11-1.

162. Liu, X., Meiresonne, N. Y. & Bouhss, A. FtsW activity and lipid II synthesis are required for recruitment of MurJ to midcell during cell division in Escherichia coli. *Mol. Microbiol.* (2018).

163. Wang, M., Fang, C., Ma, B., Luo, X. & Hou, Z. Regulation of cytokinesis: FtsZ and its accessory proteins. *Curr. Genet.* **66**, 43–49 (2020).

164. Marmont, L. S. & Bernhardt, T. G. A conserved subcomplex within the bacterial cytokinetic ring activates cell wall synthesis by the FtsW-FtsI synthase. *Proc. Natl. Acad. Sci.* **117**, 23879–23885 (2020).

165. Park, K.-T., Pichoff, S., Du, S. & Lutkenhaus, J. FtsA acts through FtsW to promote cell wall synthesis during cell division in *Escherichia coli*. *Proc. Natl. Acad. Sci.* **118**, e2107210118 (2021).

166. Adams, D. W., Wu, L. J. & Errington, J. Cell cycle regulation by the bacterial nucleoid. *Curr. Opin. Microbiol.* **22**, 94–101 (2014).

167. Wu, L. J. & Errington, J. Nucleoid occlusion and bacterial cell division. *Nat. Rev. Microbiol.* **10**, 8–12 (2012).

168. De Boer, P. A. J., Crossley, R. E. & Rothfield, L. I. A division inhibitor and a topological specificity factor coded for by the minicell locus determine proper placement of the division septum in E. coli. *Cell* **56**, 641–649 (1989).

169. Lutkenhaus, J. & Sundaramoorthy, M. MinD and role of the deviant Walker A motif, dimerization and membrane binding in oscillation. *Mol. Microbiol.* **48**, 295–303 (2003).

170. Park, K.-T. *et al.* The Min Oscillator Uses MinD-Dependent Conformational Changes in MinE to Spatially Regulate Cytokinesis. *Cell* **146**, 396–407 (2011).

171. Hu, Z., Gogol, E. P. & Lutkenhaus, J. Dynamic assembly of MinD on phospholipid vesicles regulated by ATP and MinE. *Proc. Natl. Acad. Sci.* **99**, 6761–6766 (2002).

172. Wang, N. *et al.* The C-terminal domain of MinC, a cell division regulation protein, is sufficient to form a copolymer with MinD. *FEBS J.* (2023) doi:10.1111/febs.16890.

173. Machado, L. E. S. F. *et al.* NMR study of the interaction between MinC and FtsZ and modeling of the FtsZ:MinC complex. *J. Biol. Chem.* **301**, 108169 (2025).

174. Hu, Z., Saez, C. & Lutkenhaus, J. Recruitment of MinC, an Inhibitor of Z-Ring Formation, to the Membrane in *Escherichia coli* : Role of MinD and MinE. *J. Bacteriol.* **185**, 196–203 (2003).

175. Adler, H. I., Fisher, W. D., Cohen, A. & Hardigree, A. A. Miniature escherichia colicells deficient in DNA. *Proc. Natl. Acad. Sci.* **57**, 321–326 (1967).

176. Robles-Ramos, M. Á. *et al.* The Nucleoid Occlusion Protein SlmA Binds to Lipid Membranes. *mBio* **11**, e02094-20 (2020).

177. Cho, H., McManus, H. R., Dove, S. L. & Bernhardt, T. G. Nucleoid occlusion factor SlmA is a DNA-activated FtsZ polymerization antagonist. *Proc. Natl. Acad. Sci.* **108**, 3773–3778 (2011).

178. Tonthat, N. K. *et al.* Molecular mechanism by which the nucleoid occlusion factor, SlmA, keeps cytokinesis in check: Mechanism of SlmA-mediated nucleoid occlusion. *EMBO J.* **30**, 154–164 (2011).

179. Nealson, K. H., Moser, D. P. & Saffarini, D. A. Anaerobic Electron Acceptor Chemotaxis in Shewanella Putrefaciens. *Appl Env. Microbiol* **61**, 1551 (1995).

180. Ikeda, S. *et al. Shewanella oneidensis* MR-1 as a bacterial platform for electro-biotechnology. *Essays Biochem.* **65**, 355–364 (2021).

181. Thormann, K. M. *et al.* Control of Formation and Cellular Detachment from *Shewanella oneidensis* MR-1 Biofilms by Cyclic di-GMP. *J. Bacteriol.* **188**, 2681–2691 (2006).

182. Kane, A. L. *et al.* Formate Metabolism in Shewanella oneidensis Generates Proton Motive Force and Prevents Growth without an Electron Acceptor. *J. Bacteriol.* **198**, 1337–1346 (2016).

183. Myers, C. R. & Nealson, K. H. Bacterial Manganese Reduction and Growth with Manganese Oxide as the Sole Electron Acceptor. *Science* **240**, 1319–1321 (1988).

184. Richter, K., Schicklberger, M. & Gescher, J. Dissimilatory reduction of extracellular electron acceptors in anaerobic respiration. *Appl. Environ. Microbiol.* **78**, 913–921 (2012).

185. Heidelberg, J. F. *et al.* Genome sequence of the dissimilatory metal ion–reducing bacterium Shewanella oneidensis. *Nat. Biotechnol.* **20**, 1118–1123 (2002).

186. Daraselia, N. *et al.* Reannotation of *Shewanella oneidensis* Genome. *OMICS J. Integr. Biol.* **7**, 171–175 (2003).

187. Stricker, L., Guido, I., Breithaupt, T., Mazza, M. G. & Vollmer, J. Hybrid sideways/longitudinal swimming in the monoflagellate *Shewanella oneidensis* : from aerotactic band to biofilm. *J. R. Soc. Interface* **17**, 20200559 (2020).

188. Alcalde, R. E. *et al.* Motility of Shewanella oneidensis MR-1 Allows for Nitrate Reduction in the Toxic Region of a Ciprofloxacin Concentration Gradient in a Microfluidic Reactor. *Environ. Sci. Technol.* **53**, 2778–2787 (2019).

189. Gödeke, J., Paul, K., Lassak, J. & Thormann, K. M. Phage-induced lysis enhances biofilm formation in Shewanella oneidensis MR-1. *ISME J.* **5**, 613–626 (2011).

190. Gödeke, J., Binnenkade, L. & Thormann, K. M. Transcriptome Analysis of Early Surface-Associated Growth of Shewanella oneidensis MR-1. *PLoS ONE* **7**, e42160 (2012).

191. Zeng, Z. *et al.* Cold adaptation regulated by cryptic prophage excision in *Shewanella oneidensis*. *ISME J.* **10**, 2787–2800 (2016).

192. Chen, X., Zaro, J. L. & Shen, W.-C. Fusion protein linkers: Property, design and functionality. *Adv. Drug Deliv. Rev.* **65**, 1357–1369 (2013).

193. Nanda, A. M., Thormann, K. & Frunzke, J. Impact of Spontaneous Prophage Induction on the Fitness of Bacterial Populations and Host-Microbe Interactions. *J. Bacteriol.* **197**, 410–419 (2015).

194. Paul, J. H. Prophages in marine bacteria: dangerous molecular time bombs or the key to survival in the seas? *ISME J.* **2**, 579–589 (2008).

195. Binnenkade, L., Teichmann, L. & Thormann, K. M. Iron Triggers λSo Prophage Induction and Release of Extracellular DNA in Shewanella oneidensis MR-1 Biofilms. *Appl. Environ. Microbiol.* **80**, 5304–5316 (2014).

196. Guo, Q., Chen, B., Tu, Y., Du, S. & Chen, X. Prophage LambdaSo uses replication interference to suppress reproduction of coexisting temperate phage MuSo2 in Shewanella oneidensis MR-1. *Environ. Microbiol.* **21**, 2079–2094 (2019).

197. Guo, Q., Chen, B., Tu, Y., Du, S. & Chen, X. Prophage LambdaSo uses replication interference to suppress reproduction of coexisting temperate phage MuSo2 in *Shewanella oneidensis* MR-1. *Environ. Microbiol.* **21**, 2079–2094 (2019).

198. Binnenkade, L. Molecular Control of Extracellular DNA Release and Degradation in Shewanella oneidensis MR-1 Biofilms: The Role of Phages and Nucleases. (Philipps-Universität, Marburg, 2015).

199. Tomasz, M. Mitomycin C: small, fast and deadly (but very selective). *Chem. Biol.* **2**, 575–579 (1995).

200. Otsuji, N., Sekiguchi, M., Iijima, T. & Takagi, Y. Induction of Phage Formation in the Lysogenic Escherichia coli K-12 by Mitomycin C. *Nature* (1959) doi:10.1038/1841079b0.

201. Summer, E. J. *et al.* Rz/Rz1 Lysis Gene Equivalents in Phages of Gram-negative Hosts. *J. Mol. Biol.* **373**, 1098–1112 (2007).

202. Young, R., Jeffrey Way, Susan Way, Jerry Yin ‡, & Michael Syvanen. Transposition mutagenesis of bacteriophage lambda: A new gene affecting cell lysis. *J. Mol. Biol.* (1979).

203. D'Ari, R. & Huisman, O. Novel mechanism of cell division inhibition associated with the SOS response in Escherichia coli. *J. Bacteriol.* **156**, 243–250 (1983).

204. Wang, J. *et al.* Intelligent Protein Design and Molecular Characterization Techniques: A Comprehensive Review. *Molecules* **28**, 7865 (2023).

205. Maslowska, K. H., Makiela-Dzbenska, K. & Fijalkowska, I. J. The SOS system: A complex and tightly regulated response to DNA damage. *Environ. Mol. Mutagen.* **60**, 368–384 (2019).

206. Nazir, A. & Harinarayanan, R. Inactivation of Cell Division Protein FtsZ by SulA Makes Lon Indispensable for the Viability of a $ppGpp^0$ Strain of Escherichia coli. *J. Bacteriol.* **198**, 688–700 (2016).

207. Trusca, D., Scott, S., Thompson, C. & Bramhill, D. Bacterial SOS Checkpoint Protein SulA Inhibits Polymerization of Purified FtsZ Cell Division Protein. *J. Bacteriol.* **180**, 3946–3953 (1998).

208. Kuo, D., Nie, M. & Courey, A. J. SUMO as a Solubility Tag and In Vivo Cleavage of SUMO Fusion Proteins with Ulp1. in *Protein Affinity Tags: Methods and Protocols* (eds. Giannone, R. J. & Dykstra, A. B.) (2014). doi:10.1007/978-1-4939-1034-2_6.

209. Fernando Guerrero, Annika Ciragan, & Hideo Iwaï. Tandem SUMO fusion vectors for improving soluble protein expression and purification. *Protein Expr. Purif.* 42–49 (2015).

210. Dhanoa, G. K., Kushnir, I., Qimron, U., Roper, D. I. & Sagona, A. P. Investigating the effect of bacteriophages on bacterial FtsZ localisation. *Front. Cell. Infect. Microbiol.* **12**, 863712 (2022).

211. Koskella, B. & Brockhurst, M. A. Bacteria–phage coevolution as a driver of ecological and evolutionary processes in microbial communities. *FEMS Microbiol. Rev.* **38**, 916–931 (2014).

212. Holt, A. *et al.* Phage-Encoded Cationic Antimicrobial Peptide Required for Lysis. *J. Bacteriol.* **204**, e00214-21 (2022).

213. Chamblee, J. S. *et al.* Endolysin Regulation in Phage Mu Lysis. *mBio* **13**, e00813-22 (2022).

214. Catalão, M. J. & Pimentel, M. Mycobacteriophage Lysis Enzymes: Targeting the Mycobacterial Cell Envelope. *Viruses* **10**, 428 (2018).

215. Shim, H., Shivram, H., Lei, S., Doudna, J. A. & Banfield, J. F. Diverse ATPase proteins in mobilomes constitute a large potential sink for prokaryotic host ATP. *Front Microbiol* (2021) doi:10.3389/fmicb.2021.691847.

216. Dasgupta, S., Thomas, J. A. & Ray, K. Mechanism of Viral DNA Packaging in Phage T4 Using Single-Molecule Fluorescence Approaches. *Viruses* **16**, 192 (2024).

217. Boyd, E. F., Carpenter, M. R. & Chowdhury, N. Mobile effector proteins on phage genomes. *Bacteriophage* **2**, 139–148 (2012).

218. Beliaev, A. S. *et al.* Global transcriptome analysis of Shewanella oneidensis MR-1 exposed to different terminal electron acceptors. *J. Bacteriol.* **187**, 7138–7145 (2005).

219. Qiu, X., Sundin, G. W., Wu, L., Zhou, J. & Tiedje, J. M. Comparative analysis of differentially expressed genes in Shewanella oneidensis MR-1 following exposure to UVC, UVB, and UVA radiation. *J. Bacteriol.* **187**, 3556–3564 (2005).

220. Drew, D. L. J. *et al.* Probing the local secondary structure of bacteriophage S(21) pinholin membrane protein using electron spin echo envelope modulation spectroscopy. *Biochim. Biophys. Acta Biomembr.* **1864**, 183836 (2022).

221. Steger, L. M. E. *et al.* Structural and functional characterization of the pore-forming domain of pinholin S^{21} 68. *Proc. Natl. Acad. Sci.* **117**, 29637–29646 (2020).

222. Gontijo, M. T. P., Teles, M. P., Vidigal, P. M. P. & Brocchi, M. Expanding the Database of Signal-Anchor-Release Domain Endolysins Through Metagenomics. *Probiotics Antimicrob. Proteins* **14**, 603–612 (2022).

223. Khan, R. H. *et al.* Probing the Structural Topology and Dynamic Properties of gp28 Using Continuous Wave Electron Paramagnetic Resonance Spectroscopy. *J. Phys. Chem. B* **127**, 9236–9247 (2023).

224. Koebnik, R., Locher, K. P. & Van Gelder, P. Structure and function of bacterial outer membrane proteins: barrels in a nutshell. *Mol. Microbiol.* **37**, 239–253 (2000).

225. Zückert, W. R. Secretion of Bacterial Lipoproteins: Through the Cytoplasmic Membrane, the Periplasm and Beyond. *Biochim. Biophys. Acta BBA - Mol. Cell Res.* **1843**, 1509–1516 (2014).

226. Finn, R. D., Clements, J. & Eddy, S. R. HMMER web server: interactive sequence similarity searching. *Nucleic Acids Res.* **39**, W29–W37 (2011).

227. Ahammad, T. *et al.* Conformational Differences Are Observed for the Active and Inactive Forms of Pinholin S^{21} Using DEER Spectroscopy. *J. Phys. Chem. B* **124**, 11396–11405 (2020).

228. Ahammad, T. *et al.* Structural Dynamics and Topology of the Inactive Form of S^{21} Holin in a Lipid Bilayer Using Continuous-Wave Electron Paramagnetic Resonance Spectroscopy. *J. Phys. Chem. B* **124**, 5370–5379 (2020).

229. Bednarek, A., Cena, A., Izak, W., Bigos, J. & Łobocka, M. Functional Dissection of P1 Bacteriophage Holin-like Proteins Reveals the Biological Sense of P1 Lytic System Complexity. *Int. J. Mol. Sci.* **23**, 4231 (2022).

230. Samanta, S. *et al.* The bacteriophage mu lysis system–A new mechanism of host lysis? *BIOCELL* **45**, 1175–1186 (2021).

231. Burby, P. E. & Simmons, L. A. Regulation of Cell Division in Bacteria by Monitoring Genome Integrity and DNA Replication Status. *J. Bacteriol.* **202**, (2020).

232. Egan, A. J. F. & Vollmer, W. The physiology of bacterial cell division. *Ann. N. Y. Acad. Sci.* **1277**, 8–28 (2013).

233. Errington, J., Daniel, R. A. & Scheffers, D.-J. Cytokinesis in Bacteria. *Microbiol. Mol. Biol. Rev.* **67**, 52–65 (2003).

234. Semenov, A. V. Peptidoglycan of Bacterial Cell Wall Affects Competitive Properties of Microorganisms. *Bull. Exp. Biol. Med.* **172**, 164–168 (2021).

235. Vollmer, W., Blanot, D. & de Pedro, M. A. Peptidoglycan structure and architecture. *FEMS Microbiol. Rev.* **32**, 149–167 (2008).

236. Egan, A. J. F., Errington, J. & Vollmer, W. Regulation of peptidoglycan synthesis and remodelling. *Nat. Rev. Microbiol.* **18**, 446–460 (2020).

237. Simpkin, A. J. & Rigden, D. J. GP0.4 from bacteriophage T7: in silico characterisation of its structure and interaction with E. coli FtsZ. *BMC Res. Notes* **9**, 343 (2016).

238. Suzuki, Y. Inferring natural selection operating on conservative and radical substitution at single amino acid sites. *Genes Genet. Syst.* **82**, 341–360 (2007).

239. Bustin, M. Conservative Amino-Acid Replacement in the Tyrosine Region of the Lysine-Rich Histones. *Eur. J. Biochem.* **29**, 263–267 (1972).

240. Hale, C. A., Rhee, A. C. & De Boer, P. A. J. ZipA-Induced Bundling of FtsZ Polymers Mediated by an Interaction between C-Terminal Domains. *J. Bacteriol.* **182**, 5153–5166 (2000).

241. De Boer, P. A. Advances in understanding E. coli cell fission. *Curr. Opin. Microbiol.* **13**, 730–737 (2010).

242. Rothfield, L. I. & Justice, S. S. Bacterial Cell Division: The Cycle of the Ring. *Cell* **88**, 581–584 (1997).

243. Mishra, V. Affinity Tags for Protein Purification. *Curr. Protein Pept. Sci.* **21**, 821–830 (2020).

244. Corrales-Guerrero, L. *et al.* MipZ caps the plus-end of FtsZ polymers to promote their rapid disassembly. *Proc. Natl. Acad. Sci.* **119**, e2208227119 (2022).

245. Król, E. & Scheffers, D.-J. FtsZ Polymerization Assays: Simple Protocols and Considerations. *J. Vis. Exp.* 50844 (2013) doi:10.3791/50844.

246. Mukherjee, A. Dynamic assembly of FtsZ regulated by GTP hydrolysis. *EMBO J.* **17**, 462–469 (1998).

247. De Boer, P., Crossley, R. & Rothfield, L. The essential bacterial cell-division protein FtsZ is a GTPase. *Nature* **359**, 254–256 (1992).

248. Yu, X.-C. Ca2+-mediated GTP-dependent dynamic assembly of bacterial cell division protein FtsZ into asters and polymer networks invitro. *EMBO J.* **16**, 5455–5463 (1997).

249. Venkateswaran, K. *et al.* Polyphasic taxonomy of the genus Shewanella and description of Shewanella oneidensis sp. nov. *Int. J. Syst. Bacteriol.* (1999) doi:10.1099/00207713-49-2-705.

250. Kreienbaum, M. *et al.* Isolation and Characterization of Shewanella Phage Thanatos Infecting and Lysing Shewanella oneidensis and Promoting Nascent Biofilm Formation. *Front. Microbiol.* **11**, 573260 (2020).

251. Miller, V. L. & Mekalanos, J. J. A novel suicide vector and its use in construction of insertion mutations: osmoregulation of outer membrane proteins and virulence determinants in Vibrio cholerae requires toxR. *J. Bacteriol.* **170**, 2575–2583 (1988).

252. Lassak, J., Henche, A.-L., Binnenkade, L. & Thormann, K. M. ArcS, the Cognate Sensor Kinase in an Atypical Arc System of *Shewanella oneidensis* MR-1. *Appl. Environ. Microbiol.* **76**, 3263–3274 (2010).

253. Guzman, L. M., Belin, D., Carson, M. J. & Beckwith, J. Tight regulation, modulation, and high-level expression by vectors containing the arabinose PBAD promoter. *J. Bacteriol.* **177**, 4121–4130 (1995).

254. Kovach, M. E. *et al.* Four new derivatives of the broad-host-range cloning vector pBBR1MCS, carrying different antibiotic-resistance cassettes. *Gene* **166**, 175–176 (1995).

255. Schindelin, J. *et al.* Fiji: an open-source platform for biological-image analysis. *Nat. Methods* **9**, 676–682 (2012).

256. Hartmann, R., Van Teeseling, M. C. F., Thanbichler, M. & Drescher, K. BacStalk: A comprehensive and interactive image analysis software tool for bacterial cell biology. *Mol. Microbiol.* **114**, 140–150 (2020).

257. Kropinski, A. M. Practical Advice on the One-Step Growth Curve. in *Bacteriophages: Methods and Protocols, Volume 3* (eds. Clokie, M. R. J., Kropinski, A. M. & Lavigne, R.) 41–47 (Springer New York, New York, NY, 2018).

258. Fields, S. & Song, O. A novel genetic system to detect protein–protein interactions. *Nature* **340**, 245–246 (1989).

259. Yamada, A. *et al.* Usefulness and Limitation of DiBAC4(3), a Voltage-Sensitive Fluorescent Dye, for the Measurement of Membrane Potentials Regulated by Recombinant Large Conductance Ca2+-Activated K+ Channels in HEK293 Cells. *Jpn. J. Pharmacol.* **86**, 342–350 (2001).

260. Sanger, F. & Coulson, A. R. A rapid method for determining sequences in DNA by primed synthesis with DNA polymerase. *J. Mol. Biol.* (1975).

261. McInerney, P., Adams, P. & Hadi, M. Z. Error Rate Comparison during Polymerase Chain Reaction by DNA Polymerase. *Mol. Biol. Int.* **2014**, 1–8 (2014).

262. Gibson, D. G. *et al.* Enzymatic assembly of DNA molecules up to several hundred kilobases. *Nat. Methods* **6**, 343–345 (2009).

263. Avilan, L. Assembling Multiple Fragments: The Gibson Assembly. *Methods Mol. Biol. Clifton NJ* **2633**, 45–53 (2023).

264. Gibson, D. G. Enzymatic assembly of overlapping DNA fragments. *Methods Enzymol.* **498**, 349–361 (2011).

265. Laemmli, U. K. Cleavage of Structural Proteins during the Assembly of the Head of Bacteriophage T4. *Nature* (1970) doi:10.1038/227680a0.

266. Irons, S. L., Chambers, A. C., Lissina, O., King, L. A. & Possee, R. D. Protein Production Using the Baculovirus Expression System. *Curr. Protoc. Protein Sci.* **91**, 5.5.1-5.5.22 (2018).

267. Carmignotto, G. P. & Azzoni, A. R. On the expression of recombinant Cas9 protein in E. coli BL21(DE3) and BL21(DE3) Rosetta strains. *J. Biotechnol.* **306**, 62–70 (2019).

268. Ludwiczak, J., Winski, A., Szczepaniak, K., Alva, V. & Dunin-Horkawicz, S. DeepCoil—a fast and accurate prediction of coiled-coil domains in protein sequences. *Bioinformatics* **35**, 2790–2795 (2019).

269. Teufel, F. *et al.* SignalP 6.0 predicts all five types of signal peptides using protein language models. *Nat. Biotechnol.* **40**, 1023–1025 (2022).

270. Schultz, J., Milpetz, F., Bork, P. & Ponting, C. P. SMART, a simple modular architecture research tool: Identification of signaling domains. *Proc. Natl. Acad. Sci.* **95**, 5857–5864 (1998).

271. Hallgren, J. *et al.* DeepTMHMM predicts alpha and beta transmembrane proteins using deep neural networks. Preprint at https://doi.org/10.1101/2022.04.08.487609 (2022).

272. Wilkins, M. R. *et al.* Protein identification and analysis tools in the ExPASy server. *Methods Mol. Biol. Clifton NJ* **112**, 531–552 (1999).

273. Varadi, M. *et al.* AlphaFold Protein Structure Database in 2024: providing structure coverage for over 214 million protein sequences. *Nucleic Acids Res.* **52**, D368–D375 (2024).

274. Zhou, Y., Liang, Y., Lynch, K. H., Dennis, J. J. & Wishart, D. S. PHAST: A Fast Phage Search Tool. *Nucleic Acids Res.* **39**, W347–W352 (2011).

275. Seeliger, D. & de Groot, B. L. Ligand docking and binding site analysis with PyMOL and Autodock/Vina. *J. Comput. Aided Mol. Des.* **24**, 417–422 (2010).

276. Rosignoli, S. & Paiardini, A. Boosting the Full Potential of PyMOL with Structural Biology Plugins. *Biomolecules* **12**, (2022).

277. Sievers, F. *et al.* Fast, scalable generation of high-quality protein multiple sequence alignments using Clustal Omega. *Mol. Syst. Biol.* **7**, 539 (2011).

278. Mitteer, D. R. & Greer, B. D. Using GraphPad Prism's Heat Maps for Efficient, Fine-Grained Analyses of Single-Case Data. *Behav. Anal. Pract.* **15**, 505–514 (2022).

279. Perme, M. P. & Manevski, D. Confidence intervals for the Mann-Whitney test. *Stat. Methods Med. Res.* **28**, 3755–3768 (2019).

Abbreviations

A	Alanine
aa	Amino acids
AB	Antibody
AHT	Anhydrotetracycline
AP	Alkaline phosphatase
Amp	Ampicillin
Ara	Arabinose
BACTH	Bacterial adenylate cyclase two-hybrid system
bp	Base pairs
C	Cysteine
Cm	Chloramphenicol
D	Aspartate
DAP	2,6-diamniopimelinic acid
$_{dd}H_2O$	Double-distilled water
DMSO	Dimethyl sulfoxide
DNA	Desoxyribonucleic acid
E	Glutamate
E. coli	*Escherichia coli*
EDTA	Ethylenediaminetetraacetate
et al.	Lat.: *et alii* (and others)
EtBr	Ethidium bromide

fwd	Forward
G	Glycine
GP	Gene product
H	Histidine
h	hours
HRP	Horse radish peroxidase
I	Isoleucine
IM	Inner membrane
IPTG	Isopropyl-β-D-1-thiogalactopyranoside
K	Lysine
Kan	Kanamycin
KI	Knock-in
KO	Knock-out
L	Leucine
LB	Lysogeny broth
LPS	Lipopolysaccharides
M	Methionine
MCS	Multiple cloning site
min	minutes
ml	Mililitre
NEB	New England Biolabs
OD	Optical density
ori	Origin of replication

ORF	Open reading frame
P	Proline
PCR	Polymerase chain reaction
PFU	Plaque forming units
Primer	Starter oligonucleotide
Q	Glutamine
R	Arginine
rev	Reverse
rpm	Rounds per minute
RT	Room temperature
S	Serine
S.	*Shewanella*
sfGFP	Super-folding green fluorescent protein
Suc	Succhrose
SDS	Sodium dodecyl sulphate
SDS-Page	Sodium dodecyl sulphate polyacrilamide gel-electrophoresis
T	Threonine
Taq	*Thermus aquaticus*
Temed	Tetramethyl ethylenediamine
UZ	Ultrazentrifugation
UV	Ultraviolet
V	Valine
v / v	Volume per volume

W	Tryptophan
w / v	Weight per volume
WT	Wild type
X-Gal	5-bromo-4-chloro-3-indolyl-β-D-galactopyranoside
Y	Tyrosine
YFP	Yellow fluorescent protein
λ	Lambda

Acknowledgments

It takes a village…
I don’t actually know how often I was thinking this over the last months while writing my thesis. I unfortunately won’t be able to acknowledge my whole village, but let´s start somewhere:

First of all, I would like to express my deepest gratitude to my supervisor, Prof. Dr. Kai Thormann, for giving me the opportunity to “find my feet” in this challenging academic world. I wouldn’t have been able to do it without your continuous guidance and excellent support! Thank you for helping me find my passion, pushing me to do better, and raising me up when I needed it.

I am very thankful to my thesis committee members Prof. Dr. Bork Berghoff, PD Dr. habil. Oliver Rossbach and in particular Prof. Dr. Julia Frunzke, who unhesitatingly agreed to be my second reviewer.

I am grateful to all my past and present lab members, who created a fantastic working atmosphere and who comforted me continuously during all the ups and downs. I will not only remember the times when photo shoots were held in the lab or when the entire institute was covered in 'Fredo' stickers, but especially the times when I received unwavering support from you. Thank you Nicole, Alina, Moritz, and Sebastian Pöhl from Marburg for your support with several experiments: should you ever need help - no matter what - I’m here for you! But I would especially like to thank Dorian the Dodo: without you, this work would not have been possible! Please never lose your lovable and cheerful way of facing life. You were an enrichment to my scientific career, as you consistently asked critical questions and contributed valuable ideas to a wide range of projects.

But the time during my PHD luckily wasn’t (only) marked by work: I’ve been incredibly fortunate to have a wonderful group of people in my life, who took the business of cheering me up through active, joyfully and often tipsy free time very seriously: Thank you, Siggi - for being you, and for simply standing by my side without expecting anything. Thank you, Felix, for all the coffees and countless wild nights out. Thank you, Spingli, for the wonderful getaways at your dream of a home. Thank you, Anette, for your endless support with the little devil and for breathing away my mood swings like it’s nothing.

Not mentioning my family would be a sacrilege - you made me who I am. Above all, you taught me not to give up, to persevere, and to work for the things I want in life. Here's to climbing a thousand more (fateful) mountains together…

Everyone who knows me knows that I'm not myself without my boys. Thank you, Alfi and Bubi - simply for being my main source of serotonin. Ever since I've had you in my life, I've never been alone.

But my deepest thanks goes to Luka: Thank you for being my person. For the fact that everything feels effortlessly easy with you. Without your tireless support, love, and belief in me, I probably would've given up a fantastillion times by now.